Environmental Remediation and Semiconductor Photocatalysis

Matthew Crow

2010

PhD Thesis

Department of Pure and Applied Chemistry

University of Strathclyde

This thesis is the result of the author's original research. It has been composed by the author and has not been previously submitted for examination which has led to the award of a degree.

Signed:

Date:

Abstract

Detailed studies of three areas of environmental remediation techniques which utilise semiconductor photocatalytic technologies were undertaken. These areas were: oxidation of solid inorganic contaminant layers deposited on titania (TiO_2); oxidation of inorganic gas species by ultraviolet-illuminated titania; and factors affecting wettability changes (photoinduced superhydrophilicity, *PSH*) on illuminated titania.

Soot and elemental sulfur layers, deposited onto sol-gel derived and P25 TiO_2 films were found to be completely removed upon illumination with UV light; carbon dioxide and sulfur dioxide were detected in stoichiometric quantities as the only gas-phase oxidation products. Sulfur dioxide was trapped using an irradiated flow-cell set-up, with the resulting gas-species trapped and determined by the West-Gaeke method. Remote photocatalysis of soot layers was also investigated, with results suggesting that hydroxyl radicals are potentially not the primary migratory species responsible for remote photocatalysis.

Further work concentrating on the photocatalytic oxidation of SO_2 in a static cell system containing a TiO_2 film was also carried out, with production of SO_3 and poisoning of the photocatalyst observed. The photocatalytic oxidation of carbon monoxide was also assessed, initially using sol-gel TiO_2 films before platinised films and polymer-photocatalyst matrices were assessed. The flexible polymer films were found to be degraded by the photocatalyst – including those developed using fluoropolymers – at the expense of oxidative photocatalytic activity.

The final part focused on repeatable experiments involving *PSH* – including the use of a novel environmental chamber to vary atmospheric conditions during illumination, and experiments into droplet composition and recovery of contact angle – in order to further investigate the possible mechanism(s) behind the phenomenon.

Acknowledgements

I would like to thank Professor Mills for the opportunity to undertake this work, and for challenging and focusing the research as it progressed and evolved. Thanks also to everyone who has passed through the Mills group over the past 5 years, especially George, Gerry, Paul, Cheryl, Mick, Mark, Jamie and David. I'd also like to thank Marianne for her support throughout.

Abbreviations

CA	-	Contact angle, or θ (°)
CB	-	Conductance band
DMS	-	Dimethyl sulfide
EMR	-	Electromagnetic radiation
FTIR	-	Fourier-transform infrared
PCA	-	Photocatalytic activity
PCO	-	Photocatalytic oxidation
PISR	-	Photoinduced surface reorganisation
p-RMSA	-	Pararosaniline methylsulfonic acid
PSH	-	Photoinduced superhydrophilicity
SEA	-	Sacrificial electron acceptor
SED	-	Sacrificial electron donor
SPC	-	Semiconductor photocatalysis
UV	-	Ultraviolet
UVA	-	Ultraviolet 'A' EMR between 310 nm and 400 nm
UVC	-	Ultraviolet 'C', EMR below 280 nm
UV-Vis	-	Ultraviolet-Visible
VB	-	Valence band

Environmental Remediation and Semiconductor Photocatalysis

TABLE OF CONTENTS

CHAPTER 1 INTRODUCTION 1

1.1. SEMICONDUCTOR PHOTOCATALYSIS 1
1.2. PHOTOCATALYSIS THEORY 4
1.3 PHOTOINDUCED SUPERHYDROPHILICITY 13
1.4 YOUNG'S EQUATION AND CONTACT ANGLE 14
1.5 ENVIRONMENTAL SPC – SELF-CLEANING SURFACES 15
1.6 ENVIRONMENTAL SPC – AMBIENT AND INDOOR AIR PURIFICATION 17
1.7 ENVIRONMENTAL SPC – WATERBORNE SYSTEMS 18
1.7 RESEARCH AIMS 19
1.8 REFERENCES 20

CHAPTER 2 EXPERIMENTAL 25

2.1. SYNTHESIS AND/OR PREPARATION OF PHOTOCATALYSTS 25
2.1.1. THICK FILM PHOTOCATALYSTS BY THE SOL-GEL PROCESS 25
2.1.2. ACTIV^{TM} SAMPLES 29
2.1.3. P25 FILMS 30
2.1.4. PLATINISATION OF PASTE FILMS AND P25 30
2.1.5. SYNTHESIS OF PHOTOCATALYTIC POLYMER FILMS 31
2.2. SOURCES OF IRRADIATION AND MEASUREMENT OF INTENSITY 34
2.3. SPECTROPHOTOMETRIC TECHNIQUES 35
2.3.1 ULTRAVIOLET-VISIBLE 35
2.3.1.1. UV-Vis – Cary 50 and Helios-β spectrophotometers 35
2.3.1.2. UV-Vis absorption measurements for quantitative analysis of gas species 36
2.3.2. FOURIER TRANSFORM INFRARED ANALYSIS 36
2.3.2.1. Spectrum One FTIR Spectrometer 36
2.3.2.2. FTIR monitoring of gaseous species 37
2.3.2.4. FTIR monitoring of stearic acid layers 38
2.4 LABORATORY PRODUCTION OF SULFUR DIOXIDE 39
2.5 ASSESSMENT OF CONTACT ANGLE 39

2.5.1. *REPEATED DEPOSITION* CONTACT ANGLE ASSESSMENT 40
2.5.2. *IN-SITU* CONTACT ANGLE MEASUREMENT DURING IRRADIATION 41
2.6 REFERENCES 42

CHAPTER 3 PHOTOCATALYTIC OXIDATION OF SOLID LAYERS OF INORGANIC CONTAMINANTS ON TITANIA 44

3.1 INTRODUCTION 44
3.2 EXPERIMENTAL 53
3.3 DIRECT AND REMOTE PHOTOCATALYTIC OXIDATION OF SOOT ON TiO_2[51] 56
3.4 PHOTOCATALYTIC OXIDATION OF SULFUR LAYERS ON TITANIA PASTE FILMS[48] 62
3.5 CONCLUSIONS 70
3.6 REFERENCES 72

CHAPTER 4 PHOTOCATALYTIC OXIDATION OF INORGANIC GAS SPECIES ON TITANIA 75

4.1. INTRODUCTION 75
4.2. EXPERIMENTAL 81
4.3. PHOTOOXIDATION OF SULFUR DIOXIDE ON PASTE TITANIA FILMS[62] 82
4.3. PCO OF CO ON PASTE FILMS AND PLATINISED PASTE FILMS 88
4.4. EC, P(TFE-VE-PE) AND VITON -TiO_2 FILMS FOR CO REMOVAL 91
4.5 FLUOROPOLYMER [P(TFE-VE-PE), VITON AND PTFE] DESTRUCTION BY PCO 94
4.6. CONCLUSIONS 97
4.7 REFERENCES 99

CHAPTER 5 FACTORS AFFECTING WETTABILITY CHANGES ON TITANIA 103

5.1 INTRODUCTION 103
5.2 EXPERIMENTAL 111
5.2.1. SUBSTRATES 111
5.2.2. MEASUREMENT OF CONTACT ANGLE 111
5.2.3. VARIATION OF ATMOSPHERIC COMPOSITION 111
5.2.4. VARIATION OF DROPLET COMPOSITION 112

5.2.5. SUBSTRATE ILLUMINATION IN SOLUTION 112
5.2.6. MODEL CONTAMINANT DEPOSITION – STEARIC ACID 113
5.2.7. PRE-TREATMENT TECHNIQUES 113
5.2.8. RECOVERY OF *CA* – STORAGE EXPERIMENTS 113
5.3 RESULTS AND DISCUSSION[33, 34] 114
5.3.1. IN-SITU MONITORING OF CONTACT ANGLE; EFFECT OF UV TYPE 114
5.3.2. VARIATION OF ATMOSPHERIC COMPOSITION – O_2, N_2 AND O_3 117
5.3.3 EFFECT OF UV INTENSITY ON RATE AND *PSH* PARAMETERS 120
5.3.4. VARIATION OF DROPLET COMPOSITION: THE EFFECTS OF SALTS AND *SEA*S ON *PSH* 124
5.3.5. STEARIC ACID ON TiO_2 AS A MODEL CONTAMINANT LAYER 127
5.3.6. PRE-TREATMENT – HEAT, UV/OZONE AND ACID 129
5.3.7. CONTACT ANGLE RECOVERY – EFFECT OF HEAT, VACUUM, ULTRASONIC, AND RECOVERY IN AMBIENT OR SEALED SYSTEMS 132
5.4 CONCLUSIONS 136
5.5 REFERENCES 138

CHAPTER 6 FURTHER WORK 141

6.1 PHOTOCATALYTIC OXIDATION OF SOLID INORGANIC LAYERS 141
6.2 PHOTOCATALYTIC OXIDATION OF INORGANIC GAS SPECIES ON TITANIA 141
6.3 FACTORS AFFECTING WETTABILITY CHANGES ON TITANIA 142

CHAPTER 7 GENERAL CONCLUSIONS 143

Chapter 1 Introduction

1.1. Semiconductor photocatalysis

The 1970s saw unprecedented interest in alternatives to fossil fuels for methods of energy generation. Of the solar-energy-based technologies semiconductor photocatalysis (SPC) emerged as a popular option. The formation of hydrogen and oxygen from water had long been held as an idealised potential fuel source; the potential for catalysing this reaction with a photo-sensitising material gained international recognition for photocatalysis and titanium dioxide (TiO_2). The intervening years have seen the potential applications of SPC diversify and evolve, though the original environmental emphasis has remained apparent in many of the myriad research and development projects being carried out worldwide.

The earliest examples of titanium dioxide's potential reactivity were observed as a result of its application as a pigment[1] – the fading of 'titanium white'-incorporated paints and photo-chalking were recognised as effects of ultraviolet light exposure, whereby the organic polymer binders of the matrix were being degraded by photocatalytic action[2]. The upsurge in interest in SPC came with the publishing of Fujishima and Honda's seminal paper heralding the discovery of water cleavage by solar light illumination of a TiO_2 single crystal wafer[3].

$$H_2O + 2h\nu \rightarrow \tfrac{1}{2}O_2 + H_2 \qquad (1\text{-}1)$$

The overall reaction is shown in equation 1-1, with oxygen evolved at the rutile TiO_2 electrode and hydrogen at a platinum black electrode. There have been many further studies which centre on this reaction[4], though a definitive working 'water-splitting' cell utilising solar energy is yet to be commercialised. Along similar timelines new synthetic routes utilising photocatalysis[5] and the environmental potentials of titania-mediated

photocatalysis were also being explored. From the environmental remediation approach, in the first instance, illuminated semiconductor powder dispersions were used to remove water-borne pollutants – such organic species[2, 6, 7], cyanide[8] and dissolved metals[6, 9] – from drinking water. The imparting of photocatalytic activity to robust, solid coatings allowed 'self-cleaning' surfaces to be produced[10-12], as well as those which actively 'cleaned' both ambient and indoor air of pollutant species[13, 14]. The creation of self-cleaning glass for glazing[15] followed the *discoveries*[16, 17] of photoinduced superhydrophilicity (*PSH*), a phenomenon which sees water droplets spread across illuminated titania, rather than beading as droplets. This facet of photocatalytically active titanium dioxide has also been utilised for anti-fogging coatings for mirrors and glassware.

That titanium dioxide features heavily in most discussions of semiconductor photocatalysis is of no great surprise once the key properties of an ideal photocatalyst material are considered. These include; photoactivity; ability to utilise visible or near-ultraviolet light; biological and chemical inertness; photostability; and availability/expense[18]: titania fulfils all of these requisites. Occurring naturally in two photocatalytically active forms – anatase and rutile, Figure 1-1 – and another inactive form – brookite – titanium dioxide has countless uses as a white pigment and filler, again stemming from its chemical and biological inertness.

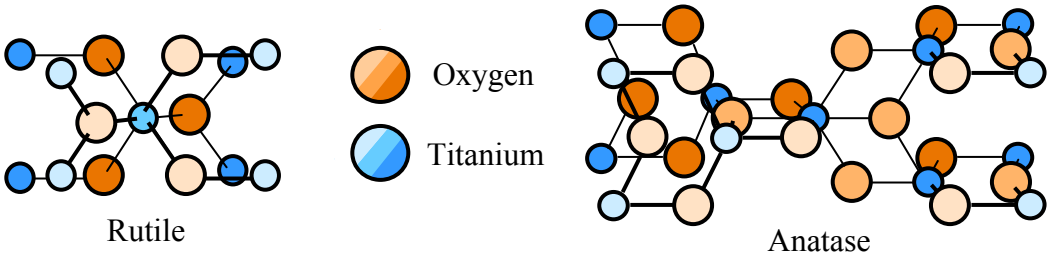

Figure 1-1 Crystal units of Rutile (left) and Anatase (right) titanium dioxide

All three forms have the same formula, TiO_2, but are distinctly different in structure. At high temperatures, >925°C, Anatase TiO_2 spontaneously restructures to the more thermodynamically stable rutile form. It is this stability which accounts for the higher natural abundance of rutile over anatase, with the brookite form found rarely.

Selected applications of photocatalytically active titania and inert titania are shown in Figure 1-2, the major differences between the two relate to particle size and morphology. As a rule larger particles reflect visible light and absorb little, appearing white as a consequence – hence titania's brilliance as a pigment[19]. At the opposite end of the scale the formation of nano-crystalline titania particles imparts novel characteristics, increasing activity whilst reflecting little light and enabling clear coatings to be formed, such as those utilised in glazing.

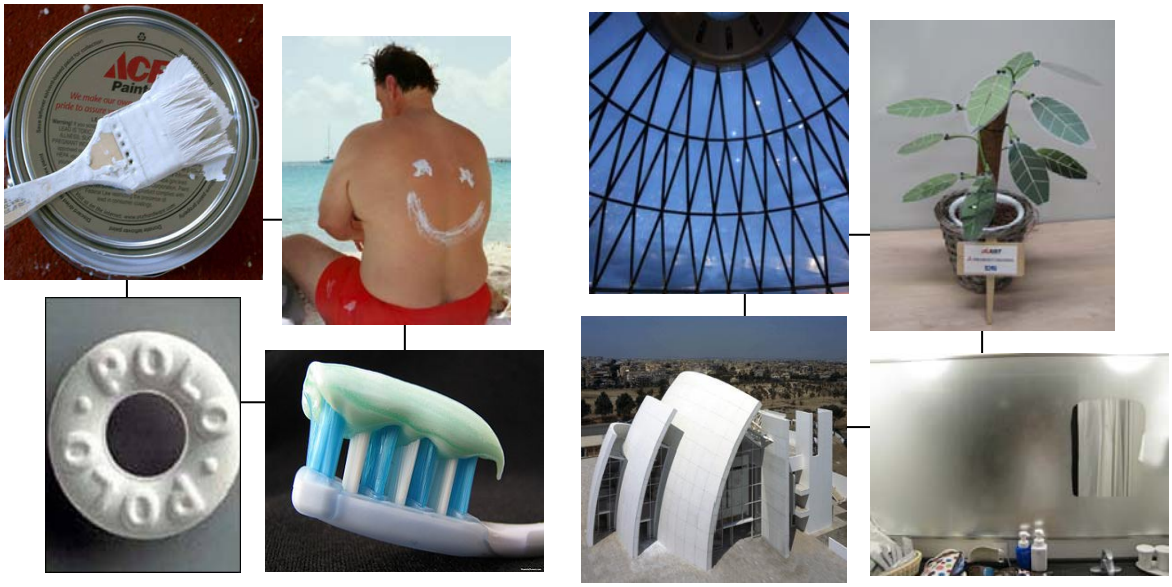

Figure 1-2 (left) selected applications of non-photocatalytic titania including sunscreen, pigment and as an inert filler, and (right) examples of photocatalytically active titania in use, as non-stain building coatings, self-cleaning glass, anti-fog coatings, and used in solar cells[20-27]

1.2. Photocatalysis theory

The fundamentals of semiconductor photocatalysis are well documented[18, 28-30]. Key factors for a photocatalytic system relate to the type of substrate, i.e. the chemical formula and the morphology, and the source of irradiation. These are intrinsically linked; to understand their relationship it is necessary to look at the theory behind semiconductors. The energy required to excite an electron from the *highest occupied molecular orbital* (HOMO) to the *lowest unoccupied molecular orbital* (LUMO), ΔE, becomes smaller as the number of monomeric units (N) increase, Figure 1-3. With the increased N of a semiconductor the electronic structure behaves as bands, with electrons present in the valence band and, for photocatalytic semiconductors via the absorption of electromagnetic radiation greater than the band-gap (E_{bg}), promoted to the conductance band, Figure 1-4.

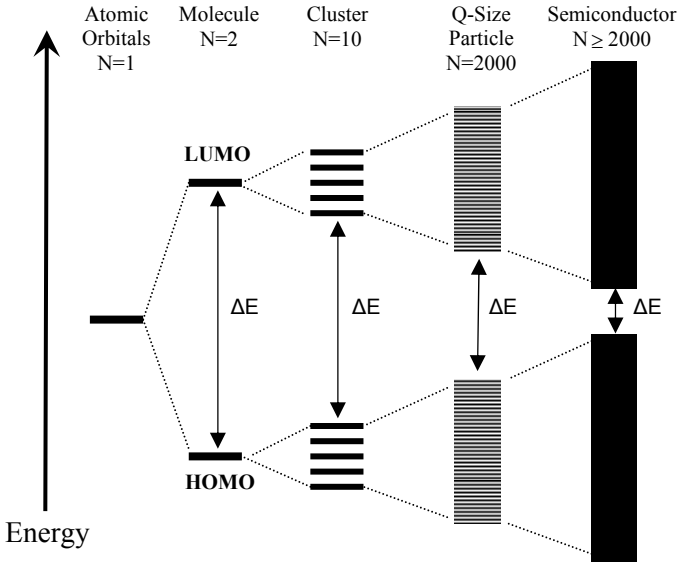

Figure 1-3 decreasing bandgap energy ΔE with increase of the number of monomeric units (N)[18]

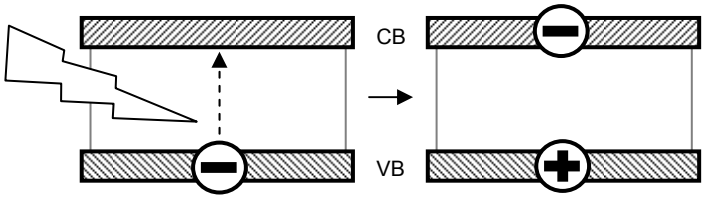

Figure 1-4 Photoexcitation of a valence band (VB) electron to the conductance band (CB) by absorption of ultra-bandgap electromagnetic radiation ($h\nu \geq E_{bg}$), creating an electron/hole pair

$$\lambda(\text{nm}) = \frac{1240}{E_{bg}(\text{eV})} \qquad (1\text{-}2)$$

The wavelength of electromagnetic radiation (EMR) required to excite electrons (λ) is dependant on E_{bg}; the two are linked by equation 1-2[31]. For titanium dioxide – which occurs in two photocatalytically active crystal forms, anatase (E_{bg} = 3.2 eV) and rutile (E_{bg} = 3.0 eV) – this equates to EMR of approximately <420 nm being necessary to initiate photocatalysis. This process creates an electron/hole pair which, following migration through the bulk can initiate redox reactions at the surface, Figure 1-5.

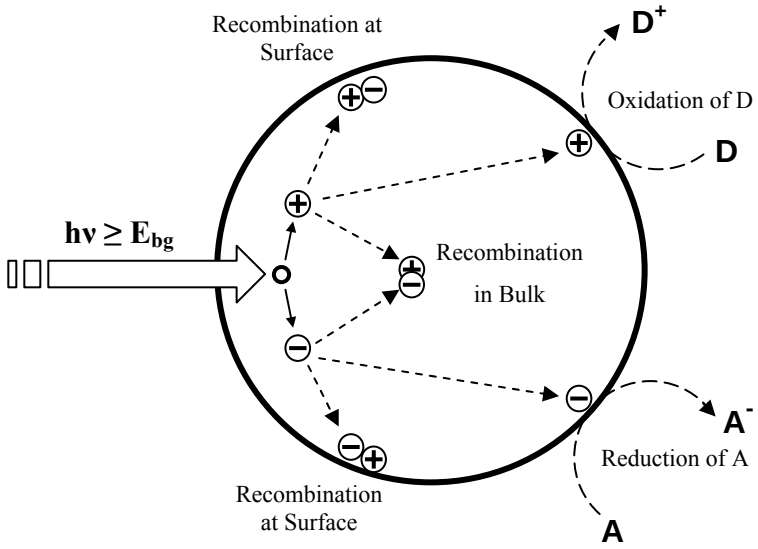

Figure 1-5 possible processes occurring within photoexcited TiO_2, including electron/hole recombination in the bulk, at the surface; and the oxidation of species D or the reduction of A

At the surface: an electron acceptor (A) can be reduced: $A + e^- \rightarrow A^-$; an electron donor (D) can be oxidised by the hole: $D + h^+ \rightarrow D^+$. In such circumstances the overall semiconductor photocatalysis process can be summarised as:

$$A + D \xrightarrow[h\nu \geq E_{bg}]{TiO_2} A^- + D^+ \qquad (1\text{-}3)$$

The oxidising and reducing potentials of the electrons and holes produced are dependant on the potentials of the conductance and valence bands. Therefore the more negative the potential of the conductance band, then the more reducing the photogenerated electrons: and the more positive the valence band potential, then the more oxidising the holes of the valence band. Figure 1-6 depicts valence and conductance band values for a number of semiconductors and their relevance to redox potentials for hydrogen and oxygen evolution. In order for photosensitised reduction to occur, the potential of the conductance band must be more negative than the reduction potential of the species, at the same time the potential of the valence band must be more positive than the oxidation potential for photo-sensitised oxidation to occur[32].

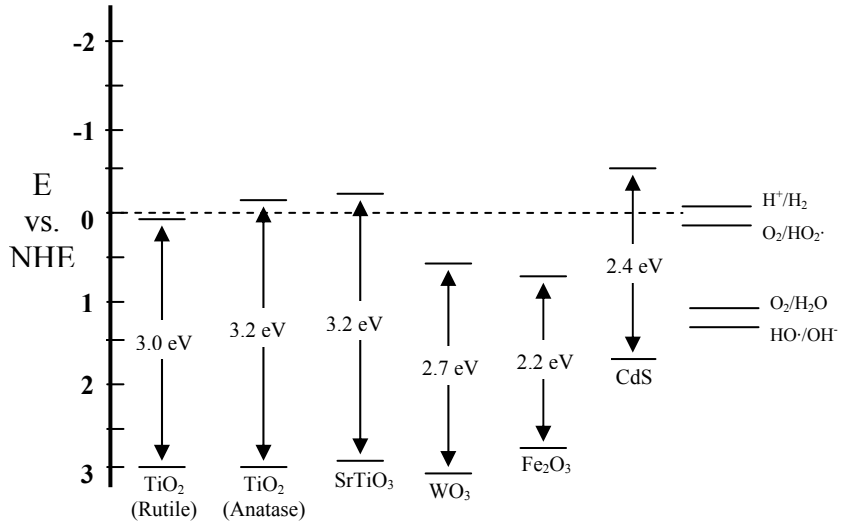

Figure 1-6 valence and conductance band positions for various semiconductors, vs. normalised hydrogen electrode potential, pH = 0[33]

The redox reactions which occur on semiconductor particles are facilitated by the interactions between adsorbed species and the electrons and holes. This is classified as the 'trapping' of the photogenerated species, and the presence of adsorbed hydroxyl groups present on the surface of TiO_2 in humid air has been shown to be significant[29]. Characteristic times of these and other processes occurring upon illumination of the photocatalyst are given in Table 1-1. The subsequently produced hydroxyl radicals are highly oxidising and play a key role in degradation of organic species by photocatalysis, equation 1-4. The active oxygen species formed during *SPC* are effectively 'burning' pollutant species in a cold-combustion reaction; therefore this can be regarded as photocatalytic oxidation (*PCO*) of the compounds. Another essential aspect of the overall process is the presence of a sacrificial electron acceptor (*SEA*); molecular oxygen fulfils this role in many systems producing superoxide ($O_2^{-\cdot}$), the subsequent degradation of which, through interaction with water and/or hydroxyl groups, is thought to produce further hydroxyl radicals which may become involved in *PCO* reactions.

Table 1-1 primary processes, and their characteristic times, for TiO_2 during illumination and subsequent reduction and oxidation reactions[29]

Primary Process	Characteristic Times
(i) charge-carrier generation	
$TiO_2 + h\upsilon \Rightarrow h_{vb}^+ + e_{cb}^-$	(*fs*)
(ii) charge-carrier trapping	
$h_{vb}^+ + >Ti^{IV}OH \Rightarrow \{>Ti^{IV}OH\cdot\}^+$	fast (*10 ns*)
$e_{cb}^- + >Ti^{IV}OH \Leftrightarrow \{>Ti^{III}OH\}$	shallow trap (*100 ps*) (dynamic equilibrium)
$e_{cb}^- + >Ti^{IV} \Rightarrow >Ti^{III}$	deep trap (*10 ns*) (irreversible)
(iii) charge-carrier recombination	
$e_{cb}^- + \{>Ti^{IV}OH\cdot\}^+ \Rightarrow >Ti^{IV}OH$	slow (*100 ns*)
$h_{vb}^+ + \{>Ti^{III}OH\} \Rightarrow >Ti^{IV}OH$	fast (*10 ns*)
(iv) Interfacial charge transfer	
$\{>Ti^{IV}OH\cdot\}^+ + Red \Rightarrow Ti^{IV}OH + Red\cdot^+$	slow *(100 ns*)
$e_{tr}^- + Ox \Rightarrow Ti^{IV}OH + Ox\cdot^-$	very slow (*ms*)

Organic species are completely degraded by *PCO* to form carbon dioxide and water, the presence of heteroatoms, such as N or S, leads to the production of mineral acids, equation 1-4[18], a list of many of the organic compounds degraded by illuminated photocatalysts is shown in table 1-2 . Stearic acid ($CH_3(CH_2)_{16}CO_2H$) is one organic compound which has been utilised as a model test compound for determining photocatalytic activity (*PCA*) of photocatalyst films[10, 34]. Integration of the relevant peaks of a Fourier-Transform Infrared (FTIR) scan allows a measure of the number of molecules of the test compound present and therefore, during irradiation, the total molecules mineralised per unit irradiation time[35]. Other species used as model pollutant compounds for testing in similar manners include gaseous organic; acetaldehyde[36], and gaseous inorganic; nitric oxide[14], as well as aqueous dyes; methylene blue[10, 37], and aqueous organics; dichloroacetic acid (DCA)[38].

$$\text{Organic pollutant} + O_2 \xrightarrow[h\nu \geq E_{bg}]{\text{semiconductor}} CO_2 + H_2O + \text{mineral acids} \qquad (1\text{-}4)$$

As previously stated, *PCO* of organic species, and many other semiconductor-mediated photocatalytic reactions, is dependant upon the wavelength of illumination and formula of substrate used – as shown if equation 1-2 and Figure 1-6 – but the structure and morphology of the semiconductor substrate are also key. A major development in photocatalytic technologies has been the synthesis of nanocrystalline materials[31]. All materials consist of 'grains' which in turn consist of many atoms. Conventional materials contain grains ranging from hundreds of microns to centimetres in size: the grains of nano-materials are in the order of 1-100 nm in size[39].

Atoms on the boundary of grains can have markedly different properties to atoms in the bulk; the distinction is shown in Figure 1-7. As grain sizes decrease the proportion of atoms on the boundaries of grains increases, and with this the material as a whole begins to take on the properties of the grain-boundary atoms, rather than of those in the bulk. This has been shown to impart novel properties on the nanocrystalline material, such as:

improved ductility, reduced density, reduced elastic modulus, enhanced diffusivity, higher electrical resistivity, and increased hardness[40].

Table 1-2 Examples of organic species destroyed or degraded by *PCO*[18]

Class	Example
Alkanes	Methane, isobutene, pentane, heptane, cyclohexane, paraffin
Haloalkanes	Mono-, di-, tri- and tetrachloromethane, tribromoethane, 1,1,1-trifluoro-2,2,2-trichloroethane
Aliphatic alcohols	Methanol, ethanol, isopropyl alcohol, glucose, sucrose
Aliphatic carboxylic acids	Formic, ethanoic, dimethylethanoic, propanoic, oxalic acids
Alkenes	Propene, cyclohexene
Haloalkenes	Perchloroethene, 1,2-dichloroethene, 1,1,2-thrichloroethene
Aromatics	Benzene, naphthalene
Haloaromatics	Chlorobenzene, 1,2-dichlorobenzene, bromobenzene
Nitrohaloaromatics	3,4-Dichloronitrobenzene, dichloronitrobenznen
Phenols	Phenol, hydroquinone, catechol, 4-methylcatechol, resorcinol, *o*-, *m*-, *p*-cresol
Halophenols	2-, 3-, 4-Chlorophenol, pentachlorophenol, 4-fluorophenol, 3,4-difluorophenol
Aromatic carboxylic acids	Benzoic, 4-aminobenzoic, phthalic, salicylic, *m*- and *p*-hydroxybenzoic, chlorohydroxybenzoic acids
Polymers	Polyethylene, poly(vinyl chloride) (PVC)
Surfactants	Sodium dodecylsulphate (SDS), polyethylene glycol, sodium dodecyl benzene sulphonate, trimethyl phosphate, tetrabutylammonium phosphate
Herbicides	Methyl viologen, atrazine, simazine, prometron, propetryne, bentazon
Pesticides	DDT, parathion, lindane
Dyes	Methylene blue, rhodamine B, methyl orange, fluorescein

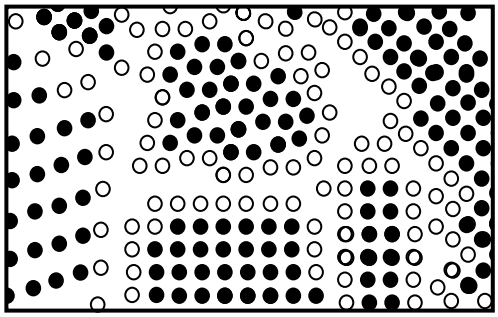

Figure 1-7 atoms in nanocrystalline material; on grain boundaries (open) and associated with the grain (closed)

For photocatalytic semiconductors, such as TiO_2, reduced grain size also means that the intra-particular distances that electrons and holes have to traverse are greatly decreased. This reduces the probability of electron/hole recombination in the bulk and increases the efficiency of the surface redox processes shown in Figure 1-5. Nanocrystalline TiO_2 also benefits from increased specific surface area, increasing hydroxyl group density and the possible sites for the creation of active oxygen species; therefore increasing the activity of the photocatalyst.

The reduced diameter of nanocrystalline particles also affects the optical properties; for TiO_2 an otherwise strong white pigment can be set as hard, clear, photoactive films, which scatter very little visible light[31]. The ultraviolet-visible (UV-Vis) absorbance spectra of a number of TiO_2 photocatalyst films can be seen in Figure 1-8, the portion at >400 nm highlights that little or no visible light is absorbed/reflected for the nanocrystalline films (Activ™ and 4μm paste film), whereas the P25 film (an average particle diameter of 21 nm is typical for Degussa P25; though these exist as aggregates of ~0.1 μm in diameter, meaning they are more accurately described as microparticles rather than nanoparticles[18]) exhibits greater scattering of visible light[10].

The fraction of incident light absorbed by the titania coating of the substrate is a major factor in determining activity of a photocatalyst. There are a number of methods which have been derived in order to calculate or estimate the catalytic properties of photocatalysts in photocatalytic systems. The majority of these terms stem from heterogeneous or homogeneous catalysis, where classical factors such as total active sites and turnover numbers are key economic drivers for a catalyst[41]. For photocatalytic systems the ideal measure of the activity/efficiency of a photocatalyst is its conversion of reactant species per photon of ultra-bandgap irradiation absorbed, this is the quantum yield (Φ), equation 1-5. Unfortunately measurement of the rate of absorption of photons is very difficult, which has meant this term is rarely used.

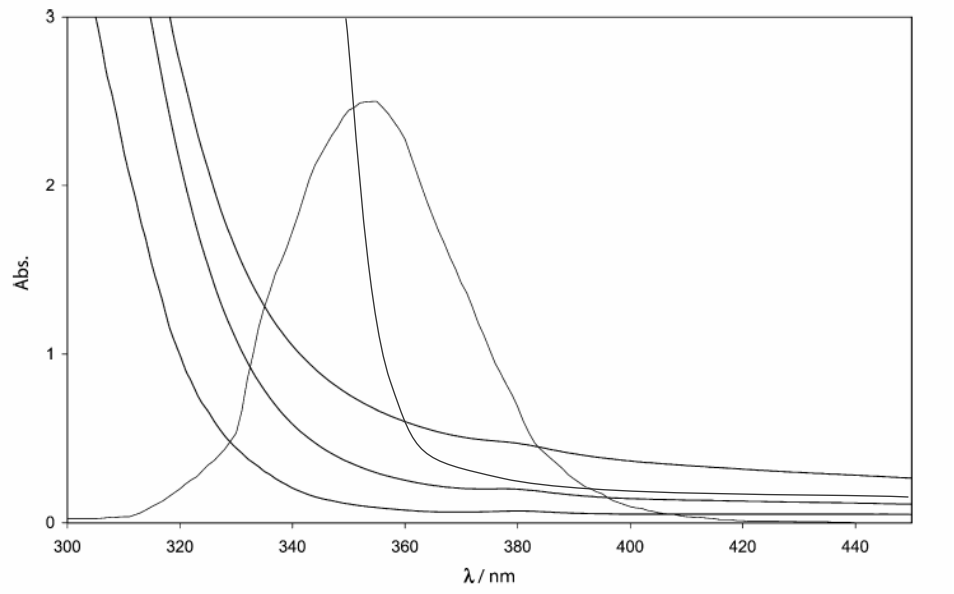

Figure 1-8 UV-Vis absorption spectra for (left to right) plain barrier glass, Activ^{TM}, barrier glass coated with 900 nm of P25, and 4 μm thick paste film. Peak spectrum is typical output of blacklight-blue UVA bulb[35, 42]

An alternative – the quantum efficiency (δ) – takes into account all incident radiation and therefore is much simpler to estimate[18]. δ is defined as the ratio of the rate of reaction over the incident light intensity, equation 1-6[18, 43]. This, when considered per unit area of photocatalyst film, per unit time, is equivalent to the molecules of pollutant degraded/removed per photon of ultra-bandgap irradiation, and is often expressed as a percentage. The caveat attached to any estimation or qualification of a photocatalyst's activity towards degradation or reaction of a specific species hinges on the multitude of other variables which may influence the progress of the reaction. Therefore quantum efficiency provides a guide to allow tentative comparison between photocatalysts rather than a rule by which to measure photocatalysts against.

$$\Phi = \frac{\text{rate of reaction}}{\text{rate of absorption of radiation}} \qquad (1\text{-}5)$$

$$\delta = \frac{\text{rate of reaction}}{\text{incident light intensity}} \qquad (1\text{-}6)$$

One method by which it has been suggested the results of photocatalytic experiments from different groups could be compared is the use of a reference photocatalyst. This would permit results for a new or modified catalyst to be published in conjunction with results for the reference. An original suggestion for such a reference, in aqueous systems which utilise catalyst dispersions, was Degussa P25[18]. Since then a large volume of work has focused on photocatalyst films, leading to suggestions that Activ™ self-cleaning glass, manufactured by Pilkington, could be utilised as a reference photocatalyst[42]. The three different types of titania substrate used in the work exhibit very different photocatalytic activities when determined by stearic acid removal rate (R_{SA})[44]. Films of P25 dip-coated onto glass are the most active – R_{SA} = 17.8 $d\mathrm{A}_{int}/t$ (10^{-3} cm^{-1} min^{-1}) – with paste films produced from a titania sol slightly less active – R_{SA} = 12.8 $d\mathrm{A}_{int}/t$ (10^{-3} cm^{-1} min^{-1}) – and Activ™ much less so – R_{SA} = 0.7 $d\mathrm{A}_{int}/t$ (10^{-3} cm^{-1} min^{-1}). This can partly be explained by comparing thicknesses for the films, intrinsically linked to the

UV absorptivity, and also considering the surface area and porosity of the films. The UV-Vis absorbance spectra of the different films, as shown in Figure 1-8, highlight the absorptivities of the different films, with the thin Activ™ films absorbing least UVA (365 nm) light (7%), followed by the P25 film and the sol-gel film, which absorbs the most (44%)[44].

1.3 Photoinduced superhydrophilicity

The activity of a photocatalyst film towards oxidation of organics translates to the film's activity when undergoing changes in hydrophilicity, i.e. *PSH*. Highly active films, such as the thick, paste-derived films undergo rapid transformation from hydrophobic to hydrophilic in comparison to thin films like Activ™ [45]. The reversible, UV-induced conversion of photocatalyst surfaces has, as mentioned before, been a major factor in the commercial production of self-cleaning surfaces. Many studies have been carried out attempting to elucidate the mechanism of PSH, but a consensus has yet to be reached over the root cause. This topic is covered in more depth in Chapter 5, but briefly; there are two major theories covering PSH, both consider the phenomenon to be photocatalytic in nature and both acknowledge that the surface chemistry of the titania substrate is the key to the process. The point where the theories diverge is once the photogenerated electrons and holes reach the surface.

In 1995 Japanese researchers working in the laboratories of TOTO Ltd. observed this phenomenon, and determined that ultraviolet radiation caused the formation of lattice defects and an increase in hydroxyl group density, resulting in an increase in hydrophilicity[17, 46]. This photoinduced surface reorganisation (*PISR)* mechanism accounts for both the forward and reverse reactions which occur on titania, and was tied in with other studies which observed UV-generated changes on TiO_2 surfaces[47]. The major alternative theory is more straightforward, considering *PSH* as merely another facet of the widely observed photocatalytic oxidation (*PCO*) reactions which occur on UV-exposed titania[16, 48, 49]. The *PCO* theory proposes that atomically clean titania

surfaces are intrinsically superhydrophilic; high energy surfaces which are wetted completely by water droplets. The suggestion is that if the surfaces are exposed to ambient conditions, extremely low levels of organic material – too low to be detected by infra-red spectrophometry for example[50] – are adsorbed, altering the surface chemistry and increasing hydrophobicity. Exposure to UV light allows *PCO* of the organic layer and returns the surface to its intrinsically hydrophilic state.

1.4 Young's equation and contact angle

Evaluation of *PSH* is invariably by the sessile drop method – a water droplet is deposited onto the horizontal subject surface and the angle between the droplet and the substrate is measured, termed the contact angle (CA, also referred to as θ in literature). Contact angle is specific to liquid and solid, and with a known liquid, such as water, contact angle is a simple method of surface analysis for solids.

The minimum surface energy for a liquid is achieved for a droplet, free of external forces, as a perfect sphere. Water has high surface energy, consisting of polar bonds exerting hydrogen bonding forces. When in contact with a solid a water droplet will minimise its surface energy, and therefore its shape, dependant upon the combination of energies of three interfaces: solid-liquid (γ_{SL}), solid-gas (γ_{SG}) and liquid-gas (γ_{LG}), Figure 1-9. A liquid on a surface will reach equilibrium when the forces acting on it are balanced and the surface tension is at a minimum. The forces at equilibrium are described by Young's equation; equation 1-7.

$$\gamma_{LG} \cos\theta = \gamma_{SG} - \gamma_{SL} \qquad (1\text{-}7)$$

The balance of forces acting upon the point where the droplet meets the surface and the gas-phase causes the droplet to stop advancing across the surface. The wetting ability of a liquid is a function of the surface energies of these three interfaces. The net effect of

this is that at the liquid-solid interface, if the attraction between the molecules of the liquid (cohesive force) is greater than their affinity for the molecules of the solid (adhesive force), then the droplet beads up and is non-wetting. If the adhesive force is greater than the cohesive force then the droplet wets the surface. When surface energies are taken into consideration, a low energy surface such as PTFE (18 mN m^{-1}) gives rise to high CA values (>100 °, highly hydrophobic) for water, a high energy liquid[51, 52].

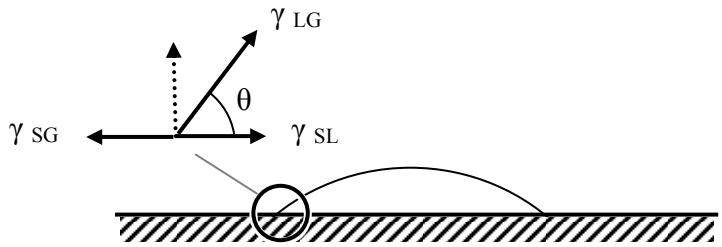

Figure 1-9 diagram of interfacial energies acting on a sessile drop resting on a surface

1.5 Environmental SPC – self-cleaning surfaces

The combination of *PCO* and *PSH* technologies has seen the creation of self-cleaning surfaces for use throughout the construction industry and beyond. The two-step process of *PCO* 'loosening' surface deposits whilst *PSH* dictates that any subsequent rainfall forms sheets of water rather than droplets to wash away the dirt has famously been utilised to fabricate self-cleaning windows[12, 15]. The primary function of self-cleaning materials is to degrade organic type materials, such as those found in greases[10], but soot has also been found to be mineralised by PCO[53-55]. This function makes the incorporation of titania into, and onto, cementitious materials an excellent way to produce stain-proof coatings, such as the coating applied to the Jubilee church in Rome, pictured in Figure 1-10, and the Marunouchi building in Tokyo[12]. Another addition to the field has been illuminated titania's anti-microbial properties, with illuminated coatings causing rupturing of cells wall membranes[56], Figure 1-11, and also degradation

of any associated toxins[57, 58]. This can potentially provide anti-bacterial properties to coatings which may be used in places where cleanliness is imperative, such as hospitals[59].

Figure 1-10 the Jubilee church in Rome features an anti-staining titania coating[27]

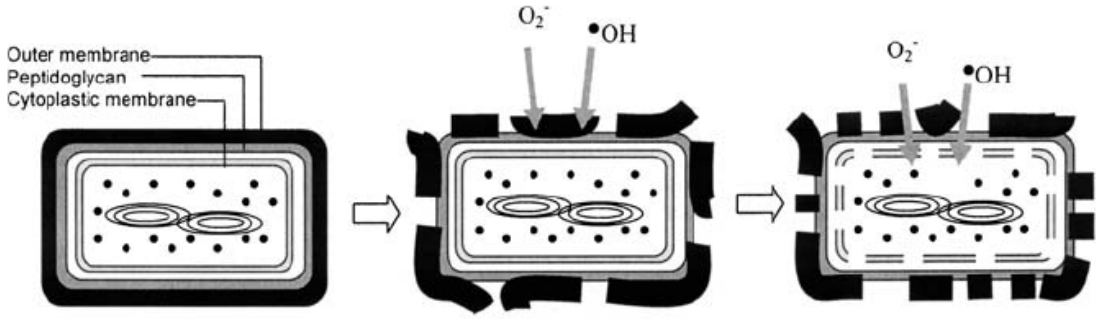

Figure 1-11photokilling of E-Coli, highlighting membrane penetration by hydroxyl radicals and superoxide[56]

1.6 Environmental SPC – ambient and indoor air purification

Another area where titania-incorporating cementitious materials have been used in environmental remediation involves removing toxic gas species from ambient air. NO_x species are a common constituent of city smog and it has been proposed that coating paving with titania can reduce NO_x levels[60, 61]. SPC-based air purifiers have also been created for indoor use, improving the quality of air for homes, offices and industrial workplaces such as factories[15]. An example of a prototype purifier and also the type of honeycomb filter which would be used are given in Figure 1-12.

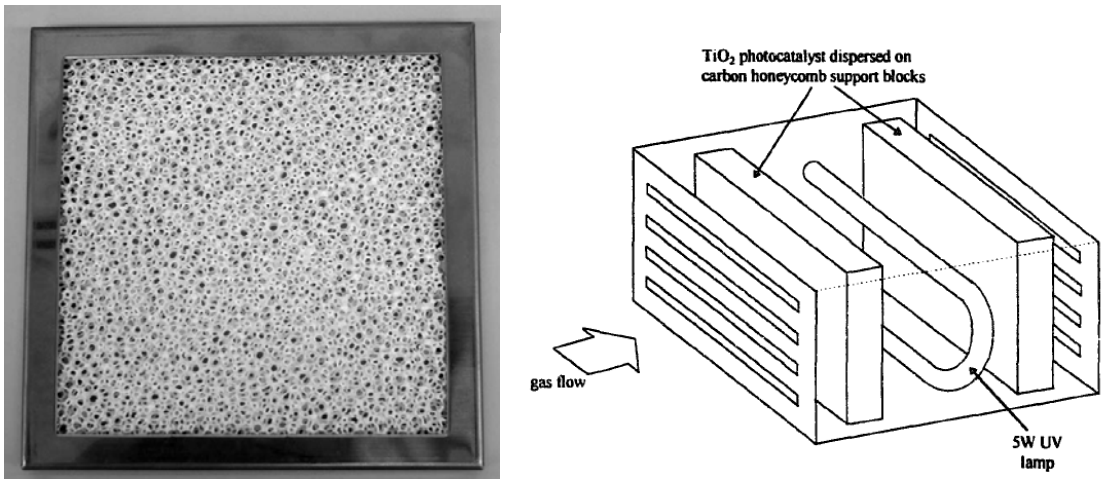

Figure 1-12 porous titania-based ceramic filter used for photocatalytic air purifiers[62] (left) and a schematic of a proposed photocatalytic air purifier[18]

Volatile organic compounds (VOCs) are thought to be a major contributor to poor indoor air quality and are commonly used in building materials – as paint solvents and in the formation of particle boards for example[63]. This class of compounds, as well as chlorinated organics[10, 64] have been shown to be removed from air streams using titania

filters in combination with UV sources[18, 65]. The degradation products of such compounds have to be monitored carefully, as it is possible that intermediates produced during mineralization may be more highly toxic than the original compound. One example of this occurs during the photocatalytic oxidation of TCE (trichloroethylene) in the gas phase, the final complete oxidation products are CO_2, CO, HCl and Cl_2, but phosgene, a highly hazardous species, has also been detected as an incomplete combustion product[32, 59]. The accumulation of acidic species – such as those generated through *PCO* of heteroatom-containing organics and inorganic gas species – would be unfavourable for acidity-sensitive materials such as masonry. Further discussion of this subject is contained in Chapter 4.

1.7 Environmental SPC – waterborne systems

The first environmental applications of SPC concerned water purification, specifically the production of potable water from polluted waterways. As an alternative to using corrosive methods like chlorination and ozone treatment, *PCO* is a much less hazardous prospect capable of degrading and destroying organic species, such as those listed in Table 1-2, as well as removing both cations and anions from water. The types of contamination which are being considered for this type of remediation are most likely to be crude oil derivatives like gasoline or pesticides and herbicides which are accumulated in ground water[66]. The photocatalytic mineralization of these organic and chlorinated organic species has been shown to be highly successful[29] using primarily powder dispersions[2, 6, 66]. Other target compounds such as cyanide and sulfite were observed to be oxidised in titania/water dispersions[8]. Bromine and iodine ions were also oxidised, with the products dependant on the pH of the medium, though chlorine ions were found to withstand oxidation[67].

Reductive pathways were observed for cations, usually metals dissolved in water, such as Ag, Au, Cd, Cr, Cu, Hg, Ni, Pb, Se and Pt[6, 9, 68]. Many of these are toxic in water and

therefore their removal by photocatalysis is another useful facet of photocatalytic purification. The development of supported photocatalysts[69], rather than powder dispersions which require a filtration step for catalyst recovery, is a useful but not essential step towards bringing these types of water-purifiers to the commercial market, as shown by the number of systems on the market which use titania slurries[15]. Self-contained reactors which do not require an electrical UV light source, i.e. solar reactors, have been piloted for effluent and wastewater purification, such as the plant situated on the site of the Menzel Temime textile factory in Tunisia[70]. Depicted in Figure 1-13, the thin-film fixed-bed reactor allows effluent to flow over the photocatalyst, removing organic compounds and reducing the chemical oxygen demand (COD) of the wastewater. Other water-borne species whose removal by PCO is desirable for drinking-water production include cyanobacteria and cyanotoxins[71].

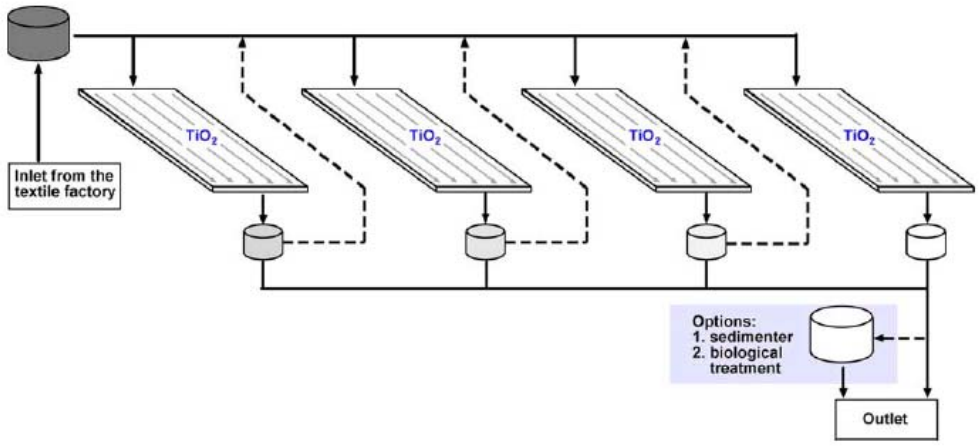

Figure 1-13 schematic of TFFBR solar reactor used to purify textile effluent in Tunisia[70]

1.7 Research aims

The aims of this work are to continue the exceptional work of the Mills group and investigate a number of areas of semiconductor photocatalysis in the context of

applications for environmental remediation. This includes the removal of solid inorganic layers from 'self-cleaning' films of titania; oxidation and removal of gas-phase pollutants by titania films and the creation of possible polymer-based photocatalyst films; and a thorough investigation into the kinetics and mechanism of both the forward and reverse reactions of *PSH*. The thread which runs through the whole body of work is the focus on using either easily fabricated or commercially-produced films of titania for repeatable experiments in order to gain insight into subjects which have provoked much debate amongst researchers.

1.8 References

1 C. F. Goodeve, and J. A. Kitchener, *T. Faraday Soc.* **34**, 570 (1938).

2 A. Mills, R. H. Davies, and D. Worsley, *Chem. Soc. Rev.* **22**, 417 (1993).

3 A. Fujishima, and K. Honda, *Nature* **238**, 37 (1972).

4 A. Mills, and G. Porter, *J.Chem. Soc., Faraday Trans.* **78**, 3659 (1982).

5 M. A. Fox, *Accounts Chem. Res.* **16**, 314 (1983).

6 M. R. Prairie, L. R. Evans, B. M. Stange, and S. L. Martinez, *Environ. Sci. Technol.* **27**, (9), 1776 (1993).

7 H. Gerischer, *Electrochimica Acta* **38**, (1), 3 (1993).

8 S. N. Frank, and A. J. Bard, *J. Phys. Chem.* **81**, (15), 1484 (1977).

9 D. Chen, and A. K. Ray, *Chem. Eng. Sci.* **56**, 1561 (2001).

10 R. Fretwell, and P. Douglas, *J. Photochem. Photobiol. A: Chem* **143**, 229 (2001).

11 A. Mills, N. Elliott, I. P. Parkin, S. A. O'Neill, and R. J. Clark, *J. Photochem. Photobiol. A: Chem* **151**, 171 (2002).

12 I. P. Parkin, and R. G. Palgrave, *J. Mater. Chem.* **15**, 1689 (2004).

13 A. Mills, S.-K. Lee, and A. Lepre, *J. Photochem. Photobiol. A: Chem* **155**, 199 (2003).

14 T. Ibusuki, and K. Takeuchi, *J. Mol. Catal. A Chem.* **88**, 93 (1994).

15 A. Mills, and S.-K. Lee, *J. Photochem. Photobiol. A: Chem* **152**, 233 (2002).

16 S. Kume, and T. Nozu, *Difficulty stainable glass product*. Japanese Patent Sho 61-243762, 1986.

17 R. Wang, K. Hashimoto, A. Fujishima, M. Chikuni, E. Kojima, A. Kitamura, M. Shimohigoshi, and T. Watanabe, *Nature* **388**, 431 (1997).

18 A. Mills, and S. Le Hunte, *J. Photochem. Photobiol. A: Chem* **108**, 1 (1997).

19 U. Diebold, *Surf. Sci. Reports* **48**, 53 (2003).

20 Webpage, *http://compmed.files.wordpress.com/2009/07/sunscreen.jpg*, (accessed 6/03/09).

21 Webpage, *http://images.travelpod.com/users/lduckett/2.1235847600.anti-fog-mirrorx.jpg*, (accessed 6/03/09).

22 Webpage, *http://media.supereco.com/media/2009/05/27/320w/white-paint-brush.jpg*, (accessed 6/03/09).

23 Webpage, *http://newsimg.bbc.co.uk/media/images/44569000/jpg/_44569543_polo226.jpg*, (accessed 6/03/09).

24 Webpage, *http://techon.nikkeibp.co.jp/english/NEWS_EN/20080527/152443/leaf1.jpg*, (accessed 6/03/09).

25 Webpage, *http://upload.wikimedia.org/wikipedia/en/thumb/b/b4/Toothpaste_and_brush.jpg/300px-Toothpaste_and_brush.jpg*, (accessed 6/03/09).

26 Webpage, *http://www.ice-productions.co.uk/Royal-Vets/Royal-Vets-132.jpg*, (accessed 6/03/09).

27 Webpage, *www.richardmeier.com*, (accessed 1/10/2007).

28 A. Fujishima, K. Hashimoto, and T. Watanabe, *TiO_2 Photocatalysis: Fundamentals and Applications*. BKC: 1999.

29 M. R. Hoffman, S. T. Martin, W. Choi, and D. Bahnemann, *Chem. Rev.* **95**, 69 (1995).

30 M. A. Fox, and M. T. Dulay, *Chem. Rev.* **93**, (1), 342 (1993).

31 A. Hagfeldt, and M. Gratzel, *Chem. Rev.* **95**, 49-68 (1995).

32 A. L. Linsebigler, G. Lu, and J. T. Yates Jr, *Chem. Rev.* **95**, 735 (1995).

33 A.Mills, and S. L. Hunte, *Journal of Photochemistry and Photobiology A: Chemistry* **108**, 1-35 (1997).

34 A. Mills, G. Hill, M. Crow, and S. Hodgen, *J. App. Electrochem.* **35**, 641-653 (2005).

35 A. Mills, G. Hill, S. Bhopal, I. P. Parkin, and S. A. O'Neill, *J. Photochem. Photobiol. A: Chem* **160**, 185 (2003).

36 I. Sopyan, S. Murasawa, K. Hashimoto, and A. Fujishima, *Chem. Letts.* **4**, 723 (1994).

37 H. Lachheb, E. Puzenat, A. Houas, M. Ksibi, E. Elaloui, C. Guillard, and J.-M. Herrmann, *Appl. Catal. B: Environ.* **39**, 75 (2002).

38 M. Lindner, D. W. Bahnemann, B. Hirthe, and W.-D. Griebler, *J. Solar Energy Eng. - Trans. ASME* **119**, 114 (1997).

39 M. Wilson, K. Kannangara, G. Smith, M. Simmons, and B. Raguse, *Nanotechnology, basic science and emerging technologies*. 1 ed.; Chapman & Hall: 2002; p 271.

40 C. Suryanarayana, *International Materials Reviews* **40**, (2), 41-64 (1995).

41 N. Serpone, A. Salinaro, A. Emeline, and V. Ryabchuk, *J. Photochem. Photobiol. A: Chem* **130**, 83 (2000).

42 A. Mills, A. Lepre, N. Elliott, S. Bhopal, I. P. Parkin, and S. A. O'Neill, *J. Photochem. Photobiol. A: Chem* **160**, 213 (2003).

43 J.-M. Herrmann, *Topics in Catalysis* **34**, (1-4), 49 (2005).

44 A. Mills, J. Wang, M. Crow, G. Taglioni, and L. Novella, *J. Photochem. Photobiol. A: Chem* **187**, 370 (2007).

45 A. Mills, N. Elliott, G. Hill, D. Fallis, J. D. Durrant, and R. L. Willis, *Photochem. Photobiol. Sci.* **2**, 591 (2003).

46 A. Fujishima, T. N. Rao, and D. A. Tryk, *J. Photochem. Photobiol. C* **1**, 1 (2000).

47 A. N. Shultz, W. Jang, W. M. Hetherington, D. R. Baer, L. Q. Wang, and M. H. Englehard, *Surf. Sci.* **339**, 114 (1995).

48 T. Zubkov, D. Stahl, T. L. Thompson, D. Panayatov, O. Diwald, and J. T. YatesJnr, *J. Phys. Chem. B* **109**, 15454 (2005).

49 J. M. White, J. Szanyi, and M. Henderson, *J. Phys. Chem. B* **107**, 9029 (2003).

50 C.-Y. Wang, H. Groenzin, and M. J. Shultz, *Langmuir* **19**, 7330 (2003).

51 A. W. Adamson, and A. P. Gast, *Physical Chemistry of Surfaces*. Sixth ed.; John Wiley & Sons: 1997.

52 D. J. Shaw, *Introduction to Colloid and Surface Chemistry*. Fourth ed.; Butterworth Heinemann: 1991.

53 M. C. Lee, and W. Choi, *J. Phys. Chem. B* **106**, 11818 (2002).

54 S.-K. Lee, S. McIntyre, and A. Mills, *J. Photochem. Photobiol. A: Chem* **162**, 203 (2004).

55 A. Mills, J. Wang, and M. Crow, *Chemosphere* **64**, 1032 (2006).

56 P.K.J. Robertson, D.W. Bahnemann, J.M.C. Robertson, and F. Wood, *Hdb Env. Chem.* **2**, (M), 367 (2005).

57 K. Sunada, Y. Kikuchi, K. Hashimoto, and A. Fujishima, *Env. Sci. Technol.* **32**, (5), 726 (1998).

58 K. Page, R. G. Palgrave, I. P. Parkin, M. Wilson, S. L. P. Savin, and A. V. Chadwick, *J. Mater. Chem.* **17**, 95 (2007).

59 L. Frazer, *Environ. Health Persp.* **109**, (4), 174 (2001).

60 H. Johnstone, *Filtr. Separat.* **41**, (4), 18 (2004).

61 K. Scrivener, and H. Van Damme, *MRS Bull.* **29**, 308 (2004).

62 A. Fujishima, and X. Zhang, *C. R. Chimie* **8**, 1 (2005).

63 Factsheet, *Indoor Air Quality: Sick Building Syndrome* **Environmental Protection Agency**, (2005).

64 S. Yamazaki-Nishida, K. J. Nagano, L. A. Phillips, S. Cervera-March, and M. A. Anderson, *J. Photochem. Photobiol. A: Chem* **70**, 95-99 (1993).

65 W.-K. Jo, and K.-H. Park, *Chemosphere* **57**, 555 (2004).

66 D. F. Ollis, E. Pelizzetti, and N. Serpone, *Environ. Sci. Technol.* **25**, (9), 1523 (1991).

67 J.-M. Herrmann, and P. Pichat, *J.C.S. Faraday I* **76**, 1138 (1980).

68 T. T. Y. Tan, D. Beydoun, and R. Amal, *J. Mol. Catal. A Chem.* **202**, 73-85 (2003).

69 R. L. Pozzo, M. A. Baltanas, and A. E. Cassano, *Catal. Today* **39**, 219 (1997).

70 D. Bahnemann, *Sol. Energy* **77**, 445 (2004).

71 P. K. J. Robertson, D. W. Bahnemann, J. M. C. Robertson, and F. Wood, *Hdb Env. Chem.* **2**, (M), 367 (2005).

Chapter 2 Experimental

2.1. Synthesis and/or Preparation of Photocatalysts

2.1.1. Thick film photocatalysts by the sol-gel process

The use of sol-gel techniques is popular for the creation of hard, glassy titania photocatalyts[1-5]. There are generally three major steps involved in sol-gel processing; hydrolysis, alcohol condensation and water condensation[6]. The following method utilised a modified sol-gel process whereby acetic acid complexation of the titanium precursor precedes acid-catalysed hydrolysis. All chemical were supplied by Aldrich unless stated otherwise.

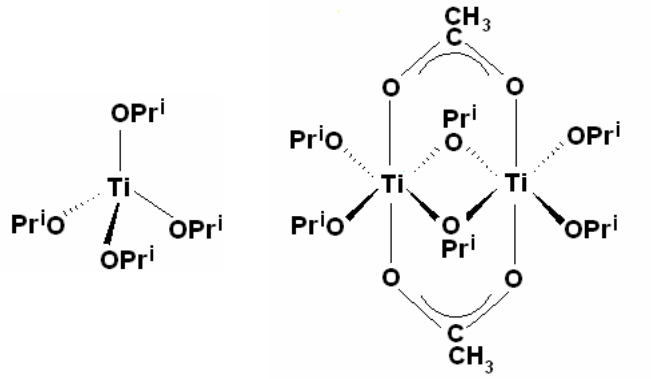

Figure 2-1 (Left) tetrahedral structure of monomeric titanium(IV) Isopropoxide, and (right) octahedral dimer of acetic acid modified titanium(IV) isopropoxide

---

Modification of precursor: Transition metal alkoxides are a common choice as precursor due to their reactive metal centres; being surrounded by electronegative –OR groups. A degree of control of the hydrolysis step is acquired by the acid modification of the precursor[7], in this case Titanium(IV) isopropoxide ($Ti(OCH(CH_3)_2)_4$ (commonly referred to as Ti ($OPr^i)_4$)). Nucleophilic substitution of the isopropoxide ligands for acetate ($–OCOCH_3$) groups controls hydrolysis by reducing the activity of the species in

two key ways: acetate groups are *less* bulky and *more* electronegative ligands than isopropoxide groups.

The procedure was as follows: titanium(IV) isopropoxide ($Ti(OPr^i)_4$, 20 ml, 97%) was added, via a 12-gauge needle connected to a glass syringe, to a 100 ml round bottomed flask containing glacial acetic acid (4.65 g). Due to the extreme moisture sensitivity of titanium(IV) isopropoxide, upon addition, the tip of the syringe was kept below the surface of the acetic acid. The reaction between the reagents was noticeably exothermic.

Synthesis of TiO_2 via hydrolysis Sol-Gel process: The overall hydrolysis reaction of acetic acid-modified titanium isopropoxide with water under acid conditions occurs via an SN2 type mechanism, a simplified version of this reaction is as follows:

$$M(OR)_4 + 4H_2O \rightarrow M(OH)_4 + 4R(OH) \qquad (2\text{-}1)$$

Condensation then occurs in two concurrent steps: water condensation and alcohol condensation, which both form ≡M–O–M≡ bonds. The formation of sub-micrometer-sized colloidal particles from many condensed oligomeric $[\equiv M–O–M\equiv]_n$ units is termed polycondensation.

To initiate hydrolysis and subsequent condensation, the modified $Ti(OPr^i)_4$ solution was added to a 250 ml conical flask containing distilled water (120 ml) and concentrated nitric acid (1.08 g) and stirred rapidly. Using a paraffin oil bath, heating plate and Fuzzy Logic temperature controller the temperature was raised to 80°C and maintained for 8 hours. After a few minutes at this temperature the solution had gelled considerably but returned to liquid state again, leaving a translucent blue/white tinted solution. Upon cooling to room temperature, the solution was filtered through a 0.45 μm syringe filter to remove any non-dispersed aggregates. At this stage a solids mass-check (carried out by sampling the solution into a glass vial and calculating the weight percentage of the remaining residue after evaporating off the water in an oven at 105°C and removing any

unreacted organics by placing in a furnace at 450°C) showed the solution to be typically 5 – 7 wt% TiO_2.

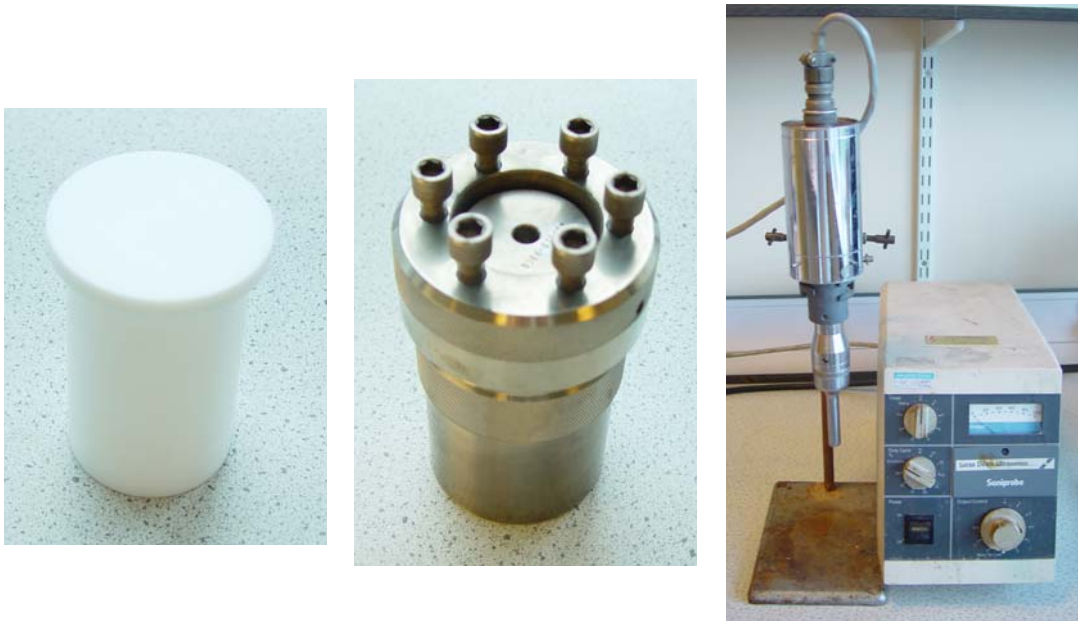

Figure 2-2 left to right; PTFE pot with lid, volume 100 mL; stainless steel autoclave; ultrasonic probe and signal generator

Particle size growth by Autoclaving: The colloidal particles formed in the condensation process are ca. 5 nm in diameter, but an extra hydrothermal particle growth step was included in order to increase particle size to ca. 10–15 nm. Autoclave treatment encourages particle growth via Östwald ripening, whereby high pressure increases the solubility of smaller particles, encouraging the growth of the less soluble larger particles, creating a white colloidal solution with a narrow particle size distribution[1].

This hydrothermal step was carried out by taking a sample of the filtered solution (80 ml) and transferring it to a Teflon™ pot, Figure 2-2, before placing it in an autoclave (Paar Instruments, also Figure 2-2) which was placed in a 220°C oven for 12 hours.

After cooling, the solution was found to have separated into two phases inside the autoclave pot, with the now white TiO_2 crystals settled to the bottom. To allow the suspension to fully re-disperse it was subjected to ultrasound using a Branson Probe 450 sonic horn probe, (Figure 2-2) on full power for 30 seconds.

Reduction of solution to form paste: The gelation step is the termination of the process in which, upon the removal of excess water, the colloidal particles form the characteristic viscous white titanium dioxide paste.

In order to concentrate the TiO_2 from ~ 5–7 wt% to ~ 12 wt% solids the solution was rotary evaporated, using a water bath set at 35°C and low-pressure pump. The rotary evaporation took in the region of 60 minutes each time. To this paste 50 wt% of polyethylene glycol ('Carbowax 20M', supplied by Supelco) was added and the paste left to stir overnight. The Carbowax acts primarily as a binder, and prevents the formation of small surface cracks in the films upon drying. The paste at this stage is very stable and will keep in a fridge for many months.

Casting and annealing of TiO_2 thick films on glass slides: The homogenised paste was cast onto glass microscope slides using the 'doctor-blade' method; whereby two tracks of Scotch Magic Tape (single thickness; 60 μm) are laid down the slide, leaving a trough template (Figure 2-3 A). Ethanol was used to clean the surface of the slide before film casting. The TiO_2 paste is applied to one end of the trough and drawn down the slide using the stem of a pasteur pipette (Figure 2-3 – B, C & D). At this stage the film was thick (~60 μm) and white, but on drying (Figure 2-3 – F & G) the thickness reduced to ~10 μm and the whiteness disappeared to leave a largely colourless film. After drying, the film was annealed in a muffle furnace; the standard temperature used for the regular films was 450°C for 30 minutes. The annealing process binds the titania particles together, and to the substrate, and burns off the PEG (leaving a porous surface) and any unreacted organic precursor[8].

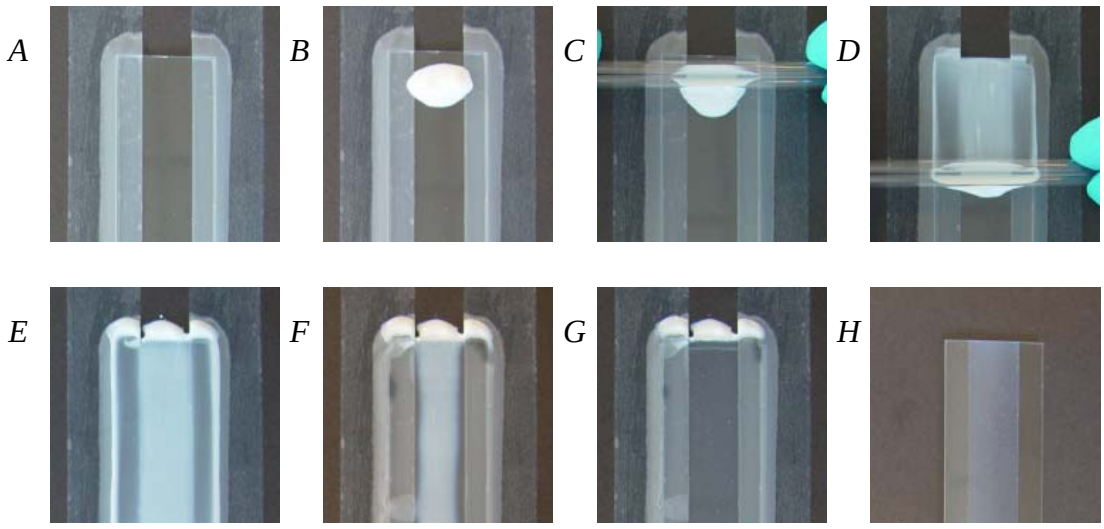

Figure 2-3 *A* – microscope slide with 'magic' tape tracks; *B, C, D* & *E* – paste deposition and 'doctor-blading'; *F* & *G* – paste drying; *H* – annealed film

---

Physical characteristics: After calcining, sol-gel paste films cast by the doctor-blade technique were observed to be ~4 μm in thickness, consisting of the anatase form of titania as determined by XRD[9]. Particles of ca. 13 nm were observed, with a BET surface area of 80 m^2 g^{-1} measured on powdered samples of the films. The films were mesoporous (average pore diameter between 2 and 50 nm) with an average porosity of ~60% [8].

2.1.2. Activ™ samples

Activ™ samples were provided by Pilkington in sheet glass form, these sheets were cut into 2 cm × 2 cm squares. The commercial fabrication of Activ™ [10, 11] utilises APCVD (atmospheric pressure chemical vapour deposition) and the TiO_2 layer is deposited onto 4 mm soda-lime silicate glass with a ~30 nm silicon oxide barrier layer – to prevent alkali metal ion migration, which can decrease photocatalytic activity by interfering with anatase crystal formation[12]. In preparation for all experiments, unless otherwise stated,

samples were cleaned in chloroform, rinsed in de-ionised water and dried with a clean compressed air stream, before being stored in a sealable box until required for use.

2.1.3. P25 films

Thick, ~0.9 μm, Degussa P25 powder films were produced by dip-coating a 1 cm × 2.5 cm section of microscope slide in a 5 wt% P25 in water solution (Figure 2-4). Coating was followed by drying at 70°C and rinsing with deionised water to remove any loose powder, before air-drying in a compressed air-stream. Three repetitions of this process produced a thick (~0.9 μm) film on both sides; the reverse was cleaned of P25 by rubbing with a damp cloth before use. P25 layers deposited in this manner were loose and easily removed by rubbing, and suffered from poor uniformity. However a specific surface area of 55 m^2 g^{-1} of P25 gave the films high photocatalytic activity. P25 consists of a mixture of titania crystal phases, featuring ca. 70% anatase titania to 30% rutile[13].

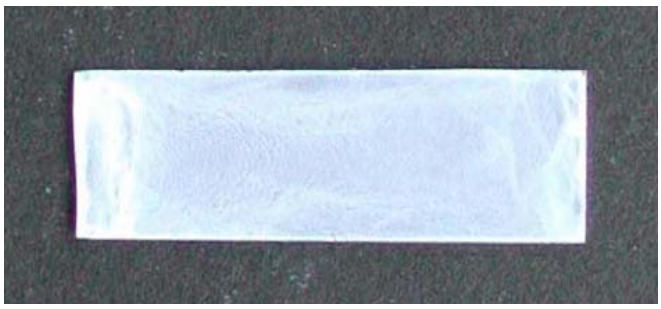

Figure 2-4 thick film of Degussa P25 deposited by repeated dip-coating in 5% aqueous slurry

2.1.4. Platinisation of paste films and P25

Titania films were cast by the doctor-blade method as described above, with the films platinised by irradiation with UVA in 10 mL of a solution containing 10^{-3} M

chloroplatinic acid in a 75%-25% methanol-water mixture. An identical solution was used for the platinisation of P25 (Figure 2-5) for use in the creation of photocatalytic polymer films. In this case 10 g of P25 was added to 500 mL of platinising solution before irradiation with two 6 × 8W BLB hemispheres with stirring. During the process darkening of the solution from white to grey indicates the reduction of platinum from Pt^{II} to Pt^{0}. After three minutes of irradiation the powder was filtered, thoroughly rinsed with deionised water and dried at 105°C, the final grey powder is also shown in Figure 2-5 beside an example of unmodified P25.

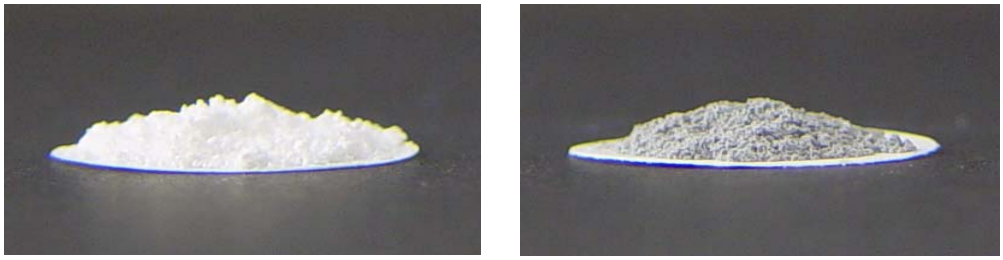

Figure 2-5 SPC platinisation of P25 using chloroplatinic acid (10^{-3} M)/methanol/water; P25 powder before (left) and after (right) platinisation, rinsing and drying

2.1.5. Synthesis of Photocatalytic polymer films

Polymer – photocatalyst films were made by addition of P25 or Pt-P25 to a polymer solution. Extensive stirring and sonication was required to fully disperse the particles in most cases. Ethyl cellulose-P25 thin films were fabricated by dissolving 10% (w/v) EC in 4:1 (v/v) toluene: ethanol mixture, before adding either P25 or P25-Pt. To create the films 10 g of polymer solution was mixed with 1g of powdered photocatalyst. Films were cast by spin-coating at 2000 rpm, resulting in thin films, of thickness ~20 μm, which when removed from the glass backing, were flexible but inelastic.

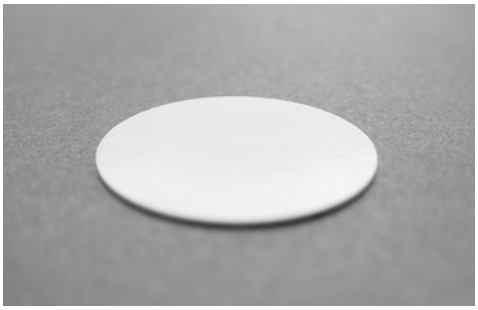

Figure 2-6 PTFE-P25 mixture pressed into 25 mm × 0.2 mm photocatalytic polymer film

---

Poly(tetrafluoroethylene-co-vinylidene fluoride-co-propylene) [P(TFE-VE-PE)] films were made using the same recipe as EC composites, but with the polymer dissolved in acetone. These films were spin-coated at 1000 rpm, producing thin, flexible films – which were 'rubbery' and more elastic than the EC composites – of ~15 μm thickness. Viton F (Terpolymer of vinylidene fluoride, hexafluoropropylene and tertrafluoroethylene) films used the same recipe as P(TFE-VE-PE) films, but were cast at 500 rpm, giving ~25 μm films which were flexible and rubbery, though it was not possible to remove the films from their backing without tearing.

Figure 2-7 0 to 15 T manual press (left) and Specac® IR die (right)

PTFE films were made by pressing disks of PTFE powder (Aldrich, 1 micron particle size) mixed with P25, in the ratio 95:5, using a 25 mm Specac® die and 0-15 T IR press, both shown in Figure 2-7. To create the films 300 mg of mixture was pressed to 5 MT for 10 minutes before rinsing in ethanol and air drying. Attempts to heat-treat the films for the creation of flexible disks[14] were unsuccessful. As a result as-pressed disks were brittle, but sufficiently robust for handling and re-use. 100% PTFE disks displayed good IR transmission ($\%T_{IR}$) but, with increasing P25 content $\%T_{IR}$ was seen to fall, and the brittle nature of the films increase. $\%T_{IR}$ was also seen to be affected by the thickness of the films, determined by mass of powder used, though very thin films were exceptionally fragile and unsuitable for use. Pressing 300 mg of 95:5 PTFE:P25 to 5T resulted in 0.2 mm disks (Figure 2-6) and provided the best trade-off between $\%T_{IR}$ and film integrity. Although the IR absorbance spectra were still relatively 'noisy', they were nonetheless suitable for observation of polymer degradation by monitoring transmission or absorbance.

2.2. Sources of Irradiation and measurement of Intensity

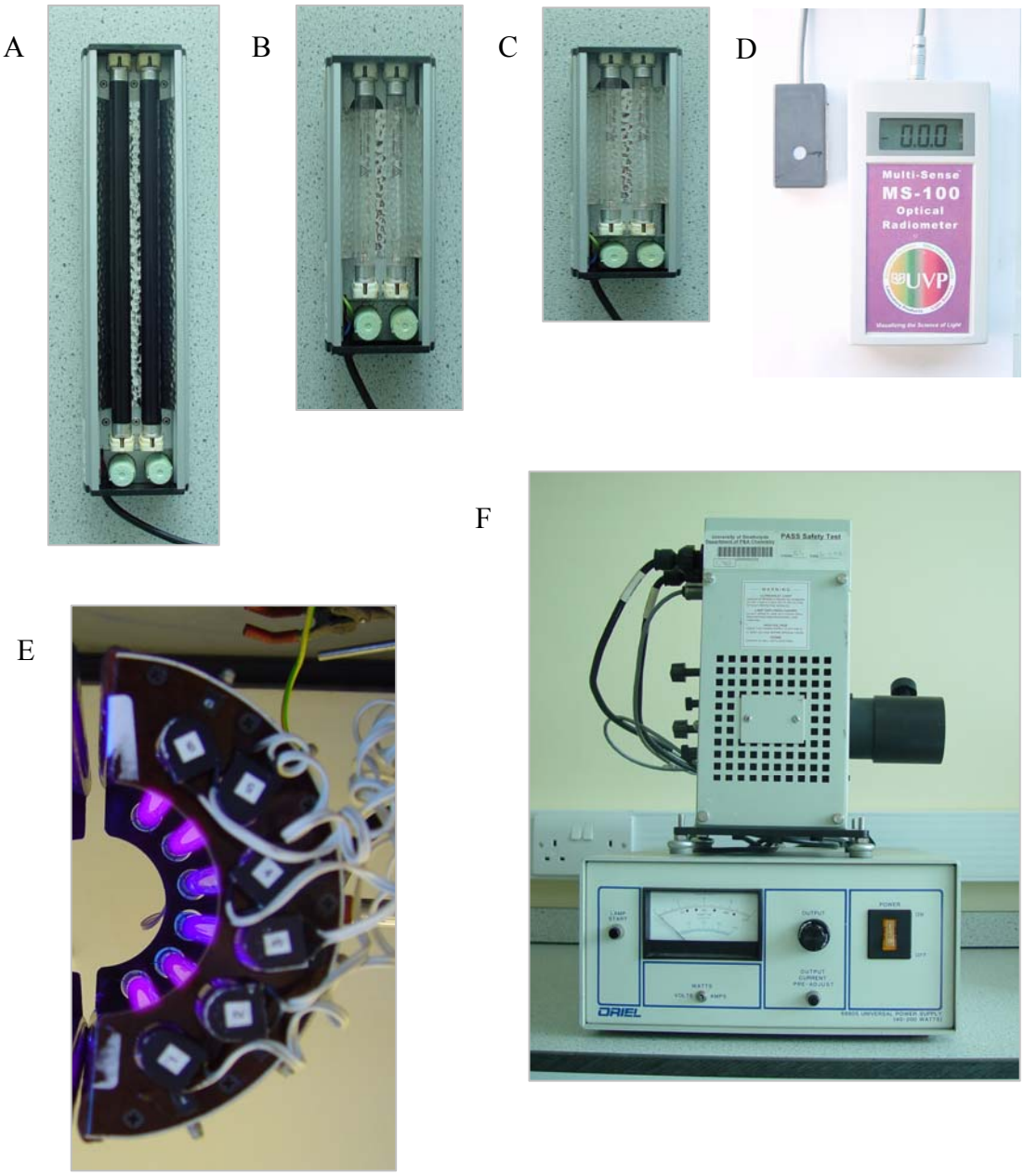

Figure 2-8 Apparatus for UV irradiation; A – 8W (with 2 × UVA); B – 6W (with 2 × UVC); C – 4W (with 2 ×UVC); A, B and C supplied by Vilber Lourmat; D – PVP UV meter with detector; E – 6 × 8W (Lidam Scientific, with UVA bulbs); F – Xenon-Arc lamp (Oriel)

Throughout this work UV irradiation was carried out with one of three forms of UV source: hand-held two-tube sources with 2×8W (Figure 2-8A), 2×6W (Figure 2-8B), or 2×4W (Figure 2-8: C) bulbs fitted; bench-top six-tube hemicylindrical sources which were fitted with 6×8W bulbs (Figure 2-8E); or a Xe-arc solar simulator (Figure 2-8F), operating at 0-150W. The two-tube and six-tube lamps were fitted with either UVA (BLB bulbs, 365 ± 20 nm) or UVC (mercury discharge bulbs, 254 nm) bulbs, the irradiation source and typical intensity value are quoted for each experiment, or at the beginning of the relevant section. Intensities were measured using a PVP ultraviolet radiation detector, supplied with both UVA and UVC attachments (Figure 2-8D). A characteristic spectrum of the output of a UVA lamp is shown in Figure 1.8, alongside the characteristic absorbance spectra of four substrates used in this work. The output of a germicidal UVC lamp is a single wavelength emission spectrum of mercury, i.e. solely 254nm in the UV region.

2.3. Spectrophotometric Techniques

2.3.1 Ultraviolet-Visible

2.3.1.1. UV-Vis – Cary 50 and Helios-β spectrophotometers

Figure 2-9 10cm gas-tight quartz cell fitted with quartz windows for UV-Vis analysis of gases

Analysis utilising the ultraviolet to visible region (UV-Vis) of the electromagnetic spectrum was carried out using the Varian Cary 50 and Thermo-Spectronic Helio-β single beam spectrophotometers.

2.3.1.2. UV-Vis absorption measurements for quantitative analysis of gas species

In order to determine the concentration of ozone present in the outlet stream of the Dryden Aqua corona-discharge ozone generator when working at full power, the stream was connected to one of the inlets of a 10 cm quartz cell (Figure 2-9) fitted with demountable quartz windows to allow UV-Vis transmission. The ozone/oxygen gas stream was then flowed through for five minutes before stopping the gas-flow and closing the inlet/outlet taps of the cell. The cell was then placed into the Cary 50 spectrophotometer and a scan taken from 200 nm to 400 nm, the measured absorbance was then used to calculate the concentration (in ppm) of ozone present using a value of 1.3×10^{-4} ppm^{-1} cm^{-1} for molar absorptivity[15]. The UV-Vis absorption spectrum of sulfur dioxide was also determined using the same technique.

2.3.2. Fourier transform infrared analysis

2.3.2.1. Spectrum One FTIR Spectrometer

The Perkin-Elmer Spectrum One Fourier transform infrared (FTIR) spectrometer was used for all infrared analysis.

2.3.2.2. FTIR monitoring of gaseous species

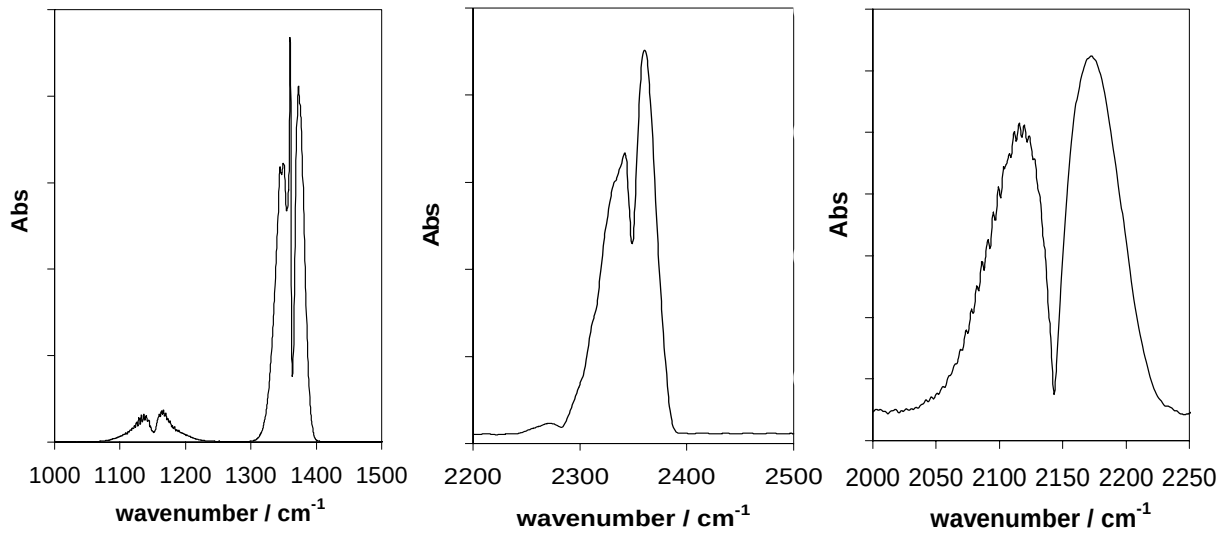

Figure 2-10 characteristic FTIR absorbance spectra of (from left) gaseous SO_2, CO_2 and CO measured using a 5 cm gas cell and Perkin-Elmer Spectrum One spectrometer

---

10 cm glass or quartz IR cells, fitted with removable CaF_2 faces and gas purge inlet and outlet taps, were employed to house both soot and sulfur coated photocatalyst films for analysis of oxidation products. The level of gas species present was determined by injecting known volumes of CO, CO_2 (both from cylinders, supplied by BOC) or SO_2 (produced in the laboratory, section 2.4) into the cell in order to create calibration graphs. The main peaks of interest for each species are shown in Figure 2-10. Major peaks of interest for CO_2 were found to occur from 2250 to 2400 cm^{-1}; while SO_2 comprised very strong bands at 1151 and 1362 cm^{-1} and a weaker one at 2499 cm^{-1},[16] with the peak at 1310 to 1400 cm^{-1} monitored. For investigations surrounding the oxidation of carbon monoxide, 0.1 mL portions were injected into the cell and the peak at 2000 to 2250 cm^{-1} was monitored, Figure 2-10.

2.3.2.4. FTIR monitoring of stearic acid layers

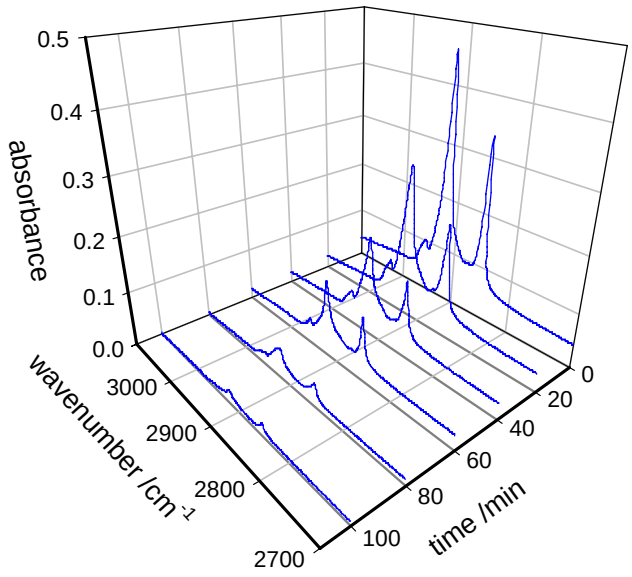

Figure 2-11 graph of FTIR absorbance of stearic acid peak decreasing with irradiation time

---

In work in which an additional layer of stearic acid (SA, i.e. $CH_3(CH_2)_{16}CO_2H$) was coated onto a sol-gel film, deposition was achieved by spin coating 3 droplets of a 2 g of SA L^{-1} in chloroform solution at 135 rpm for 10 s, which gave very thin layers of SA, typically comprising 1.2×10^{16} molecules cm^{-2}.[17] Monitoring of the SA destruction was achieved by FTIR (Perkin-Elmer Spectrum One) to measure the peak absorbance area in the region 2700-3000 cm^{-1} as a function of irradiation time, which provided a measure of the amount of SA remaining on the substrate under test, see Figure 2-11. The IR spectrum of stearic acid shows peaks of interest at: 2849.01 cm^{-1} – symmetric C–H stretching of CH_2 group; 2916.67 cm^{-1} – asymmetric C–H stretching of CH_2 group; 2953.54 cm^{-1} – asymmetric in plane C–H stretching of CH_3 group.

2.4 Laboratory Production of Sulfur Dioxide

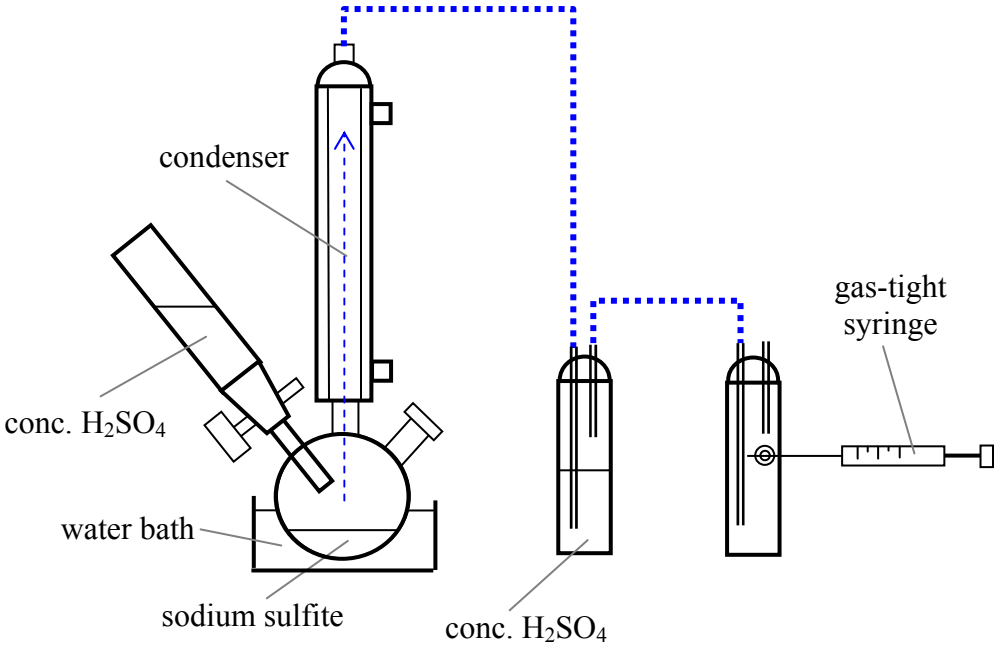

Figure 2-12 Apparatus for laboratory production of SO_2

Sulfur dioxide was produced in the laboratory by the addition of concentrated sulfuric acid (~18 M, Fluka) to powdered sodium sulfite (Aldrich), the sulfur dioxide produced passed through a condenser to removes most of the water vapour, through a drying agent (concentrated sulfuric acid) and then into a Dreschel bottle with a septum (Figure 2-12). From this point the gas was extracted using a gas-tight syringe.

2.5 Assessment of contact angle

There are two common methodologies employed for monitoring hydrophilic changes on titania substrates, and both involve capture of images of water droplets and measurement of its contact angle (*CA*) during irradiation. In the first, more common, methodology, after the measurement of the *CA*, the droplet is removed before irradiation is continued

(*repeated deposition* technique). In the second method, the same droplet is in place throughout the whole irradiation, and the series of images can be used as a movie to examine the changes during illumination (*in-situ* contact angle monitoring). However, in order to avoid evaporation problems in the latter method, the irradiation is performed in a humid (100% RH) atmosphere. Further details concerning both methods are given below.

2.5.1. *Repeated deposition* contact angle assessment

In this method, the substrate under test was placed onto the stage of the FTA-100 contact angle apparatus (Camtel, Figure 2-13). Using the computer interface and live CCTV feed, the picture was focused and a water droplet deposited onto the surface. In all experiments, the needle size used was a 30 gauge needle with a 90° bevel tip (Kahnetics) attached to a 500 μL Gastight® syringe (Hamilton), consistently delivering water droplets of ~5 μL which detach from the syringe tip under their own weight. The computer interface was then used to take a 'snapshot' of the droplet resting on the surface, and from this image the contact angle could be calculated using the associated software package. This involved marking the left and right edges of the droplet as well as the peak height, allowing the software package to calculate the angle of contact (θ). Before *CA* analysis the substrates were cleared of any dust and debris by blowing with compressed air from a cylinder, this was repeated after analysis in order to remove the water droplet. Doubly-deionised water was used for all depositions unless otherwise stated. Following measurement and removal of the droplet the substrate was then irradiated and the process repeated. The product of this work was a plot of *CA* versus irradiation time, the profile of which comprised of a series of discrete points, at typically 5-10 min intervals.

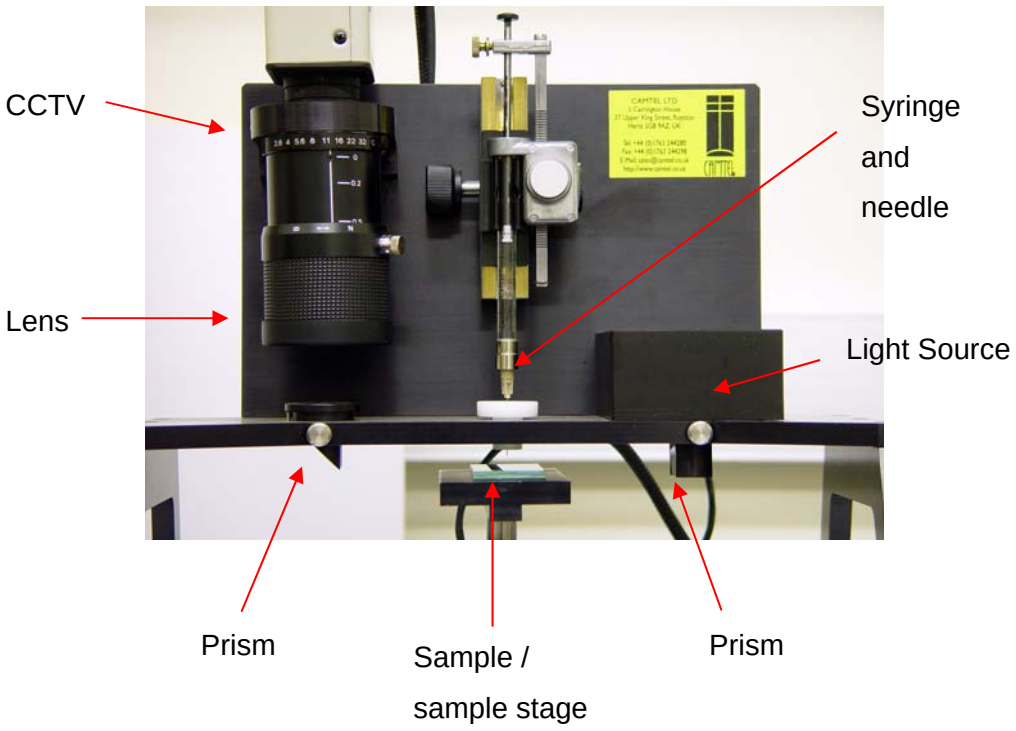

Figure 2-13 FTA-100 contact angle apparatus set up for 'repeated deposition' *CA* analysis

---

2.5.2. *In-situ* contact angle measurement during irradiation

The *in-situ* contact angle measurement method utilised an environmental chamber to contain the substrate under test and maintain it under a humid atmosphere (Figure 2-14). The chamber was made of brass, fitted with two glass side-windows to allow CCTV observation in the plane of the droplet for contact angle analysis. A circular quartz window on top permitted UVC or UVA irradiation of the TiO_2 films under test, this window also featured a rubber septum through which a syringe needle could pass for droplet deposition. The environmental chamber enabled flushing by oxygen, nitrogen or air gas streams saturated with water vapour; a typical value for flowrate of ~300 mL min^{-1} was used while flushing the cell and reduced to 100 mL min^{-1} during experiments to limit droplet evaporation. In some experiments an ozone generator (OZ500, Dryden

Aqua) was also connected in series to flush the chamber with approximately 1700 ppm O_3 in oxygen. Water saturation of the gas streams were affected by flowing through a Dreschel bottle containing either pure water, or concentrated sulfuric acid for dry gas streams.

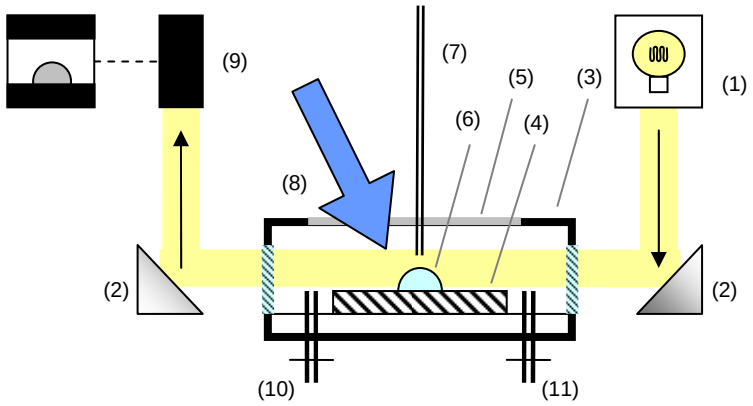

Figure 2-14 FTA-100 contact angle setup modified to include an air-tight chamber for *in-situ CA* analysis, numbered items as follows: 1 – white light source, 2 – prism, 3 – gas-tight housing, 4 – sample, 5 – quartz window, 6 – water droplet, 7 – Syringe needle, 8 – UV source, 9 – CCTV camera, computer interface, 10 & 11 – gas inlet/outlet

2.6 References

1 A. Mills, N. Elliott, G. Hill, D. Fallis, J. D. Durrant, and R. L. Willis, *Photochem. Photobiol. Sci.* **2**, 591 (2003).

2 M. Langlet, S. Permpoon, D. Riassetto, G. Berthome, E. Pernot, and J. C. Joud, *J. Photochem. Photobiol. A: Chem* **181**, 203 (2006).

3 G. Goutailler, C. Guillard, S. Daniele, and L. G. Hubert-Pfalzgraf, *J. Mater. Chem.* **13**, 342 (2003).

4 M. Wu, G. Lin, D. Chen, G. Wang, D. He, S. Feng, and R. Xu, *Chem. Mater.* **14**, 1974 (2002).

5 H.-J. Nam, T. Amemiya, M. Murabayashi, and K. Itoh, *J. Phys. Chem. B* **108**, 8254 (2004).

6 J. Livage, and C. Sanchez, *J. Non-Cryst. Solids* **145**, 11-19 (1992).

7 S. Doeuff, M. Henry, C. Sanchez, and J. Livage, *Journal of Non-Crystalline Solids* **89**, 206-216 (1987).

8 A. Mills, G. Hill, S. Bhopal, I. P. Parkin, and S. A. O'Neill, *J. Photochem. Photobiol. A: Chem* **160**, 185 (2003).

9 A. Mills, G. Hill, M. Crow, and S. Hodgen, *J. App. Electrochem.* **35**, 641-653 (2005).

10 A. Mills, A. Lepre, N. Elliott, S. Bhopal, I. P. Parkin, and S. A. O'Neill, *J. Photochem. Photobiol. A: Chem* **160**, 213 (2003).

11 D. W. Sheel, R. J. McGurdy, and S. J. Hurst, (1998).

12 Y. Paz, and A. Heller, *J. Mater. Res.* **12**, (10), 2759 (1997).

13 A. Mills, and S. Le Hunte, *J. Photochem. Photobiol. A: Chem* **108**, 1 (1997).

14 A. R. Lakshmanan, K. L. Popli, and R. C. Bhatt, *Phys. Med. Biol.* **24**, (5), 999 (1979).

15 A. Mills, S.-K. Lee, and A. Lepre, *J. Photochem. Photobiol. A: Chem* **155**, 199 (2003).

16 G. Herzberg, *Molecular Spectra and Molecular Structure*. Second ed.; Krieger Publishing: 1991; p 636.

17 A. Mills, and J. Wang, *J. Photochem. Photobiol. A: Chem* **182**, 181 (2006).

Chapter 3 Photocatalytic oxidation of solid layers of inorganic contaminants on titania

3.1 Introduction

Figure 3-1Airborne soot particles discolour stonework as well as causing health problems[1]

The 'green' applications of titania-based semiconductor photocatalysis have evolved from solar energy conversion[2, 3] and water purification[4, 5], to the development of 'smart' surfaces with the potential for anti-fouling[6, 7], self-cleaning[8-11] and ambient air purification[12-15]. The potential self-cleaning applications of titania-coated substrates began with observation of organic film destruction[16, 17] and continued apace with the recognition of the photoinduced superhydrophilic properties of TiO_2[6, 7]. Utilisation of these characteristics are of great interest for, amongst other applications, glazing[18] and construction[15, 19]. Thin nanocrystalline titania coatings on glass produce anti-fogging and anti-fouling surfaces, without impairing the optical clarity of the glazing[20]. The incorporation of titania into cementitous materials for building construction can afford self-cleaning properties, whereby dirt and deposits are loosened by photocatalytic

oxidation and washed away by rainwater, enabling exterior building surfaces to stay clean of airborne contaminants[19]. Other areas of application for this technology include coating titania onto lamp housings for use in subterranean traffic tunnels, where deposition of exhaust contaminants can block light emissions[9]. The use of 'smart' construction materials is very much on the agenda of politicians internationally, with $2.27 billion earmarked for projects by the European Union in 2004[21].

Airborne solid contaminants, also referred to as particulate matter (PM), include soot[22] (the product of vehicular internal combustion, power plants, heavy and light industry) and less commonly, sulfur, produced as a by-product of several industrial processes including sour natural gas processing[23, 24]. Fine particles ($PM_{2.5}$), those less than 2.5 μm, are recognised as causing and exacerbating serious health problems such as bronchitis and asthma[25-27], as well as reducing visibility and contributing towards urban 'smog'[26]. Deposition of PM on surfaces leads to discolouration of sandstone and other building materials (Figure 3-1) with the cleaning of these layers by mechanical or chemical processes being potentially damaging to the surfaces, increasing the potential for further staining[1]. For these reasons photocatalyst coatings, and/or the incorporation of photocatalytically active compounds into building materials, impart very desirable properties which can play a key role in environmental remediation.

The removal of soot layers on titania photocatalyst films has been illustrated previously by this group[28] and others[29]. Lee and Choi's[29] initial work found that irradiation through the soot layer reduced the efficiency of soot oxidation in contrast to irradiation through the reverse of the slide, most probably as a result of UV-scattering/blocking by the soot layer. This is highlighted in Figure 3-2A as soot loss occurs at a reduced rate with irradiation through the pollutant layer. Direct photolysis of soot with UV irradiation was not observed, and it was suggested that migration of the oxidative species throughout the diffuse soot layer was a major factor in the complete removal of soot. Irradiation in a non-oxygen atmosphere (helium) showed that initially CO_2 was produced, until – it was proposed – any oxygen adsorbed or trapped within the soot was consumed (Figure

3-2B). Thereafter a steady state was reached. Retardation of CO_2 production rate with time was ascribed to consumption of adsorbed/localised water vapour, the relative humidity (%RH) was observed to be influential on rate, implicating hydroxyl radicals as the predominant oxidative species. Direct soot oxidation was further investigated by gravimetric monitoring of mass loss and oxidation products by GC[29].

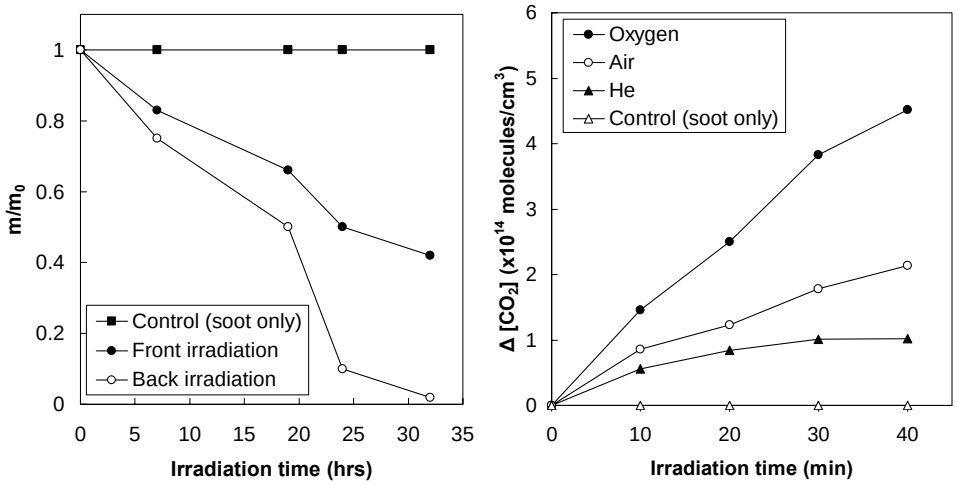

Figure 3-2 A: decrease of soot mass on TiO_2 film with UV irradiation (left) and B: CO_2 evolution from PCO of soot on TiO_2 under different atmospheres[29]

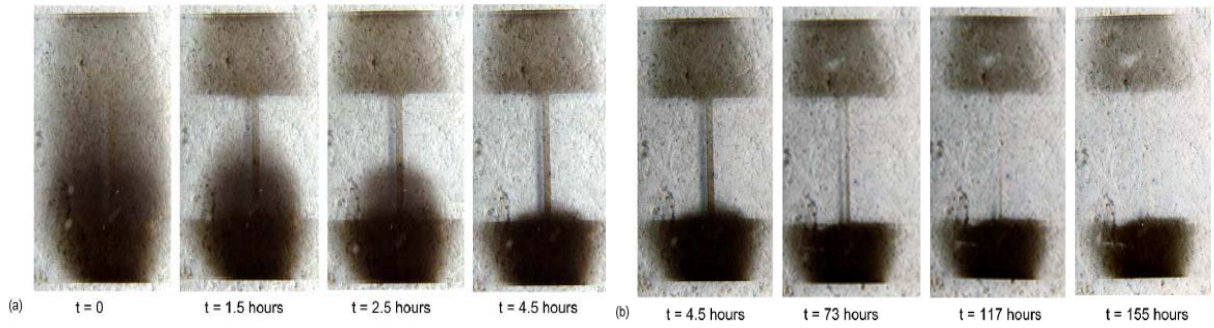

Figure 3-3 (a) *direct* PCO of soot layer on TiO_2 paste film, and (b) *lateral* removal of soot by PCO from 'gapped' portion of TiO_2 film[28]

Lateral (Figure 3-3b) and *remote* (Figure 3-4) oxidation of soot layers have been observed by leaving gaps between the photocatalytic film and the soot layer during irradiation, with *remote* PCO investigated using the apparatus described in Figure 3-5. Figure 3-3b demonstrates the *lateral* migration of gaseous oxidative species from a sol-gel paste photocatalyst; the strip of soot in the centre was deposited onto a plain glass portion of the slide, but with irradiation the soot layer was still observed to be removed by the adjacent film.

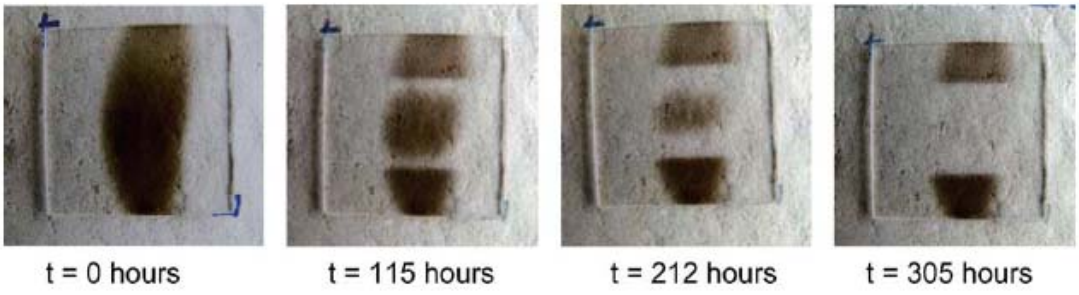

Figure 3-4 remote PCO of a soot layer separated from a TiO_2 paste film by a 175μm gap using the arrangement described in Figure 3-5[28]

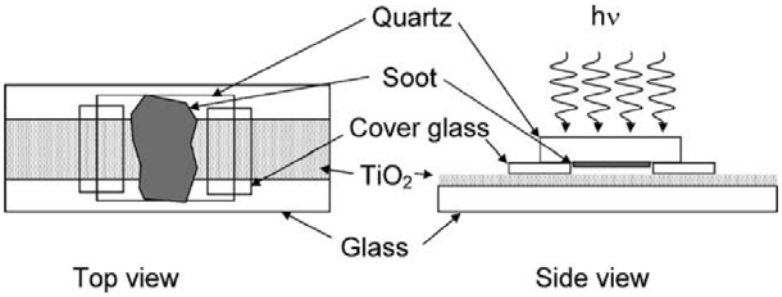

Figure 3-5 schematic of top and side-views of paste TiO_2 film and soot-covered quartz slide, separated by 175 μm glass spacers, used to demonstrate the remote PCO of soot[28]

The *remote* and *lateral* effects observed are of great interest to researchers as they demonstrate that oxidative species produced by photoinduced process on titania can

diffuse from the surface and migrate across gaps, with distances of up to 2.2 mm reported[30, 31], and potentially *through* porous or diffuse materials. Organic species[30, 32, 33], dyes[31], and soot layers[28, 29] have all been observed to be destroyed (or bleached) by remote (i.e. gas-phase) oxidation products of the UV-irradiation of titanium dioxide powders or films. A general rule determined during the investigation of PCO of soot is that, concerning the kinetics of photocatalytic processes, *direct* » *lateral* » *remote*[28].

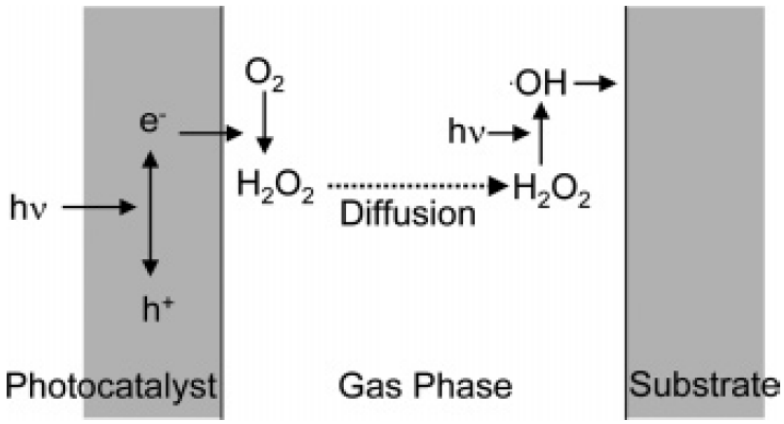

Figure 3-6 proposed mechanism of remote oxidation by a two photon process[33]

The most popular interpretation of remote photocatalysis is that the migratory oxidant species are hydroxyl radicals[29] which either directly oxidise the remote pollutant layer[34], or form hydrogen peroxide (H_2O_2) which traverses the gap before photo-cleavage forms further $OH^{\bullet}$ [30, 31], the mechanism is summarised in Figure 3-6. This is a two-photon process[33] – *(1)* photogeneration of electron-hole pair and *(2)* photo-cleavage of H_2O_2 to form hydroxyl radicals – which goes a way to explain the long periods of irradiation required, e.g.; 60 h for thin methylene blue layer[31]; and 305 h for a soot layer <0.2mm away from a paste films (compared to 4.5 h for direct PCO)[28]. The bulk of published work features UVC Hg–Xe radiation sources (which emit wavelengths predominantly <300 nm) rather than UVA blacklight-blue (BLB) sources (λ_{max} = 365 ± 20 nm). The

experience of this group is that UVA sources initiate little or no remote PCO effect, an observation which gains significance when the UV-Vis absorbance spectrum of hydrogen peroxide is considered: H_2O_2 absorbs approximately 1000 times more strongly at 250 nm than 350 nm[35].

Hydrogen peroxide production on, or at, the surface of TiO_2 occurs via superoxide ($O_2^{-\cdot}$) production and its subsequent protonation and reduction, via the following mechanism[36, 37]:

$$TiO_2 + h\nu \rightarrow e^- + h^+ \quad (3\text{-}1)$$

$$e^- + O_2 \rightarrow O_2^{-\cdot} \quad (3\text{-}2)$$

$$h^+ + H_2O \rightarrow OH^\cdot + H^+ \quad (3\text{-}3)$$

$$O_2^{-\cdot} + H^+ \leftrightarrow HO_2^\cdot \quad (3\text{-}4)$$

$$HO_2^\cdot + e^- + H^+ \rightarrow H_2O_2 \quad (3\text{-}5)$$

$$OH^\cdot + OH^\cdot \rightarrow H_2O_2 \quad (3\text{-}6)$$

An example of the analytical observation of photocatalytically-produced hydrogen peroxide is one which utilised a UV-irradiated flow-through cell packed with TiO_2-coated beads. The gas stream was flushed through a trapping solution and a colorimetric change was only observed if catalase (a H_2O_2 decomposition catalyst) was absent[38]. Further evidence has been presented which uses fluorescent dyes as molecular flags to the presence of H_2O_2[39, 40]. Laser-induced fluorescent spectroscopy has also been used to directly detect hydroxyl radicals, rather than H_2O_2, over TiO_2 powders[34], the researchers concluding that $OH^\cdot$ was not formed from superoxide reduction to hydrogen peroxide and photo-cleavage.

An interesting effect which has been observed is the UV-sensitised removal of octadecyltriethoxysilane (ODS) – its presence monitored by contact angle measurement – using H_2O_2-saturated humid air[33]. This is of interest as it is presented as proof that the second of the two-photon effects (photo-cleavage of H_2O_2) forms species with sufficient

oxidising potential to remove aliphatic carbon chains. The conditions under which this experiment was carried out are worth noting for later reference; the 60% RH air flow passes through a H_2O_2 solution, into the empty glass cell (heated to ~55°C) and through Teflon tubing to the ODC coated substrate, which was irradiated with λ <300 nm photons of 100 mW cm^{-2} intensity.

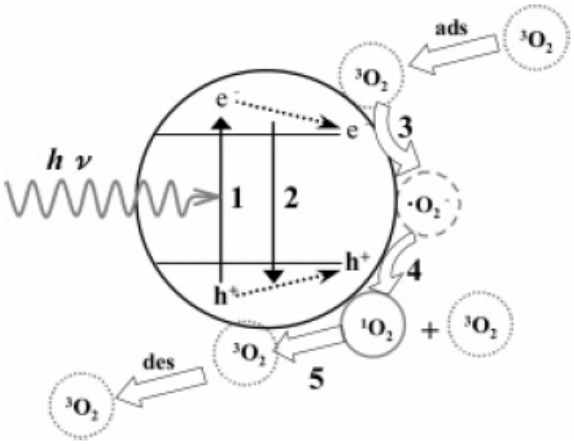

Figure 3-7 photoinduced processes on TiO_2 involving molecular oxygen; 1 – electron/hole pair production; 2 – e^-/h^+ recombination; 3 – electron transfer and superoxide formation; 4 – oxidation of superoxide and formation of singlet oxygen; 5 – quenching of $^1O_2$ at surface to reform molecular oxygen[41]

The same research group state, alongside their proposed mechanism for remote PCO, that "…*there is another possibility that ozone is the diffusing species*…" although they do, rightly, further explain that ozone production by photocatalysis has not been reported[33]. In fact the TiO_2-mediated destruction of ozone has been investigated by a number of groups, including this one[13, 42]. This would appear to rule out the possibility that ozone is a significant gas-phase product of PCO, although ozone does absorb strongly at wavelengths <300 nm, becoming electronically excited and more highly reactive. Other oxidative species formed on the surface of illuminated TiO_2 include singlet oxygen ($^1O_2$)[43], which is formed directly or indirectly during electron transfer between the semiconductor and ground state oxygen ($^3O_2$)[41] (Figure 3-7). Lifetime

studies in air and in suspensions, using near-infrared (NIR) phosphorescence measurements, have been interpreted as to suggest that singlet oxygen remains at the surface of the semiconductor particles, rather than being released into air or the solution[43]. With this in mind it would appear that hydroxyl radicals (and hydrogen peroxide), or possibly ozone, are the likely airborne oxidative species formed by TiO_2 during illumination, with hydroxyl radicals appearing to be the most plausible.

$$C + O_2 \xrightarrow[h\nu \geq E_{bg}]{TiO_2} CO_2 \qquad (3\text{-}7)$$

Soot removal is believed to follow the scheme shown in Equation 3.7 with no incomplete oxidation products, such as carbon monoxide observed in the gas phase. This is important because contaminant soot removal would be unacceptable as a green process if environmentally damaging, or toxic, by-products were generated as a result.

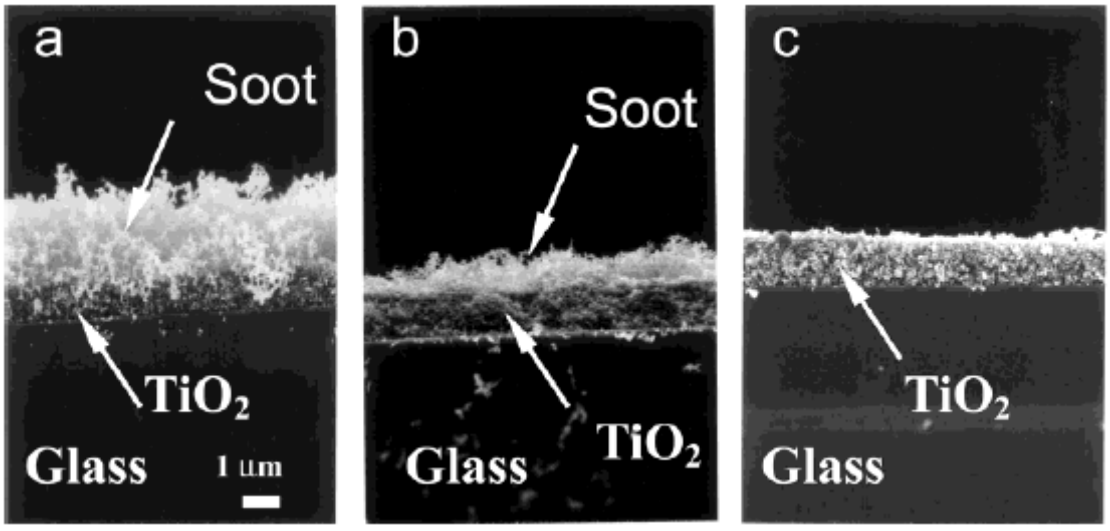

Figure 3-8 cross-sectional SEM observation of the PCO of a fibrous, wispy soot layer on a thin titania film during irradiation[29]

While not as atmospherically common as ultrafine carbon pollution, airborne particulate sulfur is a significant constituent of fly ash[22] and has been shown to be environmentally damaging[23, 24]. The photocatalytic oxidation of sulfur in aqueous systems has been observed to directly produce sulphuric acid, with hydrogen sulfide also produced[44, 45]; this work was carried out using powder dispersions in neutral, acidic and alkaline solutions using crystalline sulfur particles. There has been to date no investigation into the photocatalytic removal of solid sulfur layers, deposited onto photocatalysts. Some work has been carried out investigating S atom-containing organic species[46], with irreversible catalytic deactivation observed after photocatalysis using P25 titania. As the oxidation products of sulfur (SO_x) are in themselves far more environmentally damaging than elemental sulfur[22, 47], the degradation, or elimination of gaseous SO_x by photocatalysis is addressed in the next chapter (chapter 4).

In this work the sulfur and soot layers were directly monitored during irradiation using UV-Vis spectrophotometry and gravimetric analysis and oxidation products monitored by FTIR, or by trapping with subsequent determination for SO_2. The stoichiometry for each reaction was established and the formal quantum efficiencies estimated. A brief investigation into remote photocatalysis is also included, using soot as a model pollutant.

3.2 Experimental

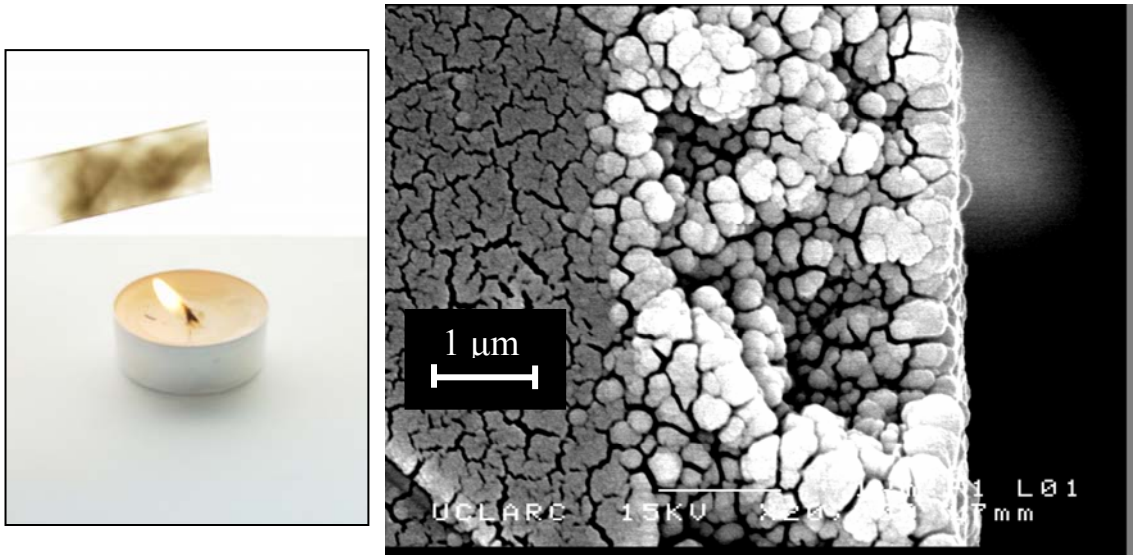

Figure 3-9 Deposition of soot from a candle flame (left); typical side-on SEM image of amorphous sulfur on titania; sulfur particles distinguishable as white spheroids in contrast to darker titania film (right)[48]

For this work the substrates used were sol-gel derived paste films, fabricated as described in section 2.1.1. Films were cast in 1 cm × 7.6 cm strips on glass microscope slides, before calcining to give ~4 µm anatase titania films. For preliminary bench top experiments with sulfur layers, 2cm × 2cm glass slides with 1.6 cm × 2 cm paste titania coatings were used. Also used were Degussa P25 powder films, produced by dip-coating a 1 cm × 2.5 cm section of microscope slide as described in section 2.1.3. Soot layers were deposited from the flames of 'tea-light' candles, simply by holding the titania films over the flame, as shown in Figure 3-9. A typical layer of soot was approximately 0.5 µm thick and consisted of thin fibrous 'wisps' of soot, in accordance with observations made by others[29], an example of which is depicted in Figure 3-8. The amorphous sulfur layers were deposited by dip-coating using a 4.0 mol dm^{-3} sulfur (100-mesh) in carbon disulfide solution. The initially colourless carbon disulfide solution acquired a yellow

hue with the addition of sulfur. Analysis of side-on SEM images, an example of which is shown in Figure 3-9, allowed estimation of the sulfur layer thickness. The layers were found to be ~2.8 μm thick and containing particles of typically ~260 nm, though ranging from 60 – 500 nm, in diameter. Sulfur on glass blanks were made by dip-coating a microscope slide 'roughened' by sand-blasting, in order to allow the sulfur to attach to the surface.

UV-Vis spectra for both soot and sulfur layers were taken using a single beam spectrophotometer (Cary 50), the titania film with the deposited pollutant layer was placed directly into the beam and absorbance measurements taken at five predetermined points along the slide. Gravimetric analysis used a balance (Mettler-Toledo) accurate to five figures (0.01 mg); the average of five measurements is again quoted. FTIR (Perkin Elmer Spectrum One spectrometer) absorbance spectra were recorded with the soot or sulfur coated titania slide contained within a 10 cm glass cell.

Investigation into the mechanism behind remote photocatalysis utilised a PTFE-bodied cell featuring gas input and outputs, the top of the cell was sealed with a brass plate containing a quartz window (76mm × 24 mm). A schematic of the cell is shown in Figure 3-5. Oxygen, containing either ozone (~1700 ppm) – produced by a corona-discharge ozone generator (Dryden Aqua), or hydrogen peroxide, from a Dreschel bottle containing 30 vol. H_2O_2 – was flowed through the cell (flowrate typically 200 mL min^{-1}) during irradiation with 2×8W UVC bulbs ($I_{UVC} \sim 7.0$ mW cm^{-2}). The presence of hydrogen peroxide was confirmed by subsequent bubbling through 0.1 M potassium iodide solution, which gave a 'positive' brown/orange colour change.

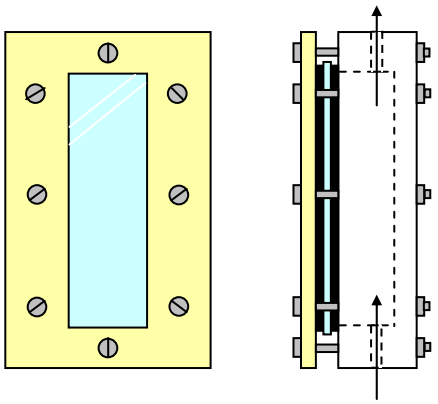

Figure 3-10 schematic showing top and side views of brass/PTFE cell used for investigation of remote photocatalysis, featuring a quartz window and gas inlet/outlet

---

Trapping of photocatalytically produced SO_2 and subsequent colourimetric determination of the produced complex was by the West-Gaeke method[49]. This utilises the reaction of sulfurous acid (aqueous sulfur dioxide) with formaldehyde and the dye ρ-rosaniline under acidic conditions (acidified ρ-rosaniline with sulfite is named 'Schiff's reagent' and is used for the determination of aldehydes), with the concentration of the coloured species generated proportional to the concentration of sulfurous acid[50].

The sulfur-coated titania film was housed in an IR cell, with oxygen flowed through the cell at ~100 cm^{-3} min^{-1}, a graphical scheme of the apparatus is shown in Figure 3-11. The gas stream was then scrubbed through 100 mL of 0.1 M sodium tetrachloromercurate and the concentration of SO_2-mercury complex colourimetrically determined from 1 mL portions removed at regular intervals. The colour development method was as follows: 1 mL of trapping solution mixed with 1 mL bleached ρ-rosaniline hydrochloride aqueous solution (0.04 wt% dye & 6 wt% conc. HCl), 1 mL formaldehyde solution (0.2 wt%) and 4 mL of 0.1 M fresh, unexposed TCM solution. Absorbance of a portion of this solution was measured using a 10 mm glass cell (Cary 50 spectrophotometer) and scanning from 300 nm to 800 nm; the absorbance at 560 nm is quoted.

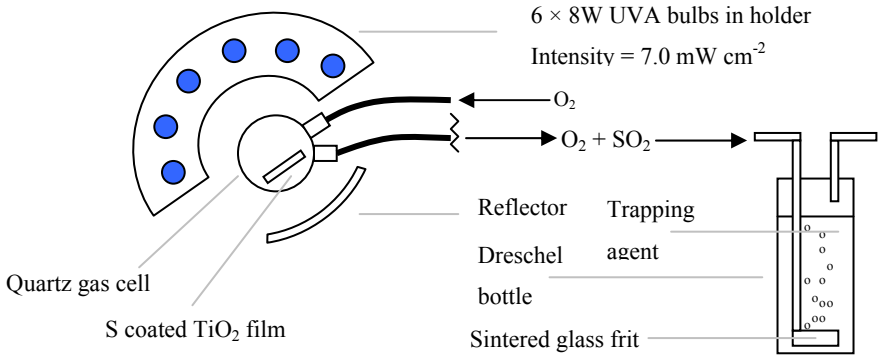

Figure 3-11 Apparatus for trapping of SO_2 produced by photocatalysis of sulfur deposited on sol-gel derived titania film

3.3 Direct and Remote Photocatalytic Oxidation of Soot on TiO_2[51]

By placing the soot-covered photocatalyst film directly into the beam of a UV-Vis spectrometer the absorbance readings allowed direct monitoring of the pollutant layer as it was oxidised with UV irradiation. Figure 3-12 shows visual evidence that during irradiation in a non-sealed system, with UVC (I_{UVC} = 5 mW cm^{-2}) in this case, a deposited layer of soot is completely removed from a titania paste film within 720 minutes. The pictures highlight that soot deposition by exposure to a candle flame gives uneven layers, and, as would be expected and the thicker areas took longer to oxidise.

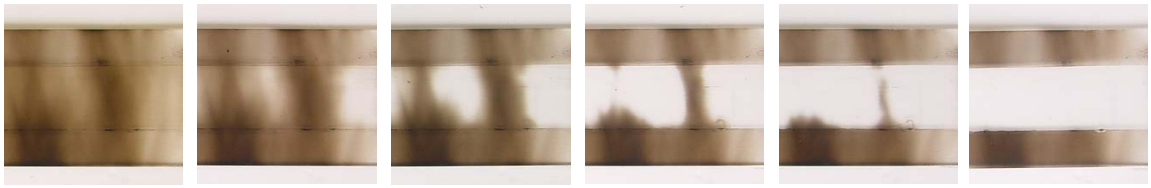

Figure 3-12 Soot layer oxidation by thick TiO_2 paste film, t = (from left) 0, 180, 360, 540, 630 and 720 min

Direct monitoring of the soot layer using a UV-Vis spectrophotometer was possible, with the amount of soot present seen to be directly proportional to the measured absorbance. As irradiation time progressed the spectra exhibited reduced absorbance (Figure 3-13). An arbitrary value of wavelength, in this case 600 nm, was chosen and plotted versus irradiation time, (Figure 3-13). Further evidence of this relationship was gleaned by accurately weighing the slides during irradiation. The kinetics of soot removal were observed to be approximately zero-order with respect to the level of soot when present in a continuous film across the slide. This is in accordance with kinetics observed for stearic acid layers[17, 52], and represents saturation kinetics, whereby all photocatalytic sites are occupied during the oxidation process.

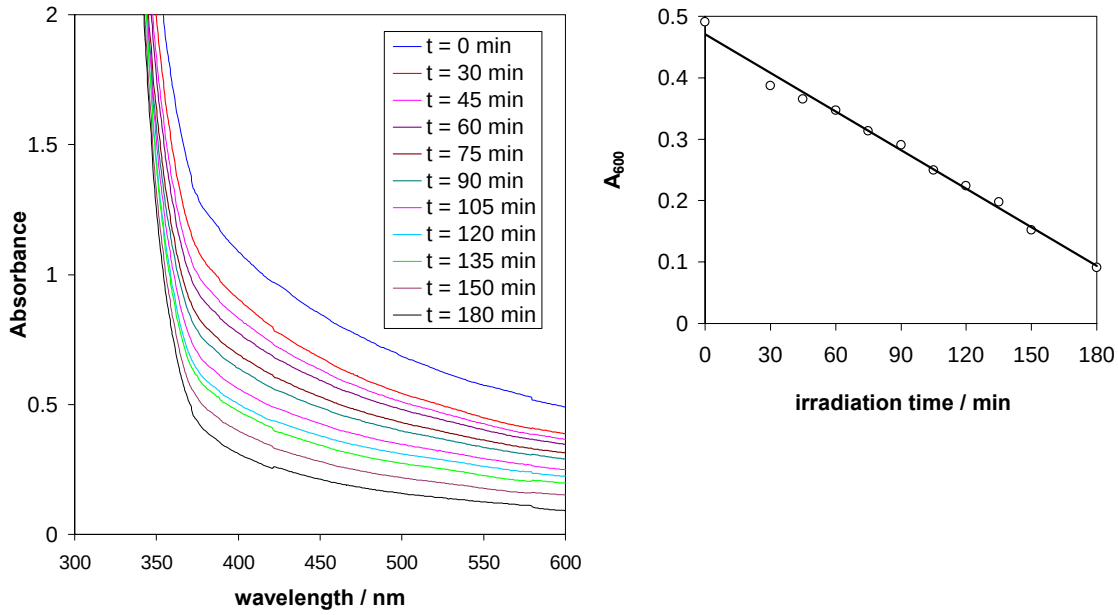

Figure 3-13 UV-Vis absorbance spectra of soot-covered titania paste film taken at intervals during irradiation and, right; $Abs_{600\ nm}$ versus irradiation time

---

In parallel with changes in absorbance, mass changes during irradiation were monitored (Figure 3-14) indicating that the changes in absorbance were directly proportional to changes in mass. The correlation for this plot, $R^2 = 0.9633$, reflects the poor uniformity

of the soot layers; Figure 3-14 plots the average absorbance across the slide versus the total mass of the slide. A method of coating the soot more uniformly, such as sputtering, may give better agreement between the absorbance and mass data to allow more detail on the kinetic factors influencing reaction 3-7.

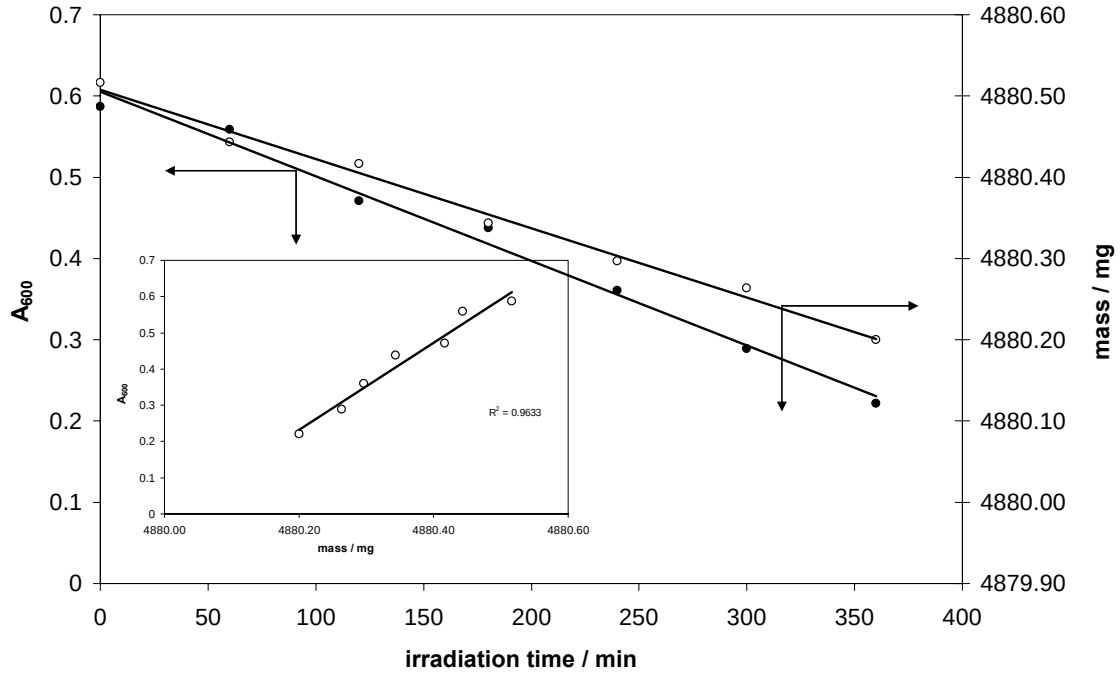

Figure 3-14 UV-Vis absorbance (open) and mass (closed) of a soot-covered titania paste film during UVC irradiation (I = 5 mW cm^{-2}) and, inset; Absorbance at 600 nm plotted against mass

In the aforementioned experiments the soot layers were seen to be completely removed by photocatalysis, and it was suggested that all mass due to soot is removed to the gas-phase as CO_2, i.e. that the reaction proceeds via reaction 3-7. To determine stoichiometry, irradiation of soot on P25 titania films was carried out within a sealed IR cell, shown in Figure 3-15. Throughout the irradiation time it was possible to monitor carbon dioxide, characterised by a large peak at 2400 – 2200 cm^{-1}, which was the only gas-phase product observed. Through calibration of the cell, by injecting known volumes of CO_2, the number of moles produced after 1100 h could be calculated (22.5 × 10^{-6} mol), this corresponded perfectly, giving a 100% yield, with the number of moles of

soot removed by photo-oxidation; determined by the measured mass loss of the film (0.27 mg).

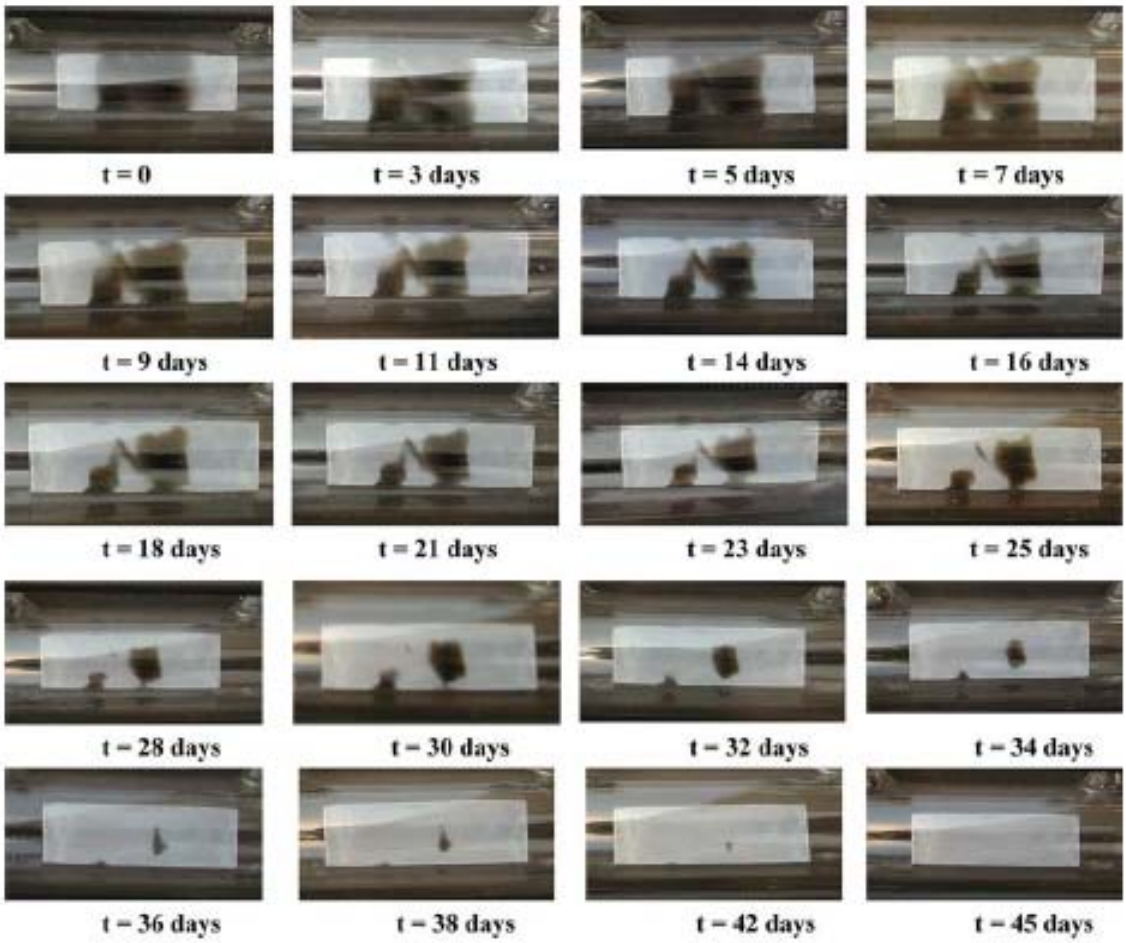

Figure 3-15 Soot layer destruction by photocatalysis on P25 titania film sealed within gas-tight glass IR cell (I_{UVA} = 4.28 mW cm^{-2}).

The plot depicted in Figure 3-16 allowed estimation of the initial rate (1.91×10^{-11} mol s^{-1}), from this it was possible to calculate, using the incident light intensity (1.04×10^{17} photons s^{-1}), that the formal quantum efficiency (FQE) for the process was 1.1×10^{-4} molecules $photon^{-1}$ (0.011% efficiency), suggesting an electron/photon FQE of 4.4×10^{-4}. This is much reduced from that observed for stearic acid layer removal[52], ca. 640 times lower. An explanation for this may be the fibrous nature of the soot layers, i.e. the

lack of intimate contact between titania and soot, this reflects the findings of Lee and Choi[29], who suggested that the diffuse, fibrous soot layer experienced photocatalysis by desorbed oxidative species, such as hydroxyl radicals, this would explain the lower quantum efficiency.

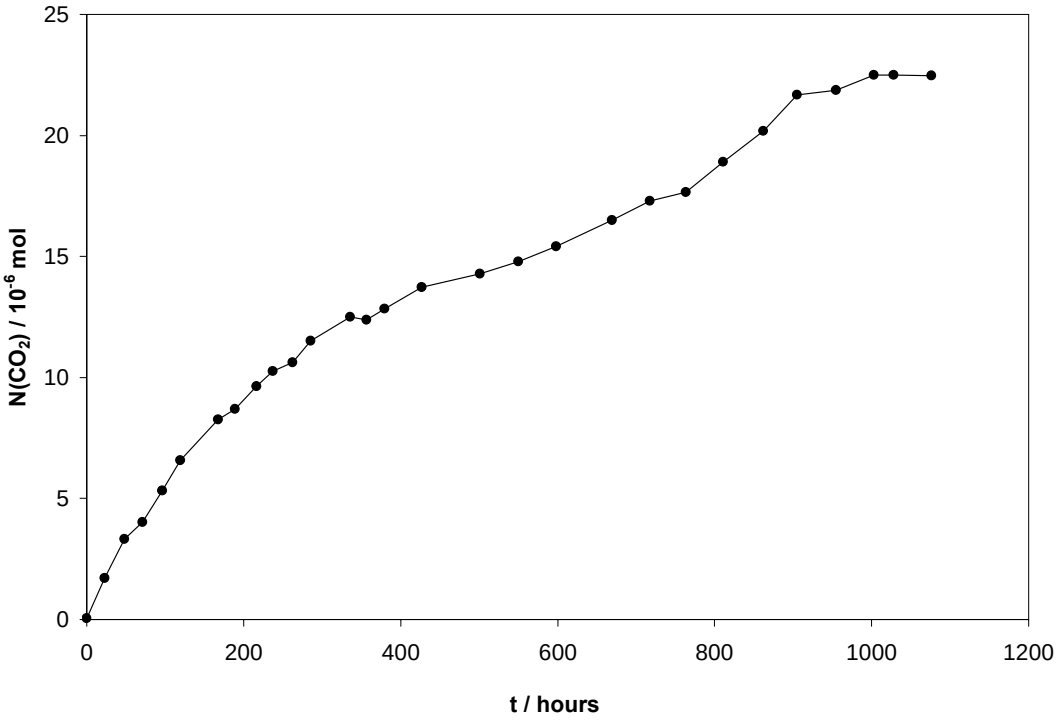

Figure 3-16 Number of moles of CO_2 generated by PCO versus UVA irradiation time, graph relates to data obtained during experiment illustrated in Figure 3-15

While the above experiments were designed to focus on the *direct* effects of photocatalysis on soot layers, further experiments were carried out to investigate the *remote* photocatalysis phenomenon. Figure 3-17 depicts an example of remote photocatalysis, whereby a titania paste star was placed in a similar arrangement to that described in Figure 3-5, with the soot layer 185 μm from the star. This is an example of the potential for the development of photoinduced etching processes via remote photocatalysis. One suggested mechanism for remote photocatalysis, a representation of which is shown in Figure 3-6, features the two-photon process of hydroxyl radical

formation, hydrogen peroxide formation, and hydrogen peroxide cleavage. Kubo and Tatsuma[33] produced evidence for this mechanism by observing octadecyltriethoxysilane (ODS) degradation upon UV irradiation of a H_2O_2-containing air stream.

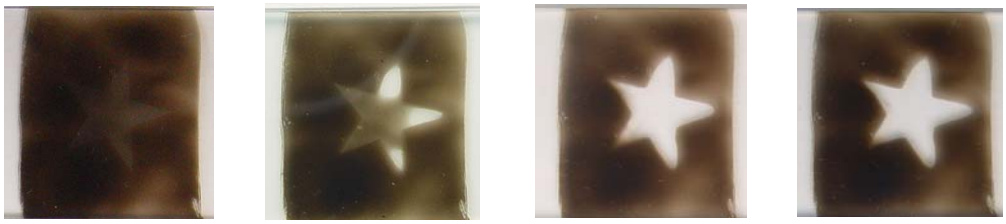

Figure 3-17 'remote' oxidation of soot by a star-shaped paste film using a set-up similar to that described in Figure 3-5 (gap ~2 mm), irradiation was by UVC (~5 mW cm^{-2}) from reverse of paste film. Pictures taken after (left to right) 0, 100, 250, 300 h

Using a similar scheme, this time with soot as the model contaminant, a H_2O_2-containing oxygen stream was flowed into a PTFE and brass cell, the brass side of which featured a quartz window with the inside coated with soot (Figure 3-10). It was expected that irradiation with UVC (I_{UVC} ~5 mW cm^{-2}) through the window would cause rapid removal of the soot. In fact, as shown in Figure 3-18 A&B, after 72 hours of irradiation there was no visible effect on the soot deposit. A possible reason behind this may be that hydroxyl radicals are not sufficiently oxidising to remove soot deposits. This experiment not only casts doubt on the two photon mechanism proposed by Kubo and Tatsuma[33], but also on the identification of hydroxyl radicals as the probable remote oxidant species[29, 34]. If hydrogen peroxide is not the migratory species, and hydroxyl radicals are not the oxidant, then another gas-phase species must be responsible. The same experimental set-up was utilised for a further experiment, whereby an ozone-containing oxygen stream replaced the hydrogen peroxide stream. In this case, as depicted in Figure 3-18 C&D, the soot layer was removed within 18 hours. Much more work is required before the hydroxyl mechanism can be discounted, but the effect of ozone on soot during irradiation is remarkable; and the lack of effect with UVC/H_2O_2 is equally noteworthy. A third possibility is singlet oxygen, which, despite observations suggesting that the

species is not significantly migratory[43], should be investigated to assess its potential involvement in remote photocatalysis.

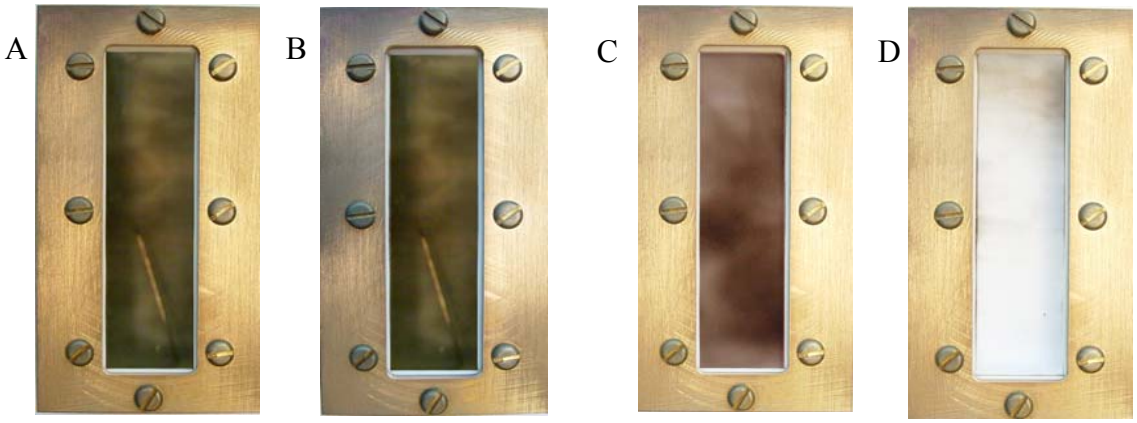

Figure 3-18 before and after pictures of photoinduced soot removal, effected by UVC irradiation of a flowing oxygen stream containing (A&B) H_2O_2 and (C&D) ozone; timings of pictures are: (H_2O_2-UVC) A = 0 h, B = 72 h; and (ozone-UVC) C = 0 h, D = 18 h

3.4 Photocatalytic oxidation of Sulfur Layers on Titania Paste Films[48]

$$S + O_2 \xrightarrow[h\nu \geq E_{bg}]{TiO_2} SO_2 \quad (3\text{-}8)$$

$$2S + 3O_2 + 2H_2O \xrightarrow{UVC} 2H_2SO_4 \quad (3\text{-}9)$$

$$S + O_2 \xrightarrow{UVC} SO_2 \quad (3\text{-}10)$$

$$SO_2 + \tfrac{1}{2}O_2 \xrightarrow{UVC} SO_3 \quad (3\text{-}11)$$

$$SO_2 + \tfrac{1}{2}O_2 \xrightarrow[h\nu \geq E_{bg}]{TiO_2} SO_3 \quad (3\text{-}12)$$

$$2SO_3 + 2H_2O \longrightarrow 2H_2SO_4 \quad (3\text{-}13)$$

The photocatalytic oxidation of sulfur on titania, summarised by equation 3-8, is complicated by two factors. Firstly; the UV-induced photolysis of sulfur has been documented to occur in aerated aqueous conditions with irradiation by UVC (but not

UVA or visible light)[44, 45], as described in equations 3-9 and 3-10. As direct UVC photolysis is observed in aerated aqueous solution, it must be assumed that it also occurs in ambient humid air. Secondly is the further oxidation of SO_2, by (a) homogeneous photolysis – initiated by wavelengths <300 nm, i.e. reaction 3-11 – and (b) heterogeneous photocatalysis, i.e. reaction 3-12.

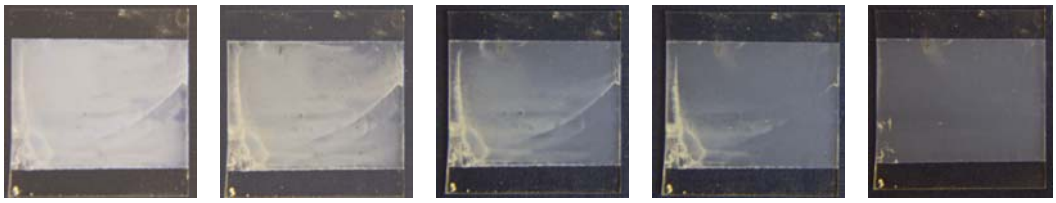

0 min 120 min 240 min 360 min 480 min

Figure 3-19 2cm × 2cm glass square with 1.6 cm × 2cm titania coating covered in amorphous sulfur pictured during irradiation on open bench top with UVC light source, I_{UVC} = 5.6 mW cm^{-2}

Preliminary experiments carried out on the benchtop with UVC irradiation of a sulfur-coated titania-paste film, depicted in Figure 3-19, showed the light yellow/white sulfur layer to be removed completely within 8 hours of irradiation. Small deposits of sulfur on the plain glass indicate that in these conditions, i.e. 50-60% RH and ambient flowing air over the substrate, the rate of sulfur photolysis is not competitive in comparison with the rate of photocatalytic sulfur oxidation; i.e. reaction 3-8 is much faster than reaction 3-10. UV-Vis monitoring of the sulfur layer in this experiment produced the spectra shown in Figure 3-20, and illustrated that the sulfur layer was removed linearly with irradiation time, displaying what are most probably zero-order kinetics with respect to the level of sulfur present. Such kinetics are not uncommon in studies of surface films (organic or carbon) destruction by titana photocatalyst layers.

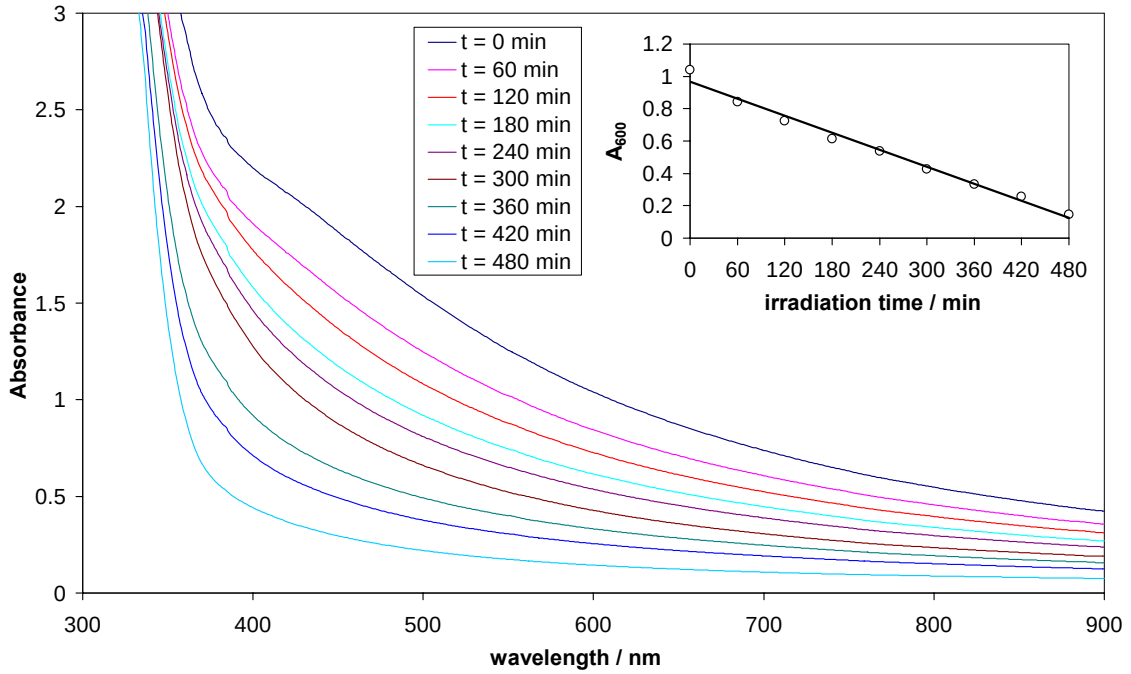

Figure 3-20 UV-Vis absorbance spectra for sulfur on titania film during irradiation with UVC, I_{UVC} = 5.6 mW cm^{-2} and, inset, absorbance at 600 nm versus irradiation time

---

The combination of monitoring by UV-Vis absorbance and accurate mass measurement, as shown in Figure 3-21, illustrates that no persistent species are formed on the substrate during irradiation, as both absorbance and mass return to approximately initial, i.e. before sulfur deposition, values – indicated by the grey dashed line. Figure 3-21 also illustrates a good correlation between absorbance and mass, with a factor of 0.9906 calculated, and further evidence of zero-order kinetics, as a linear correlation was observed while full layer coverage maintained.

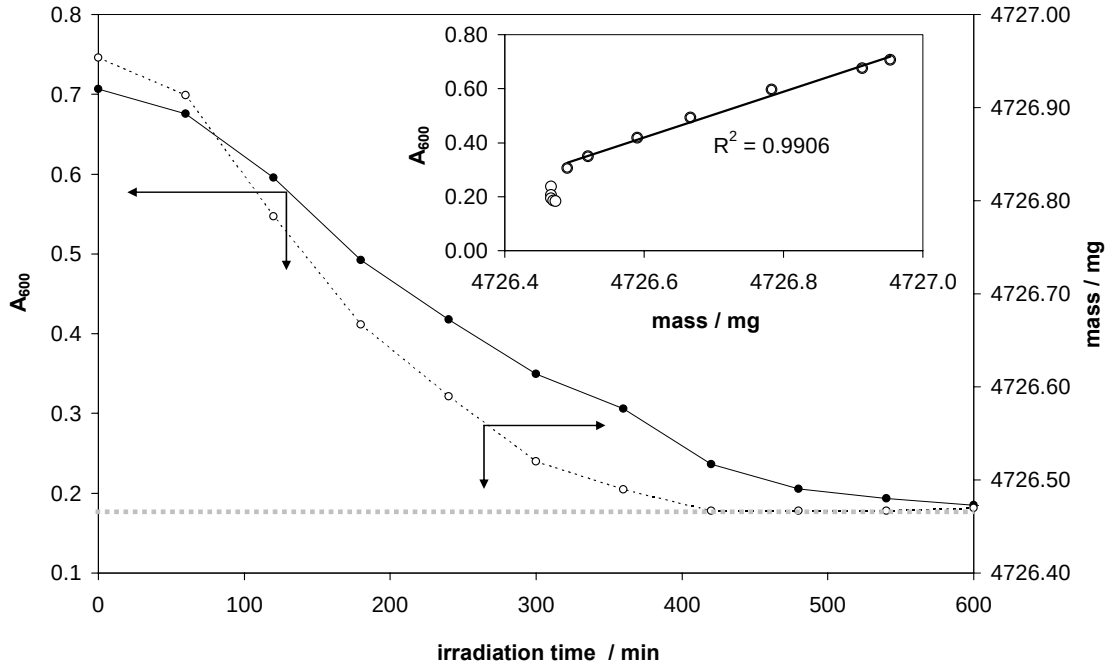

Figure 3-21 UV-Vis (closed) and gravimetric (open) monitoring of sulfur on titania film during UVC irradiation with, (inset) correlation between both y-axes plotted. Initial (before sulfur deposition) values of mass ans absorbance indicated by grey dotted line. I_{UVC} = 5.6 mW cm^{-2}

When a UVA light source was used instead of UVC, with both sources emitting similar intensities (~5.6 mW cm^{-2}), the change in absorbance was seen to occur at a reduced rate, (Figure 3-22). Concurrent mass measurements give initial sulfur removal rates of 90 μg h^{-1} and 41 μg h^{-1} for UVC and UVA respectively, the ratio (~2.3 times) correlates well with the ratio of UV absorbance of titania films for UVA (44%) and UVC (100%). With UVC irradiation, a possible contributing factor in the increased rate of sulfur removal is the direct photolysis of sulfur, i.e. reaction 3-10. Mass measurements for sulfur deposited onto frosted glass, during UVC irradiation in ambient conditions, suggested an initial rate of sulfur removal by photolysis of ~18 μg h^{-1}, approximately 5 times slower than that observed with a photocatalyst film.

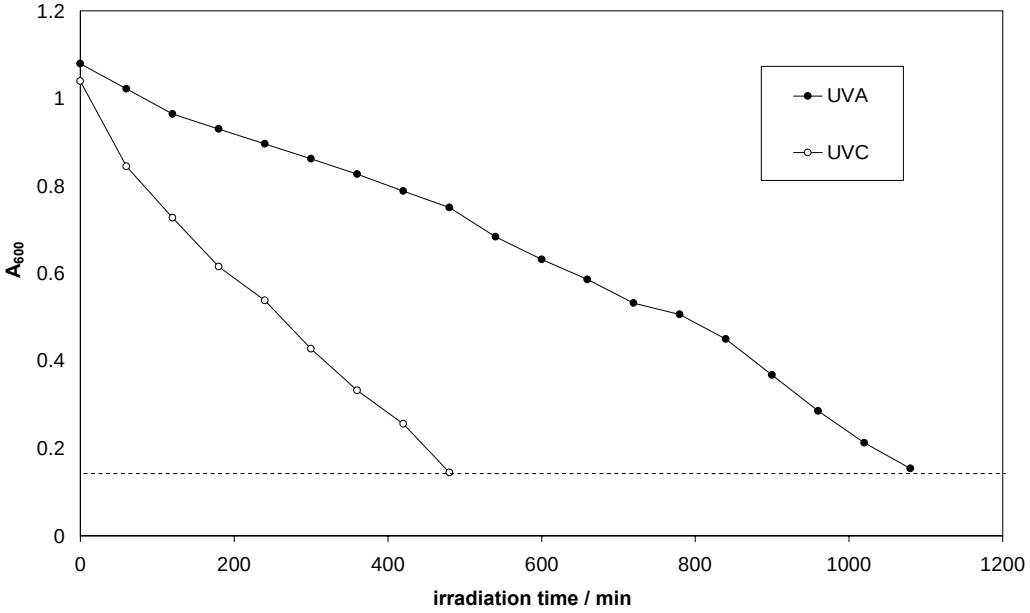

Figure 3-22 Comparison of changes in absorbance at 600 nm for two titania films coated in sulfur, irradiated with UVC (open) or UVA (closed) $I_{UVC/UVA}$ = 5.6 mW cm^{-2}. Initial absorbance, i.e. before sulfur deposition, indicated by dashed line

---

Experiments with a sealed FTIR cell indicated that SO_2 was the only gaseous oxidation product; calculation of initial rate with these conditions gave a value of 20 μg h^{-1} with UVC irradiation. Calculation of stoichiometry at this stage gave very low, ~20%, yields when the moles of SO_2 formed were compared to the moles of S removed. This was thought to be due to the S and SO_2 direct photolysis removal reactions, i.e. 3-10 and 3-11, with liquid SO_3 or H_2SO_4 produced. In order to limit these processes the cell was flushed after three hours' irradiation, with the sum of the total SO_2 produced calculated. When sulfur was coated onto roughened glass and irradiated with UVC in the sealed cell an initial rate of ~4 μg h^{-1} for sulfur removal was observed. Figure 3-23 shows that the rate of sulfur removal during each three hour period, from this data it can be seen that the rate was initially ~14 μg h^{-1}, but fell away rapidly despite the SO_2 being removed at 180 minute intervals. From this it became apparent that the photocatalyst was being

poisoned, and that the most probable cause was that SO_3 and/or H_2SO_4, produced by photocatalysis and photolysis, were blocking the photocatalyst surface. This was occurring to such an extent that the predominant reaction was seen to shift away from photocatalytic equation 3-8, with the resulting sulfur removal most likely to occur via direct UV photolysis, equation 3-10. Figure 3-23 plots the calculated rates of sulfur removal as the experiment progressed and clearly indicates this shift from photocatalytic oxidation of sulfur, with some photolysis, to the simple photolysis of sulfur by UVC after a combined irradiation period of approximately 150 hours.

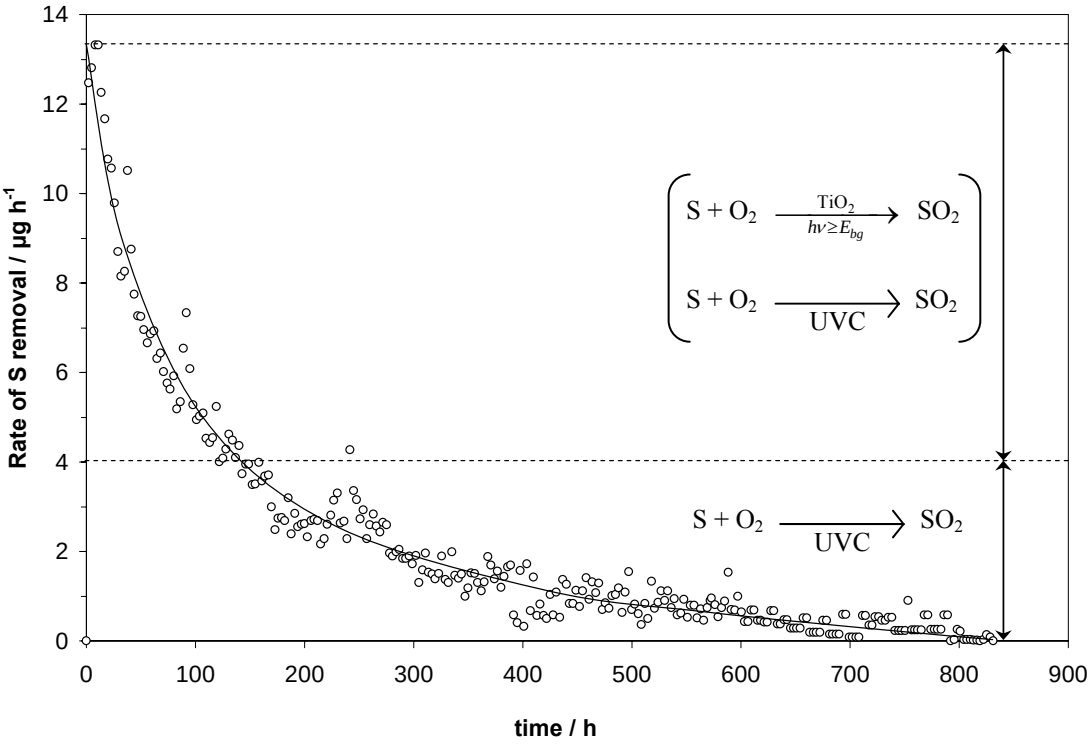

Figure 3-23 Rate of sulfur removal on titania film in sealed system with UVC irradiation, oxidation products are determined and flushed with oxygen every three hours

Because SO_3 (and, in the presence of water vapour, H_2SO_4) appeared to be blocking the photocatalytic activity of the films it became clear that another method for the evaluation of stoichiometry for reaction 3-8 was required. The simple replacement of UVC light

with UVA removed the influence of the direct photolysis of both S and SO_2, i.e. reactions 3-10 and 3-11, but the further photocatalytic reaction of SO_2 at the titania surface, i.e. 3-12, was still to be addressed. As seen with the initial ambient bench top experiments, where oxidation products were permitted to diffuse from the surface with gas flow, it followed that a flowing system was necessary to limit the heterogeneous photocatalytic reaction of SO_2. In order to determine stoichiometry, and estimate a quantum yield for reaction 3-8, a trapping agent and subsequent colourimetric determination method were employed. The trap chosen was sodium tetrachloromercurate (TCM) which, upon exposure to SO_2, sulfite or sulfurous acid, rapidly forms a stable, non-volatile, soluble disulfitomercury (II) salt (DSM) via equation 3-14[49].

$$[HgCl_4]^{2-} + 2SO_2 + 2H_2O \rightarrow [Hg(SO_3)_2]^{2-} + 4HCl \qquad (3\text{-}14)$$

It is then possible to determine the trapped SO_2 colourimetrically using acidified ρ-rosaniline/formaldehyde solution; the trapped SO_2, formaldehyde and ρ-rosaniline reacting to form ρ-rosaniline methylsulfonic acid (ρ-RMSA), reaction 3-15.

amine group + sulfur dioxide + formaldehyde → ρ-rosaniline methylsulfonic acid

$$R\text{–}NH_2 + SO_2 + HCHO \rightarrow R\text{–}NH\text{–}CH_2\text{–}SO_3H \qquad (3\text{-}15)$$

Calibration of the absorbance of the coloured species, λ_{max} = 560 nm, versus $[SO_2]$, using sodium metabisulfite solution standardised with standard sodium thiosulfate, allowed calculation of SO_2 produced by photocatalysis as a function of irradiation time. Figure 3-24 depicts the spectral change observed during irradiation with UVA as the concentration of SO_2 increased. Inset is the absorbance at 560 nm versus time.

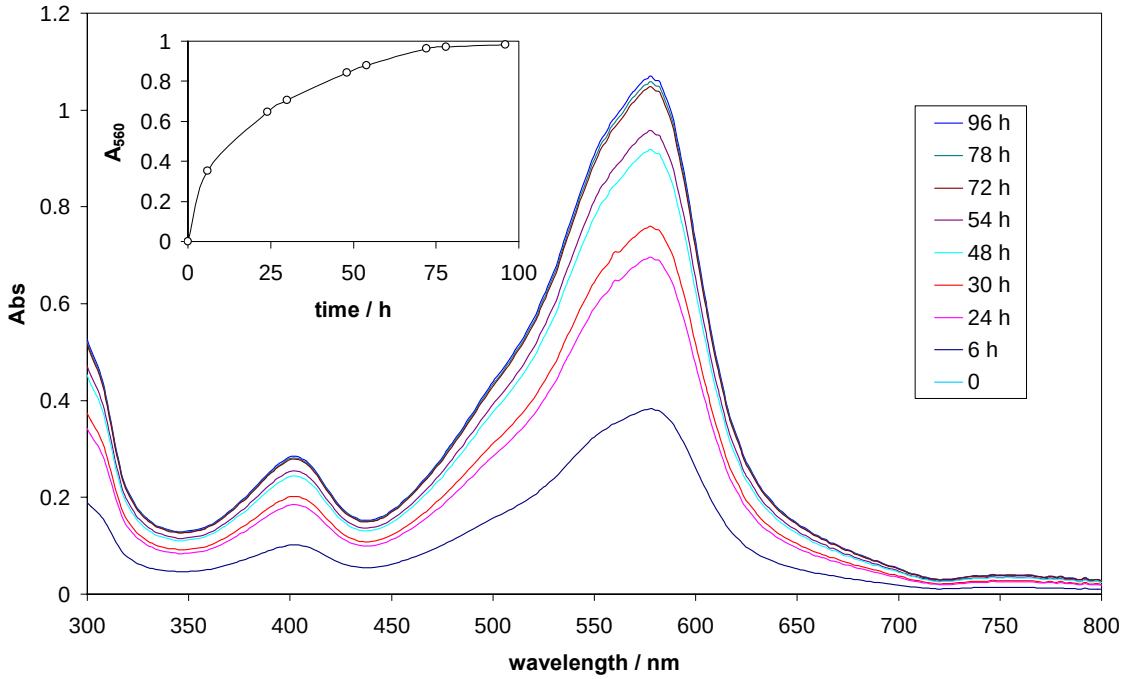

Figure 3-24 Absorption spectra of ρ-RMSA-developed solution with increasing irradiation time for a sulfur-coated titania film under UVA irradiation in a dry oxygen stream and, inset, A_{560} versus irradiation time

---

Using the calibration factor determined (0.5008 μg mL^{-1} Abs^{-1}), the concentration of SO_2 trapped, and subsequently the mass of SO_2 produced, were calculated. By measuring the mass of the sulfur-coated slide before and after irradiation a mass balance was possible. From the plot it is apparent that 903 μg of sulfur dioxide were produced (Figure 3-25), via reaction 3-8, for a loss of 470 μg of sulfur. The yield is therefore ~96%, a similar efficiency to that found for soot oxidation over titania with UVA light (100%, section 3.3). An initial rate of sulfur dioxide production of 58.9 μg h^{-1} was estimated from Figure 3-25. This was equivalent to 0.129 μg cm^{-2} min^{-1}, as the area of the film was 7.6 cm^2. Typical UVA intensity for this system was 7 mW cm^{-2}; equivalent to 7.7×10^{17} 365 nm photons cm^{-2} min^{-1}. From this a formal quantum efficiency of ~0.16% could be estimated. This is approximately a 15 times increase in comparison to that found for soot on P25 titania films. A possible reason could be the closer intimate contact observed for

sulfur on titania, suggesting oxidative species react at the surface in a more efficient process.

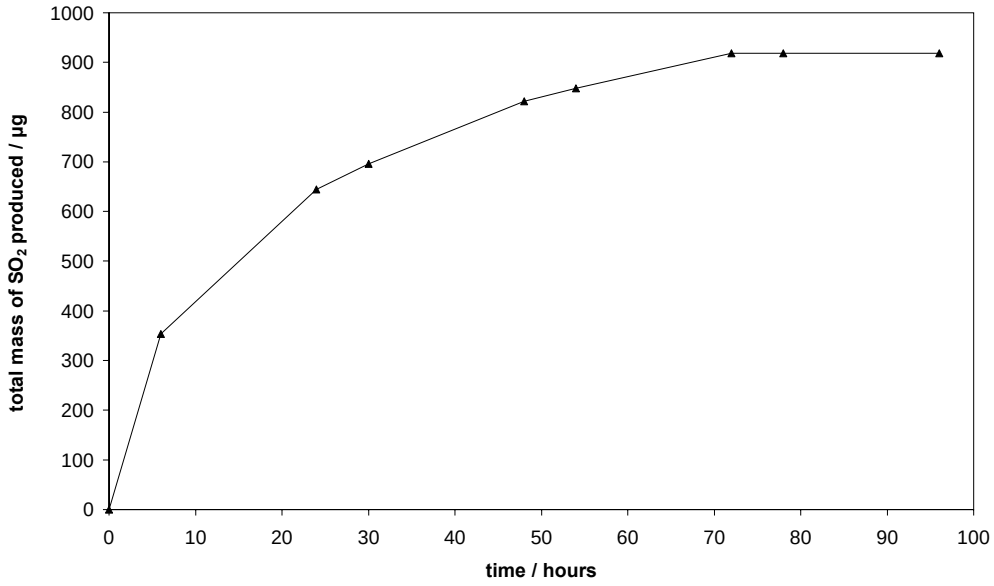

Figure 3-25 Calculated mass of sulfur dioxide produced by photocatalysis of sulfur layer on titania film during UVA irradiation in flowing oxygen

3.5 Conclusions

It has been possible to supplement the existing work covering the photocatalytic oxidation of soot on titania films with further methods of soot-layer monitoring and establishment of stoichiometry. Carbon dioxide was identified as the only oxidation product, in accordance with equation 3-7, and was seen to be produced stoichiometrically (100% yield when compared to moles of soot removed). Throughout the work it became apparent that deposition of soot from a candle flame was an inefficient and unreliable model and that for a full kinetic study to be possible an

improved deposition method may be required. The fibrous nature of flame-deposited soot layers seems to have been the cause of the low quantum efficiency (0.011%), in comparison to stearic acid removal (c. 640 times smaller). Investigation into the remote photocatalysis of soot showed no removal of the soot layer with UVC-irradiated hydrogen peroxide vapour. This, and the rapid removal of soot by UVC-ozone, casts doubts over the hydrogen peroxide/hydroxyl radical mechanisms proposed for remote PCO.

Sulfur layers dip-coated onto titania were removed completely by PCO with UVC and UVA irradiation. With UVC irradiation, a portion of the sulfur loss was likely to be as a result of direct photolysis, whereas UVA irradiation appeared to only initiate photocatalytic oxidation. FTIR analysis of the gas-phase indicated that SO_2 was the only direct product of photocatalysis, but the further oxidation of SO_2 by PCO or photolysis meant that stoichiometry could not be determined by this method. UVA irradiation was used in conjunction with a trapping agent (sodium tetrachloromercurate) in a flow-through set-up, with the trapped SO_2 determined colourimetrically using acid-bleached ρ-rosaniline and formaldehyde to form the coloured species ρ-rosaniline methylsulfonic acid. A mass balance between sulfur removed by PCO and SO_2 trapped gave a yield of 96%, and from the 'mass of SO_2 produced' versus time plot an initial rate was calculated, from this a formal quantum yield of 0.16% was estimated, approximately 15 times higher than found for soot oxidation by a P25 film. This was concluded to be as a result of closer contact between the film and the sulfur due to the denser nature of the sulfur layer.

3.6 References

1 R. G. M. Webster, C. A. Andrew, S. Baxter, J. MacDonald, M. Rocha, B. W. Thomson, K. H. Tonge, D. C. M. Urquhart, and M. E. Young, *Stonecleaning in Scotland, Research Report to Historic Scotland and Scottish Enterprise by Masonry Conservation Research Group, Gilcomston Litho, Aberdeen*. 1992.

2 A. Fujishima, and K. Honda, *Nature* **238**, 37 (1972).

3 A. Hagfeldt, and M. Gratzel, *Chem. Rev.* **95**, 49-68 (1995).

4 C. S. Turchi, and D. F. Ollis, *J. Catal.* **122**, 178-192 (1990).

5 S. N. Frank, and A. J. Bard, *J. Phys. Chem.* **81**, (15), 1484 (1977).

6 R. Wang, K. Hashimoto, A. Fujishima, M. Chikuni, E. Kojima, A. Kitamura, M. Shimohigoshi, and T. Watanabe, *Nature* **388**, 431 (1997).

7 S. Kume, and T. Nozu, *Difficulty stainable glass product*. Japanese Patent Sho 61-243762, 1986.

8 R. Fretwell, and P. Douglas, *J. Photochem. Photobiol. A: Chem* **143**, 229 (2001).

9 A. Fujishima, K. Hashimoto, and T. Watanabe, *TiO_2 Photocatalysis: Fundamentals and Applications*. BKC: 1999.

10 D. W. Sheel, R. J. McGurdy, and S. J. Hurst, (1998).

11 I. P. Parkin, and R. G. Palgrave, *J. Mater. Chem.* **15**, 1689 (2004).

12 H. Einaga, M. Harada, S. Futamura, and T. Ibusuki, *J. Phys. Chem. B* **107**, 9290 (2003).

13 A. Mills, S.-K. Lee, and A. Lepre, *J. Photochem. Photobiol. A: Chem* **155**, 199 (2003).

14 J. Zhang, T. Ayusawa, M. Minagawa, K. Kinugawa, H. Yamashita, M. Matsuoka, and M. Anpo, *J. Catal.* **198**, (1), 1 (2001).

15 L. Frazer, *Environ. Health Persp.* **109**, (4), 174 (2001).

16 A. Heller, *Accounts Chem. Res.* **28**, 503 (1995).

17 M. Minabe, D. A. Tryk, P. Sawunyama, K. Y, K. Hashimoto, and A. Fujishima, *J. Photochem. Photobiol. A: Chem* **137**, 53 (2000).

18 A. Mills, and S.-K. Lee, *J. Photochem. Photobiol. A: Chem* **152**, 233 (2002).

19 K. Scrivener, and H. Van Damme, *MRS Bull.* **29**, 308 (2004).

20 A. Mills, N. Elliott, I. P. Parkin, S. A. O'Neill, and R. J. Clark, *J. Photochem. Photobiol. A: Chem* **151**, 171 (2002).

21 K. Ritter, and (Associated-Press), in *Chicago Tribune* http://www.titaniasun.com/downloads/chicagotrib_article.pdf, Chicago, 22/7/2005.

22 S. E. Manahan, *Environmental Chemistry*. Sixth ed.; Lewis: 1994.

23 K. A. Kennedy, P. A. Addison, and D. G. Maynard, *Environ. Pollut.* **51**, 121 (1988).

24 K. A. Kennedy, P. A. Addison, and D. G. Maynard, *Environ. Pollut. A* **39**, 71-77 (1985).

25 T. R. Barfknecht, *Prog. Energy Combust. Sci.* **9**, 199 (1983).

26 EPA, *Fact sheet on the new ozone (smog) and particulate (soot) air quality standards*. 1997.

27 M. J. Abramson, and T. Beer, *Med. J. Australia* **169**, 452 (1998).

28 S.-K. Lee, S. McIntyre, and A. Mills, *J. Photochem. Photobiol. A: Chem* **162**, 203 (2004).

29 M. C. Lee, and W. Choi, *J. Phys. Chem. B* **106**, 11818 (2002).

30 T. Tatsuma, S. Tachibana, and A. Fujishima, *J. Phys. Chem. B* **105**, 6987-6992 (2001).

31 T. Tatsuma, S. Tachibana, T. Miwa, D. A. Tryk, and A. Fujishima, *J. Phys. Chem. B* **103**, (38), 8033-8035 (1999).

32 H. Haick, and Y. Paz, *J. Phys. Chem. B* **105**, 3045-3051 (2001).

33 W. Kubo, and T. Tatsuma, *J. Am. Chem. Soc.* **128**, 16034 (2006).

34 Y. Murakami, E. Kenji, A. Y. Nosaka, and Y. Nosaka, *J. Phys. Chem. B Letts* **110**, 16808 (2006).

35 *Physical and Chemical Properties of Hydrogen Peroxide; Radiation Properties of H_2O_2, US Peroxide*, http://www.h2o2.com/intro/properties/radiation.html

36 Y. Nosaka, M. Nakamura, and T. Hirakawa, *Phys. Chem. Chem. Phys.* **4**, 1088 (2002).

37 H. Goto, Y. Hanada, T. Ohno, and M. Matsumara, *J. Catal.* **225**, 223 (2004).

38 W. Kubo, and T. Tatsuma, *Anal. Sci.* **20**, 591 (2004).

39 K.-I. Ishibashi, A. Fujishima, T. Watanabe, and K. Hashimoto, *J. Photochem. Photobiol. A: Chem* **134**, 139 (2000).

40 K. Naito, T. Tachikawa, M. Fujitsuka, and T. Majima, *J. Phys. Chem. B Letts* **109**, 23138 (2005).

41 T. Tachikawa, and T. Majima, *J. Fluoresc.*, (2007).

42 K.-C. Cho, K.-C. Hwang, T. Sano, K. Takeuchi, and S. Matsuzawa, *J. Photochem. Photobiol. A: Chem* **161**, 155 (2004).

43 T. Daimon, and Y. Nosaka, *J. Phys. Chem. C* **111**, 4420 (2007).

44 Y. Matsumoto, H. Nagal, and E. Sato, *J. Phys. Chem.* **86**, 4664 (1982).

45 Y. Matsumoto, Y. Yamaguchi, and E. Sato, *Bull. Chem. Soc. Jpn.* **58**, 1255 (1985).

46 J. Peral, and D. F. Ollis, *J. Mol. Catal. A: Chem.* **115**, 347 (1997).

47 World-Bank-Group, *Pollution Prevention and Abatement Handbook* **July 1998**,

48 A. Mills, M. Crow, J. Wang, I. P. Parkin, and N. Boscher, *J. Phys. Chem. C* **111**, 5520 (2007).

49 P. W. West, and G. C. Gaeke, *Anal. Chem.* **28**, (12), 1816-1819 (1956).

50 A. Steigman, *J. Soc. Chem. Ind.* **61**, 18-19 (1942).

51 A. Mills, J. Wang, and M. Crow, *Chemosphere* **64**, 1032 (2006).

52 Y. Paz, Z. Luo, L. Rabenberg, and A. Heller, *J. Mater. Res.* **10**, (11), 2842 (1995).

Chapter 4 Photocatalytic Oxidation of Inorganic Gas Species on Titania

4.1. Introduction

Organic, chlorinated organic, and inorganic gas species such as NO_x (NO, NO_2, N_2O), SO_x (SO_2, SO_3), O_3 and CO, are primary pollutant species, recognised as harmful to humans, and damaging to the environment[1-4]. The commercial applications of SPC for the elimination of such compounds are directed towards two fields: ambient air purification, and improvement of indoor air quality. The former has been more high profile of the two, with 7000 m^2 of road surface in Milan coated in photocatalyst-composite cementitious material in order to demonstrate its worth in the removal of NO_x species (a 60% decrease in street-level NO_x was claimed)[5]. Further to this the Mitsubishi Materials Corporation have developed a photocatalytic NO_x-removing concrete tile called 'Noxer', which features a 5–7 nm surface layer of TiO_2, these tiles have been deployed on the streets of London in the burgh of Westminster[6]. NO_x, i.e. nitric oxide (NO), nitrous oxide (N_2O), and nitrogen dioxide (NO_2), are oxidised to nitric acid (HNO_3) and nitrates by PCO[7], removing them from the air.

Of the most popular routes for metal oxide production, specifically for use as photocatalysts, sol-gel and CVD synthesis stand out for their creation of hard ceramic materials of nanocrystalline material, ideal for use as glazes and robust coatings, which can be produced simply and applied in-process to tiles and building materials, or sheet glass for glazing. For the creation of glazes, in the pursuit of optical clarity film, thickness is minimised, therefore PCO activity is often relatively low for such products[8-11]. TiO_2 products which display higher PCA are often white particulate solids and are unsuitable for creation of clear glazes but which nonetheless form highly active photocatalyst films when deposited[12-16]. The major problem with these films, apart from a white appearance due to light-scattering, is a distinct lack of robustness. For this

reason researchers have attempted to fix or bind titania particles within a continuous phase[16-23]. The two main stipulations of a binder in these composites are that they afford sufficient surface area to the photocatalyst, and that they themselves are not degraded by PCO. Silicate and ceramic binders satisfy both parameters, leaving hard, robust coatings similar to sol-gel and CVD coatings[16, 18, 19, 21].

An area of interest within this sphere is the production of films which feature both high PCA but are also flexible and not brittle as ceramic-type films can be. This would give the possibility of imparting self-cleaning and deodorising properties unto plastics and other 'soft' materials like fabrics. As with cementitious building materials[24], incorporation of photocatalytically active compounds into plastics is a simple way to functionalise common products, and titania pigments have been used as whiteners and fillers in plastics for many years[17]. Photocatalytically active titania though, has been observed to degrade poly-vinyl-chloride (PVC) in sunlight[25], prompting researchers to suggest its potential for creating photo-degradable plastics. In order to create polymer-titania materials which *do not* degrade, fluoropolymer based systems have been suggested[23, 26]. Fluoropolymers, which are extremely corrosion resistant and thermally stable (e.g. PTFE is stable >250°C)[27], are suggested to be inert enough to resist PCO[26], and photo-ageing experiments showed little obvious degradation of fluororesin binders[23]. Other applications of polymer-photocatalyst films include the fabrication of oxygen scavenger films for insertion into modified atmosphere packaging (MAP) to limit oxidative spoiling of foodstuffs[20].

A number of products have been developed to remove the compounds associated with indoor air phenomena such as 'sick building syndrome' (SBS). The term SBS applies to cases where a significant proportion of occupants of both commercial and residential buildings suffer from the acute health effects which can be directly linked to their time spent in the building[4]. The causes of SBS are believed to include poor indoor air quality; including exposure to species such as NO_x, SO_2, CO, O_3 and volatile organic compounds (VOCs). The sources of these species are either common processes – vehicular exhaust,

electrical sparking in office equipment, cigarette smoke, or release of residual solvents from building materials, paints, adhesives, particle board, textiles, and cleaning products. PCO of VOCs (such as formaldehyde, benzene, toluene and methane) and chlorinated VOCs (such as trichloroethylene and 4-chlorophenol) has been extensively studied[2, 28-35] and have been targeted specifically for their prevalence in indoor air[36]. Other PCO systems include those which are specifically designed for the oxidation of ethylene gas in refrigeration units for the storage of fruit and vegetables[6, 37]. Ethylene is released by, and promotes the ripening of many fruit and vegetables and its removal by PCO, along with any pathogens present, can prolong the storage life of the produce. The homogeneous degradation of ozone has been observed to be expedited by PCO over titania films[38] and platinised titania[39].

SPC is a viable technology for the removal of many species, such as carbon monoxide, which has been a long-term target compound for SPC due to its toxicity, lack of colour and odour, and common formation in incomplete combustion of solid, liquid and gaseous fuels[40]. Some researchers have used acetaldehyde degradation as the model system to demonstrate SPC for fluoropolymer composites[23], and NO_x removal is also popular for the assessment of air-purification photocatalysts[7]. For this section of work carbon monoxide oxidation was chosen to investigate polymer-titania films, with a view to creating thin, flexible films of photocatalytically active material which can be coated onto non-rigid surfaces.

Carbon monoxide oxidation by SPC has been observed to be an unfavourable process on unmodified titania, with platinum deposition necessary in order to make it viable[41-43]. Figure 4-1 shows the findings of Hwang et al[42], who compared three commercial photocatalysts before and after platinisation. Reports vary within the body of literature as to the extent of PCO of CO on 'naked' titania; Einaga et al[41] observed no PCO activity towards CO with P25 titania, whereas Vorontsov et al[43] found 'Hombikat' titania oxidised CO but with very low quantum yields compared to the same material after platinisation. Van Damme and Hall[44] and Linsebigler et al[45] both reported

successful oxidation of CO on titania, the latter suggesting that both CO and O_2 adsorb at the same sites on titania (these sites being identified as oxygen vacancies, created by heating to >400°C) and pre-exposure to CO reduces the rate of PCO, as active oxygen species are not formed.

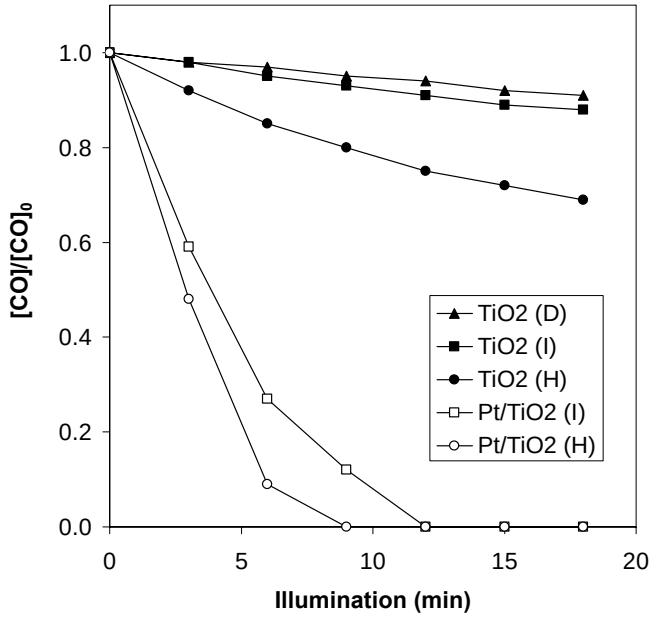

Figure 4-1 Variation of [CO] with UV illumination time (3 mW m^{-2}) for naked and platinised TiO_2, $[CO]_0$ was 500 ppmv[42]

The platinum enhancement of CO oxidation on titania is generally associated with the creation of active sites for CO to react with photogenerated oxidative species, rather than enhancement of charge separation within the photocatalyst[42]. Einaga et al[41] proposed that platinisation allows efficient adsorption of the CO which would not otherwise occur, but did not go so far as to investigate the oxidative species present. These are not thought to be hydroxyl radicals, as humidity had no effect on CO oxidation rate[42],

instead it has been proposed that adsorbed oxygen species O^{2-} and O_2^{2-} are the significant photo-generated oxidants[45].

Another common group of inorganic gas species are the oxides of sulfur, i.e. SO_x; SO_2 and SO_3, and reduced sulfur (such as H_2S), which are present in the atmosphere due to both natural and anthropogenic sources. The most common sources of SO_2 are industrial, e.g. fossil-fuel burning, while reduced sulfur, such as hydrogen sulfide, is commonly released anaerobic organic matter degradation[1]. In the industrial process for the production of sulfuric acid, sulfur is burnt to form SO_2, which is then heated (450 °C) with air under pressure, and in the presence of a vanadium catalyst, to form SO_3. The atmospheric sulfur cycle is complex, with sulfur dioxide produced homogeneously from H_2S. SO_2 and sulfur trioxide (SO_3) are solvated to sulfurous acid (H_2SO_3) and sulfuric acid (H_2SO_4) respectively. Sulfates are produced from H_2SO_4, SO_2 and H_2S[1]. The presence of sulfurous acid and sulfuric acid in the atmosphere are major contributors to acid rain, a global phenomenon linked inexorably with the burning of sulfur-containing fuels, which damages plant life and animal life, as well as causing costly damage to building materials[1]. Sulfur dioxide itself is harmful to humans; exacerbating respiratory illnesses and causing death above 500 ppm[46].

The removal, by SPC, of many sulfur compounds is of interest as they can be malodorous as well as toxic. Compounds such as hydrogen sulfide[47-49], methyl-[47] and ethyl-mercaptan (ethanethiol)[50], and dimethylsulfide (DMS)[51, 52] have all been successfully degraded by SPC. Sulfur dioxide in the aqueous phase has been observed to produce sulfate (SO_4^{2-}) when photocatalytically oxidised by P25 powder[53, 54]. There is a small amount of previous research addressing the photocatalytic removal of SO_2 from air, though it is inconclusive as to the effectiveness of SPC for this compound, and its use has been confined to powders and not films. It has been reported that powdered titania (and zinc oxide) photocatalysts oxidised SO_2 to SO_3 and H_2SO_4 under moderate UVA irradiation in a static system, with a decrease in kinetic rate reported with each subsequent run using the same photocatalyst[55, 56]. The catalysts were then regenerated by

sonication in pure water. Ao et al[57] found that, at ppb levels of SO_2, SPC had no effect, and the only effect observed was adsorption onto the filter. It was also reported that SO_2 adsorption inhibited the SPC of NO_x and VOCs when synchronous pollutants were tested. The suggestion of this research group[57] was that at high levels of SO_2 (4000 ppm) SPC proceeds, but at low levels (ppb) the adsorption of SO_2 is too low for SPC to progress.

Catalyst deactivation during treatment of sulfur-containing compounds is widely reported. Although deactivation was not observed by Peral and Ollis[52] when investigating the photocatalysis of dimethyl sulfide ($(CH_3)_2S$), their conclusion was that SO_2 and SO_3 were produced and removed continuously during reaction in a flowing system. Kako et al.[48] studied the prevention of hydrogen sulfide poisoning on Pd/TiO_2 catalysts by UV photocatalysis of H_2S to sulfate, and mentioned briefly that sulfate is also a PCO poisoning species, and it should be removed by washing. Vidal and Luengo[58] observed the inactivation of P25 titania during photocatalytic degradation of Vapam® (monoalkyl dithiocarbamate), a common pesticide/fungicide.

SPC of gaseous species, specifically in the cases of sulfur, nitrogen and halogenated compounds, can result in the release of hazardous products and intermediates. For example, SPC of trichloroethylene (TCE) has been observed to yield carbon monoxide, chloroform and phosgene[2, 59, 60], an extremely poisonous species, arguably more hazardous than TCE[40]. PCO of sulfur-containing compounds can form SO_2, SO_3 and H_2SO_4[47, 51, 56], all of which are environmentally hazardous. PCO of NO forms some NO_2 which is not always further oxidised to HNO_3[7, 61] and NO_2 is as much of a pollutant gas as NO. For these reasons it is paramount that SPC systems are environmentally sound, and that any by-products and intermediates are identified and removed if possible. As a follow up to the work documented in Chapter 3, whereby layers of elemental carbon and sulfur were successfully removed from the surface of titania paste films as CO_2 and SO_2 respectively, this section of work was designed to investigate the heterogeneous photocatalysis of SO_2, and any concomitant PCA deactivation observed, as well as

investigating the oxidation of carbon monoxide, and the potential creation of polymer-binder based photocatalysts for CO removal.

4.2. Experimental

Sulfur dioxide was produced in the laboratory as described in section 2.4. Gas-phase oxidation of sulfur dioxide was carried out in 5cm quartz IR cells, as described in section 2.3.2.3. Titania paste films (7.5 mm × 25 mm titania films cast on 10 mm × 25 mm cut glass slides) were placed inside the IR cell before sealing and flushing with dry (RH ≈ 0%) air. Sulfur dioxide was then injected into the cell through a rubber septum. The level of sulfur dioxide inside the cell was determined by FTIR analysis (further details are contained in 2.3.2.3). For all carbon monoxide oxidation experiments 100% CO (BOC) was injected into quartz IR cells with one CaF_2 window replaced by the photocatalyst substrate cast onto a 24 mm cover slip. Titania films were cast by the doctor-blade method (2.1.1.), with the films platinised by the method described in section 2.1.4. The platinisation of P25 for use in polymer films in also documented in section 2.1.4.

Irradiation for all experiments in this section were with 6 × 8W UVA bulbs arranged in a hemisphere, depicted in section 2.2.1. IR cells with photocatalyst films fitted in the end window were irradiated through the glass backing, i.e. from the reverse of the photocatalyst. Carbon monoxide and carbon dioxide were monitored using FTIR spectroscopy, the technique is described fully in 2.3.2.3. Polymer degradation was observed by the decrease in IR absorbance during irradiation, and degradation products observed in the gas-phase where applicable.

4.3. Photooxidation of sulfur dioxide on paste titania films[62]

In order to investigate the potential removal of sulfur dioxide by PCO, a set of experiments were designed whereby 0.3 mL portions of SO_2 were injected into a 5 cm quartz-bodied gas cell, previously flushed with dry (i.e. RH ≈ 0%) oxygen, and containing either titania-paste films or, for blank experiments, no film at all. Subsequently, the SO_2 levels present were determined by FTIR as the cells were irradiated with either a UVA or UVC source of typical intensity = 4 mW cm^{-2}. Figure 4-4 shows examples of the initial, i.e. before irradiation, and post irradiation IR spectra.

$$SO_2 + ½O_2 \xrightarrow[h\nu \geq E_{bg}]{TiO_2} SO_3 \quad (4\text{-}1)$$

$$SO_2 + ½O_2 \xrightarrow[UVC]{} SO_3 \quad (4\text{-}2)$$

$$2SO_3 + 2H_2O \longrightarrow 2H_2SO_4 \quad (4\text{-}3)$$

The observed product of sulfur dioxide oxidation via both PCO and direct photolysis was sulfur trioxide, equations 4-1 and 4-2 respectively, which reacts with water to form H_2SO_4, reaction 4-3. Sulfur trioxide is a liquid at room temperature (m.p. 17 °C, b.p. 49 °C) therefore it was not possible to monitor the accumulation of SO_3 in the gas phase during photocatalysis. A small proportion was left in the gas phase, and some was also seen to deposit onto the CaF_2 windows, causing interference with the spectrum of SO_2, as shown in Figure 4-4, with peaks at ~600 cm^{-1}, 900 cm^{-1} and a broad absorbance between 1000 cm^{-1} and 1300 cm^{-1}. The majority of SO_3 produced was seen to be deposited as a liquid onto the interior surfaces of the cell, Figure 4-3.

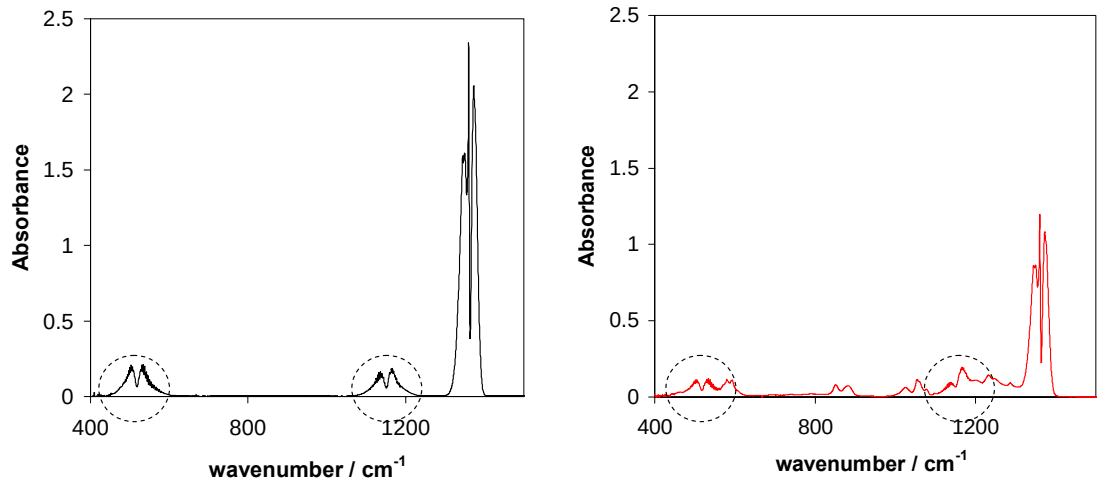

Figure 4-2 FTIR absorbance spectra for SO_2 before (left) and after (right) UVA irradiation in the presence of sol-gel paste titania film

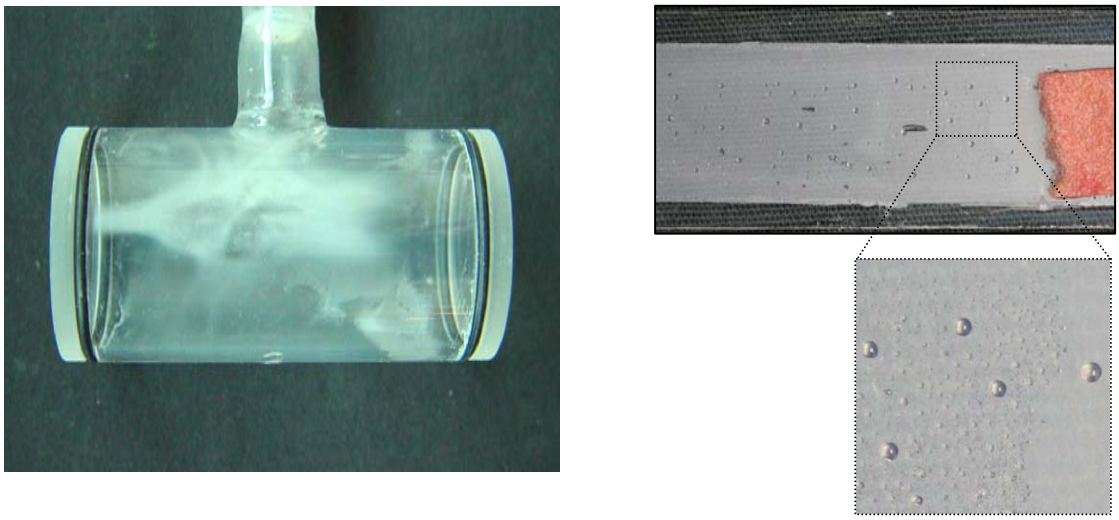

Figure 4-3 (left) Photograph of IR cell after SO_2/UVC photolysis, clearly displaying deposits of SO_3/H_2SO4; and (right) liquid deposits observed on paste titania films as a result of UVA-TiO_2 photocatalysis of SO_2, featuring wet pH indicator paper highlighting the strongly acidic liquid formed by oxidation of sulfur dioxide

The experiments carried out with and without paste titania films (TiO_2 area ≈ 2 cm^2), as shown in Figure 4-4, highlighted two important observations: (1) that UVC light photolysed SO_2 homogeneously and (2) UVA irradiation had little effect on the SO_2 level without the presence of a titania photocatalyst. These observations were in line with interpretation of the UV-Vis absorbance spectrum of SO_2, as UVC (254 nm) light is strongly absorbed but UVA (365 ± 20 nm) absorbs very little (Figure 4-5). The runs with titania films indicated that nanocrystalline solid films can remove SO_2 from the gas phase successfully by photocatalysis with UVA light.

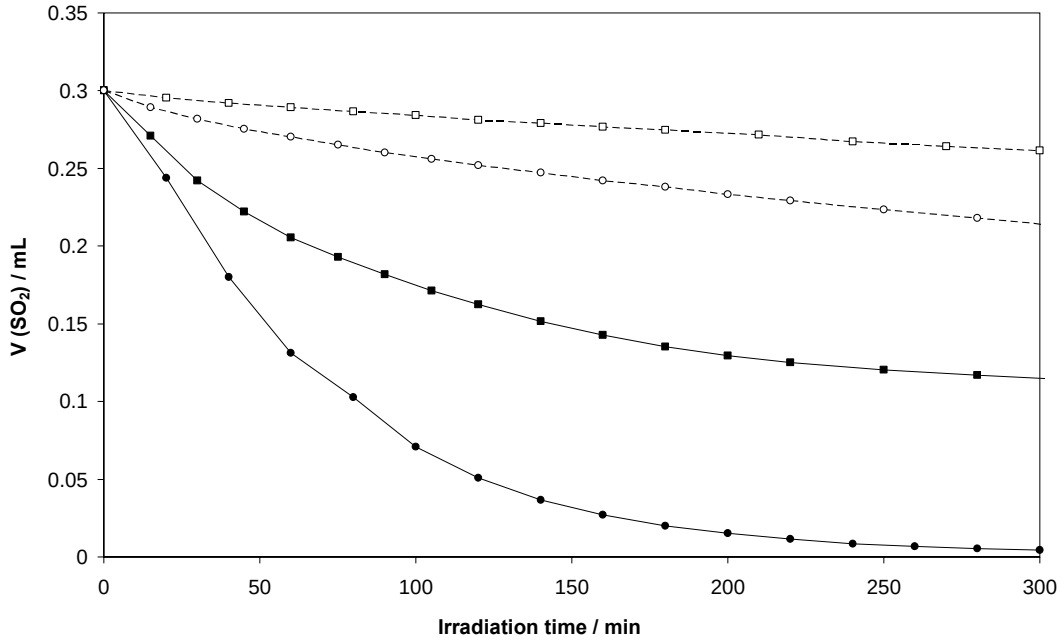

Figure 4-4 Heterogeneous oxidation of sulfur dioxide by photocatalysis with UVC/TiO_2 (●) and UVA/TiO_2 (■); and homogeneous photolysis by UVC (○) and UVA (□)

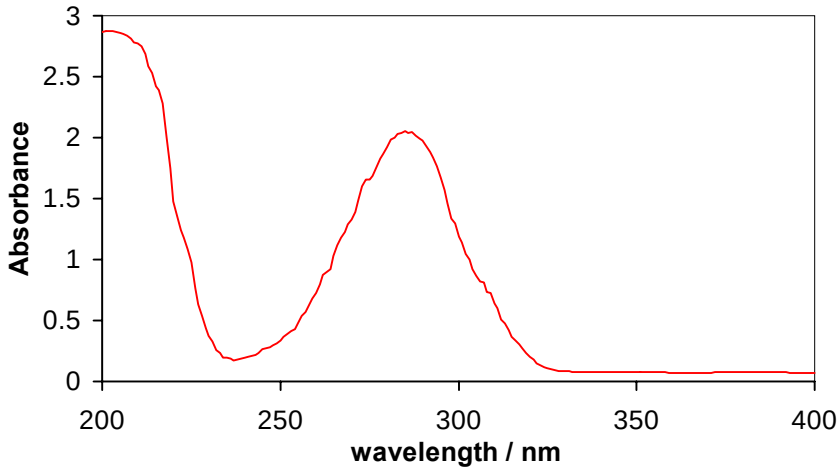

Figure 4-5 UV-Vis absorbance spectrum of SO_2; measured using 10 cm quartz cell, fitted with quartz windows, containing 1.5 mL of laboratory-produced SO_2

The deposition of oxidation products was observed to have a negative effect on photocatalytic activity when further SO_2 oxidation experiments were carried out using the same titania film, shown in Figure 4-6. From the SO_2 volume versus time plots, with $V(SO_2)$ calculated from the IR data, initial rates of SO_2 oxidation (r_i) were calculated, using the time taken for the first 20% change in volume. These values were then plotted versus the total volume of SO_2 removed from the gas phase by SPC; calculated using the sum of ΔV_{SO_2} ($V_0 - V_t$ for each repetition). The inset of Figure 4-6 shows that as the total volume of SO_2 removed increases, the initial rate of SO_2 oxidation decreases rapidly. By the sixth usage (total irradiation t = 1800 min) the initial rate of SO_2 removal was seen to be reduced by approximately ten-fold.

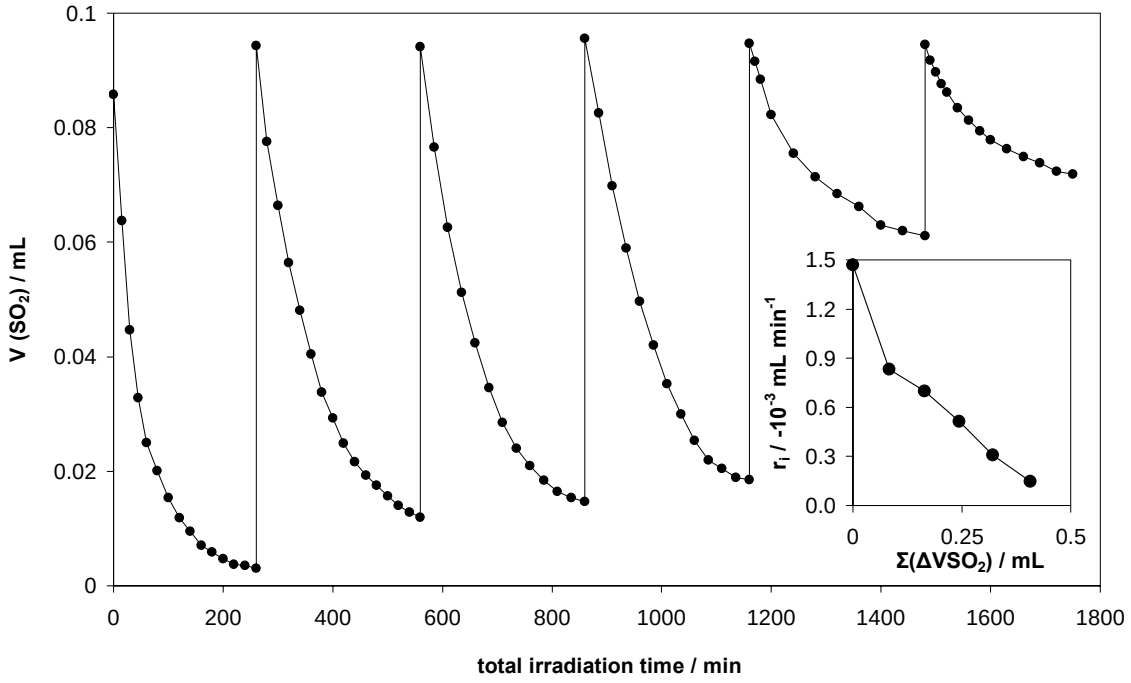

Figure 4-6 repeated PCO of SO_2 using same paste titania film under UVA irradiation (0.1 mL SO_2, balance; air) in 5 cm quartz cell,) and (inset) initial rate of SO_2 removal (r_i) for each repetition versus the total volume of SO_2 removed by the titania film $\Sigma(\Delta V_{SO_2})$

In order to estimate a value of quantum efficiency for SO_2 removal on TiO_2 by PCO, the initial rate of SO_2 oxidation on a titania slide for its first use was considered. This value, 1.47×10^{-3} mL min^{-1}, was converted into molecules of SO_2 oxidised per minute per cm^2 of TiO_2; giving a value of 1.98×10^{16} molecules cm^{-2} min^{-1}. As the measured UVA intensity was equal to 4.0 mW cm^{-2}, the number of incident photons per cm^2 was calculated to be 1.672×10^{18} UVA photons cm^{-2} min^{-1}, giving a quantum efficiency (δ) value for SO_2 oxidation by a titania paste film under in a static system of 1.18%. No value of quantum efficiency has been published before for PCO of this specific gas, but it compares favourably with δ for deposited sulfur oxidation by titania paste films, most probably due to there being no solid layer to block the UVA photons in this system.

The deactivation of titania powders by deposition of $SO_3/H_2SO_4/SO_4^{2-}$ was reversed in literature by sonication in pure water[55, 56]. Although titania films used for this experiment are more robust than powdered films, they will not withstand sonication. For this reason the deactivated samples were simply soaked in pure water (1 L) for 8 hours before drying and re-testing. Another regeneration method was to heat the film in a muffle furnace to 400°C, which is higher than the boiling points of both SO_3 (45°C) and H_2SO_4 (340°C), for 8 hours. Both methods regenerated the activity of the titania films (Figure 4-7) with soaking giving a ten-fold increase in activity and heating a five-fold increase. The discrepancy between the two might be explained by the presence of sulfate on the films which may be removed by solvation but not heating.

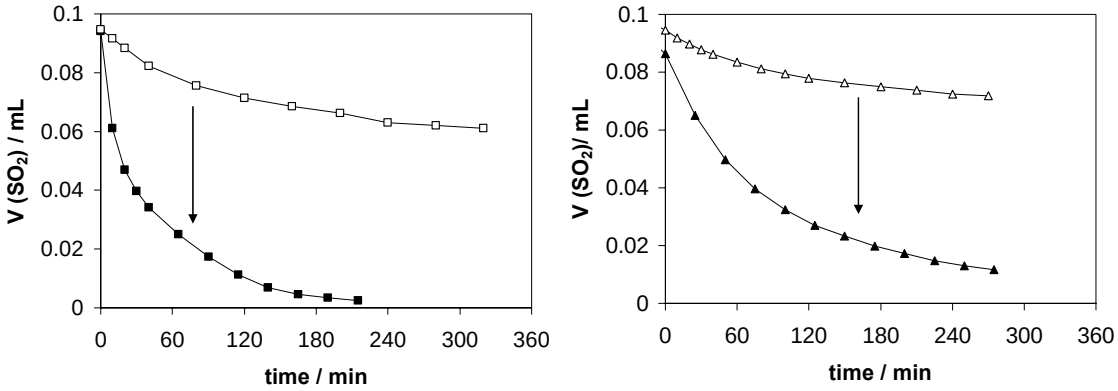

Figure 4-7 Regeneration of SO_3/H_2SO_4 deactivated titania films by soaking in pure water (left) and heating to 300 °C (right)

4.3. PCO of CO on paste films and platinised paste films

In an identical set of experiments to those carried out with SO_2, 0.1 mL portions of carbon monoxide (CO) were injected into 5 cm quartz cells containing a titania-paste film. The corresponding FTIR spectra, examples of which are shown in Figure 4-8, illustrate that carbon monoxide (ν = 2000 cm^{-1} to 2250 cm^{-1}) oxidation progresses via SPC to form carbon dioxide (ν = 2250 cm^{-1} to 2400 cm^{-1}) on both paste-titania films and platinised paste-titania films. Carbon dioxide was the only oxidation product observed, and was produced in approximately stoichiometric amounts, as shown in Figure 4-9, i.e. volume of CO removed ≈ volume of CO_2 produced. The ratio of typical initial rates for each substrate was ~10, i.e. Pt-paste films were 10 times more active towards oxidation of CO [mean r_i (paste) ≈ 3.9×10^{-4} mL min^{-1}; mean r_i (Pt-paste) ≈ 3.9×10^{-3} mL min^{-1}]. Quantum efficiencies, calculated as described in section 4.2, for the two types of film were 0.31% for titania-paste films and 3.14% for the Pt-paste films.

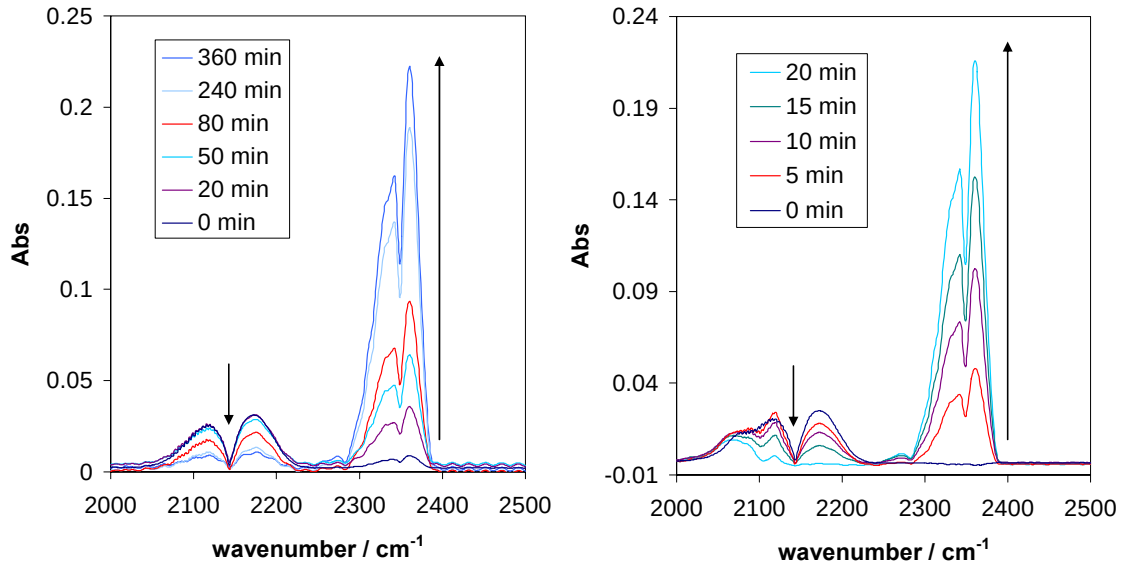

Figure 4-8 PCO of carbon monoxide with titania paste (left) and Pt-titania paste (right)

IR absorbance spectra of Pt-paste clearly show the characteristic absorbance peak of CO adsorption on Pt-TiO_2[63], occurring at ~2080cm^{-1}, in addition to the gas-phase CO peak. Examples of both spectra are shown in Figure 4-9. This peak was seen to persist after the gas-phase CO was no longer detected, suggesting that carbon monoxide is strongly adsorbed onto Pt-TiO_2, and some CO is not oxidised during the irradiation times quoted here.

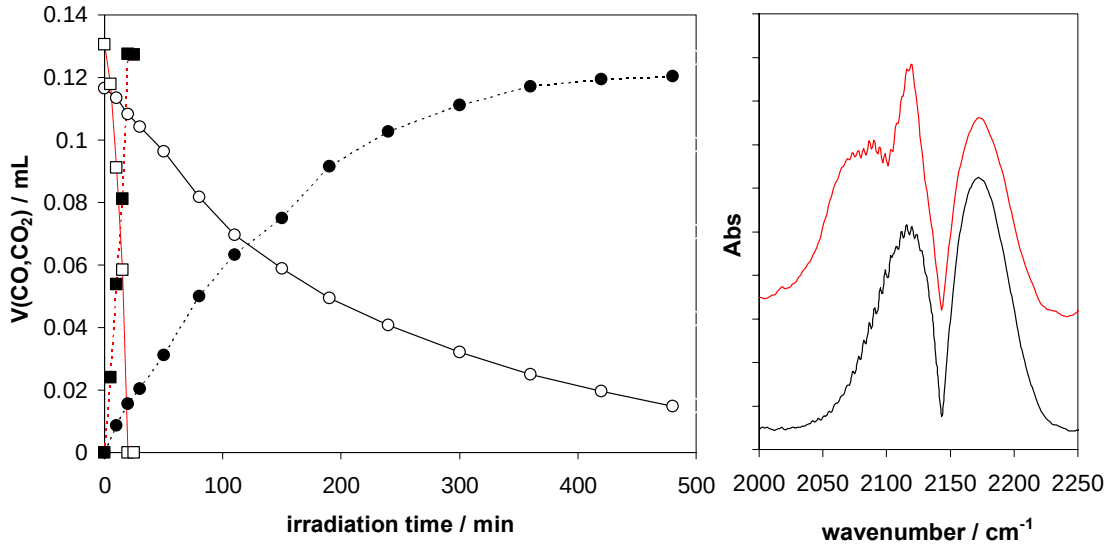

Figure 4-9 (left) the volumes of CO and CO_2 were calculated by the area under the peaks shown in Figure 4-8, these were used to illustrate the PCO of carbon monoxide (open) and production of CO_2 (closed) using paste (○, ●) and Pt-paste (□, ■) films and a UVA source; (right) the characteristic absorbance peak of CO (black) and the extra peak at 2080 cm^{-1} as a result of strong CO-Pt interaction

Repeated use of titania films showed no sign of deactivation (Figure 4-10) with initial rates for both Pt-paste and paste presenting no significant retardation in striking contrast to the PCO of SO_2 on paste TiO_2 films (Figure 4-11). Quantum efficiencies for the three

systems were as follows: SO_2/titania = 1.18%; CO/titania = 0.31%; CO/Pt-titania = 3.14%.

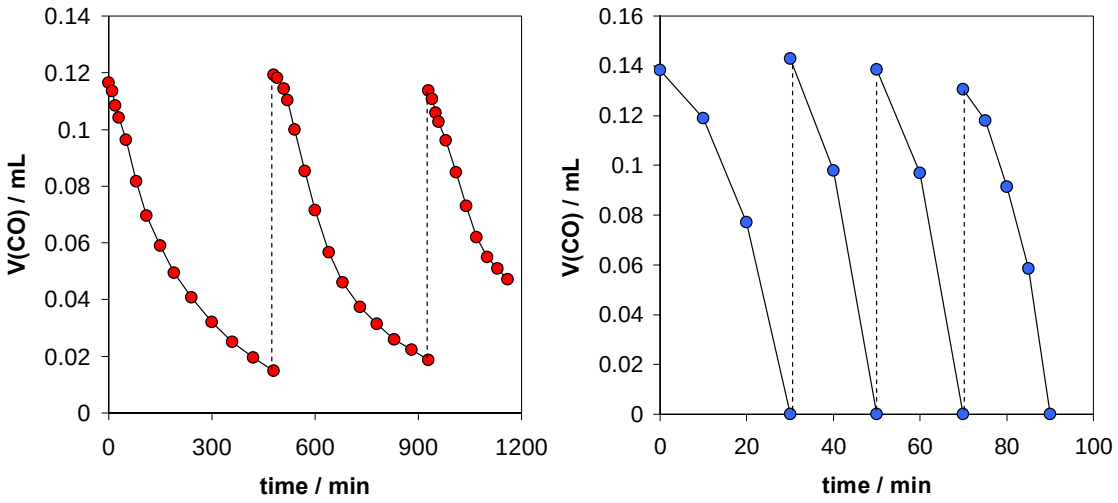

Figure 4-10 Repeated oxidation of CO with paste film (left) and Pt-paste film (right)

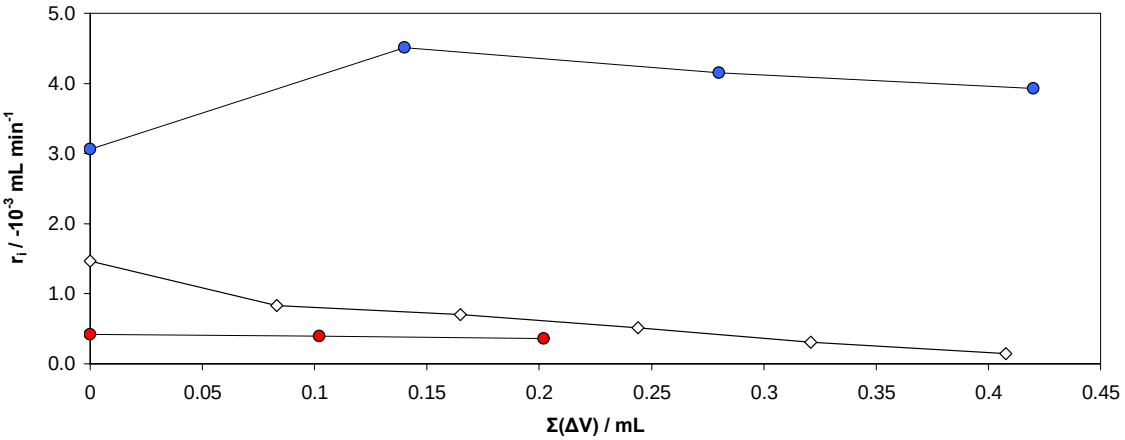

Figure 4-11 Initial PCO rate versus total volume of species oxidised for repeated use of substrate; (□) CO on Pt-paste, (Δ) CO on paste, (○) SO_2 on paste

4.4. EC, P(TFE-VE-PE) and Viton -TiO_2 films for CO removal

In order to investigate the possibility of creating flexible photocatalysts – using powdered titania dispersed into a polymer solution before casting into a film – ethyl cellulose (EC) was chosen as the starting point. EC has already been proven as a binder for oxygen-scavenging films containing titania[20]. The polymer-titania (10% w/v EC in a 4:1 mixture of ethanol and toluene, 10g of which was mixed with 1g of P25 or Pt-P25) films were spun onto 24 mm diameter glass cover slips, approximately giving a 1:1 ratio of EC to titania upon drying in the final film. The films were then placed directly into the end of a 5 cm quartz-bodied IR cell, acting as one of the windows through which the IR beam passed though. The photocatalytic activity (PCA) of these films was then assessed for the oxidation of carbon monoxide, and the results compared to titania-paste and platinised titania-paste films. A blank, consisting of a 100% EC film, produced no CO_2 during prolonged irradiation with UVA (in excess of 20 hours).

The rates of CO_2 production and the volume of CO_2 produced (Figure 4-12 and Figure 4-13) were in vast excess to that of CO oxidation for both photocatalyst-polymer films. This strongly implied that the polymer was being degraded by PCO. It was also observed that r_i (CO) increased with repeated use of the same film, shown in Figure 4-13, suggesting that PCO of the polymer binder was increasing the active area of the photocatalyst material. Irradiation to completion on the open bench left only a powdered catalyst film, easily rubbed off the glass backing. The initial rates of CO oxidation observed were very low for both P25 and platinised P25. Figure 4-13 illustrates the comparison with titania paste films, with EC/P25 approximately half as active for CO oxidation, whereas the EC/P25-Pt films were approximately 5 times less active than Pt-paste. EC/P25-Pt films were in the order of 4/5 times more active than EC/P25.

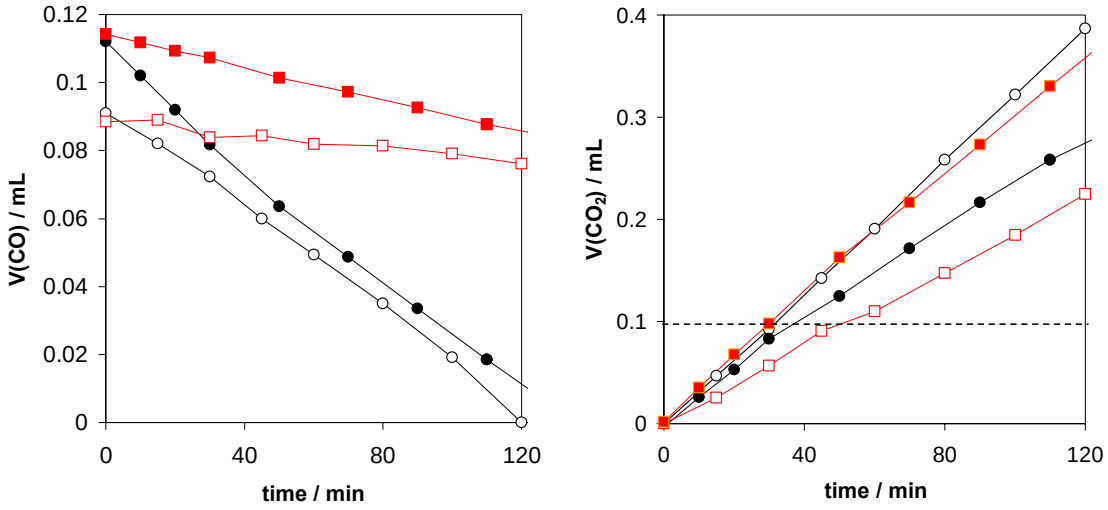

Figure 4-12 CO oxidation (left) and CO_2 production (right) for 1st (open) and 2nd (closed) use of EC/P25 (■, □) and EC/P25-Pt (●, ○) polymer-photocatalyst films under UVA irradiation. The dashed line indicates approximate CO_2 level for balanced stoichiometry

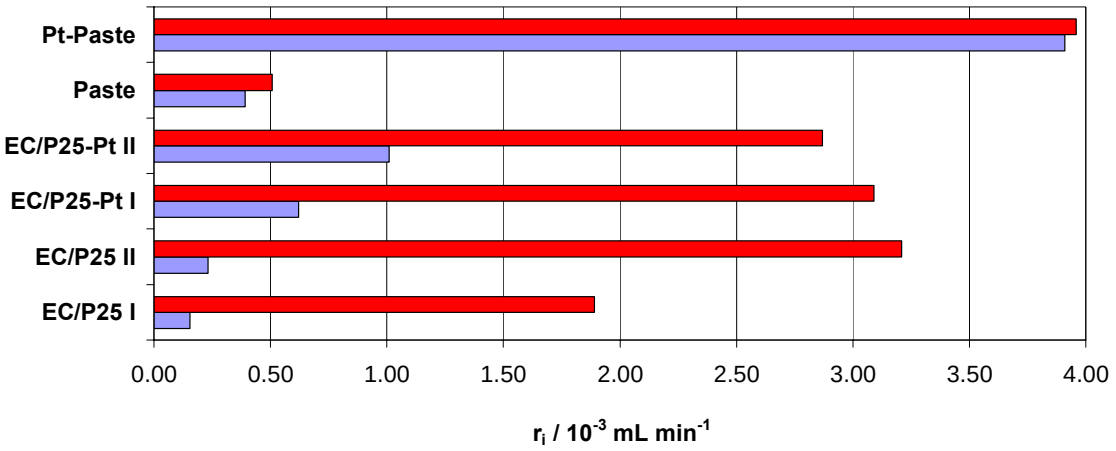

Figure 4-13 Initial rate of CO oxidation (blue) and CO_2 production (red) for polymer/TiO_2 films

---

The degradation of ethyl cellulose by SPC understandably meant it was an unsuitable polymer to bind the photocatalyst in possible flexible films. To this end the resistance of fluoropolymers to corrosion and thermal degradation should make them ideal for

polymer-based photocatalysts[23, 26]. For this work two solvent-soluble fluoropolymers were chosen; Poly(tetrafluoroethylene-co-vinylidene fluoride-co-propylene) P(TFE-VE-PE), sometimes referred to by its trade name Aflas® (Du Pont); and Viton F, a terpolymer of vinylidene fluoride, hexafluoropropylene and tertrafluoroethylene used for corrosion resistant gaskets and o-rings. The initial rates of identical testing to the EC/titania films using CO are shown in Figure 4-14. These indicated that films of both P(TFE-VE-PE)/P25 and Viton/P25 had little or no activity towards CO oxidation, and that the polymer was again rapidly degrading due to PCO. The platinised titania analogues of both polymer types also registered very low CO oxidation activity, if slightly improved in comparison to the non-platinised P25 films, whilst also being degraded by PCO. This set of experiments casts doubt over the suitability of solvent-soluble fluoropolymers for making photocatalyst films and also strongly indicates that illuminated titania is oxidising enough to degrade very stable polymers over long periods.

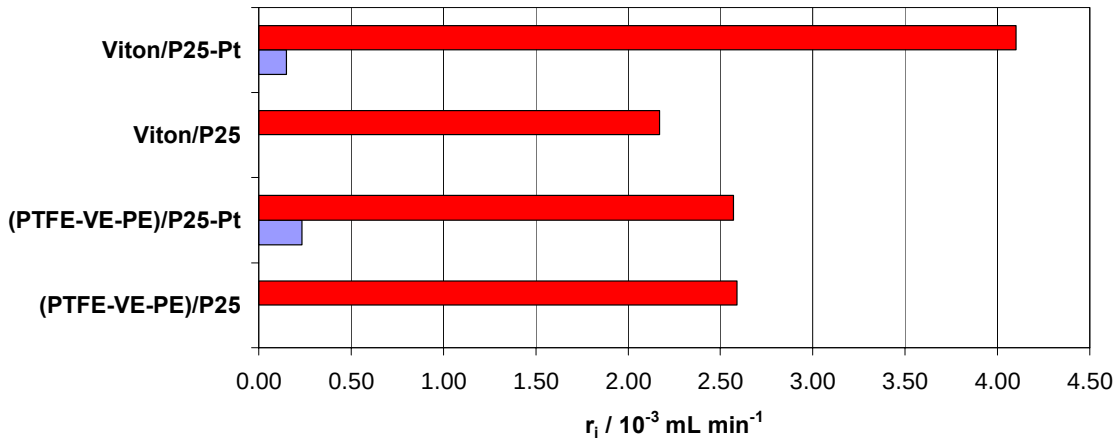

Figure 4-14 Initial rate of CO oxidation (blue) and CO_2 production (red) for fluoropolymer/titania films

4.5 Fluoropolymer [P(TFE-VE-PE), Viton and PTFE] destruction by PCO

As an extension to the previous section's work, during which it was observed that polymer-photocatalyst films of fluoropolymer/P25 mixtures were degraded by PCO, further work was carried out to determine the degradation products of these reactions. Direct FTIR monitoring of the polymer-photocatalyst films, and of the gas phase above these films, indicated that one intermediate produced during PCO of fluoropolymers was carbonyl fluoride, characterised by an absorbance stretch in the region 1875-2000 cm^{-1}, highlighted in the insets of Figure 4-15 and Figure 4-16.

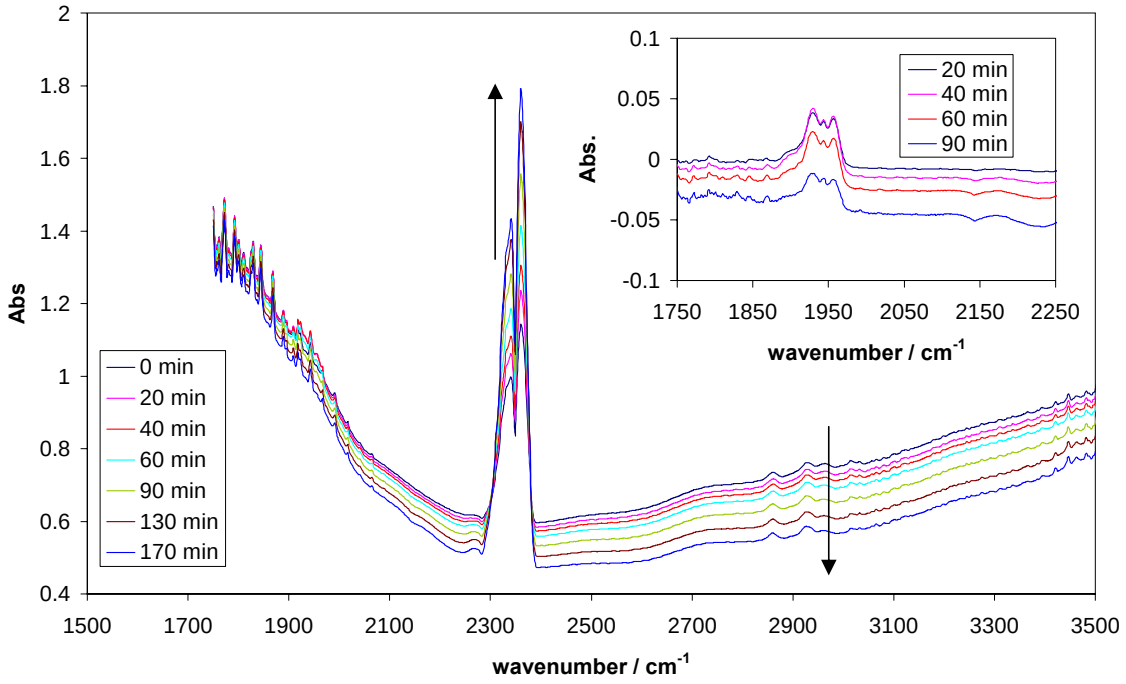

Figure 4-15 FTIR monitoring of p(TFE-VE-PE)-P25 composite film during UVA irradiation, and, inset, spectra of gas phase products of polymer/photocatalyst PCO

Carbonyl fluoride is the fluorine analogue of phosgene, a species observed as an intermediate during PCO of TCE[2, 59]. Both are highly toxic species. The carbonyl fluoride peaks were seen to decrease with irradiation time, suggesting that PCO can destroy the fluorinated intermediates produced, presumably leading to HF and CO_2, although long term irradiation of Viton films (>200 h) led to production of another gas-phase species (Figure 4-17).

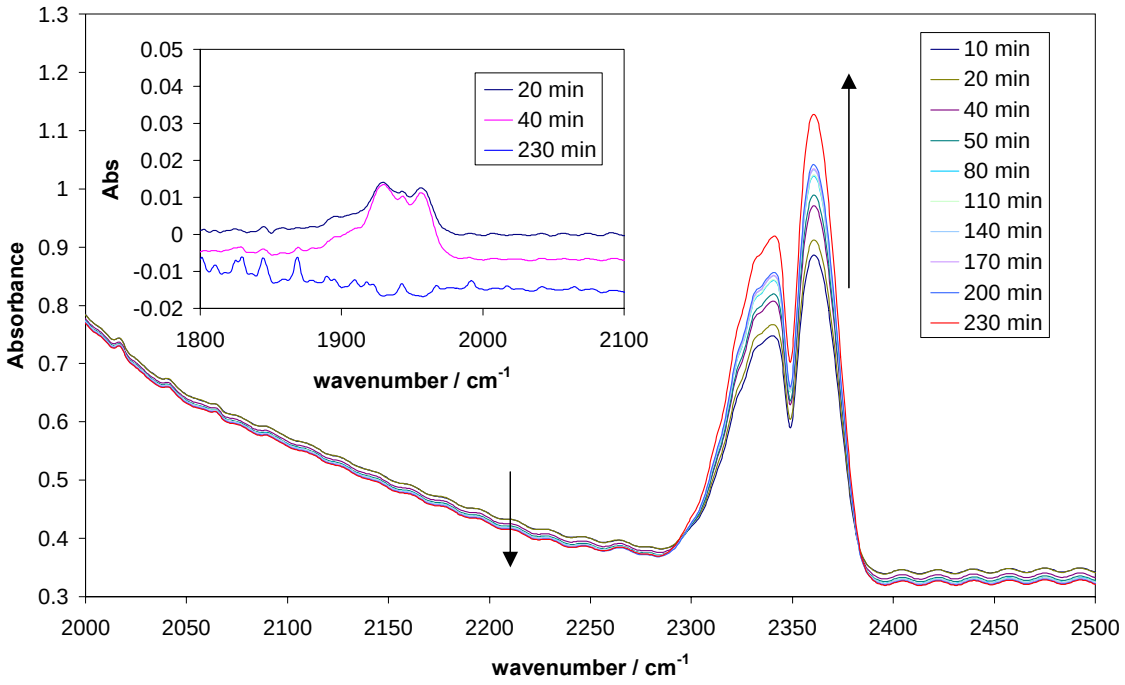

Figure 4-16 FTIR monitoring of Viton-P25 composite film during UVA irradiation, inset; gas phase products of PCO

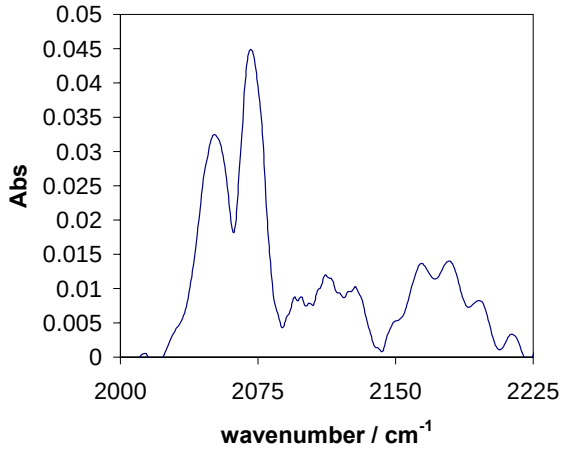

Figure 4-17 Initial spectrum subtracted from spectrum taken after 200 h irradiation in order to investigate gaseous products of PCO for Viton-P25 films

---

Irradiation of PTFE/P25 disks with UVA was seen to initiate degradation of the polymer, highlighted by a decrease in IR absorbance (Figure 4-18-A). Analysis of the gas phase showed production of carbon dioxide and carbon monoxide, with no indication of carbonyl fluoride. The same absorbance stretching observed for long-term irradiation of Viton (Figure 4-17) was observed for PTFE.

It is possible that during PCO carbonyl fluoride reacts with fluorine to produce CF_3OF [64], which has characteristic absorbance stretching in the region 2000 cm^{-1} – 2100 cm^{-1} [65]. This corresponds well with the spectra of Figure 4-17 and Figure 4-18-B. The possible production of CF_3OF appears to take a long periods of irradiation, and it is not possible to determine if this is a PCO-mediated or photolytic phenomenon, though it does appear to be at the expense of COF_2 and CO.

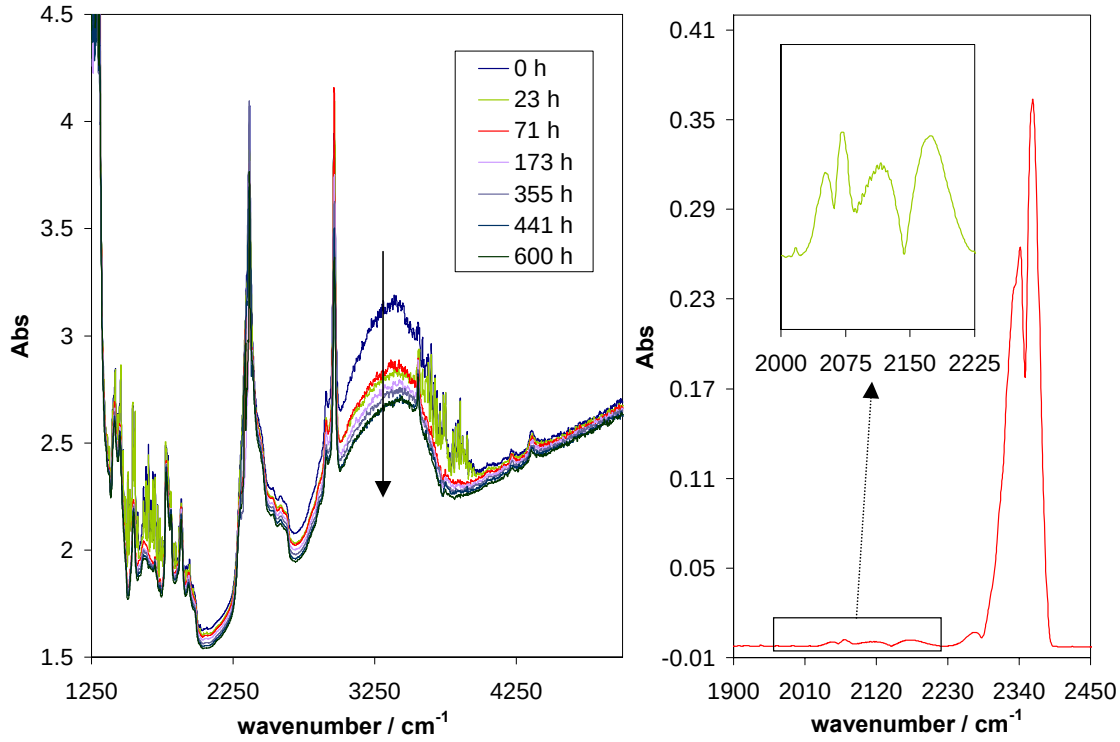

Figure 4-18 A: FTIR monitoring of PTFE destruction by PCO (left) and B: FTIR spectrum of gas-phase products observed after 330 h irradiation (right), with region 2000-2225 cm^{-1} expanded (inset)

4.6. Conclusions

In agreement with research by others carried out using powder films[55, 56], it was observed that sulfur dioxide was removed from the gas-phase by semiconductor photocatalysis, with the concomitant effect of deactivation of the photocatalyst. Deposited droplets of high acidity on the titania films used, as well as on the interior surfaces of the cell, indicated that the oxidation products were SO_3 and H_2SO_4. UVA irradiation of SO_2 without titania did not initiate photolysis, as was observed with a UVC source. It was possible to monitor photocatalyst activity as a function of total sulfur dioxide oxidised, with activity seen to decrease rapidly and be reduced by ten-fold after six repetitions. The films were regenerated by soaking and heating, with soaking

the more successful technique, suggesting that sulfate was also present as an oxidation product on the titania surface. A quantum efficiency value of 1.18% was estimated for the PCO of SO_2 on paste-titania during UVA illumination.

Platinised paste titania films were observed to removed CO as CO_2 at rates 10 times faster than non-platinised standard paste films. Significant deactivation was not observed for either type of film. Quantum efficiency values for these two systems were estimated to be 0.31% for CO removal by paste films, and 3.14% for Pt-paste films, both using UVA illumination. P25-titania-polymer and platinised P25-titania-polymer films were fabricated using ethyl cellulose, poly(tetrafluoroethylene-co-vinylidene fluoride-co-propylene) and Viton F. When tested for PCO activity using carbon monoxide as a model species, the platinised films were seen to oxidise CO, but at a very much reduced rate in comparison to platinised paste-titania films. Further to this, it was observed that PCO degrades non-fluorinated *and* fluorinated polymers. Carbon dioxide and carbon monoxide were determined as the major products of fluoropolymer PCO, but carbonyl fluoride was also initially observed for P(TFE-VE-PE) and Viton. It was also suggested that CF_3OF was being formed during long-term irradiation of both PTFE-P25 and Viton-P25 films, but whether or not this is a photocatalytic or photolytic process is unclear at this stage.

4.7 References

1 S. E. Manahan, *Environmental Chemistry*. Sixth ed.; Lewis: 1994.

2 M. R. Hoffman, S. T. Martin, W. Choi, and D. Bahnemann, *Chem. Rev.* **95**, 69 (1995).

3 EPA, *Fact sheet on the new ozone (smog) and particulate (soot) air quality standards*. 1997.

4 EPA, *IAQ: Sick Building Syndrome Factsheet*. 2005.

5 H. Johnstone, *Filtr. Sep.* **41**, (4), 18 (2004).

6 L. Frazer, *Environ. Health Persp.* **109**, (4), 174 (2001).

7 T. Ibusuki, and K. Takeuchi, *J. Mol. Catal. A Chem.* **88**, 93 (1994).

8 A. Mills, N. Elliott, I. P. Parkin, S. A. O'Neill, and R. J. Clark, *J. Photochem. Photobiol. A: Chem* **151**, 171 (2002).

9 A. Mills, S. K. Lee, A. Lepre, I. P. Parkin, and S. A. O'Neill, *Photochem. Photobiol. Sci.* **1**, 865-868 (2002).

10 A. Mills, A. Lepre, N. Elliott, S. Bhopal, I. P. Parkin, and S. A. O'Neill, *J. Photochem. Photobiol. A: Chem* **160**, 213 (2003).

11 A. Mills, J. Wang, M. Crow, G. Taglioni, and L. Novella, *J. Photochem. Photobiol. A: Chem* **187**, 370 (2007).

12 S. Ahmed, C. E. Jones, T. J. Kemp, and P. R. Unwin, *Phys. Chem. Chem. Phys.* **1**, 5229 (1999).

13 A. Mills, and J. Wang, *J. Photochem. Photobiol. A: Chem* **118**, 53 (1998).

14 A. Mills, and J. Wang, *J. Photochem. Photobiol. A: Chem* **182**, 181 (2006).

15 A. Mills, J. Wang, and M. Crow, *Chemosphere* **64**, 1032 (2006).

16 Y. Paz, Z. Luo, L. Rabenberg, and A. Heller, *J. Mater. Res.* **10**, (11), 2842 (1995).

17 N. Allen, M. Edge, G. Sandoval, J. Verran, J. Stratton, and J. Maltby, *Photochem. Photobiol.* **81**, 279 (2005).

18 R. Fretwell, and P. Douglas, *J. Photochem. Photobiol. A: Chem* **143**, 229 (2001).

19 A. Heller, *Accounts Chem. Res.* **28**, 503 (1995).

20 A. Mills, G. Doyle, A. M. Peiro, and J. R. Durrant, *J. Photochem. Photobiol. A: Chem* **177**, 328 (2006).

21 M. Minabe, D. A. Tryk, P. Sawunyama, K. Y, K. Hashimoto, and A. Fujishima, *J. Photochem. Photobiol. A: Chem* **137**, 53 (2000).

22 R. L. Pozzo, M. A. Baltanas, and A. E. Cassano, *Catal. Today* **39**, 219 (1997).

23 I. Sopyan, M. Watanabe, S. Murasawa, K. Hashimoto, and A. Fujishima, *J. Electroanal. Chem.* **415**, 183 (1996).

24 K. Scrivener, and H. Van Damme, *MRS Bull.* **29**, 308 (2004).

25 S. Cho, and W. Choi, *J. Photochem. Photobiol. A: Chem* **143**, 221 (2001).

26 J. D. Weir, D. Dimarzio, and R. G. Pirich, (2004).

27 D. Walton, and P. Lorimer, *Polymers*. 2000; Vol. 85.

28 P. Pichat, J.-M. Herrmann, H. Courbon, J. Disdier, and M.-N. Mozzanega, *Can. J. Chem. Eng.* **60**, 27 (1982).

29 J. Peral, X. Domenech, and D. F. Ollis, *J. Chem. Technol. Biotechnol.* **70**, 117 (1997).

30 R. M. Alberici, and W. F. Jardim, *Appl. Catal. B: Environ.* **14**, 55 (1997).

31 A. J. Maira, J. M. Coronado, V. Augugliaro, K. L. Yeung, J. C. Conesa, and J. Soria, *J. Catal.* **202**, 413 (2001).

32 I. Sopyan, S. Murasawa, K. Hashimoto, and A. Fujishima, *Chem. Letts.* **4**, 723 (1994).

33 H. Liu, X. Ye, Z. Lian, Y. Wen, and W. Shangguan, *Res. Chem. Intermed.* **32**, (1), 9 (2006).

34 D. V. Kozlov, A. A. Panchenko, D. V. Bavykin, E. N. Savinov, and P. G. Smirniotis, *Russ. Chem. Bull., Int. Ed.* **52**, (5), 1100 (2003).

35 S. T. Martin, A. T. Lee, and M. R. Hoffman, *Environ. Sci. Technol.* **29**, 2567 (1995).

36 W.-K. Jo, and K.-H. Park, *Chemosphere* **57**, 555 (2004).

37 A. Mills, and S.-K. Lee, *J. Photochem. Photobiol. A: Chem* **152**, 233 (2002).

38 A. Mills, S.-K. Lee, and A. Lepre, *J. Photochem. Photobiol. A: Chem* **155**, 199 (2003).

39 K.-C. Cho, K.-C. Hwang, T. Sano, K. Takeuchi, and S. Matsuzawa, *J. Photochem. Photobiol. A: Chem* **161**, 155 (2004).

40 D. W. A. Sharp, *Dictionary of Chemistry*. 2nd ed.; Penguin: 1990.

41 H. Einaga, M. Harada, S. Futamura, and T. Ibusuki, *J. Phys. Chem. B* **107**, 9290 (2003).

42 S. Hwang, C. Lee, and W. Choi, *Appl. Catal. B: Environ.* **46**, 49 (2003).

43 A. V. Vorontsov, E. N. Savinov, G. B. Barannik, V. N. Troitsky, and V. N. Parmon, *Catal. Today* **39**, 207 (1997).

44 H. vanDamme, and W. K. Hall, *J. Catal.* **69**, 371 (1981).

45 A. L. Linsebigler, G. Lu, and J. T. Yates, *J. Phys. Chem.* **100**, 6631 (1996).

46 World-Bank-Group, *Pollution Prevention and Abatement Handbook* **July 1998**,

47 S. Kato, Y. Hirano, M. Iwata, T. Sano, K. Takeuchi, and S. Matsuzawa, *Appl. Catal. B: Environ.* **57**, 109 (2005).

48 T. Kako, H. Irie, and K. Hashimoto, *J. Photochem. Photobiol. A: Chem* **171**, 131 (2005).

49 S. Kataoka, E. Lee, I. Tejedor-Tejedor, and M. A. Anderson, *Appl. Catal. B: Environ.* **61**, 159 (2005).

50 A. Kachina, S. Preis, and J. Kallas, *Environ. Chem. Letts.* **4**, (2), 107 (2006).

51 C. Guillard, D. Baldassare, C. Duchamp, M. N. Ghazzal, and S. Daniele, *Catal. Today*, (2007).

52 J. Peral, and D. F. Ollis, *J. Mol. Catal. A: Chem.* **115**, 347 (1997).

53 S. N. Frank, and A. J. Bard, *J. Phys. Chem.* **81**, (15), 1484 (1977).

54 A. Romero, G. Hernandez, and M. F. Suarez, *J. Chem. Ed.* **82**, (8), 1234 (2005).

55 J. Liqiang, X. Baifu, F. Y., W. Baiqi, S. Keying, C. Weimin, and F. Honggang, *Appl. Catal. A: General* **275**, 49 (2004).

56 J. Shang, Y. Zhu, Y. Du, and Z. Xu, *J. Solid State Chem.* **166**, 395 (2002).

57 C. H. Ao, S. C. Lee, S. C. Zou, and C. L. Mak, *Appl. Catal. B: Environ.* **49**, 187 (2004).

58 A. Vidal, and M. A. Luengo, *Appl. Catal. B: Environ.* **32**, 1 (2001).

59 J. R. Kittrel, C. R. Dupre, and D. A. Gerrish, *Remediation* **16**, (3), 81 (2006).

60 A. L. Linsebigler, G. Lu, and J. T. Yates Jr, *Chem. Rev.* **95**, 735 (1995).

61 C. H. Ao, and S. C. Lee, *J. Photochem. Photobiol. A: Chem* **161**, 131 (2004).

62 A. Mills, M. Crow, J. Wang, I. P. Parkin, and N. Boscher, *J. Phys. Chem. C* **111**, 5520 (2007).

63 E. V. Benvenutti, L. Franken, and C. C. Moro, *Langmuir* **15**, 8140 (1999).

64 M. Wechsberg, and G. H. Cady, *J. Am. Chem. Soc.* **91**, (16), 4432 (1968).

65 R. T. Lagemann, E. A. Jones, and P. J. H. Woltz, *J. Chem. Phys.* **20**, (11), 1768 (1952).

Chapter 5 Factors affecting wettability changes on titania

5.1 Introduction

Titanium dioxide films have been widely observed to become superhydrophilic, i.e. water droplet contact angle < 5°, when exposed to UV light, a phenomenon termed photoinduced superhydrophilicity (*PSH*)[1-7]. Its effects have been pivotal in the development of self-cleaning surfaces for glazing and other applications, but the precise mechanism by which this change is effected remains the subject of some debate. Although it is clear that *PSH* is initiated by the photogeneration of electron/hole pairs and their migration to the surface. The kinetics of hydrophilic conversion are also yet to be fully elucidated, being inextricably linked to the changes in surface energies and therefore an intrinsic part of any discussion of mechanism. An essential feature of the overall *PSH* phenomenon is not only the initial photoinduced hydrophobic to hydrophilic change, but also the reverse dark process, whereby a superhydrophilic titania film recovers its original hydrophobic form. Any mechanism of *PSH* must embrace both the light-induced superhydrophilic process and the dark hydrophobic-recovery step. In 1985 Kume and Nozu of Nihon Itagarasu, Japan reported that sheet glass coated with TiO_2 had the ability to stay clean by *"…rapidly and automatically decomposing and removing organic stains adhered to the glass surface…"*[8] Part of their patent application centred on the observation that the contact angle made by a water droplet on the glass was reduced as a function of UV irradiation time. This appears to be the first clear claim of a *PSH* effect relating to titania films on glass and was attributed to the photocatalyst removing the hydrophobic organic stains on the surface, via the well-established, photocatalytic oxidative (*PCO*) process, equation 5-1.

$$\text{organic} + O_2 \xrightarrow[h\nu \geq 3.2\text{eV}]{TiO_2} \text{minerals (such as } CO_2 \text{ and } H_2O) \qquad (5\text{-}1)$$

In contrast, in 1997, Wang et al[6] – reporting on the UV-induced hydrophilic conversion of TiO_2/SiO_2 films – proposed that the effect was not due to *PCO*, but rather by a photoinduced surface re-organisation (*PISR*), summarised in Figure 5-1. In this mechanism water is dissociatively adsorbed at surface defects created by UV light[9]. The defects, it was suggested, were formed by the trapping of holes at bridging oxygen lattice points close to the surface, the Ti^{4+} sites being reduced to Ti^{3+} by the electrons and oxygen atoms being ejected to form vacancies[10]. The oxygen vacancies were thought to cause an increase in the adsorbed hydroxyl group density and lead to the formation of hydrophilic regions. Storage in the dark, in the presence of oxygen, was thought to 'heal' the defects, replacing the chemisorbed hydroxyl groups with oxygen and so returning the surface to its original hydrophobic state.

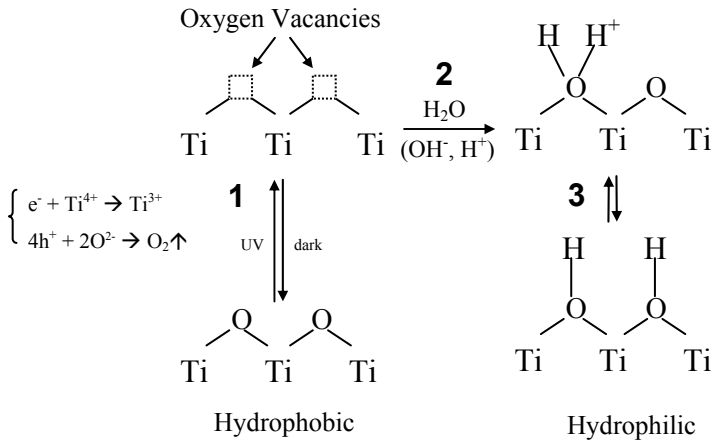

Figure 5-1 *PISR* mechanism of *PSH* on TiO_2; whereby surface defects are generated by UV exposure (**1**) leading to dissociative adsorption of H_2O (**2**) and reversible formation of hydrophilic state (**3**)[10]

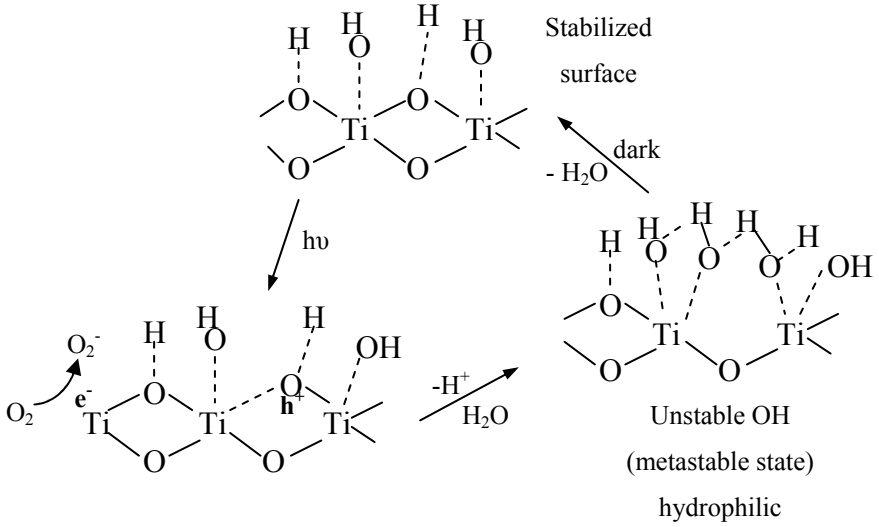

Figure 5-2 Schematic of alternate *PISR PSH* mechanism; ultra band-gap irradiation causes elongation of Ti–O bonds and reversible formation of a metastable state via adsorption of molecular water[11]

A further *PISR* mechanism was proposed by Sakai et al in 2003[12], this version involved the photoinduced absorption of H_2O as a result of Ti–O lattice bond elongation. This model was further refined to include the trapping, and exchange with ambient O_2, of electrons at Ti atoms[11] (Figure 5-2). Both *PISR* mechanisms have the surface hydroxyl density as the hydrophilicity-defining parameters, with increases in OH density the root cause of *PSH*.

The photo-induced surface reorganisation models of *PSH* have received support from a number of studies. The formation of surface defects was supported by the examination of Ti^{3+} defect creation on single-crystal rutile TiO_2 using X-ray photoelectron spectroscopy (XPS)[13]. FTIR measurements were also interpreted as showing that anatase TiO_2 reversibly adsorbs water as a result of UV irradiation[10] and AFM studies highlighted apparent 'roughening' of the surface as a result of UV exposure (attributed to defect formation)[14]. The importance of bridging oxygen atoms, an integral part of the *PISR* model, has also been illustrated using rutile single crystals, with the (001) face,

which does not feature bridging oxygen, showing the least propensity to photoinduced hydrophilic change[10, 15].

Recently, support for the more simplistic *PCO* model of *PSH*, based on equation 5-1 (namely the photocatalytic removal of hydrophobic organic surface contaminants) has increased, with a number of different groups reporting evidence for this model using test hydrophobic surface contaminants, such as trimethyl acetate[16] and hexane[17], and the detection of previously unobserved layers of hydrocarbons on titania surfaces[18]. Support for *PCO* over *PISR* has also been garnered by investigation of the effect of thermal treatment on the surface hydroxyl character of SiO_2 and TiO_2[19]. XPS monitoring of hydrocarbons on titania before and after a number of different pre-treatment techniques (rinsing with distilled water; rinsing with 2M NaOH; calcination at 723K; UV irradiation) also strongly suggested that removal of hydrocarbons was closely linked to changes in contact angle[20].

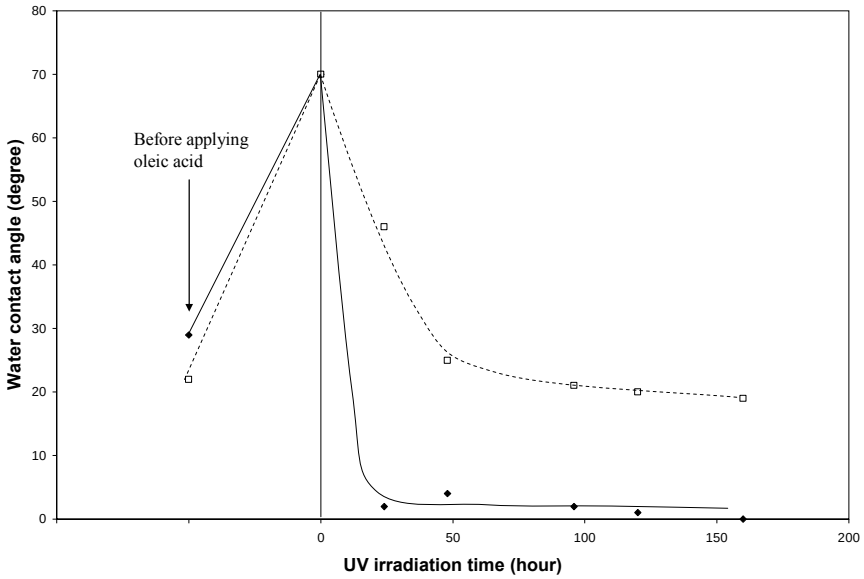

Figure 5-3 time dependence of water contact angle under UV irradiation, after applying oleic acid to the surfaces of TiO_2 (♦) and $SrTiO_3$ (□). UV irradiation was 1mW/cm^{-2} under ambient conditions[21]

It has been suggested that the *PISR* mechanism is specific to only a few materials, of which titania is most notable; for example it is not exhibited by silica substrates. Of the metal oxides which have been shown to initiate photocatalytic processes i.e. TiO_2, ZnO, $SrTiO_3$ and SnO_2, only TiO_2, ZnO and SnO_2 have also been shown to undergo *PSH*[3]. It is the example of $SrTiO_3$ which is often used as evidence *against* the *PCO* mechanism. As shown in Figure 5-3, oleic acid deposition increases the *CA* for both TiO_2 and $SrTiO_3$, the *CA* is then observed to decrease with illumination as the compound is mineralised, but whereas *CA* falls to <5° for TiO_2, the *CA* for $SrTiO_3$ returns to the pre-deposition value[21]. This, along with metal oxide films which display *PSH* but no photocatalytic activity i.e. WO_3, V_2O_5, highlights the complexity of the subject and also the importance of film production method when comparing films of different materials[3, 5, 21].

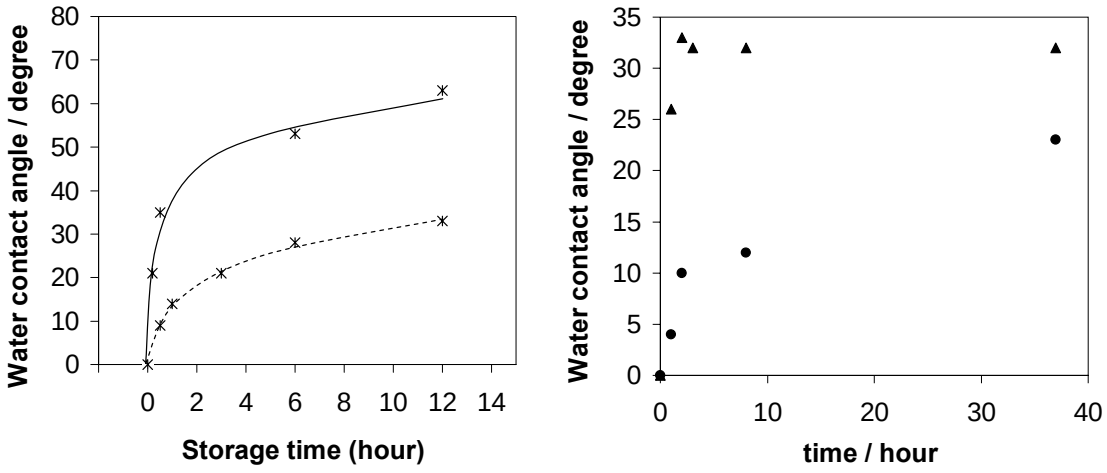

Figure 5-4 (left) variation of water *CA* of a highly hydrophilic TiO_2 (110) single crystal upon storage in air (dashed) and oxygen (solid)[15], and (right) variation of water *CA* on highly hydrophilic TiO_2 surface in the dark in a vacuum (▲) and ambient conditions (●)[11]

As noted earlier, key to any model of *PSH* is an explanation of the dark recovery step. Thus, significant support for the *PISR* model of *PSH* has been provided by studies of this process[10, 11, 22], effectively a dehydration step (see Figure 5-1 & Figure 5-2), with the

observation that titania films regain their original hydrophobicity at an increased rate when stored at increased temperatures[22, 23], or under an evacuated (H_2O free) atmosphere, Figure 5-4[11]. The *PISR* model rationale behind these phenomena is that heat and vacuum cause the meta-stable water/hydroxyl groups, responsible for the superhydrophilic surface of titania, to dissociate more quickly. Of course the proponents of the *PCO* mechanism would claim that the surface is merely being recontaminated by airborne organic species. It has also been claimed that hydrophilic TiO_2-glass films exhibit a measurable increase in contact angle when subjected to ultrasound[24]. The use of ultrasound to render a superhydrophilic film slightly more hydrophobic was interpreted initially by the proponents of *PISR* as being due to the re-oxidation of the surface by sonically-produced OH radicals[24], but more recently as simply the breaking down of the photo-induced hydrophilic meta-stable state by an external stimulus[22]. A similar interpretation has been used to explain the effect of wet-rubbing[25], which re-converts superhydrophilic titania to its original hydrophobic state.

To this point hydrophobic conversion has been simply described as the condition whereby water contact angle falls to below 5° with ultraviolet illumination, though there appears to be much information about the mechanism of *PSH* to be gained through the investigation, and modelling, of the kinetics. The two distinct methodologies which are employed in the analysis of *PSH* kinetics both involve taking a succession of still images from which the *CA* can be measured. The distinction centres on the deposition of the droplet; for *in-situ* analysis (the method used most commonly throughout this work) after deposition, the same droplet is observed during the full period of illumination[16, 17]. The second, and to date more common[10, 12, 26-28] method sees the repeated cycle of droplet deposition, *CA* measurement, and the droplet removal, between periods of illumination.

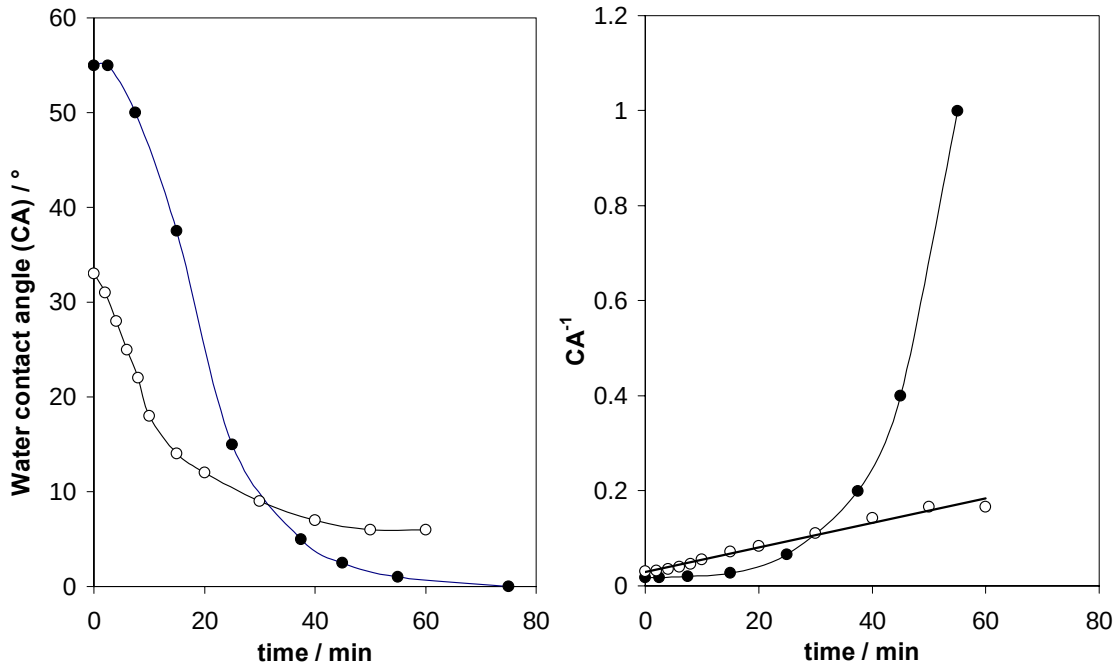

Figure 5-5 Time dependence of (left) water *CA* on TiO_2 films under UV illumination with varying light intensities, showing non-hyperbolic (● 0.1 mW cm^{-2})[5] and hyperbolic (○ 0.2 mW cm^{-2})[12] *CA* vs. time profiles and (right) reciprocal of *CA* versus time for same intensities

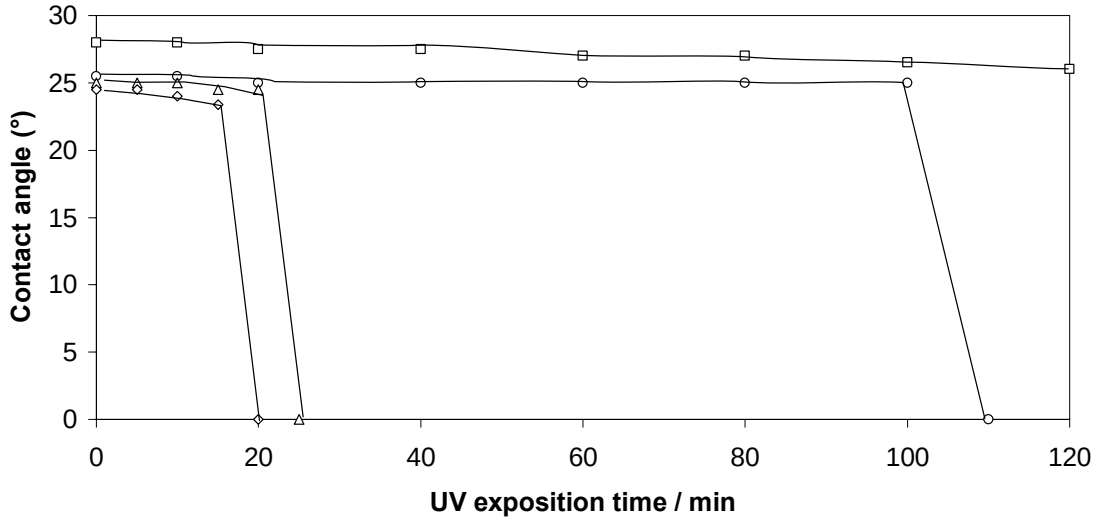

Figure 5-6 Example of 'sudden wetting' of water droplets on sol-gel derived films under UV irradiation, and effect of film thickness (□ = 8 nm, ○ = 15 nm, Δ = 40 nm, ◊ = 160 nm) on elapsed time before wetting[1]

There are two commonly observed types of *CA* versus irradiation time profile; hyperbolic and non-hyperbolic. Both types of profile, depicted in Figure 5-5, are observed for both *in-situ* and *repeated deposition* monitoring. Non-hyperbolic profiles commonly feature a 'delay' type phenomenon. During this delay the contact angle decreases only slowly for a period, before falling more rapidly (Figure 5-5 and Figure 5-6). Hyperbolic profiles do not feature any such delay feature; with *CA* falling immediately after irradiation is commenced. With the more recent increase in *in-situ* style analysis a further class of non-hyperbolic profile has been observed. This type features a more pronounced delay, during which only evaporation causes change in *CA*, followed by very sudden wetting of the droplet across the surface[1] (Figure 5-6). This type of profile has also been observed with model organic layers of hexane[17]. Studies have found the rate of hydrophilic change to be dependant on light intensity[24]. Further work has demonstrated that the profile of contact angle versus irradiation time was dependant upon the photonic absorptivity of the substrates. Thick (8 μm) sol-gel paste films displayed hyperbolic profiles[29, 30], characterised by a linear plot of the reciprocal of the contact angle versus time[12], see Figure 5-5 and very thin (15 nm) films coated by CVD gave non-hyperbolic profiles[29], as did moderately thick (0.4 μm) films under low (0.1 mW cm^{-2}) UV intensity[5]. It was suggested that this non-hyperbolic behaviour could be due to a preliminary surface-conditioning process, possibly the removal of low levels of organic impurities[29].

There have been two notable attempts to model the kinetics of *PSH* algebraically. The first uses the reciprocal of the *CA* plotted against irradiation time which was shown to give a straight line through the initial part of the profile and the slope of this segment is defined as the hydrophilic conversion rate (k_f)[12]. k_f was found to be a function of incident UV intensity, with 0.4 mW cm^{-2} found to be the boundary value between two linear regions of a log-log plot of k_f versus incident UV intensity. The second kinetic model used the same data as the work of Sakai et al[12], but was based upon Young's equation[31, 32] (see section 1.5, equation 1-7) and used the cosine of the *CA* rather than the

reciprocal[28]. Both models include discussions of the reverse reaction and attempted to overcome issues deriving from inconsistent initial *CA* values.

These observations (the effect of light intensity on *PSH*, the use of a model contaminant layer, and utilisation of pre-treatments to render surfaces hydrophilic) along with the discussions on recovery of hydrophobicity, the effect of droplet and atmospheric composition on *PSH*, and the role of electron acceptors in *PSH*, form the starting point of this investigation into *PSH*.

5.2 Experimental

5.2.1. Substrates

Descriptions of the substrates used i.e. thick sol-gel films, Activ™ titania-coated glass, and microscope slide blanks, and preparation/cleaning methods are contained in sections 2.1.2. and 2.1.3.

5.2.2. Measurement of Contact Angle

The two methods used to assess changes in contact angle i.e. *repeated deposition* and *in-situ*, are detailed in sections 2.5.1. and 2.5.2.

5.2.3. Variation of Atmospheric Composition

When in use, the sealed environmental chamber apparatus allowed control of the gas-phase surrounding the observed water droplet. The standard setup, as described in section 2.5.2, used for all *in-situ* experiments unless otherwise stated, featured 100 mL min^{-1} flowing oxygen, bubbled through a dreschel bottle to attain 100% relative humidity. For the variation of atmospheric composition the oxygen stream was either

replaced with nitrogen, or an ozone generator was attached in-line. Before deposition the water droplet was held at the end of the syringe for 10 minutes with the gas flowing through the cell in order to flush any dissolved gas species from the water.

5.2.4. Variation of Droplet Composition

For the investigation into the possible incorporation of a sacrificial electron acceptor into the deposited water droplet, 0.1M solutions of potassium chloride, sodium persulfate and sodium dithionite (all supplied by Aldrich) were used.

5.2.5. Substrate Illumination in Solution

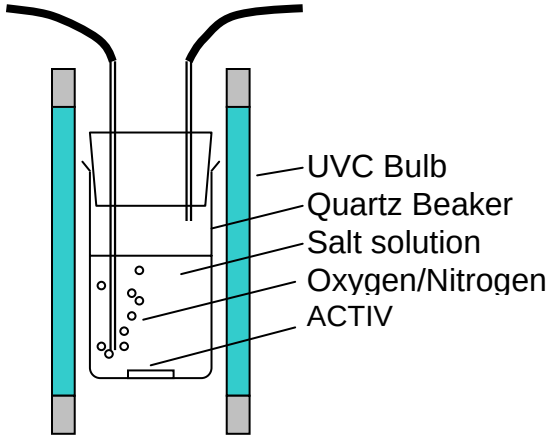

Figure 5-7 Diagram of setup used for the UVC illumination of a titania substrate in an oxygenated or deoxygenated solution of KCl or $Na_2S_2O_8$

In order to irradiate a titania substrate in oxygenated and deoxygenated solutions of potassium chloride or sodium persulfate, a 500 mL quartz beaker, fitted with a removable bung closure with gas inlet and outlet (Figure 5-7) was utilised. The irradiation sources were two 2 × 8W mercury discharge UVC lamps. Initially hydrophobic samples were placed in the beaker followed by the salt solution and oxygen

or nitrogen bubbled through for 1 hour before commencement of illumination. After irradiation the samples were removed, washed with DI water, dried in a clean gas stream, and the *CA* measured in triplicate.

5.2.6. Model Contaminant Deposition – Stearic Acid

The stearic acid (SA) model contaminant layer deposition is described in further detail in 2.3.2.4 with the description of the method for monitoring the layer by FTIR also included.

5.2.7. Pre-treatment techniques

Substrates were pre-treated by three methods: UV/ozone exposure, heat treatment, and acid deposition. Both plain glass and Activ glass were rendered superhydrophilic by pre-treating with UVC/ozone, effected by irradiation with 2×6W UVC (254 nm) bulbs (Vilber-Lourmat), irradiance ~1 mW cm^{-2}, in a water-saturated, i.e. 100% relative humidity (RH), oxygen atmosphere containing ~1700 ppm ozone, produced by a corona-discharge ozone generator (OZ500, Dryden Aqua). Other pre-treatment methods used included a heat-treatment process, using a muffle-furnace, in which the samples were kept at the desired temperature for 1 hour before removing to cool to room temperature in a covered Petri dish. Aqua regia was also used as a pre-treatment method and involved immersing the samples for 1 hour in the aqua regia before being removed, rinsed with doubly-distilled, deionised water and dried in a compressed air stream

5.2.8. Recovery of *CA* – Storage Experiments

For recovery experiments, samples were rendered superhydrophilic by the same UV/ozone pre-treatment method described above (section 5.2.7). The study of the kinetics of contact angle recovery of samples held under vacuum was carried out using a vacuum desiccator connected to a vacuum line. Non-covered samples were simply left on the bench top in a light-free laboratory. For the investigation of ultrasonic (US)

recovery, samples of superhydrophilic Activ™ or glass were immersed in doubly-distilled, deionised water and placed in a US bath (VWR model: USC100T). All glassware for this section was thoroughly cleaned with chloroform and rinsed with water before use. Sample handling was carried out using plastic forceps and the samples were dried with compressed air from a cylinder.

5.3 Results and Discussion[33, 34]

5.3.1. In-situ monitoring of contact angle; effect of UV type

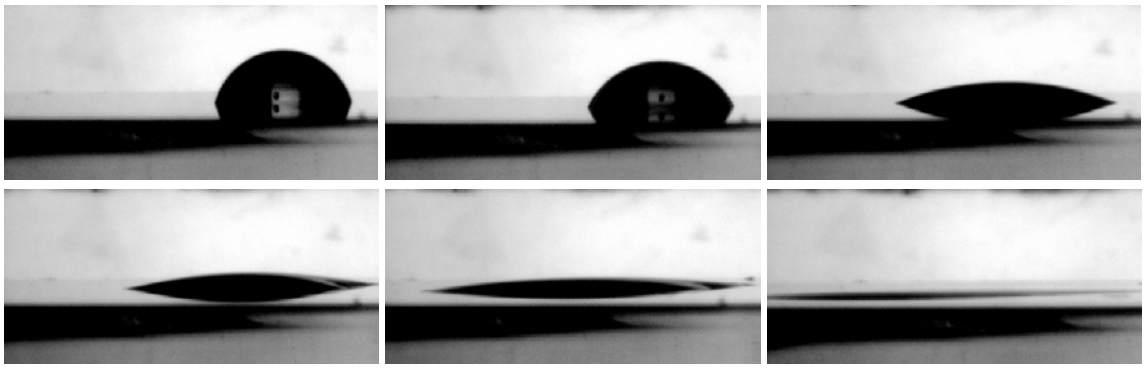

Figure 5-8 Images of water droplet on Activ sample after (from top left) 0, 6, 12, 15, 18 and 20 minutes' UVC irradiation; I_{UVC} = 0.5 mW cm^{-2}

In order to take a different approach to investigating PSH, a series of experiments were designed which permitted monitoring of water-droplet contact angle (*CA*) during irradiation, with a water droplet *in-situ* (continuous monitoring), rather than droplets being deposited and removed in between periods of irradiation (discontinuous monitoring). Figure 5-8 features a series of images taken during the irradiation of a square of Activ titania-coated glass which had a water droplet (5 μL) deposited onto the surface. The droplet was seen to slowly spread across the surface before a critical point (be it the *CA*, diameter, circumference, or another factor) was reached and the droplet spread rapidly, the angle falling to <5°.

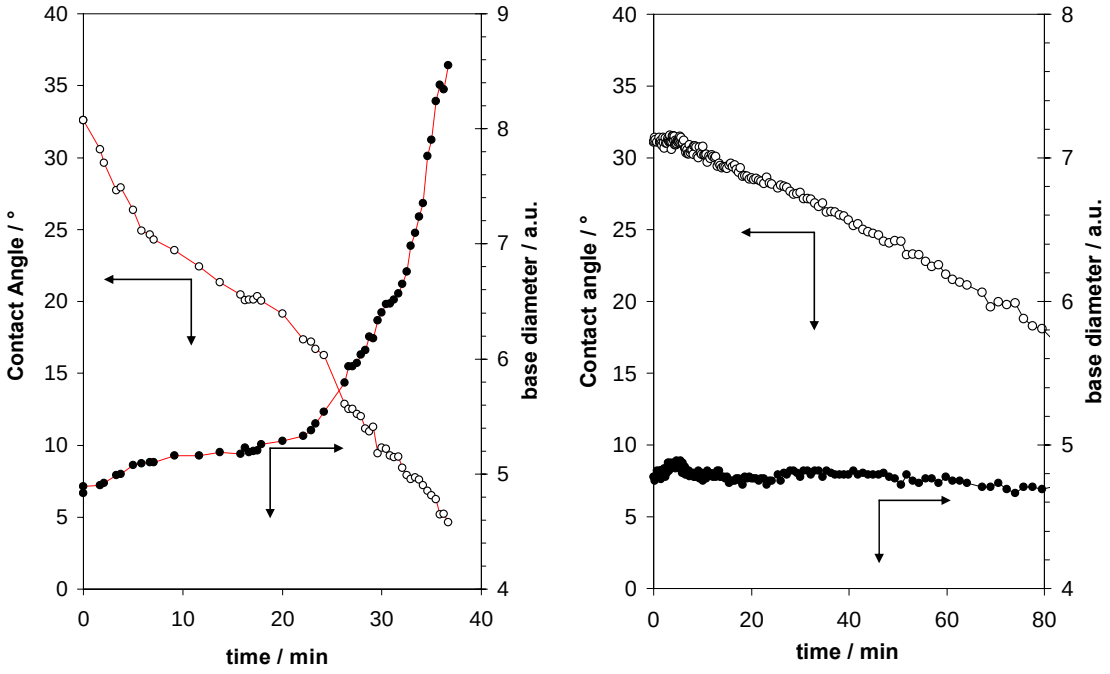

Figure 5-9 *CA* vs. irradiation time and base diameter vs. irradiation time for titania paste film (left) and plain glass (right). I_{UVC} = 0.5 mW cm^{-2}

Preliminary studies on a titania paste film showed *CA* to fall rapidly, but use of a plain glass blank also indicated that evaporation of the droplet (Figure 5-10B) could give the impression of *PSH*. Analysis of the base diameter of the droplet (Figure 5-10B) clearly indicated no spreading, whereas with titania-paste films the diameter is seen to increase steadily throughout irradiation. This was a key observation in distinguishing between *PSH* and evaporation, and led to the employment of an environmental chamber with water-saturated gas flowing through the cell throughout irradiation. This, along with a small fan included to cool the lamp employed as the irradiation source, allowed the deposited droplets to be monitored during illumination with limited evaporation.

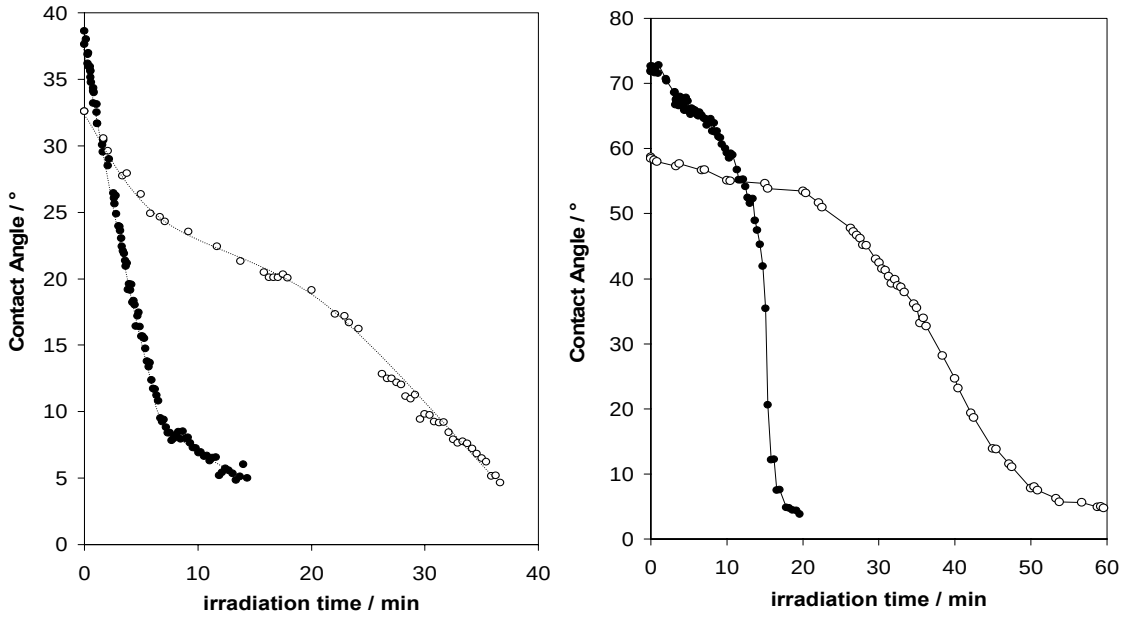

Figure 5-10 *CA* vs. irradiation time for A: titania paste films (left) and B: Activ films (right) under UVA (open) and UVC (closed) irradiation, $I_{UVC/UVA}$ = 0.5 mW cm^{-2}

A quartz window had been fitted into the top of the environmental chamber to allow irradiation by UVA and UVC sources. A comparison of *PSH* profiles during each type of irradiation for paste and Activ samples (Figure 5-10) showed much more rapid hydrophilic conversion occurring with UVC. Initial rates of *PSH*, calculated from the profiles displayed in Figure 5-10, for Activ-UVC (r_i = 1.38 °min^{-1}) Activ-UVA (0.27 °min^{-1}) paste-UVC (4.50 °min^{-1}) and paste-UVA (1.28 °min^{-1}) support this observation. This is consistent with titania films having higher absorptivity in the UVC region than UVA[2, 26, 29]. An interesting feature of this work are the 'delays' observed in both the *CA* vs. irradiation time profiles for Activ™, illustrated in Figure 5-10, when using UVA or UVC light. For UVA, the fastest rate of change of *CA* ($-r_{max}$) is 2.0 °min^{-1} but the time at which this occurs, around the time of the rapid spreading of the droplet, was after ~35 min UV irradiation. With UVC irradiation the fastest rate of change of *CA* ($-r_{max}$) is 22.4 °min^{-1} and the rapid photoinduced conversion of the titania surface began after only ca. 10 minutes.

The profiles are consistent with the idea of an initiation period before more rapid wetting occurs. Previous work[29] suggested that these non-hyperbolic profiles were due to a preliminary surface conditioning, possibly the removal of low levels of organic impurities, which are significant at low intensities of UV light or with very thin films[1, 10, 35]. The 'delay' observed for ACTIV when irradiated by UVA does appear to suggest that such a long-lived phenomenon might be occurring, rather than the surface restructuring mechanism described earlier. The profile also fits with the 'sudden wetting' which follows an induction period, described when using hexane as a model contaminant[17].

It appears likely that $-r_{max}$ and the delay time (δ), before a rapid decrease in *CA* as a function of illumination time, are negatively correlated in some way, with the larger the r_{max} value the lower the value of δ. Clearly both *CA* vs. time profiles for Activ illustrated in Figure 5-10 are decidedly non-hyperbolic in shape, which is typical of a low-activity titania photocatalyst film. The hyperbolic profiles observed for paste films are, again, indicative of the type of film under test. In this case no delay is observed for either UV-type, a feature characteristic of high-activity (thick) films.

5.3.2. Variation of atmospheric composition – O_2, N_2 and O_3

Using the environmental cell the influence of atmospheric composition was then investigated. As shown in section 5.3.1, in an oxygenated atmosphere *PSH* occurs for water droplets on both paste and Activ substrates under both UVC and UVA irradiation. When the cell was flushed with a water-saturated nitrogen gas stream before commencement of UVC irradiation, no *PSH* effect was observed for either type of substrate, illustrated in Figure 5-11, which is in agreement with recently published results of others[17]. This observation highlights the need for oxygen, or some other sacrificial electron acceptor, for *PSH* to proceed, a feature that is common to both major *PSH* mechanistic theories.

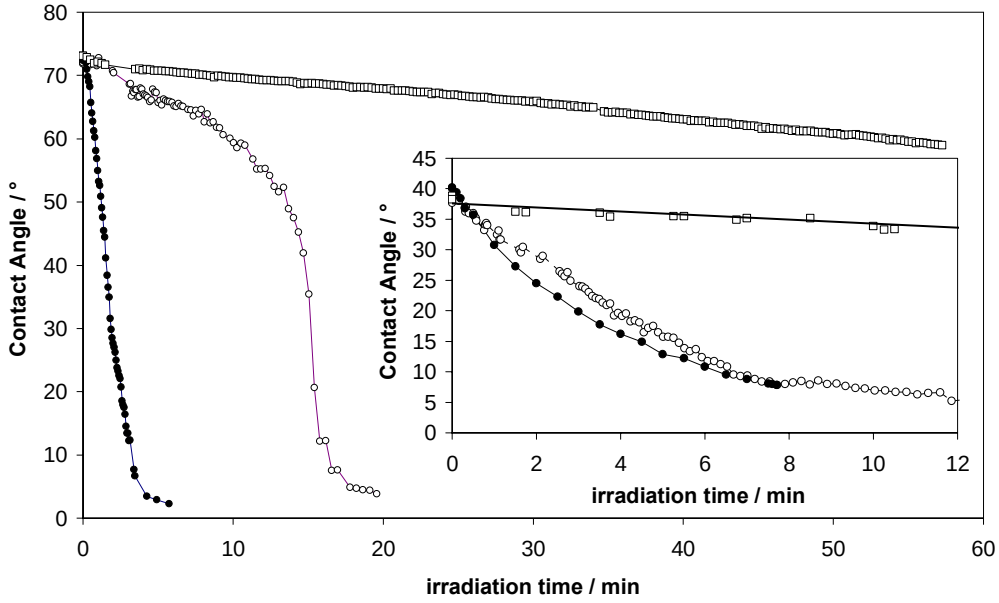

Figure 5-11 *CA* vs. UVC irradiation time for Activ films under water-saturated nitrogen (□), oxygen (○) and ~1700 ppm ozone (●) atmospheres; and (inset) paste-titania films under nitrogen (□), oxygen (○) and ozone (●) atmospheres; I_{UVC} = 0.5 mW cm^{-2}

Another set of experiments also utilised the chamber, but this time it was flushed with an oxygen stream that also contained ~1700 ppm of ozone. Upon irradiation with UVC *PSH* was seen to occur more rapidly for the Activ substrate, whilst *PSH* appeared to already be at a maximum on paste films. Short wavelengths of UV light are well known to both produce (at 198 nm) and electronically excite (at 254 nm) ozone[36, 37]. Electronically excited ozone can be used to scour organic contaminants from semiconductor surfaces, the suggestion here being that the combination of UVC and ozone is removing adventitious, hydrophobic organic material from the surface. In effect cleaning the surface and causing the hydrophilic change. UVA irradiation does not excite ozone, yet illumination of both Activ and paste films in the ozone-containing atmosphere with a UVA source was seen to initiate *PSH*. The effect of the presence of O_3 markedly reduces the time taken to render the surface hydrophilic; for Activ from ~55 min to <5 min and from ~38 min to ~8 min for paste films. The conclusion which

can be drawn from this is that ozone is acting as a more efficient electron acceptor than oxygen. This suggestion is not without precedent, as ozone in combination with UVA light has been shown to increase the rate of the photocatalytic decomposition of toluene[38].

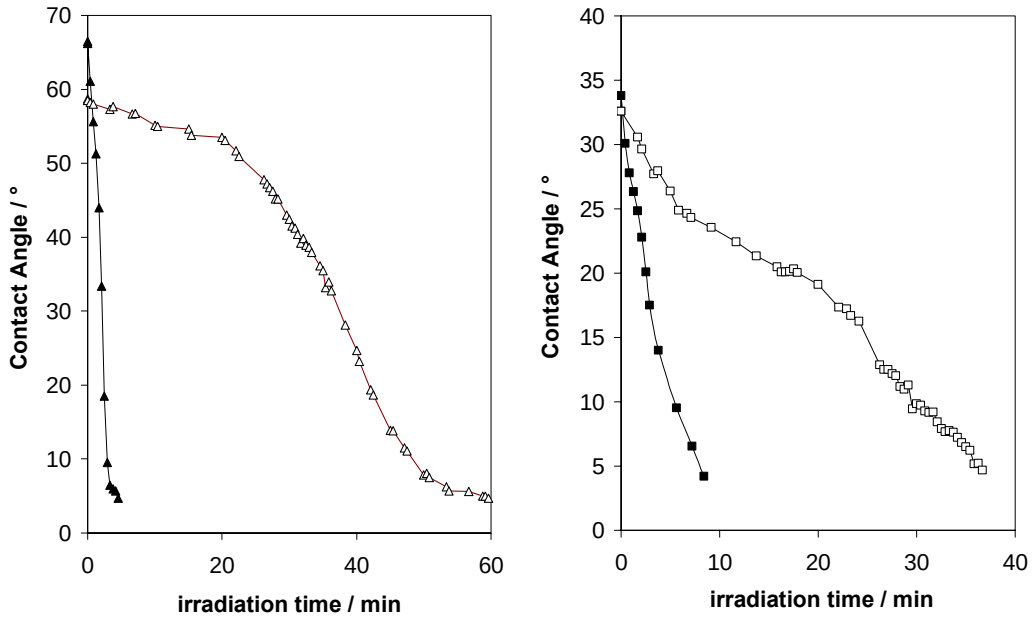

Figure 5-12 *CA* versus UVA irradiation time for (left) Activ and (right) titania-paste films in water-saturated oxygen (open) and ozone (closed) atmospheres; I_{UVA} = 0.5 mW cm^{-2}

A further confirmation of this electron-acceptor effect is provided by the combination of UVC-O_2/O_3 and UVA-O_2/O_3 on a water droplet resting on a plain glass substrate (Figure 5-13). In this case no *PSH* effect is observed for UVA-O_2/O_3, whereas the shorter wavelength radiation provides a false-positive for *PSH* as the electronically-excited ozone removes surface organics.

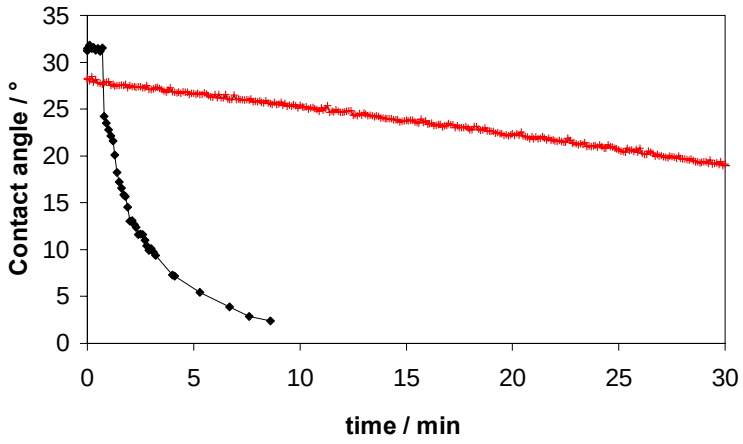

Figure 5-13 *CA* versus irradiation time for plain glass in O_2/O_3 atmosphere with UVC (black) and UVA (red) irradiation

---

5.3.3 Effect of UV intensity on rate and *PSH* parameters

In literature it has been suggested that *PSH* activity is analogous to SPC activity, in that it is a function of the substrate's absorptivity of ultra-bandgap irradiation[5, 29, 30]. Therefore it can be expected that thin films, of low absorptivity, will undergo hydrophilic change at reduced rates compared to thick films, of higher absorptivity. The hyperbolic and non-hyperbolic profiles observed are indicative of what is essentially a 'path-length' phenomenon, whereby, in accordance to Beer's law, increasing path-length (film thickness) is directly related to absorbance, and therefore activity.

In order to investigate this phenomenon further, and to possibly determine a relationship/relationships between the delay time (δ), the maximum rate (r_{max}) (features observed previously in section 5.3.1.) and incident UV intensity (I), the hydrophilic change of paste films and Activ samples was monitored at varying light intensities. Two sets of samples, one of paste-titania films and one of Activ glass, were cleaned and dark-stored in a sealed box for in excess of 5 months. When water droplets were applied to

these samples it became apparent, especially for the titania-paste films, that long term dark-storage had affected a significant increase in contact angle. The paste samples displayed *CA*s of 60° to 70°, effectively twice as high as the values observed previously.

When illuminated at increasing UVA intensities and exposed to ozone/oxygen atmospheres, Activ samples (Figure 5-14) exhibited a decrease in δ with increasing I, and the profiles were seen to shift from classically non-hyperbolic to hyperbolic. Paste films, which generally display hyperbolic profiles, were observed to shift from hyperbolic to non-hyperbolic with decreasing UV intensity (Figure 5-15). High UV intensity was seen to give an almost immediate fall in *CA,* which initially appeared to feature no delay. Plots of the reciprocal (inset of Figure 5-15) were used to estimate delay times for these high intensity cases, the delay period observed as the time before CA^{-1} deviates from the horizontal, highlighted with vertical lines.

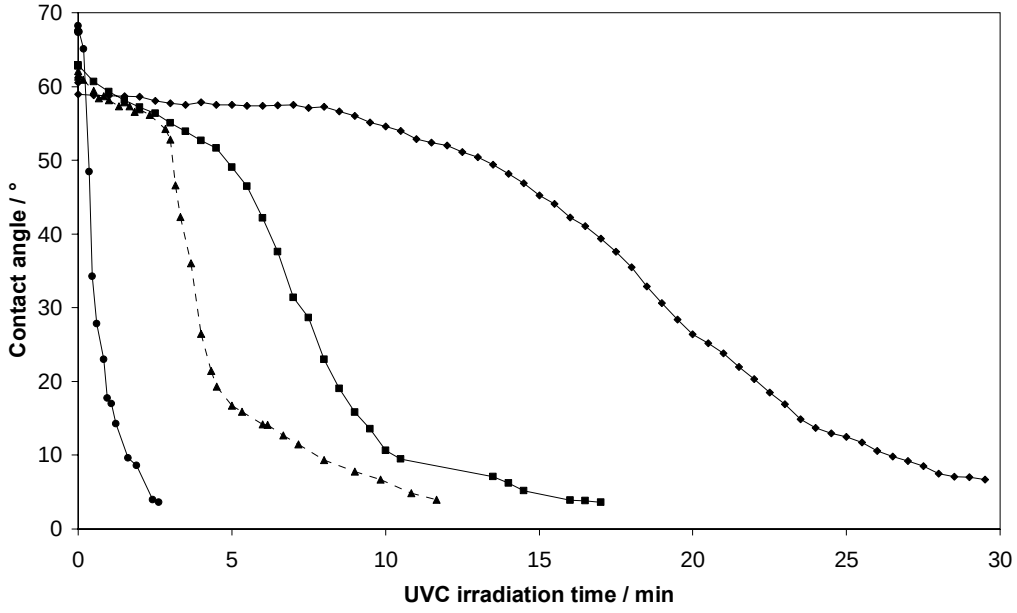

Figure 5-14 *CA* vs. time for Activ irradiated in water-saturated oxygen/ozone stream with I_{UVA} = (from left) 4.96, 1.01, 0.32 and 0.18 mW cm^{-2}

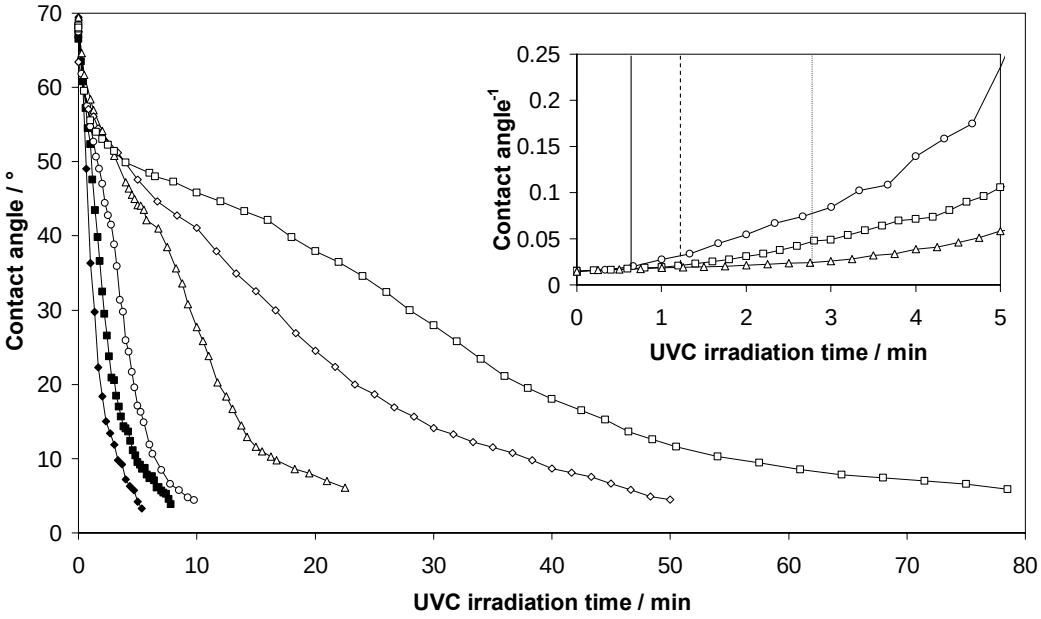

Figure 5-15 *CA* vs. time for paste films irradiated in water-saturated oxygen/ozone stream with I_{UVA} = (from left) 1.01, 0.69, 0.34, 0.18, 0.09 and 0.04 mW cm^{-2}, inset: reciprocal of *CA* used to highlight end of 'delay' for higher intensities

---

Both sets of data fit in with the 'initiation process' theory, in that with variations of UV intensity, thin and thick films show decreasing δ with increasing irradiance. Using values of δ and r_{max}, estimated from Figure 5-14 and Figure 5-15, and the measured incident UV intensity tentative attempts were made to link the parameters for both substrates. Approximately linear correlations were found for plots of the reciprocal of δ versus I_{UVA} (Figure 5-16) as well as for $-r_{max}$ and I_{UVA}, and also $-r_{max}$ and δ^{-1}, for both Activ and titania-paste films (Figure 5-17 and Figure 5-18).

These results give hope that it will be possible to link *PSH* parameters across substrates, potentially including the absorptivity, in order to build a complete kinetic model for *PSH*. Investigation of further substrates is the next obvious step, but the clarification that both profile types, those which fit hyperbolic degradation and those which don't, are

interchangeable dependant on intensity of illumination is a major step towards fully understanding the factors which determine the kinetics of *PSH*.

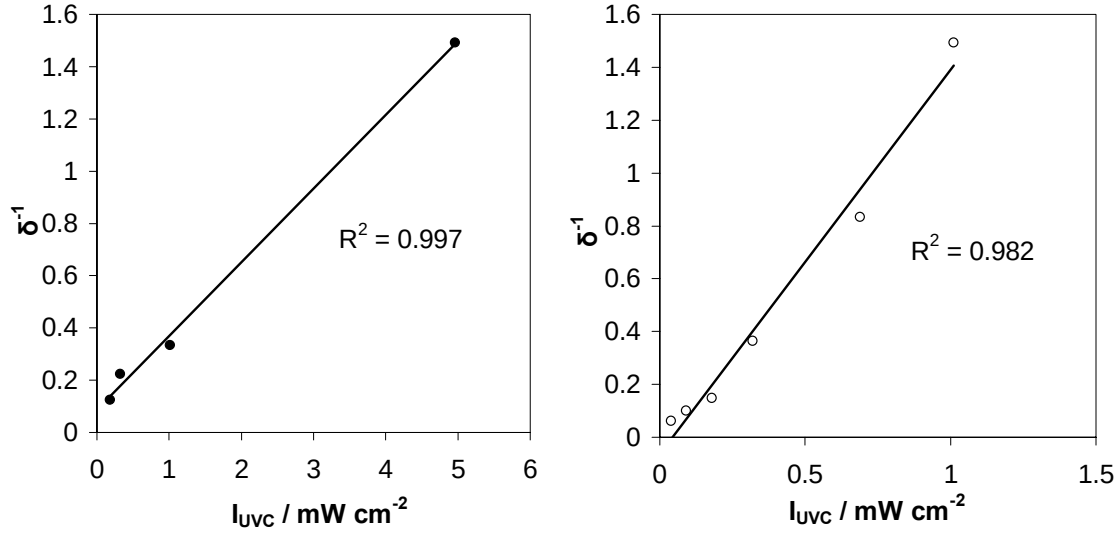

Figure 5-16 values of δ^{-1} (reciprocal of delay time) versus incident UV intensity for Activ (left) and thick paste films (right). R^2 values are displayed for best-fit lines.

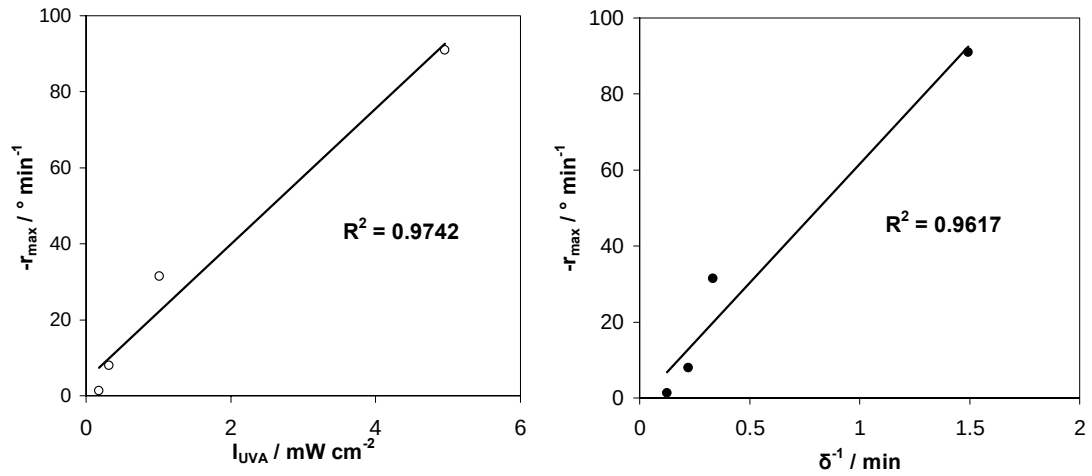

Figure 5-17 plots of maximum rate ($-r_{max}$) versus, left, UVA intensity (I_{UVA}) and, right, reciprocal of delay time (δ^{-1}) for Activ films irradiated in ozone/oxygen atmosphere

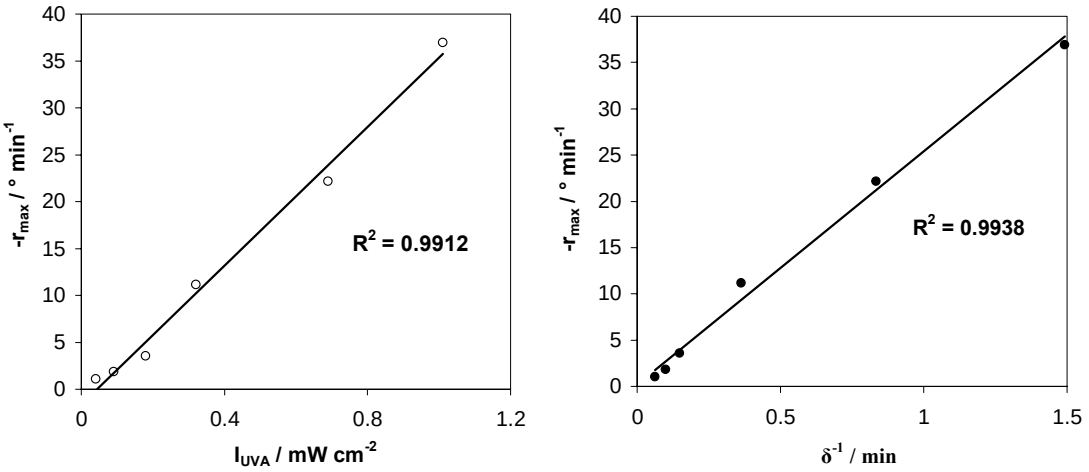

Figure 5-18 plots of maximum rate ($-r_{max}$) versus, left, UVA intensity (I_{UVA}) and, right, reciprocal of delay time (δ^{-1}) for titania-paste films irradiated in ozone/oxygen atmosphere

---

5.3.4. Variation of Droplet Composition: the effects of salts and *SEA*s on *PSH*

In the previous section ozone was seen to increase the rate of *PSH* by acting as a super, i.e., much more effective than O_2, sacrificial electron acceptor, and no *PSH* effect was observed on Activ and sol-gel samples in the absence of an electron acceptor such as ozone, or atmospheric oxygen. These results raise the following question: Does the electron acceptor have to be oxygen or oxygen-containing, or can it be another SEA? Certainly in some examples of semiconductor photocatalysis, i.e., equation 5-1, other *SEA*s have been used with great effect[39]. Thus, in this work the role of electron-acceptor in *PSH* was investigated further by dissolving various salts in the water used to generate the deposited water droplets. Thus, water droplets containing 0.1 M sodium persulfate (an SEA), potassium chloride, and sodium dithionite (an oxygen scavenger) were each, in turn, deposited onto an Activ titania film. As shown in Figure 5-19 all three salt-containing drops made the *PSH* process faster, i.e., typically reaching a CA < 5° in <10 min rather than the usual ~18 min, in 100% RH oxygen. The CA vs. *t* profiles generated

by this work suggest that having an electrolyte in the water droplet accelerates the photocatalytic process and thus the rate of *PSH*. The fact that the electrolyte may also act as either an SEA (as in the case of persulfate) or a scavenger of O_2 (as in the case of dithionite) in the water droplet appears to make no difference to the kinetics of *PSH*.

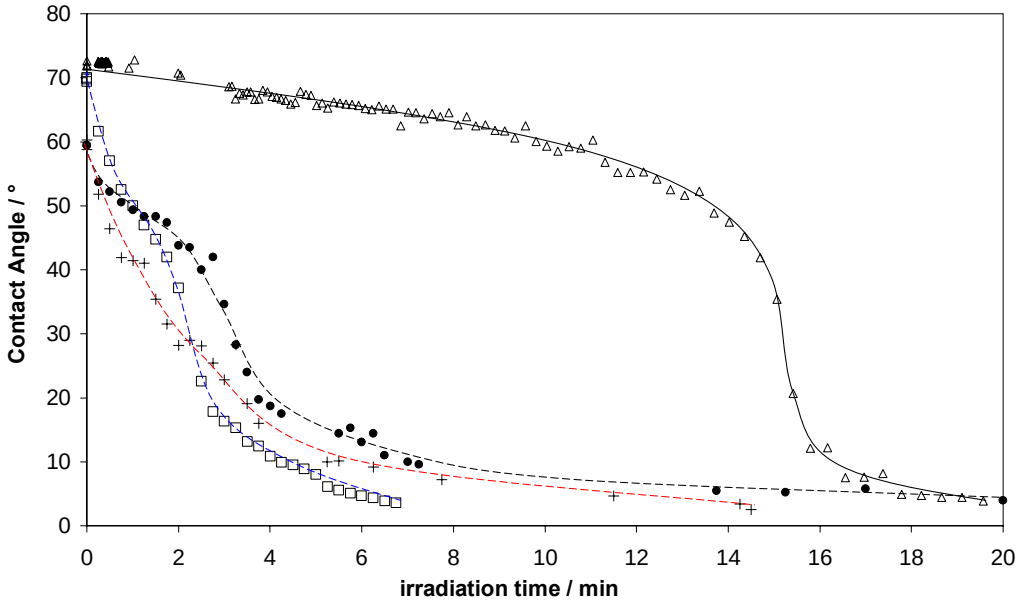

Figure 5-19 *CA* vs. UVC irradiation time for pure water (Δ), 0.1M KCl (black), 0.1M $Na_2S_2O_8$ (blue) and 0.1M $Na_2S_2O_4$ (red) in water-saturated oxygen atmospheres

These results imply that *PSH* depends more on what happens to the surface surrounding the water droplet rather than underneath the droplet itself. Possibly of greater initial surprise is the observation that *PSH* is not exhibited by Activ with use of any of the different salt-containing droplets under an anaerobic, rather than oxygen, atmosphere (Figure 5-20). This is surprising because sodium persulfate is a proven effective SEA for the TiO_2-sensitized photooxidation of organics in water[39] so if the photocatalytic model of *PSH* is correct, persulfate's presence in a water droplet, in an otherwise anaerobic atmosphere, should allow any organic material directly beneath the water droplet to be

destroyed, effectively burning a hole into any underlying organic film. Given this, initially it seems odd that the water droplet does not spread, i.e., no *PSH* activity is exhibited, when a persulfate droplet is UV irradiated under anaerobic conditions.

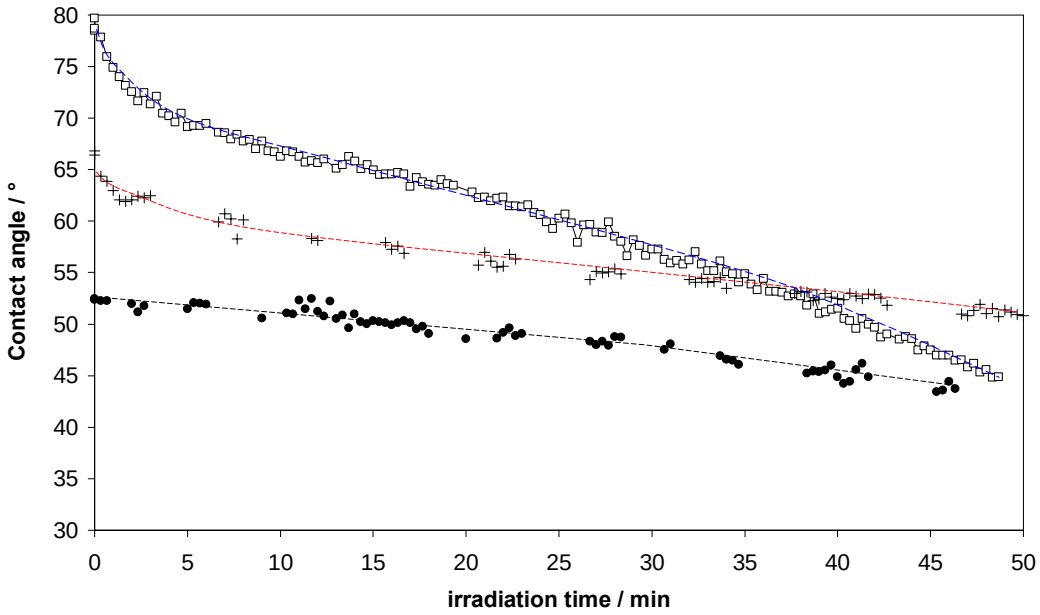

Figure 5-20 *CA* vs. UVC irradiation time for 0.1M KCl (black), 0.1M $Na_2S_2O_8$ (blue) and 0.1M $Na_2S_2O_4$ (red) in water-saturated nitrogen atmospheres

However, a possible reason for the persulfate-containing water droplet not spreading would be that, apart from underneath the water droplet, the surrounding titania film would, presumably, remain covered with a thin, albeit undetectable (by FTIR at least), layer of organic material that renders it hydrophobic, as indicated by the schematic illustration in Figure 5-21. Support for the above "hole-burning" model was provided by a demonstration that persulfate is able to effect readily the complete cleaning of the surface of an Activ sample of the hydrophobic organics on its surface by semiconductor photocatalysis under anaerobic conditions, thereby rendering it superhydrophilic. This was achieved by pre-irradiating an Activ film, submerged in an anaerobic, 0.1 M

persulfate solution, with UVC light, apparatus shown in Figure 5-7. The results of this work showed that the titania film was rendered superhydrophilic by this process whereas, in contrast, films which had been treated similarly, but with 0.1 M KCl or sodium dithionite as the immersion solution, retained their initial hydrophobic character.

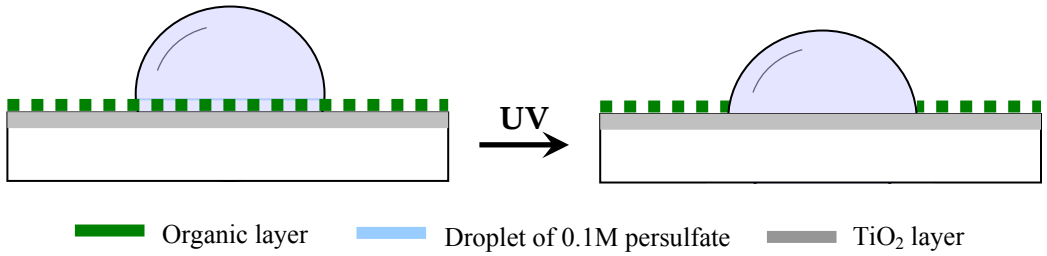

Figure 5-21 schematic of the suggested 'hole-burning' effect of irradiation on 0.1 M persulfate solution droplet on Activ in deoxygenated atmosphere

5.3.5. Stearic acid on TiO_2 as a model contaminant layer

It was observed in a previous section that thick titania paste films do not normally exhibit any delay in their CA vs t plots, even in the absence of ozone (Figure 5-10) and follow a more conventional hyperbolic profile, as would be expected for films of high activity, which absorb strongly any incident UV light, based on the photocatalyst model of *PSH*. In contrast, and as indicated earlier, thin titania films and/or low incident UV light intensities have been shown to give rise to such non-hyperbolic CA vs. irradiation time profiles and appear associated with low rates of *PSH*[5, 29]. Interestingly and not surprisingly, such non-hyperbolic CA vs. t profiles can be effected when using very active, thick, sol-gel films, even in an ozone-containing environment, through the application of a stearic acid (SA) film onto the substrate's surface before water droplet deposition, as shown by the CA vs. UVA irradiation time profile in Figure 5-22. Figure

5-22 also illustrates the variation of the integrated area under the FTIR peaks due to the SA layer on the same thick paste titania film, i.e., A_{int} vs. UV irradiation time. This concomitant monitoring of the SA layer by FTIR on an identical film shows that there is a strong correlation between the end of the induction period (characterized by a sudden wetting process) and the removal of the final, FTIR-detectable, traces of the stearic acid layer. These results appear to lend support to the elegant work of Yates et al[17] and their proposal that such delay periods are due to organic film contaminant removal by photocatalysis.

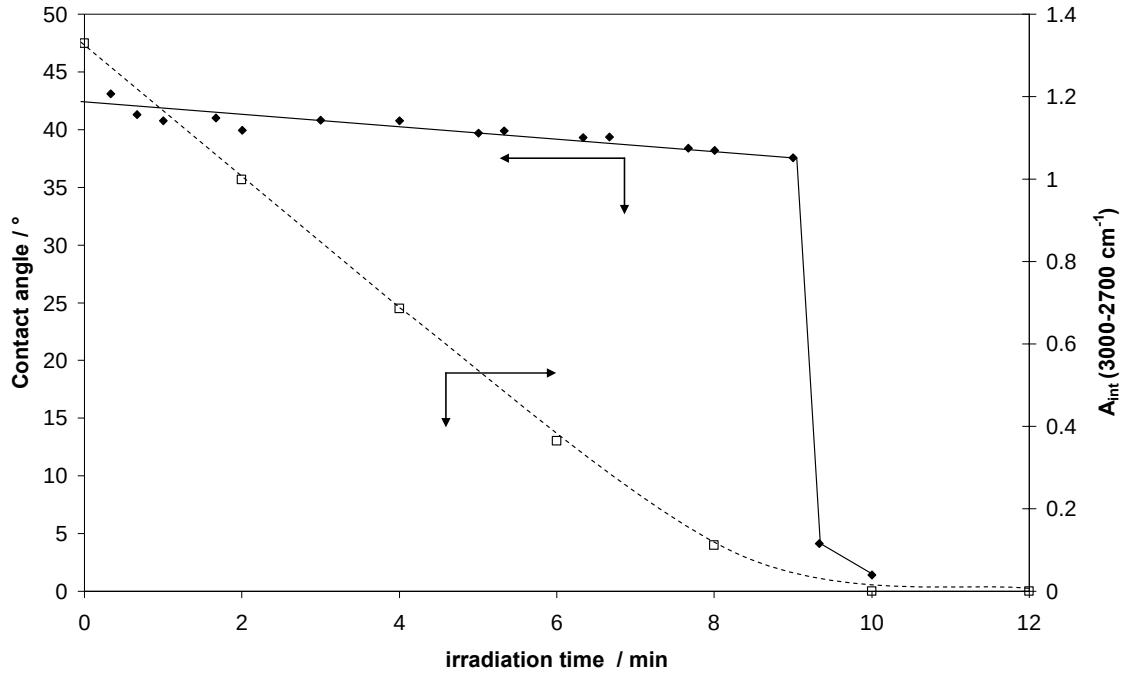

Figure 5-22 CA (♦) and FTIR (□) integrated area, A_{int}, measured from 2700 to 3000 cm^{-1}, versus UVA irradiation time for stearic acid coated paste film in an ozone-containing (1700 ppm) oxygen, water-saturated atmosphere. A blank of a stearic acid-coated paste film treated with only ozone produced no change in integrated area over 30 min.

5.3.6. Pre-treatment – heat, UV/ozone and acid

Table 1 Water contact angles for Activ™ and glass samples before and after pre-treatment

Pre-treatment Method	Activ™		Plain Glass	
	initial CA / °	final CA / °	initial CA / °	final CA / °
UVC/O_3 [a]	71	< 5	35	< 5
Δ 500°C [b]	70	< 5	37	< 5
Aqua Regia [c]	70	< 5	38	< 5

[a] Samples irradiated by 2×6W UVC bulbs in ~1700 ppm O_3 for 1 hour

[b] Samples heated to 500°C and held at temp for 1 hour before cooling under Petri dish

[c] Immersion in 25 mL Aqua Regia for 1 hour before rinsing and drying

---

The combination of short wavelength ultraviolet light and ozone to create electronically excited ozone, O_3*, which is a very effective oxidising agent is well documented in its use for destroying organic materials and scouring the latter from surfaces such as semiconductor wafers[36, 37]. As previously stated (section 5.3.2.) it has been observed that the combination of UVC and ozone as a pre-treatment produces a superhydrophilic surface on Activ™ and plain glass. These findings imply that the intrinsic state of a titania film or pristine glass is superhydrophilic, as indicated by other work on both plain glass[40] and titania[20] (such as found on Activ™) and that this state requires simply the removal of all surface contaminants, particularly hydrophobic organics, for its production.

This finding, that UV/O_3 pre-treatment renders Activ™ superhydrophilic, fits in with both the *PSIR* model, and the *PCO* model of *PSH*. However, the observation that plain glass is also rendered superhydrophilic indicates that the initial hydrophobic nature of the plain glass, and most probably Activ™, is due to contamination of the surface by

hydrophobic organics, at a level too low to detect by simple FTIR. UVC excitation of the O_3 creates O_3* that effectively oxidises and removes organics from the surfaces of these two substrates, to reveal the pristine, intrinsically superhydrophilic surfaces of the substrates. Thus, there appears no need to invoke a surface reorganisation mechanism, i.e. *PISR*, to explain *PSH* in titania as *PCO*, since such work implies any oxidative process that removes hydrophobic surface organics, such as UVC/O_3, will render the surface of titania superhydrophilic. The typical water droplet contact angles of plain and Activ^{TM} glass samples before and after UV/O_3 treatment are given in Table 1.

A series of experiments were carried out to investigate a variety of other oxidising pre-treatment methods, including heating and strong acid immersion, to ascertain if all were able to render Activ^{TM} and plain glass superhydrophilic (i.e. CA < 5°). Thus, heating Activ^{TM} and plain glass at different temperatures and testing their hydrophilic natures, via CA measurements produced the results illustrated in Figure 5-23. These results show that for both substrates the CA decreased with increasing temperature, with glass falling from an initial contact angle, CA_i, ~35° to < 5° by 300° and Activ^{TM} from CA_i ~ 70° to <5° by 550°.

That the titania substrates become hydrophilic with heat treatment appears at odds with the PSIR model of *PSH*, i.e. Figure 5-1, which suggests that the dark dehydration process should be promoted by high temperatures [19], leading to either no change, or an increase in its hydrophobic nature. Instead, the results in Figure 5-23 indicate that the initial hydrophobic character of Activ^{TM} and plain glass is due to organic surface contaminants that are readily oxidised by high heat treatment to reveal the intrinsic superhydrophilic nature of glass and titania films. From the data in Figure 5-23 it appears that the plain glass samples become hydrophilic at lower temperatures than Activ^{TM}, probably due to a lower level of contamination on glass, which is much smoother than the titania films, rendering the latter more susceptible to organic adsorption. Initially hydrophobic Activ^{TM} and plain glass samples were also pre-treated

with the very oxidising reagent, aqua regia, and found to be rendered superhydrophilic by this treatment, (see Table 1).

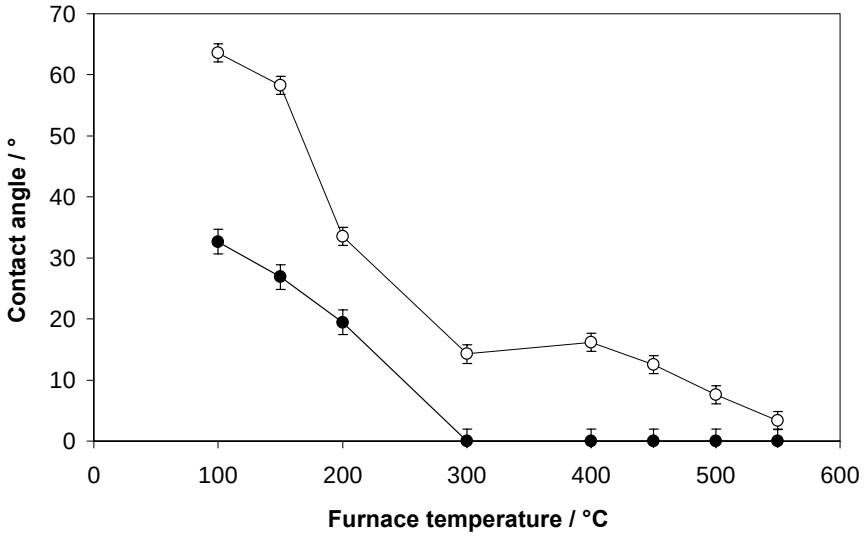

Figure 5-23 Plot of Contact angle vs. pre-treatment furnace temperature for Activ^{TM} (○) and for plain glass (●)

In conclusion, all three methods of pre-treatment, i.e. UVC/O_3, heat (> 550°C) and aqua regia are able to effect the conversion of both Activ^{TM} and plain glass samples from an initial hydrophobic state to a superhydrophilic state. All three methods use very strong oxidising agents to render plain and Activ^{TM} glass samples superhydrophilic, most probably due to the oxidation of any surface hydrophobic organic species. These results therefore provide significant support for the *PCO* model of *PSH*. These results also imply that the pristine, i.e. organic-free, surfaces of these materials are superhydrophilic.

5.3.7. Contact Angle Recovery – effect of heat, vacuum, ultrasonic, and recovery in ambient or sealed systems

The 'dark' recovery of contact angle i.e. the regeneration of hydrophobicity, exhibited by superhydrophilic titania films has been widely reported[10-12, 29] and opinion over its cause is polarised between a re-contamination of the surface by air-borne organics (*PCO* model of *PSH*) and the reverse process of Figure 5-1, i.e. a dehydroxylation/dehydration process on the surface of the titania (*PISR* model of *PSH*). Work carried out by others[11] shows that superhydrophilic samples of titania become more hydrophobic when stored in an evacuated atmosphere. These results are interpreted as evidence of the *PISR* model, in which vacuum storage accelerates OH^- desorption and therefore CA recovery in superhydrophilic samples of titania. In replicating this work we also found that the CA of Activ^{TM} increases markedly when the samples are stored under vacuum, but also, and more revealing, that plain glass exhibits the same feature, although to a lesser extent.

These results, illustrated in Figure 5-24, indicate that the phenomena of CA increasing for superhydrophilic titania films held under vacuum (used to support the 'surface reorganisation' model, i.e. Figure 5-1) is not specific to titania films, but is also exhibited by plain glass and so not likely to be associated with a *PISR* mechanism, attributed to titania but not to glass. Instead, the more likely explanation is that it is due to organic contamination of a clean surface, i.e. glass or titania in this work, produced by exposing the sample to air when making the CA measurement after storage in a vacuum.

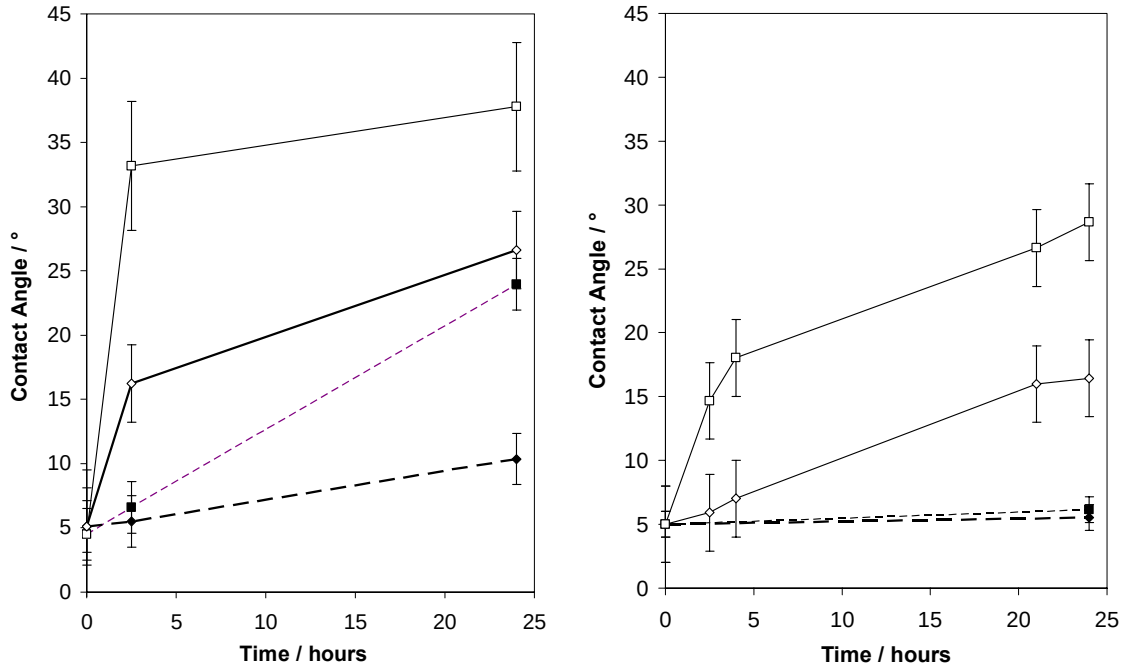

Figure 5-24 Water contact angle vs. exposure time in (left) an evacuated (solid line) or hydrated (dashed line) atmosphere, and (right) ambient laboratory storage (solid) and ambient contained storage (dashed); for Activ™ (square) and glass (diamond), CA measurements recorded under ambient conditions

---

The observation of accelerated recovery of *CA* on titania films via storage at elevated temperatures was again, as with the case of vacuum storage, suggested to be as a result of the reverse process of Figure 5-1[11]. To investigate the effect of elevated temperature on a titania and plain glass, pre-cleaned (by UV-ozone) samples were stored for 18 hours at 100°C, 200°C and 300°C using three different ovens/furnaces. Numbered 1 to 3, typical use temperature ranges were as follows: oven #1 was used in the range 70°C to 100°C; oven #2 from 100°C to 200 °C; and #3 was a furnace commonly used from 400°C to 800°C. Figure 5-25 shows the measured contact angles after 18 hours' storage, with a marked increase observed for the titania films in oven #1 at 100°C. The second plot is telling, in that when stored in the muffle furnace at 100°C the *CA* recovers to a

lesser extent. This strongly implies that prior usage and organic contamination are key factors in *CA* changes due to heating. That heating to 300°C caused little or no increase in *CA*, and that analogous effects were observed for titania films and plain glass, add further weight to this suggestion of re-contamination rather than a *PISR* effect.

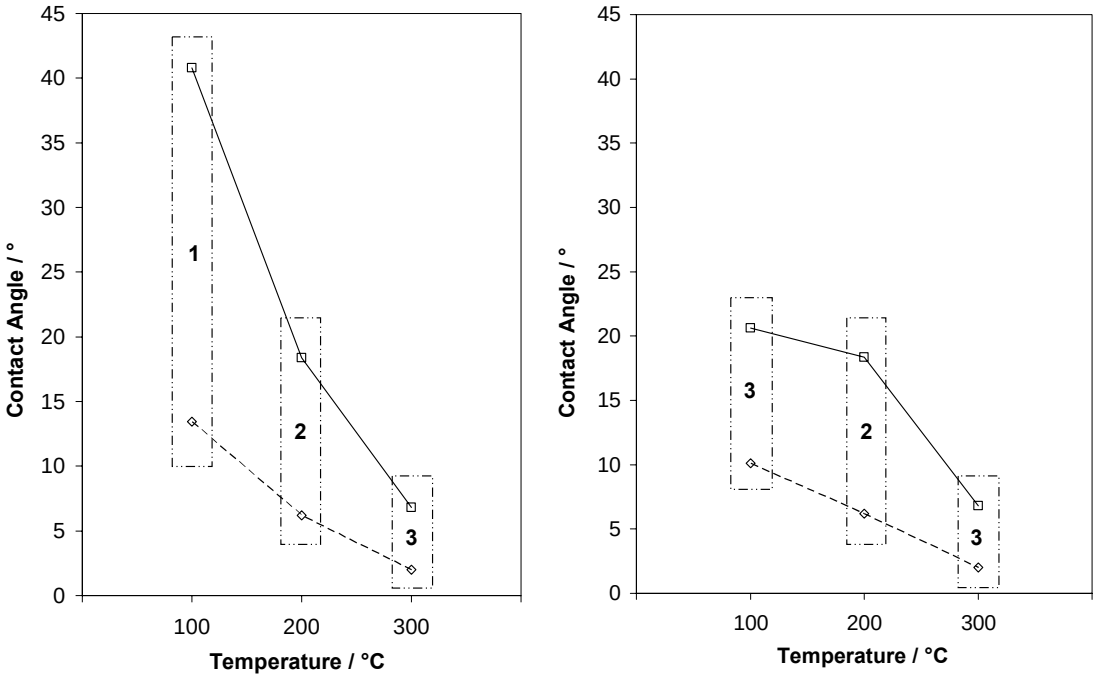

Figure 5-25 Contact angle for Activ (□) and plain glass (◊) after 18 hours' storage using: 1 – small oven; 2 – medium oven, and; 3 – muffle furnace, at indicated temperatures

The effect of air-borne contamination of a pristine, superhydrophilic glass and Activ™ surface was demonstrated by leaving two freshly-prepared samples out on the bench and monitoring the change in CA as a function of time. The results of this work are illustrated in Figure 5-24. From these results it is clear that, on the open bench, a pristine, superhydrophilic sample of glass or Activ™ can be rendered noticeably hydrophobic within a few hours of exposure. Note that, as expected from its lower

surface roughness, over the same time plain glass is rendered less hydrophobic than Activ™ due to this surface contamination. Simple IR analysis of these glass samples revealed no indication of contamination of their surfaces by hydrophobic organics, implying that the level is very low and below the level of detection of normal FTIR spectroscopy.

Table 2 Table of water contact angle for Activ™ and glass samples before and after either sonication or immersion for 10 minutes in deionised (DI) water

Treatment	**Activ™**		**Glass**	
	initial CA / °	**final CA / °**	**initial CA / °**	**final CA / °**
Sonication for 10 min in DI water	< 5	8.9	3.8	8.2
DI water immersion for 10 min	< 5	6.4	4.3	5.3

Previous work carried out by others[24] has shown that a superhydrophilic titania film is rendered more hydrophobic upon exposure to ultrasound (10 min). In another set of experiments both glass and titania films, rendered superhydrophilic by treatment with UVC/O_3, were placed in high purity water in clean beakers and treated with ultrasound. The measured CAs of these samples before and after exposure to ultrasound are given in Table 2 and show that for both samples, upon sonication the CA rises slightly, by 3–5°, whereas without sonication the CA remains largely unchanged. These results imply that the effect of ultrasound on superhydrophilic films, be they glass or titania, is very small and most probably due to a roughening of the substrate, and/or some organic contamination, and is not specific to titania.

Other work shows that any wiping or rubbing of a pristine superhydrophilic glass or titania film using a tissue or cloth renders the film hydrophobic, and this is attributed, once again, to organic contamination of the surfaces of these substrates. It appears unlikely that rubbing is able to effect the reverse of reaction (2) via a mechano-chemical effect as claimed by others[25], since plain glass is affected in the same way as titania.

5.4 Conclusions

The results of this work provide a greater understanding of *PSH*. Firstly it was observed that a number of factors can affect the progress of *PSH* on titania substrates. These factors include the type of UV irradiation i.e. more highly absorbed UVC gave much more rapid hydrophilic change than UVA. The intensity of UV irradiation was also significant, with 'switching' between the two characteristic profile types observed for thick films and thin films. The atmospheric composition surrounding the droplet was also observed to be vital as *PSH* requires an electron-acceptor to progress, and can be expedited by using more efficient SEAs such as ozone. The composition of the deposited droplet was also investigated, leading to the suggestion of a 'hole-burning effect'. That a doped SEA *could* replace atmospheric oxygen, proven by irradiation in a deoxygenated solution, but *in-situ* irradiation only removes organic material beneath the droplet itself, prohibiting spreading. The use of stearic acid as a model contaminant layer provided another example of 'sudden wetting', and concomitant monitoring of the layer by FTIR illustrated correlation between the sudden wetting and complete removal of the organic layer, to the limits of detection by this method.

The second part took in the use of pre-treatments to effect hydrophilic change on both titania (Pilkington Activ) and plain glass. Heat, strong acid immersion, and UVC/ozone were all observed to render both glass and Activ superhydrophilic. As each technique utilised highly oxidising conditions and an analogous effect was found for both types of substrates it is becoming increasingly likely that hydrophilic change, and photoinduced

superhydrophilicity, is, as suggested by Nozu and Kume[8], caused by the photocatalytic removal of organic pollutants rather than any surface reorganisation process. This theme was continued when the reverse process, the recovery of hydrophobicity, was considered. The proposed expedition of *CA* recovery by heat and vacuum were investigated for Activ and plain glass along with samples subjected to a hydrated gas stream. Increases in *CA* were observed for both substrates in each set of conditions. A comparison of the degree of recovery when hydrophilic samples were stored in either air-tight beakers or left open to the atmosphere on the benchtop found virtually no increase in *CA* for the former and significant increase for the latter over 24 hours. The final part investigated the suggested influence of external stimulus, such as rubbing or sonication, on the hydrophilicity of superhydrophilic glass and Activ. Storage in pure water with and without sonication highlighted that some effect is occurring for both substrates during sonication. That this effect is directly, or indirectly, linked to a surface reorganisation is unlikely, though it would appear that, in this case, organic recontamination is not the cause.

In summary, a number of factors concerning both the 'forward' and 'reverse' processes of *PSH* have been explored, and in each circumstance the *PCO* model rather than the *PISR* model has been the best fit to explain the observed phenomena. The implication being that photocatalytic removal of adventitious organic material, and subsequent recontamination by airborne organics, are the root causes of hydrophilic changes observed on titania during illumination by ultraviolet radiation and dark storage.

5.5 References

1 M. Langlet, S. Permpoon, D. Riassetto, G. Berthome, E. Pernot, and J. C. Joud, *J. Photochem. Photobiol. A: Chem* **181**, 203 (2006).

2 A. Mills, G. Hill, S. Bhopal, I. P. Parkin, and S. A. O'Neill, *J. Photochem. Photobiol. A: Chem* **160**, 185 (2003).

3 M. Miyauchi, A. Nakajima, T. Watanabe, and K. Hashimoto, *Chem. Mater.* **14**, 2812 (2002).

4 I. P. Parkin, and R. G. Palgrave, *J. Mater. Chem.* **15**, 1689 (2004).

5 R. Sun, A. Fujishima, T. Watanabe, and K. Hashimoto, *J. Phys. Chem. B* **105**, 1984 (2001).

6 R. Wang, K. Hashimoto, A. Fujishima, M. Chikuni, E. Kojima, A. Kitamura, M. Shimohigoshi, and T. Watanabe, *Nature* **388**, 431 (1997).

7 N. Stevens, C. I. Priest, R. Sedev, and J. Ralston, *Langmuir* **19**, 3272 (2003).

8 S. Kume, and T. Nozu, *Difficulty stainable glass product*. Japanese Patent Sho 61-243762, 1986.

9 A. Fujishima, K. Hashimoto, and T. Watanabe, *TiO_2 Photocatalysis: Fundamentals and Applications*. BKC: 1999.

10 A. Fujishima, T. N. Rao, and D. A. Tryk, *J. Photochem. Photobiol. C* **1**, 1 (2000).

11 H. Irie, and K. Hashimoto, *Environmental Photochemistry pt. II: Photocatalytic Active Surfaces and Photo-Induced High Hydrophilicity/High Hydrophobicity; Eds: P. Boule, P.K.J. Robertson, D.W. Bahnemann*. Springer-Verlag: 2005; Vol. 2.

12 N. Sakai, A. Fujishima, T. Watanabe, and K. Hashimoto, *J. Phys. Chem. B* **107**, 1028 (2003).

13 A. N. Shultz, W. Jang, W. M. Hetherington, D. R. Baer, L. Q. Wang, and M. H. Englehard, *Surf. Sci.* **339**, 114 (1995).

14 Katsumata. K, Nakajima. A, Shiota. T, Yoshida. N, W. T, Kameshima. Y, and O. K, *J. Photochem. Photobiol. A: Chem* **180**, 75 (2006).

15 R. Wang, N. Sakai, A. Fujishima, T. Watanabe, and K. Hashimoto, *J. Phys. Chem. B* **103**, 2188 (1999).

16 J. M. White, J. Szanyi, and M. Henderson, *J. Phys. Chem. B* **107**, 9029 (2003).

17 T. Zubkov, D. Stahl, T. L. Thompson, D. Panayatov, O. Diwald, and J. T. YatesJnr, *J. Phys. Chem. B* **109**, 15454 (2005).

18 C.-Y. Wang, H. Groenzin, and M. J. Shultz, *Langmuir* **19**, 7330 (2003).

19 A. Kanta, R. Sedev, and J. Ralston, *Langmuir* **21**, 2400 (2005).

20 M. Takeuchi, K. Sakamoto, G. Martra, S. Coluccia, and M. Anpo, *J. Phys. Chem. B* **109**, 15422 (2005).

21 M. Miyauchi, A. Nakajima, A. Fujishima, K. Hashimoto, and T. Watanabe, *Chem. Mater.* **12**, 3 (2000).

22 K. Hashimoto, H. Irie, and A. Fujishima, *Jap. J. App. Phys.* **44**, (12), 8269 (2005).

23 M. Miyauchi, N. Kieda, S. Hishita, T. Mitsuhashi, A. Nakajima, T. Watanabe, and K. Hashimoto, *Surf. Sci.* **511**, 401 (2002).

24 N. Sakai, R. Wang, A. Fujishima, T. Watanabe, and K. Hashimoto, *Langmuir* **14**, 5918 (1998).

25 M. Kamei, and T. Mitsuhashi, *Surf. Sci.* **463**, L609 (2000).

26 A. Mills, N. Elliott, G. Hill, D. Fallis, J. D. Durrant, and R. L. Willis, *Photochem. Photobiol. Sci.* **2**, 591 (2003).

27 A. Mills, N. Elliott, I. P. Parkin, S. A. O'Neill, and R. J. Clark, *J. Photochem. Photobiol. A: Chem* **151**, 171 (2002).

28 K. Seki, and M. Tachiya, *J. Phys. Chem. B* **108**, 4806 (2004).

29 A. Mills, A. Lepre, N. Elliott, S. Bhopal, I. P. Parkin, and S. A. O'Neill, *J. Photochem. Photobiol. A: Chem* **160**, 213 (2003).

30 N. Sakai, K. Fukuda, T. Shibata, Y. Ebina, K. Takada, and T. Sasaki, *J. Phys. Chem. B* **110**, 6198 (2006).

31 A. W. Adamson, and A. P. Gast, *Physical Chemistry of Surfaces*. Sixth ed.; John Wiley & Sons: 1997.

32 D. J. Shaw, *Introduction to Colloid and Surface Chemistry*. Fourth ed.; Butterworth Heinemann: 1992.

33 A. Mills, and M. Crow, *Int. J. Photoenergy*, Article ID. 70670 doi: 10.1155/2008/7670 (2008).

34 A. Mills, and M. Crow, *J. Phys. Chem. C* **111**, 6009 (2007).

35 N. Sakai, A. Fujishima, T. Watanabe, and K. Hashimoto, *J. Phys. Chem. B* **105**, 3023 (2001).

36 R. R. Sowell, R. E. Cuthrell, D. M. Mattox, and R. D. Bland, *J. Vac. Sci. Technol. A* **11**, (1), 474 (1974).

37 J. R. Vig, *J. Vac. Sci. Technol. A* **3**, (3), 1027 (1985).

38 Z. Pengyi, L. Fuyan, Y. Gang, C. Qing, and Z. Wanpeng, *J. Photochem. Photobiol. A: Chem* **156**, 189 (2003).

39 A. Mills, and M. A. Valenzuela, *J. Photochem. Photobiol. A: Chem* **165**, 25 (2004).

40 S. Takeda, M. Fukawa, Y. Hayashi, and K. Matsumoto, *Thin Solid FIlms* **339**, 220 (1999).

Chapter 6 Further Work

6.1 Photocatalytic Oxidation of Solid Inorganic Layers

Whilst further work involving soot and sulfur layers on titania films may not be necessary, with the oxidation products monitored or trapped and determined in stoichiometric quantities, the area of remote photocatalysis and identification of the migratory species produced at the surface could still yield considerable interest. Further work addressing the possible role of ozone or singlet oxygen, potentially involving a cold trap to remove ozone from a gas stream flowing over UV-illuminated titania, or singlet oxygen generating dyes, may be able to elucidate the mechanism behind this phenomenon.

6.2 Photocatalytic Oxidation of Inorganic Gas Species on Titania

From this chapter there would appear to be potential for further work around the photo-oxidation of CO on thick titania films, potentially using CO as a model species to investigate the activities of different photocatalytic substrates. The creation of flexible, polymer-based photocatalyst films is an area where further research could prove fruitful. A combination of polymer and photocatalyst which do not lead to the matrix itself being degraded may be found, potentially using non-photocatalytically degradable compounds such as silicates. Photocatalytic degradation of PTFE is in itself novel research, but the applications are at present unclear and the hazardous nature of the oxidation products would render the pursuit of photo-degradable fluoropolymers undesirable.

6.3 Factors affecting wettability changes on titania

With such a contentious subject matter, further work to support the findings of the body of work regarding *PSH* is always likely to be necessary. Areas of specific interest include exploring the possibility of there being a universal kinetic model which includes both thick and thin film types and the characteristic features associated with them. In order to fully elucidate the mechanism of *PSH* the creation of a 'killer' experiment, one that discounts either of the two major hypotheses is likely to be necessary. The nature of this experiment may be along the lines of those included here, but including clean-room synthesis and highly sensitive in-situ analytical techniques in order to prove that intrinsically clean titania surfaces are hydrophilic, and that adventitious organics render them hydrophobic.

Chapter 7 General Conclusions

The three sections of this work, whilst being linked as research into semiconductor photocatalysis under the banner of environmental remediation, all occupy distinct area of the SPC spectrum. Chapter 3 gave further instances of photocatalytic oxidation of solid contaminant layers, whilst documenting the complete removal to the gas phase of soot and elemental sulfur. The remote photo-oxidation of soot layers and the related experiments which attempted to determine the migratory oxidising species added further intrigue to the existing research in the area. That a hydrogen peroxide-saturated gas stream, under UVC irradiation, had no effect on a soot layer strongly suggests that a species other than hydroxyl radicals is behind the remote photocatalysis phenomenon.

In Chapter 4 further oxidation of the gaseous products of the PCO of elemental sulfur was investigated; highly acidic species were found to be deposited onto the films, sulfite and sulfuric acid, poisoning the photocatalyst. When using carbon monoxide as a model pollutant species it was again shown that platinisation of titania, either as sol-gel films or powder incorporated into a matrix, increases the activity of the photocatalyst. Polymer matrices were found to be degraded by the incorporated photocatalyst, in these cases CO_2 was produced in vast stoichiometric excess to the initial CO as the polymer was oxidised. Thermally and chemically stable fluoropolymers were also found to be degraded by an incorporated photocatalyst.

The experiments documented in Chapter 5 were designed to explore the current adopted theories surrounding photoinduced superhydrophilicity (*PSH*). Through assessing the changes in wettability affected by UVA and UVC illumination of a droplet on titania surfaces it became apparent that the two, previously distinct, modes of kinetics observed for *PSH* can in fact be made interchangeable by varying the intensity of irradiation. The atmosphere surrounding the droplet was also found to be a determining factor in the

progression of *PSH*, providing evidence that the electron acceptor essential for *PSH* to proceed can be gaseous or in solution – sodium persulfate in this work. When the recovery of contact angle for the films was investigated it became apparent that intrinsically clean titania has a contact angle of 0°, and further experiments suggested that the contact angle recovers due to re-contamination of the surface with organic material, rather than a structural re-organisation of the titania surface. All of the evidence garnered from these experiments points towards photocatalytic oxidation of organic contaminants as being the cause of *PSH*.

Journal of Applied Electrochemistry (2005) 35:641–653
DOI 10.1007/s10800-005-1628-5

Reviews in Applied Electrochemistry Number 57

Thick titania films for semiconductor photocatalysis

ANDREW MILLS,* GEORGE HILL, MATTHEW CROW and STEPHANIE HODGEN
Department of Pure and Applied Chemistry, University of Strathclyde, Glasgow, G1 1XL, UK
*(*author for correspondence, e-mail: a.mills@strath.ac.uk)*

Received 26 July 2004; accepted in revised form 24 October 2004

Key words: semiconductor, photocatalysis, titania, thick-films, stearic acid, porosity

Abstract

A brief overview of work carried out by this group on thick (>1 μm), optically clear, robust titania films prepared by a sol–gel method, as well as new results regarding these films, are described. Such films are very active as photocatalysts and able to destroy stearic acid with a quantum yield of 0.32%. The activity of such films is largely unaffected by annealing temperatures below 760 °C, but is drastically reduced above this temperature. The drop in photocatalyst activity of such films as a function of annealing temperature appears to correlate well with the change in porosity of the films and suggests that the latter parameter is very important in deciding the overall activity of such films. The importance of porosity in semiconductor photocatalysed cold combustion may be due to the effect it has on access of oxygen to the active sites, rather like the effect the position of a fire grate (open or closed) has on the rate of burning, i.e., hot combustion, that takes place in a fireplace.

1. Introduction

Self-cleaning glass has been hailed as one of the greatest of all inventions [1] and certainly represents the most important advance in glass technology for many decades. A key feature of self-cleaning glass is a thin layer, typically 15 nm thick, of titanium dioxide which is able to absorb some of the UV component of sunlight to drive the photocatalytic mineralisation of many carbon-containing compounds [1–5]. The overall process of semiconductor photomineralisation may be summarised as follows:

$$\text{organic pollutant} + O_2 \xrightarrow[TiO_2]{h\nu \geq E_{bg}} \text{mineralised products} \quad (1)$$

Obviously, with self-cleaning glass the outer titania film must adhere strongly to the glass substrate and be optically clear. Most manufacturers of self-cleaning glass have been able to achieve this using nanocrystalline titania laid down via a chemical vapour deposition method [1, 2, 6]. The titania films must usually be very thin, ca. 15 nm as noted earlier and comprised of nanocrystalline particles, since any thicker, with bigger particles, and the film develops a degree of opacity and/or fragility that renders it unacceptable as a commercial product. Unfortunately titania is an indirect semiconductor and, as a result, although it possesses a bandgap of 3–3.2 eV, it does not absorb strongly in the UVA region (320–380 nm), where most of the UV component of sunlight lies [7]. For example, the absorption coefficient for nanocrstalline anatase, α, is ca. 5×10^4 cm^{-1} at 365 nm [7] and, given for any film:

$$\text{Absorbance} = 0.434\,\alpha\,d(1-p) \quad (2)$$

where p is the porosity and d is the thickness of the film. It follows that a 15 nm, non-porous, titania film, such as Activ^{TM} will only absorb ca. 7% of the incident UVA irradiation at this wavelength [7]. There is interest, therefore, in ways to generate thick films of titania, typically >1 μm, which are optically clear and robust. In a recent series of papers [8–10] this group has reported on a method for producing such films and shown them to be highly active for mediating the photocatalytic destruction of carbon-containing materials, such as stearic acid and soot. This paper highlights the results of this work and also describes more recent work that may help further our understanding of the key factors that decide the overall activity of photocatalytic films.

2. Experimental

2.1. *Materials and methods*

Unless stated otherwise all chemicals were purchased from Aldrich Chemicals (UK) and used as received.

UV/Vis absorption spectra were recorded using a Lambda 20 UV/Vis spectrophotometer (Perkin Elmer, UK).

In the study of the photocatalytic activities of the various titanium dioxide films, stearic acid was used as the test organic material for mineralisation. Stearic acid was chosen as it provides a good representation of the organic solid films that deposit on window glass and because it is very readily deposited to create films that are easily analysed by transmission FT-IR. Each film under test was coated with an initial layer of stearic acid by dropping 0.3 cm^3 of a stearic acid in chloroform solution (30 g dm^{-3}) onto the surface of the film and then spinning it at 500 rpm for 10 s. Each film was then placed in an oven at 100 °C for 30 s and then allowed to cool to room temperature. A 1600 FT-IR (Perkin Elmer, UK) was used to record the FT-IR spectra of the films with an initial stearic acid coating, before and after any illumination. For any and every film, the FT-IR spectrum of the stearic acid coating was used to calculate the integrated area under the stearic acid peaks over the range 2500–3500 cm^{-1}, from which the concentration of stearic acid on the film was calculated as a function of irradiation time, given an integrated absorbance of 1 cm^{-1} is equivalent to 3.13×10^{15} molecules of stearic acid per cm^2 [11]. Through this process, FT-IR absorption spectroscopy allowed the concentration of stearic acid on a test substrate to be measured (in units of molecules of stearic acid cm^{-2}) and monitored as a function of irradiation time.

In the study of the photocatalytic activities of the various films using the stearic acid test system the irradiation source comprised six 8 W black blue fluorescent tubes, set in a half cylinder unit, with a backing aluminum reflector. In all cases the sample under test was placed on the bench and the irradiation unit placed 13 cm above it and facing the film. The light output of this illumination source was determined by ferrioxalate actinometry to be 8.02×10^{17} photons cm^{-2} min^{-1}.

2.2. *Preparation of the thick titanium dioxide films*

The general preparation of thick titanium dioxide films by a sol–gel method is described in detail elsewhere [9]. Briefly 4.65 g of acetic acid was added to 20 ml of titanium isopropoxide under an inert nitrogen atmosphere. To this was added 120 ml of 0.1 mol dm^{-3} nitric acid and, after mixing, the reaction solution was heated rapidly to 80 °C whereupon it turned milky white and opaque. Within a few minutes at this temperature the reaction solution gelled but became fluid again within 1–2 h. The reaction solution was maintained at 80 °C for 8 h whereupon it was allowed to cool to room temperature and any remaining aggregate particles were removed using a 0.45 μm syringe filter. 80 ml of the colloidal solution product were then placed in a Teflon pot with a lid in an autoclave (Parr Instruments, UK) and heated and maintained at 220 °C for 12 h. This hydrothermal step was used to grow the titania particles from ca. 5 to 15 nm. Upon removal of the solution from the autoclave the separated out colloidal particles were redispersed using ultrasound. The reaction solution was then concentrated to about 12 wt% using a rotary evaporator, followed by the addition of 50 wt% Carbowax 20M to help prevent the formation of small surface cracks that are often produced when the paste is cast and allowed to dry.

The final form of the titanium dioxide paste is a white, mayonnaise-like, substance which is stable for many months if kept in the fridge. Unless stated otherwise, all titanium dioxide films produced in this work were generated from the white titanium dioxide paste and so are referred to as 'TiO_2 paste films.' It is assumed that the white colour of the TiO_2 white paste is due to light-scattering by loosely bound, large aggregates of the electrostatically stabilised, small (10–15 nm) colloidal particles of titania. Work carried out by Zaban and his co-workers on a similar system indicates that such aggregated particles may be as large as 3 μm [12]. A striking feature of this paste is that, although initially white when wet, when cast as a film it dries to produce a clear film. The paste can be cast to produce thick ($>>1\mu$m) films using a doctor-blade technique, in which a small amount of the paste is placed on a standard glass microscope slide, between two tracks of Scotch Magic Tape^{TM}, typically ca. 1 cm apart, and subsequently smeared along the gap between the tracks by a flat blade, to produce a final long strip of the TiO_2 paste film on the slide.

Figure 1 illustrates the typical variation in the absorption spectrum of the titania paste film produced by this doctor blade method as it dries and clarifies. The thickness of the film, typically 60 μm when wet, decreases as the film dries and eventually approaches a value of 4–5 μm. How and why the loosely held networks of large aggregates of nanocrystalline titania particles that form the white paste produce a final film that is devoid of such large, light-scattering, aggregates during the drying/clarification process, is not obvious and requires further investigation. However, that the final product is optically clear, i.e. non-scattering and strongly UVA-absorbing is illustrated by the UV/Visible absorption spectrum of the final, dried film in Figure 1.

Although the final stage of the titania film synthesis involved placing the freshly dried film directly into a furnace set at 450 °C for 30 min, no change in the optical characteristics of the 4–5 μm titania films were observed as a result of this treatment. Instead, this final high temperature treatment appears simply to fuse the nanocrystalline titania particles together, burn off any organic present and help bind the titania to the glass to produce a more robust film. Further work shows that even without this heat-treatment step the titania photocatalyst film is very active. X-ray analysis of the titanium dioxide films showed the films before and after the final annealing step to be anatase and SEM analysis showed that the final films comprised particles typically

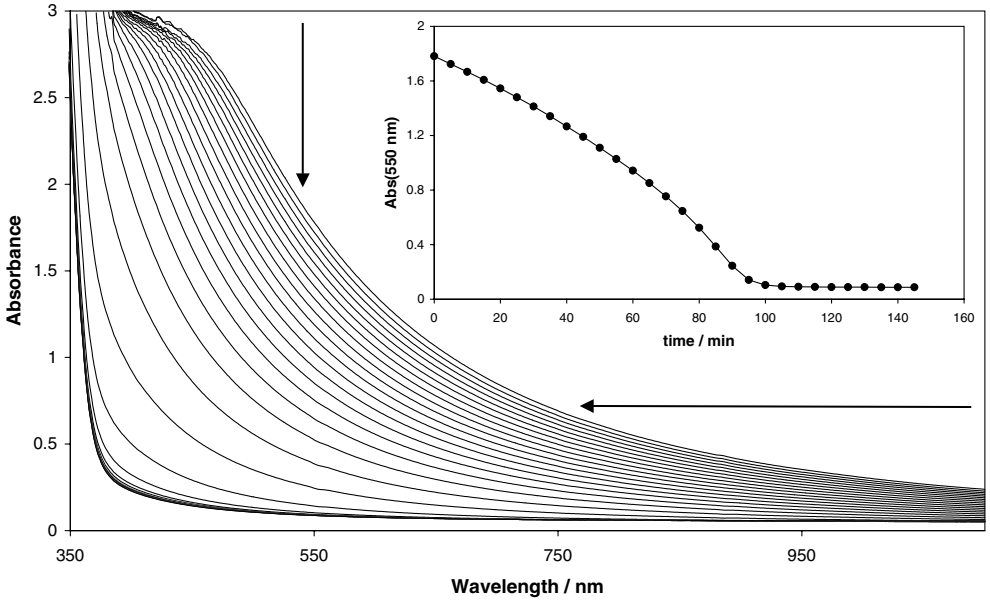

Fig. 1. UV/Vis absorption spectra of a thick paste TiO_2 freshly cast film as it dries in air under ambient conditions. The absorption spectra were recorded every 5 min and the absorbance of the film decreased with increasing drying time. This feature is highlighted in the insert diagram, a plot of the absorbance of the film at 550 nm as a function of drying time, with the data taken from the main diagram.

13 ± 1 nm in diameter. Work by others showed that such films were largely mesoporous with an average porosity of ca. 50–60%.

X-ray powder diffraction patterns for the different titania films were recorded using a Siemens D500 powder diffractometer, fitted with a Kristalloflex 710 generator with a tube head mounted at an angle of 30° from the vertical and operated at 40 kV and 20 mA. The target material was copper producing X-rays of 1.5406 Å. The post-sample radiation was detected by a scintillation counter, after first passing through a post-sample monochromator. Samples were scanned over a range of 2θ values from 20° to 80° using a step scan mode (0.05 degrees step size and 2 s count time per step). Intensity readings were recorded as a function of 2θ°.

AFM images of the films were recorded in air using a Digital Instruments Nanoscope Multimode SPM with a JV-type scanner and a Nanoscope III controller. Olympus tapping mode, silicon pyramidal, cantilevers were used, with a tip curvature <10 nm and a normal force constant of 42 N/m. For all samples both amplitude and height scans were carried out with scan sizes from 1 to 5 μm, recorded at a scan rate of 0.5–1.0 Hz and with a resolution of 512 scan lines per image. No image processing was carried out on the presented data.

3. Results and discussion

3.1. *Photocatalytic activity studies*

The rate of the photocatalytic destruction of stearic acid ($CH_3(CH_2)_{16}CO_2H$) is commonly used to provide a measure of the photocatalytic activity of any new material [11, 13–15]. The overall process may be summarised as follows:

$$CH_3(CH_2)_{16}CO_2H + 26O_2 \xrightarrow[\text{Semiconductor}]{h\nu \geq \text{band gap energy}} 18CO_2 + 18H_2O \quad (3)$$

Since the process involves the transfer of 104 electrons, it follows that the quantum yield for this process will be, at best, ca. 0.01, and this fact should be borne in mind when the measured quantum yields for Reaction (3) are considered later in this article. Since the melting point of stearic acid is markedly above room temperature, i.e. 69.3 °C, it forms solid films when deposited, usually by a spin- or dip-coating technique, on the substrate under test. As noted earlier, the destruction of stearic acid is readily monitored by FT-IR absorbance spectroscopy, since this compound has a peak at 2957.5 cm^{-1}, due to the asymmetric in-plane C–H stretching mode of the CH_3 group, and peaks at 2922.8 and 2853.4 cm^{-1}, due to the asymmetric and symmetric C–H stretching modes of the CH_2 group, respectively.

The FT-IR method employed in this work actually measures the kinetics of the disappearance of stearic acid and here and elsewhere it is assumed that this is also a direct measure of the kinetics of Reaction (3), the photocatalytic destruction of stearic acid, as would be the case if no major long-lived intermediates were generated. Support for this assumption is provided by the work of others [13–15] that shows: (a) the removal of stearic acid by semiconductor photocatalysis produces no film component other than stearic acid that is detectable by FT-IR, (b) no gas phase products other than carbon

dioxide and water are generated during the course of the photocatalytic reaction and (c) the calculated ratio of the number of moles lost due to the disappearance of stearic acid and the concomitant appearance of carbon dioxide is 1:18, as expected for the photocatalytic mineralisation of stearic acid, described by Reaction (3).

Figure 2 illustrates the observed variation in the FT-IR absorbance spectrum of a typical stearic acid film, deposited on a thick (4.5 μm) paste TiO_2 film on a glass slide, as a function of irradiation time with UVA light (365 $\pm$ 25 nm) from the six 8 W BLB illumination system. From the data in Figure 2 it is clear that the stearic acid FT-IR peaks disappear with ultra-band gap irradiation of a TiO_2 paste film, as expected from Reaction (3). Using the data illustrated in Figure 2, the integrated areas under the absorption peaks, due to stearic acid, as a function of irradiation time were calculated and plotted to generate an integrated absorbance versus irradiation time decay profile. The results of this work are illustrated in Figure 3, along with the decay profile, calculated in a similar fashion, for a stearic acid film on plain glass. Stearic acid does not absorb UVA light, thus it is no real surprise that, in the absence of titania film coating, it does not undergo any appreciable decomposition upon illumination with UVA light, as illustrated by the results in Figure 3 for plain glass. In contrast, the FT-IR absorbance versus time profiles recorded for the thick paste TiO_2 film irradiated with 365 nm light, also illustrated in Figure 3, show that under the experimental conditions employed the film is able to photocatalyse the complete destruction of stearic acid within ca. 50 min.

3.2. *Kinetics of photocatalysis*

The kinetics of the photocatalytic destruction of stearic acid, via Reaction (3), were studied as a function of initial stearic acid concentration, over the range: $(1.2–5.6) \times 10^{16}$ molecules of stearic acid cm^{-2}, i.e. 64–300 nm thick. Some of the stearic acid concentration versus irradiation time decay profiles did show some evidence of a tail to the decay profiles, particularly at high stearic acid levels, as illustrated in Figure 3. This latter feature has been suggested by others to be due to the accumulation of a small amount of material that is more difficult to destroy [14]. However, for the most part, the rate of decay appeared largely independent of the stearic acid concentration as illustrated by the results in Figure 4, and the subsequent plot of the initial rate data versus stearic acid concentration, illustrated in the insert diagram of Figure 4. Such zero-order kinetics for Reaction (3) have been reported by others [14, 15] in similar studies and are usually attributed to the complete coverage of the titania photocatalyic active sites by the stearic acid. This appears a likely situation in this work given that the initial stearic acid concentrations employed corresponded to films 25–120 monolayers thick [8].

The FT-IR absorbance versus time decay profiles, as illustrated in Figure 3, were determined for a commercial, self-cleaning, titania film (Activ^{TM}) as well as a thick titania film. For each recorded profile it was possible to determine the initial rate of destruction of stearic acid as a function of time for the film under test, first in units of integrated absorbance (i.e. peak area)/min (simply the gradient of the initial part of the decay

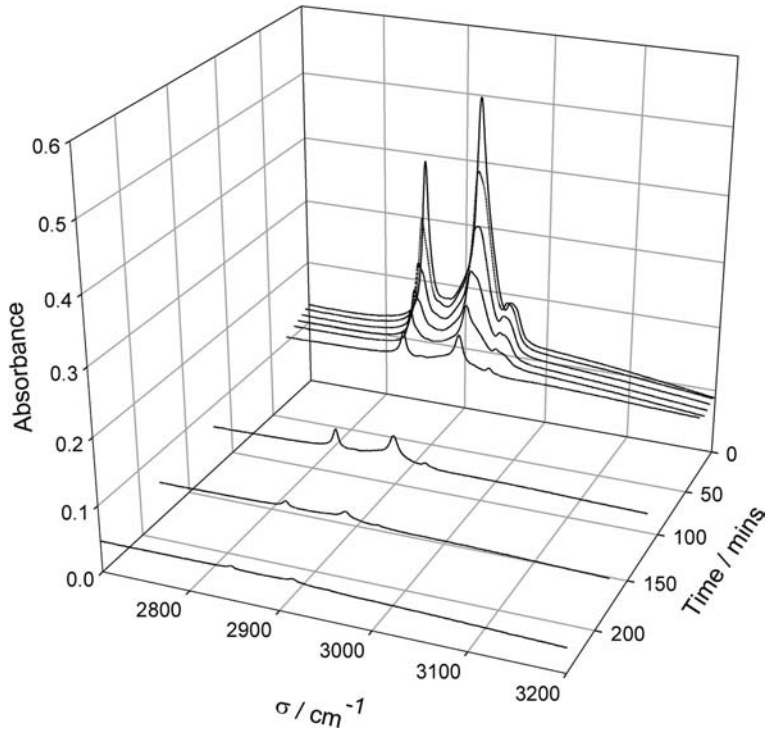

Fig. 2. Recorded decrease in the FT-IR absorbance spectrum of a stearic acid film on a typical, 4.5 μm thick paste TiO_2 film as a function of irradiation time.

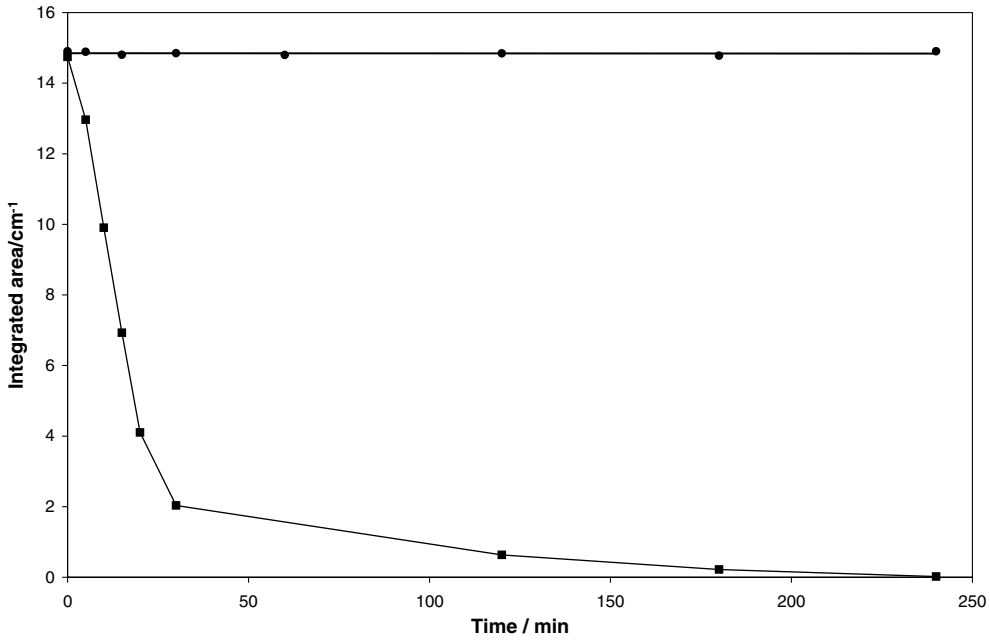

Fig. 3. Plot of the integrated area under the FT-IR absorbance spectrum of a stearic acid layer on: a typical thick TiO_2 paste film (■) and on plain glass (●), as a function of irradiation time.

curves in Figure 3) and then, as the more useful parameter, R_i, (units: molecules of stearic acid/cm^2/min). The calculated initial rates for Reaction (3), in these latter units, for a typical thick paste and Activ^{TM} titania film are listed in Table 1. For each sample, the incident light intensity, I_o, and the fraction of UV light absorbed by the film f, are known or readily calculated, thus it was possible to calculate the quantum yield for each film tested for the overall photomineralisation process, Reaction (3), ϕ, where

$$\phi = \frac{\text{initial rate of disappearance of stearic acid}(R_i)}{\text{rate of light absorption}(= I_o \times f \times (1 - R_{refl}))} \quad (4)$$

where, R_{refl} is the fraction of light reflected by the film. For smooth films of anatase (refractive index = 2.5), such as the Activ^{TM} and paste films, a value of 0.18 can be estimated for R_{refl}. The results of the quantum yield calculations for the Activ^{TM} and paste films are given in

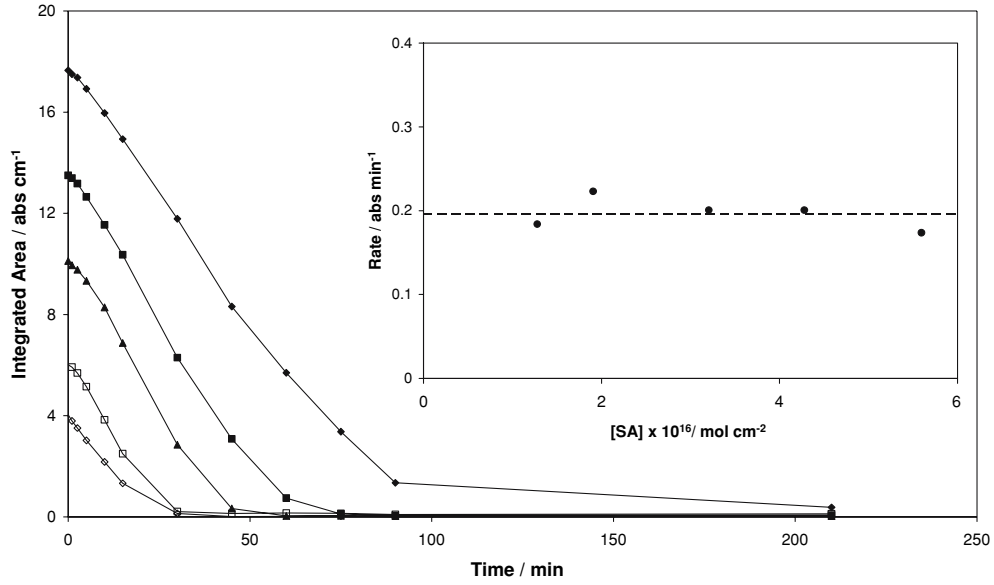

Fig. 4. Plot of a series of profiles of the form: integrated area under the stearic acid peaks, as measured by FT-IR, as a function of irradiation time. Each profile corresponds to a different initial amount of stearic acid, but the same thick TiO_2 paste film was used throughout. The insert diagram is a plot of the initial rate (taken from the data in the main diagram) as a function of initial stearic acid concentration, as determined from the measured initial integrated area [8].

Table 1. Optical and photocatalytic properties of titania-coated glass samples

Film type	Film thickness (d) /nm	Initial rate (R_i)/(10^{13} molecules/cm^2/min)	Fraction of light absorbed (f)[a]	Quantum yield[b] /(10^{-2})
Paste (thick)	4500	144.0	0.70	0.32
Activ^{TM}	15	0.6	0.07	0.01
P25	1300	–	1[c]	0.15[c]

[a]f, calculated using $f = (1 - 10^{-Abs(\lambda)})$ for Activ^{TM}, with absorbance calculated using the formula: $Abs_\lambda = 0.434\alpha_\lambda d(1-p)$, where $\alpha_{365} = 5\times10^4$ cm^{-1} [7] and $p = 0$; for the Paste(thick) films f was calculated from an analysis of the overlap of the UV/Vis spectra of the film with that of the emission spectrum of the lamp.

[b]Quantum yield, ϕ, calculated as: $\phi =$ initial rate/($f \times I_o$ (1-R_{refl})); where $I_0 = 8.02 \times 10^{17}$ photons cm^{-2} min^{-1} and $R_{refl} = (2.5-1)^2/(2.5+1)^2 = 0.18$.

[c]Actually the formal quantum efficiency (FQE), δ, for this material reported by others [11], given it has had to be assumed $f = 1$ and $R_{refl} = 0$ and, by definition, δ = rate of stearic acid destruction (molecules removed/cm^2/min)/incident light intensity (photons/cm^2/min).

Table 1, along with those, reported by others, for a 1.3 μm film of the ubiquitous titania pigment, Degussa P25 [11]; a material which is noted for its high photocatalyst activity and commonly employed as a reference photocatalyst material. The quantum yield data in Table 1 for the thick paste, and P25 films are not highly dissimilar, i.e 0.32 and 0.15, respectively, with the thick paste TiO_2 film appearing somewhat more active than the P25 film. However, the apparent enhanced photocatalytic activity of the thick paste titania film over one of P25 is likely to be fortuitous, since the latter films are white, opaque and scattering and so values for f and R_{refl} cannot be easily determined. Instead, the values for f and R_{refl} for this latter film are assumed to be unity and zero, respectively and, thus the reported quantum yield for this film should be more accurately referred to as a measure of its formal quantum efficiency, the value of which is likely to be a lower estimate of the film's true quantum yield [3]. The results in Table 1 are encouraging in that the subject of this work, namely: thick paste films, appear at least to be on a par with P25 titania, a material which is recognized as being one of the most active commercial forms of titania.

The major problem with films of Degussa P25 TiO_2 is their lack of mechanical stability, since they can be readily wiped off and are easily damaged. In contrast, thick sol–gel films are mechanically robust, undamaged, when wiped, and are not removed by successive applications and removals of Scotch Tape^{TM}; the so-called 'Scotch Tape^{TM} test'. Note that since the maximum quantum yield for this process is likely to be ca. 1%, the calculated quantum efficiency of the thick paste film of 0.32% is very high and indicates that the material is very efficient for promoting the photocatalytic Reaction (3).

In contrast to thick paste and P25 titania films, Activ^{TM} appears to comprise particles that are relatively inactive in terms of photocatalytic activity. Thus, the quantum yield for Reaction (3) was estimated as 0.01%, for Activ^{TM}, ca. 32 times lower than that for a typical thick paste film. It could be that, for reasons not clear at present, the titania produced by a CVD process is inherently less active than that produced using a sol–gel thick paste or flame-hydrolysis (P25) route. However, another suggestion is that photocatalytic activity may be related to film porosity, since both the sol–gel and the P25 films are very porous (% porosity > 50%), whereas, from SEM and AFM images, the Activ^{TM} film is comprised of particles which are very closely packed, producing largely non-mesoporous films [6, 8]. Additional evidence that film porosity may play an important role in deciding the activity of a semiconductor photocatalyst is provided later on in this paper.

3.3. *Photocatalyst durability*

An important characteristic of any photocatalyst is durability. Certainly, many semiconductors appear, on paper at least, to be a much better choice as a photocatalyst than titania, especially if the overall goal is to utilise sunlight to drive the photocatalytic process forward. However, almost all fail to deliver, usually on the grounds of poor durability. Few semiconducting materials can match titania's chemical and biological inertness, high photocatalytic activity and excellent resistance to photochemical ageing. Figure 5 illustrates the observed variation in integrated area due to stearic acid on a thick paste TiO_2 film as a function of irradiation time in an experiment which involved the repeated deposition of stearic acid on the same titania paste film and its subsequent irradiation [8]. The results in Figure 5 indicate that the photoactivity of a thick paste titania film does not diminish with repeated irradiation and help reinforce the reputation of this photocatalyst material for high photochemical durability. In contrast, most other semiconducting materials, especially those with bandgaps that fall into the visible region, either exhibit little or no photocatalytic activity or readily undergo photocorrosion and/or inhibition. The search for a photocatalyst with all the positive features of titania as a photocatalyst and an ability to absorb visible as well as UV light is one of the continuing great quests in photochemistry.

3.4. *Photocatalyst activity: Effect of final annealing temperature*

Usually in the sol–gel synthesis of titania, the titania is largely in an amorphous, hydrated form, $Ti(OH)_4$, and the final high temperature annealing step

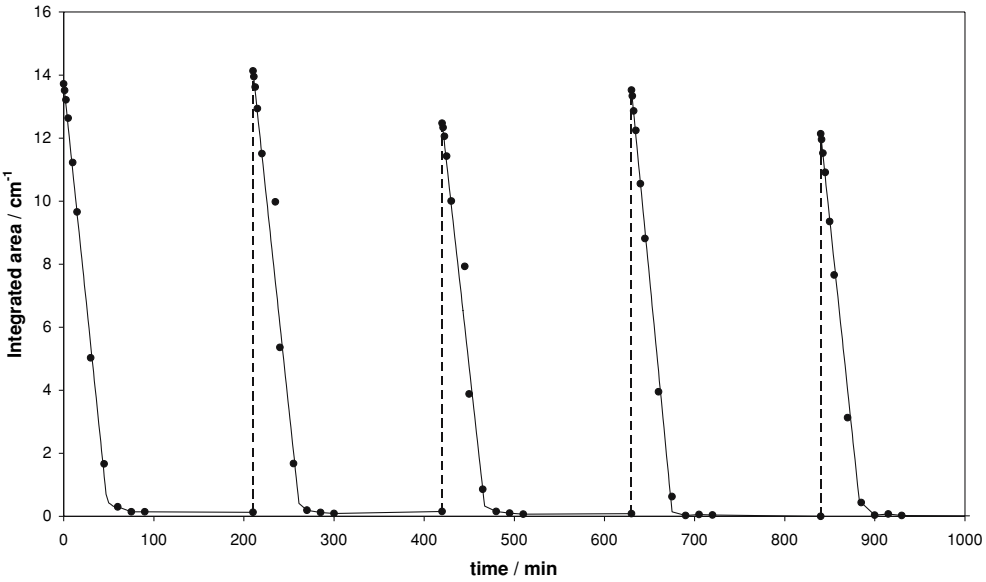

Fig. 5. Plot of a profile of the integrated area under the stearic acid peaks as a function of irradiation time, recorded using the same thick TiO_2 paste film. The broken lines indicate the point of addition of a further amount of stearic acid after the complete removal of the previous one [8].

($T \geq 450$ °C) promotes the processes of dehydration and crystallisation, often leading to the formation of anatase particles [16–18]. However, the hydro-thermal particle growth step employed here in the preparation of the titania thick paste appears not only to promote particle growth, but also crystallisation. Thus, XRD analysis of the final paste reveals the titania particles to be largely anatase even before the final heat-treatment step is applied. Although the photocatalytic activities of an annealed (450 °C for 30 min) and non-annealed thick titania paste film are the very similar, at higher annealing temperatures the photocatalytic activity of the film is expected to change, either due to particle sintering or a change in crystal phase (from anatase to rutile). In a study of this effect, the photocatalytic activities of the thick paste films were measured, as a function of final annealing temperature, applied for 30 min to a set of typical non-annealed films. In this work quartz was used as the glass substrate in order to allow the application of high (up to 900 °C) annealing temperatures and each film generated was also characterised by UV/Vis spectrophotometry, XRD, AFM and profilometry.

The measured variation in UV/Vis spectrum of these films as a function of annealing temperature is illustrated in Figure 6 and reveals that whereas there is little

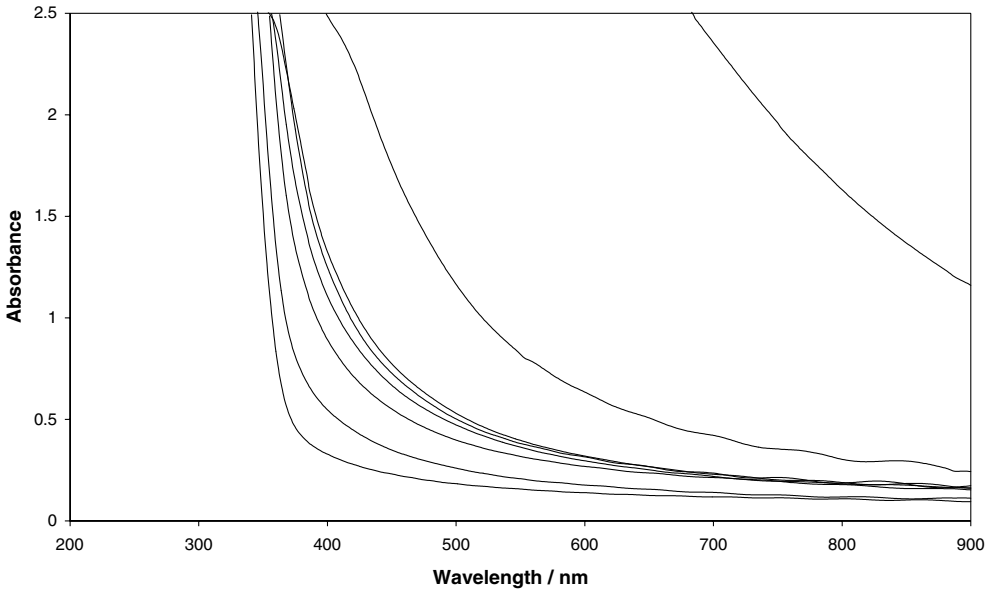

Fig. 6. UV/visible absorbance spectra for a series of thick paste films (initially, ca. 4.5 μm thick) annealed at the following temperatures for 30 min (from left to right): 450, 700, 730, 740, 750, 760, 800 and 900 °C, respectively.

difference between the absorption spectrum of a film annealed at 450 °C and one annealed at 700 °C, the films become more opalescent and light-scattering as the annealing temperatures is increased above 700 °C. In particular, the films become highly scattering at annealing temperatures > 760 °C, and, as a consequence, films annealed at 900 °C are white and opaque. This variation in UV/Vis absorption spectrum is mainly due to particle growth through sintering.

Direct evidence for the sintering of titania particles in the thick paste films, with annealing temperatures > 760 °C, was gained from an AFM study of the different films, some of the results of which are illustrated in Figure 7. Thus, although the AFM's of the 450 and 700 °C annealed films are quite similar, comprising particles typically 50–60 nm in diameter, films annealed at 800 °C and, especially, 900 °C are comprised of much bigger particles, i.e. typically, 99 and 217 nm, respectively. From this AFM study it is not surprising that the films become more scattering at high annealing temperatures, since particle growth is significant at these elevated temperatures, especially at temperatures ≥800 °C.

Particle growth at temperatures ≥ 800°C is important, but another critical process, which should not be ignored, is the phase change of titania from anatase to rutile, which also occurs in this region and a good way to study this process is through the use of XRD. Thus, the variation in the XRDs of the annealed titania films was studied as a function of annealing temperature and the results of this work are illustrated in Figure 8(a). Anatase titania has major XRD peaks associated with the following crystal planes and spacings, i.e. (*hkl*, *d*/Å): (101, 3.51), (200, 1.89), (0 0 4, 2.38) and (05, 1.70), respectively, whereas rutile has peaks at: (110, 3.25), (211, 1.69), (101, 2.49) and (111, 2.19), respectively. Given that the wavelength of the X-radiation used in this work was 1.5406 Å, and the value of *d* is related to the Bragg angle associated with a specific crystal spacing, θ, via the following equation:

$$d(\text{in Å}) = 1.5406/(2\sin\theta) \tag{5}$$

It follows that anatase is expected to exhibit major peaks at 2θ values of: 25.4°, 48.1°, 37.8° and 53.9° and rutile at: 27.4°, 54.3°, 36.1° and 41.2 ° and some, or all,

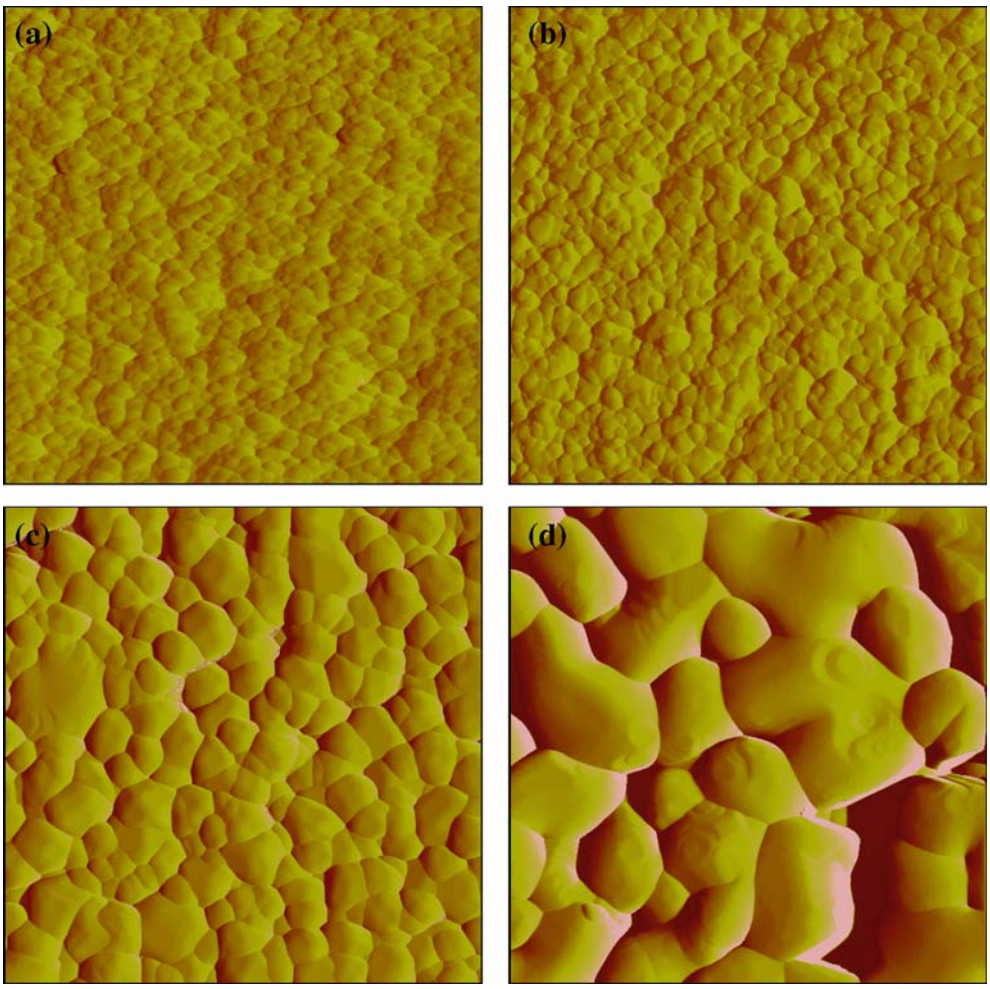

Fig. 7. AFM images of a series of thick paste films (initially, ca. 4.5 μm thick) annealed at the following temperatures for 30 min: (a) 450, (b) 700, (c) 800 and (d) 900 °C, respectively; all illustrated AFM's are for a scanned area of 1 μm^2.

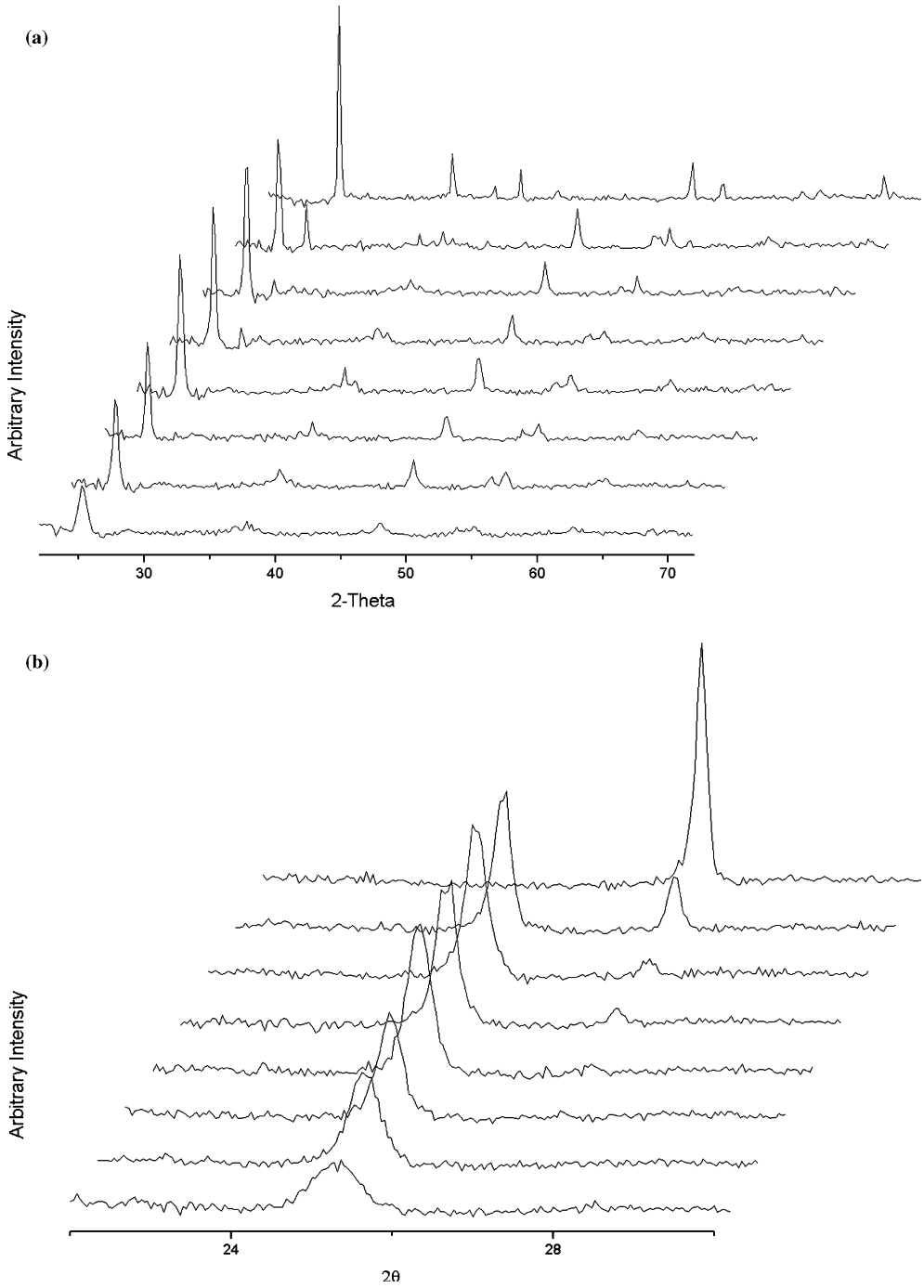

Fig. 8. (a) Powder XRD patterns recorded for a series of thick paste films (initially, ca. 4.5 μm thick) annealed at the following temperatures for 30 min (front to back): 450, 700, 730, 740, 750, 760, 800 and 900 °C, respectively. (b) Enlargement of the XRD spectra in (a), spanning the range $22 \leq 2\theta \leq 30$.

of these peaks can be seen in the XRD spectra illustrated in figure 8(a). Figure 8(b) illustrates an expanded section in the XRD spectra in Figure 8(a) and shows that with increasing annealing temperature, the presence of rutile (major peak (110) at $2\theta = 27.4°$) in the film emerges only at annealing temperatures ≥ 740 °C and in significant amounts only $T \geq 800$ °C. In addition, in all films annealed at temperatures < 900 °C, anatase is the predominant species. Spurr and Meyers used the intensities of the lines at $2\theta = 25.4°$ for the (101) plane of anatase and $2\theta = 27.4°$ for the (110) plane of rutile, i.e. the lines depicted in figure 8(b), to calculate the fraction of anatase, x_A, using the following expression:

$$x_A = \frac{1}{1 + 1.26(I_R/I_A)} \tag{6}$$

where I_R and I_A are the intensities of the reflections for the (110) plane of rutile and the (101) plane of anatase, respectively [19]. Using this formula, and the data in figure 8(b), the variation in x_A was determined as a function of annealing temperature and the results of this

work are illustrated in figure 9. The results show that the level of rutile in the films is only ca. 25% even at an annealing temperature of 800 °C and that only at 900 °C is the film fully transformed in rutile.

From the peak width of the XRD peaks at $2\theta = 25.3$ and 27.4 it is possible to estimate the average size of the crystal domains in each of the films as a function of annealing temperature using the Scherrer equation [20]. A plot of particle size, as measured by AFM, versus crystal domain size, as calculated from XRD data using the Scherrer equation, is illustrated in figure 10 and shows that at low annealing temperatures, i.e. ≤ 730 °C, the particle size is almost independent of annealing temperature, whereas the crystal domain size increases markedly. Thus, at these low annealing temperatures, crystal growth within particles dominates over the process of particle sintering and growth. At higher annealing temperatures, i.e. ≥ 740 °C, particle growth is more significant than crystal growth, with the size of the titania particles growing due to particle sintering ca. 5–6 times faster than that of crystal domain size.

Of critical significance to a self-cleaning film is the observed variation in its photocatalytic activity as a function of annealing temperature. In this work the measured rates of destruction of stearic acid, via Reaction (3) for each of the annealed films was used to assess the variation in the photocatalytic activity of the thick paste TiO_2 films as a function of annealing temperature and the results of this work are illustrated in Figure 11.

The significant feature of these results is the marked loss of photocatalytic activity of the titania films annealed at temperatures ≥ 760 °C. This loss as a function of annealing temperature does not correspond very well, with either the observed variation in particle or crystal domain size, or with the crystal phase, with annealing temperature. Thus, at 760 °C the particle size and crystal domain sizes are still relatively small (i.e. 82 and 24 nm, respectively) and there is little rutile present (7%). Instead, the drop in photocatalytic activity, illustrated in Figure 11, appears to correlate best with the apparent change in the porosity of the film. An approximate estimate of the fractional porosity, p, of the film can be made using the following formula:

$$p = \frac{h - h_0}{h} \tag{7}$$

where h and h_0 are the thicknesses of paste titania films with porosities, p, and zero, respectively.

In this work the thicknesses of all the films were measured by profilometry. Assuming that the films annealed at 900 °C have zero porosity, (AFM analysis of these films show them to be very compact), then the measured value of its thickness, which is 2.13 μm, is, according to Equation (7), h_o. Using this value for h_o, and the measured thicknesses for the other films and Equation (7), it is possible to calculate the variation in porosity, p, as a function of film annealing temperature and these results are illustrated in Figure 12. Some support for this approach for estimating porosity is that the value calculated using Equation (7), 51%, for 450 °C annealed films, is similar to that estimated for similar films by others [21], using gas adsorption methods (50–60%). Significantly, a plot of film photocatalyst rate versus its calculated porosity yields a good straight line, as illustrated by the insert diagram in Figure 12, i.e. there appears to be a linear correlation between the photocatalytic activity of a titania film and its porosity.

As noted earlier, the apparently low photocatalytic activity of commercial self-cleaning titania films, made by CVD, has been attributed previously to the low porosity of these materials, compared to most sol–gel

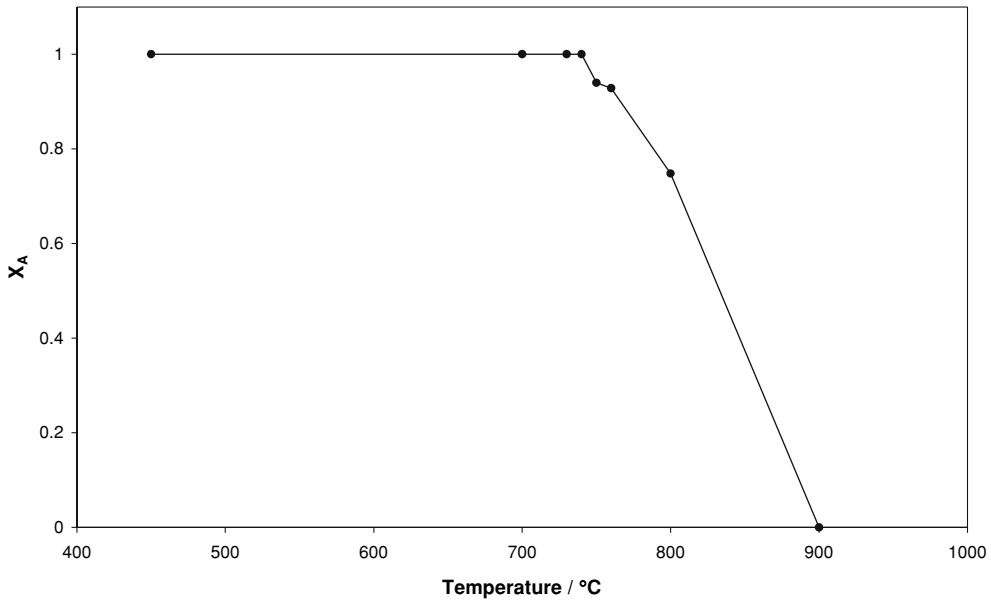

Fig. 9. Fraction of particles that are in the anatase form, x_A, as a function of film annealing temperature. The values of x_A for the different films were calculated using Equation (6) and the intensity data in Figure 8.

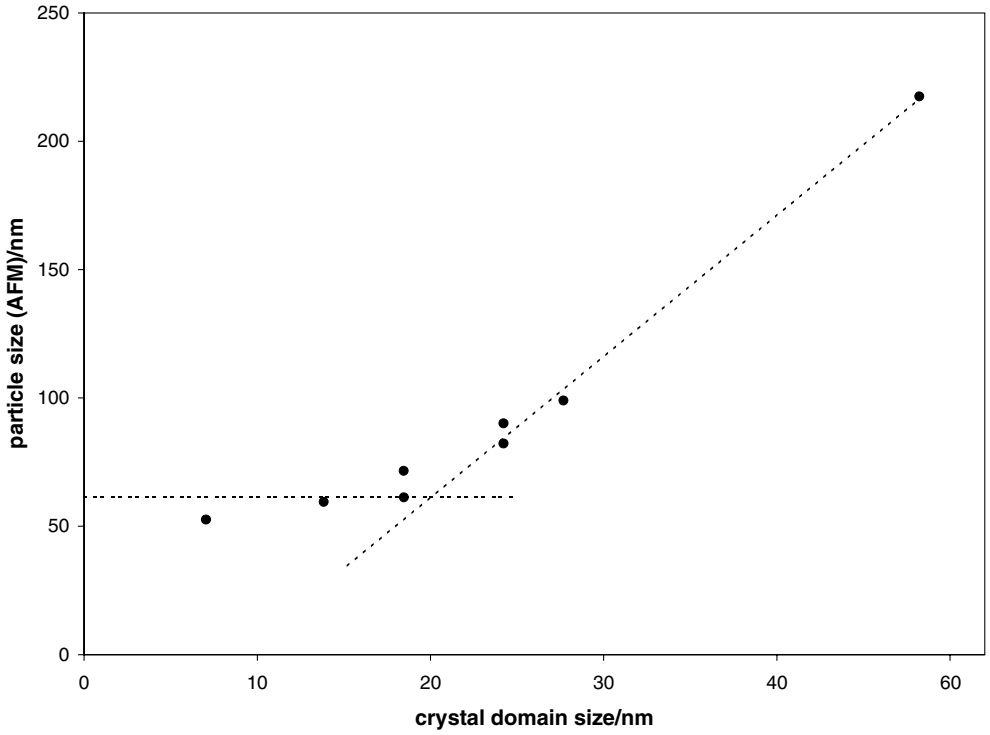

Fig. 10. Plot of particle size, as measured by AFM and crystal domain size, as measured using the data in Figure 8 and the Scherrer equation [20], for the different thick paste TiO_2 films annealed at different temperatures.

films [8]. One possible way in which porosity might be expected to positively influence photocatalyst activity is by providing a route, other than through the largely gas-impermeable stearic acid layer, for oxygen to diffuse to the active sites; effectively a 'fire-grate' effect. The prolonged photocatalytic mineralisation of organics by semiconductor photocatalysis is not possible without oxygen; the overall process is, after all, simply the photocatalysed 'cold-combustion' of the organic material. A porous film might be expected to provide channels through which the essential co-reactant, oxygen can diffuse to the surfaces of the titania and allow the photocatalytic process to occur unhindered. In contrast, a compact, non-porous, titania film will lack such channels, the rate of diffusion to the active sites will be expected to be less and, as a consequence, the rate of overall photocatalysis will be slower.

In a fire-grate, the rate of combustion can be controlled to some extent by the position of the grate. When open, the access of air to the burning embers

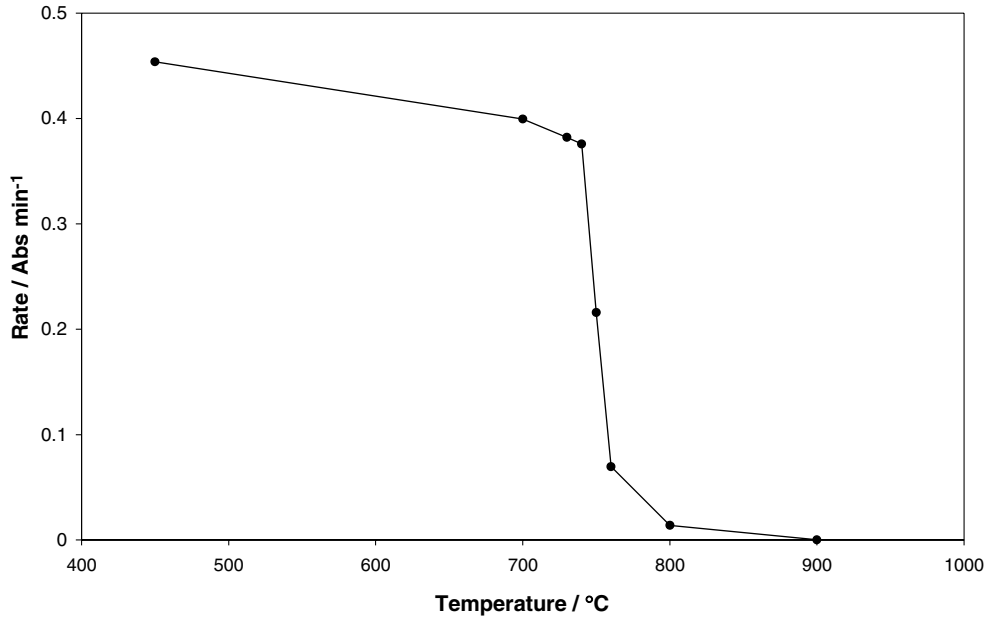

Fig. 11. Measured initial rate of the photocatalytic destruction of stearic acid as a function of annealing temperature for the thick paste TiO_2 films.

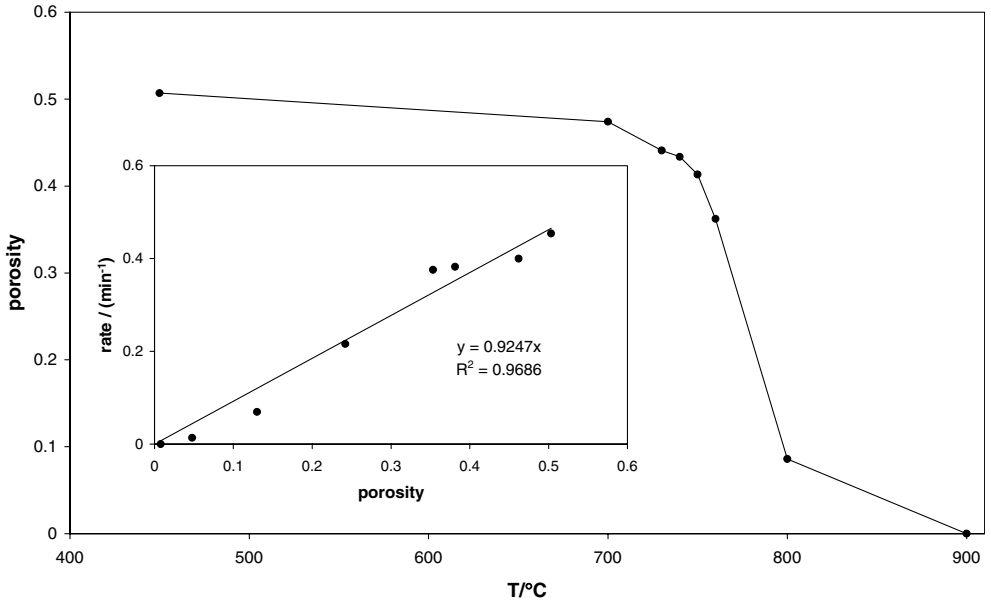

Fig. 12. Calculated variation in the porosity of the thick paste films, determined using Equation (7) and film thickness data obtained by profilometry, as a function of film annealing temperature. The insert diagram highlights the apparent linear relationship between the measured rate of photocatalysis (data from Figure 11) and the calculated porosity (from main diagram) for the thick paste TiO_2 films annealed at different temperatures.

nearest the grate is unlimited and combustion is rapid. When closed, the flow of air is appreciably curtailed and combustion is greatly reduced. As a consequence, the enhanced photocatalytic activity of porous titania films may be likened to an 'open fire-grate' effect, whereas the markedly reduced activity of compact, non-porous films is like a 'closed fire-grate' effect.

Although, from the results of this work, film porosity appears to be an important, and until now largely unrecognised, parameter in deciding the overall photocatalytic activity of titania films, the role of crystal phase may be just as important and should not be ignored. Certainly some researchers report rutile to be inactive as a photocatalyst material [22, 23], whereas others, after taking into consideration its usually reduced specific surface area, have found it to be similar in activity as anatase [24, 25]. In order to separate the roles of crystal phase and porosity on photocatalytic activity more work is required. In particular the generation of thick paste, porous rutile films of similar particle sizes and morphology to the ones reported in this work and thin, non-porous rutile and anatase films would help resolve some of these issues. Further work is in progress to develop such materials.

4. Conclusions

Thick paste TiO_2 films are optically clear, durable and very active as photocatalysts for the destruction of stearic acid on their surfaces. Although all the key features of such photocatalyst films are unchanged at annealing temperatures below 700 °C, above this temperature they are altered markedly. Thus, the films become increasing opaque, especially at temperatures >760 °C and much less active. The marked decrease in photocatalytic activity appears to correlate well with the change in the calculated porosity of thick paste films as a function of annealing temperature. This finding may help explain the low photocatalytic activity associated with most commercial samples of self-cleaning glass, since their active outer coating usually comprises nancrystalline, non-porous thin films of titania.

References

1. R. Bridgeman, *1000 Inventions and Discoveries* (Dorling, Kindersley, 2002).
2. V. Ashton, *Chem. Brit*. June (2002) 26.
3. A. Mills and S. LeHunte, *J. Photochem. Photobiol. A: Chem*. **108** (1997) 1.
4. A. Fujishima, T.N. Rao and D. Tryk, *J. Photochem. Photobiol. C: Photochem. Rev*. **1** (2000) 1.
5. A. Mills and S.-K. Lee, *J. Photochem. Photobiol. A: Chem*. **152** (2002) 233.
6. A. Mills, A. Lepre, N. Elliott, S. Bhopal, I.P. Parkin and S.A. O'Neill, *J. Photochem. Photobiol. A: Chem*. **160** (2003) 213.
7. A. Mills, S.-K Lee, A. Lepre, I.P. Parkin and S.A. O'Neill, *Photochem. Photobiol. Sci*. **1** (2002) 865.
8. A. Mills, G. Hill, S. Bhopal, I.P. Parkin and S.A. O'Neill, *J. Photochem. Photobiol. A: Chem*. **160** (2003) 185.
9. A. Mills, N. Elliott, G. Hill, D. Fallis, J.R. Durrent and R.L. Willis, *Photochem. Photobiol. Sci*. **2** (2003) 591.
10. S.-K. Lee, S. McIntyre and A. Mills, *J. Photochem. Photobiol. A: Chem*. **162** (2004) 203.
11. Y. Paz, Z. Luo, L. Rabenberg and A. Heller, *J. Mater. Res*. **10** (1995) 2842.
12. A. Zaban, S.T. Aruna, S. Tirosh, B.A. Gregg and Y. Mastai, *J. Phys. Chem. B* **104** (2002) 4130.
13. P. Sawanyama, L. Jiang, A. Fujishima and K. Hashimoto, *J. Phys. Chem. B* **101** (1997) 11000.

14. T. Minabe, D.A. Tryk, P. Sawanyama, Y. Kikuchi, K. Hashimoto and A. Fujishima, *J. Photochem. Photobiol. A: Chem.* **137** (2000) 53.
15. S. Sitkiewitz and A. Heller, *New J. Chem.* **20** (1996) 233.
16. S. Doeff, M. Henry, C. Sanchez and J. Livage, *J. Non-Cryst. Solids* **89** (1987) 206.
17. J. Livage and C. Sanchez, *J. Non-Cryst. Solids* **145** (1992) 11.
18. F. Babonneau, C. Sanchez and J. Livage, *J. Non-Cryst. Solids* **106** (1988) 170.
19. R.A. Spurr and H. Myers, *Anal. Chem.* **29** (1957) 760.
20. H.P. Klug and L.E. Alexander, *X-Ray Diffraction Procedures for Polycrystalline and Amorphous Materials* (Wiley, NY, 1954), p. 512.
21. C.J. Barbé, F. Arendse, P. Comte, M. Jirousek, F. Lenzmann, V. Shklover and M. Grätzel, *J. Am. Ceram. Soc.* **80** (1997) 3157.
22. K. Okamoto, Y. Yamamoto, H. Tanaka and A. Itaya, *Bull. Chem. Soc. Jpn.* **58** (1985) 2015.
23. V. Augugliaro, L. Palmisano, A. Sclafani, C. Minero and E. Pelizzetti, *Toxicol. Environ. Chem.* **16** (1988) 89.
24. A. Sclafani, L. Palmisano and M. Schiavello, *J. Phys. Chem.* **94** (1990) 829.
25. A. Mills and S. Morris, *J. Photochem. Photobiol. A: Chem.* **71** (1993) 285–289.

Available online at www.sciencedirect.com
ScienceDirect
Journal of Photochemistry and Photobiology A: Chemistry 187 (2007) 370–376
Journal of Photochemistry and Photobiology A:Chemistry
www.elsevier.com/locate/jphotochem

Novel low-temperature photocatalytic titania films produced by plasma-assisted reactive dc magnetron sputtering

Andrew Mills [a,*], Jishun Wang [a], Matthew Crow [a], Giovanni Taglioni [b], Luca Novella [b]

[a] *Department of Pure & Applied Chemistry, University of Strathclyde, Glasgow G1 1XL, UK*
[b] *Galileo Avionica, Via Turanense km. 44, 67061 Carsoli (Aquila), Italy*

Received 10 September 2006; received in revised form 20 October 2006; accepted 3 November 2006
Available online 9 November 2006

Abstract

Robust, active, anatase titania films, 250 nm thick, are deposited onto glass at low temperatures, i.e., <100 °C, using plasma-assisted, reactive dc magnetron sputtering (PAR-DC-MS). The films are transparent and colourless and truly photocatalytic, exhibiting turnover numbers >2.0 for the photocatalytic mineralization of stearic acid. These films are typically 6.9 times more active than a sample of commercial self-cleaning glass, comprising a 15 nm layer of titania deposited by CVD, mainly because they are much thicker and, therefore, absorb more of the incident UV light. The most active of the films tested comprised particles of P25, but lacked any significant physical robustness. Similar results, but much more quickly obtained, were generated using a photocatalyst-sensitive ink, based on the redox dye, resazurin, Rz. All titania films tested, including those produced by magnetron sputtering exhibited photo-induced superhydrophilicity. The possible future application of PAR-DC-MS for producing very active photocatalytic films on substrates not renowned for their high temperature stabilities, such as plastics, is noted.

Keywords: Photocatalysis; Plasma-assisted; Magnetron sputtering; Low-temperature; Titania; Stearic acid; Resazurin

1. Introduction

Semiconductor photocatalysis (SPC) continues to be the focus of many research groups, especially with regard to the ability of many semiconductors, most notably titania, to mediate the photomineralisation of many organics by oxygen [1–4], i.e.,

$$\text{organic} + O_2 \xrightarrow[h\nu \geq E_{bg}]{TiO_2} \text{minerals} \quad (1)$$

where E_{bg} is the bandgap of the semiconductor, 3.0–3.2 eV for TiO_2. Such is the ability of titania to mediate reaction (1) that several major commercial products, based on titania photocatalyst films, have been launched successfully in recent years [5]. These include self-cleaning glass and tiles, such as Activ™ [6] and Hydrotech™ [7], sold by Pilkington Glass and TOTO, respectively.

In most commercial manifestations of SPC, the active layer is a film of titania, usually produced via some high temperature treatment process, involving CVD or a sol–gel process. The high temperatures (typically ≥450 °C) are needed to convert a largely inactive amorphous titania into a much more active crystalline form, usually anatase and to help produce a physically robust film. It follows that, so far, the titania-film supporting substrate must be resistant to such high-temperature treatment; clearly not a problem when it comes to self-cleaning glass and tiles [6–8]. However, there is an obvious future market for transparent photocatalytic films on plastics for use in street-light covers, car and plane windows and corrugated sheet roofing, for example. Exploitation of this potentially large market has been largely hindered by the inherent high-temperature step in titania film production.

Reactive magnetron sputtering is an example of a physical vapour deposition (PVD) method by which titania films can be generated [9–17]. However, this along with most other PVD methods, produces titania films which are usually non-stoichiometric, amorphous, not very active photocatalytically and poorly attached to the substrate (usually glass) without a post heat-treatment step to anneal and crystallise the film [10,13,17]. Note: a rather elegant method to produce low temperature active films of titania involves the combination of a sol–gel process, followed by a low-temperature oxygen plasma

* Corresponding author. Tel.: +44 141 548 2458; fax: +44 141 548 4822.
E-mail address: a.mills@strath.ac.uk (A. Mills).

1010-6030/$ – see front matter © 2006 Elsevier B.V. All rights reserved.
doi:10.1016/j.jphotochem.2006.11.004

treatment [18]; however, use of the latter might pose problems if the substrate was easily oxidised, as might be in the case of a plastic.

Typically, in reactive dc sputtering, argon gas is used as the sputtering gas and a titanium metal target is bombarded with argon ions, producing a vapour of titanium atoms, which then reacts with the oxygen reactive gas, to produce TiO_2 that deposits onto the substrate. A ring magnet placed below the target enhances the sputtering process. The mechanical characteristics of the titania film that forms, in particular adhesion and compactness, depend upon the energy of the condensing particles and in most cases, this energy is insufficient to create mechanically robust, active, stoichiometric titania films [13]. However, by applying a radio-frequency ac-voltage to the non-conducting substrate, a plasma is created over the substrate area that allows the condensing particles to gain sufficient energy, via chemical activation and acceleration, to create mechanically robust, active, stoichiometric films of titania. Interestingly, these films are also quite crystalline, thus, no post high-temperature treatment step is required to activate these plasma-assisted, reactive dc magnetron sputtered (PAR-DC-MS) titania films and the maximum temperature endured by the substrate can be $\leq$100 °C. Previous work has reported on the use of dc magnetron sputtering as a route to produce thin titania films. However, most require temperatures >100 °C to produce the most active films [9–17] and few report on the mechanical stability of these films [13]. In this initial paper, the use of this low-temperature deposition technique to create robust titania films on glass is described. The photocatalytic activity of the titania films is assessed by two different methods and compared to that of a typical, commercial self-cleaning glass film, Activ^{TM}. This system allows 3D objects, up to 30 cm across in any direction, as well as planar substrates, as used in this work, to be coated with titania.

2. Experimental

The plasma assisted reactive dc sputtering deposition, PAR-DC-MS, system used in this work was built on site. The system comprised a deposition chamber which utilised a batch vacuum system with a configuration commonly used for the production of optical components, i.e. a turbo-molecular pump and gas flow and process pressure control systems. The sputtering component comprised a standard dc magnetron sputtering source (Galileo Avionica) fed by a dc pulsed generator (Advanced Energy) that typically operated under the following conditions: power 3 kW, voltage 430 V, current 6.8 A, pulse frequency 10 kHz and pulse width 1 μs. A conductive target, 4 mm thick TiO_x, where x lies in the range 1–2, with planar dimensions 305 mm × 127 mm, supplied by Bekaert VDS (Deinze), was used in this work. In most other work in which titania films are produced by reactive sputtering a titanium metal target is used, and a TiO_x target is used here because the sputtered sub-oxide of titania is easy to oxidise fully to titania and yet, being a sub-oxide is still sufficiently conducting to be sputtered using a dc magnetron. A fully oxidised titanium target would require an RF magnetron with significantly lower sputtering rates. The plasma assistance

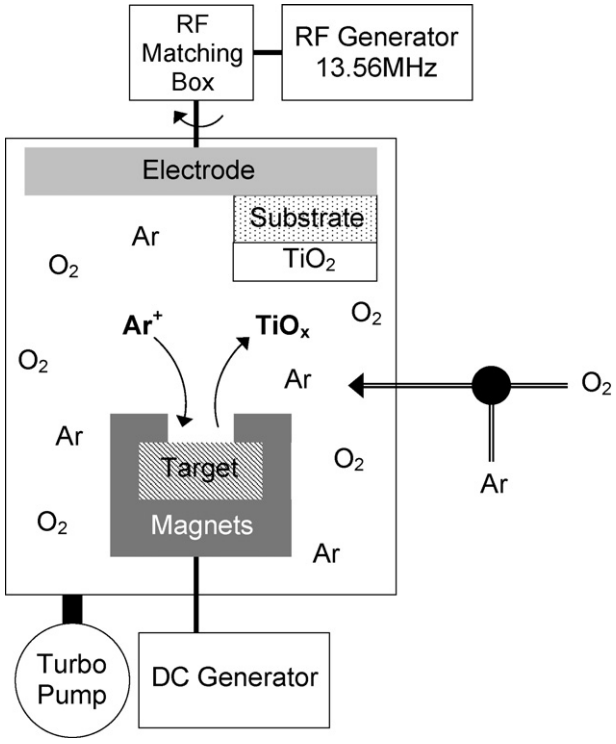

Fig. 1. Schematic illustration of the PAR-DC-MS system for producing low-temperature, active titania films.

was provided by a rotary metallic substrate holder connected to an RF system, operating at 13.56 MHz with a power density of 0.013 W cm^{-2}. Fig. 1 provides a schematic illustration of the PAR-DC-MS system, with its various major components.

In a typical run using this system, 3 mm thick glass samples (diameter: 25 mm) were placed in the chamber which was then pumped down to 10^{-4} mbar after which a 4:1 mixture of argon and oxygen was pumped in, to achieve a process pressure of 2×10^{-2} mbar. A typical run time was 270 min and the final thickness of the deposited titania film was ca. 250 nm. A long deposition time is required to ensure no excessive local heating of the substrate and the creation of a robust, crack-free, uniform film. The films produced using this procedure were optically clear and exhibited an XRD spectrum typical of anatase titania. In particular, the XRD spectrum, illustrated in Fig. 2(a), showed peaks corresponding to the 101, 200 and 211 crystal planes, with d-spacings of 3.52, 1.89 and 1.67 Å, i.e., $2\theta_B = 25.3°$, 48.1° and 54.9° for CuKα_1 radiation, respectively.

The films were mechanically very robust and were not removed or damaged by numerous abrasion and adhesion tests including: a pull test using 3M Scotch Tape^{TM} and a moderate abrasion test, using a cheesecloth pad, with a 0.5 kg weight attached to the rubbing head for pressure, which was rubbed 25 times over the sample [13]. A typical AFM of the titania film is illustrated in Fig. 2(b) and shows the film to be comprised of closely packed particles, typically 60 nm in diameter. The R_q and R_{max} values for the PAR-DC-MS film were 4.6 and 41.7 nm, respectively; approximately twice those for Activ^{TM}, indicating that the former are approximately twice as rough.

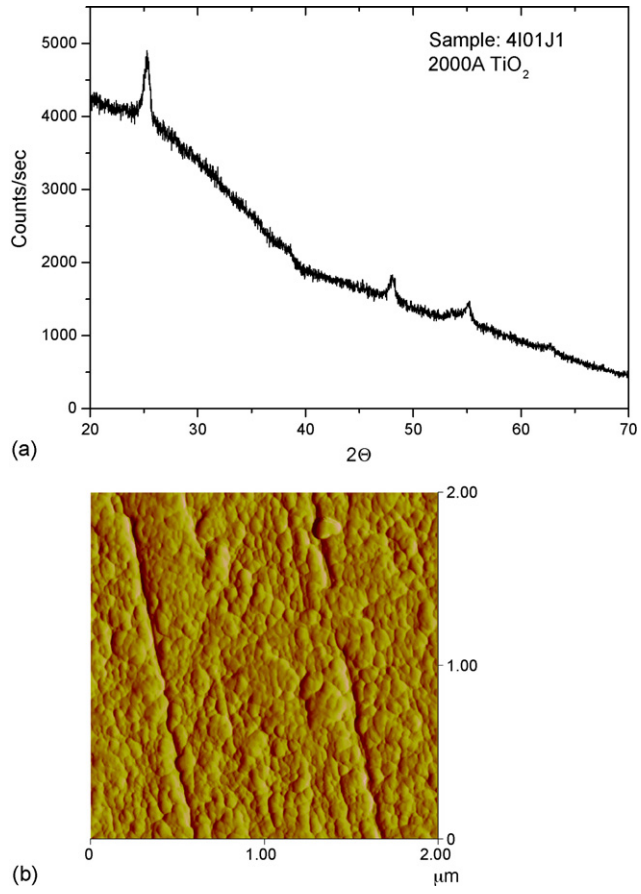

Fig. 2. (a) CuKα_1 XRD spectra of PAR-DC-MS titania film on glass, with peaks at 25.3°, 48.1° and 54.9°, indicating an anatase only crystal phase present and (b) AFM image of the titania film produced by PAR-DC-MS, with most titania particles ca. 60 nm in diameter.

Other titania films used in this work were a commercial self-cleaning glass, Activ^{TM} (Pilkington Glass), comprising a 15 nm thick titania film as the active coating, prepared by a CVD technique [19] and thick, 4 μm, titania films prepared by a sol–gel method [20]. In both cases, the titania was anatase. P25 titania films 90 nm thick were prepared using a dip-coat method described elsewhere [19]. As part of the assessment of the photocatalytic activities of the various TiO_2 films, stearic acid was used as the organic material to be mineralized via reaction (1) [20–26]. For each film tested, 1.0 ml of a 0.02 M stearic acid in chloroform solution was spread over the film, and then spun at 500 rpm for 15 s, in order to coat the film with a thin layer of stearic acid. The final coated film was dried in an oven at 80 °C for 10 min, allowed to cool and then used directly. The infra-red spectrum of the film before and after the addition of the stearic acid layer was recorded using a Spectrum 1 FT-IR spectrometer (Perkin Elmer, UK). The same instrument was used to record the FT-IR spectrum of the film as a function of time of irradiation with ultra-band gap light. The FT-IR's software allowed the integrated area under the stearic acid peaks to be determined over the range 2800–3000 cm^{-1} for each FT-IR spectrum recorded and a plot of A_{int} versus irradiation time to be generated. A typical stearic acid film had an initial integrated absorbance over this range of 1.0 cm^{-1}, corresponding to ca. 9.7×10^{15} molecules of stearic acid cm^{-2} [27]. In the stearic acid tests, all irradiation were performed using six 8 W blacklight bulbs (i.e. 365 ± 20 nm) set in a half cylinder unit, with back aluminium reflector, held 13 cm above the sample. In this work, the incident light intensity was 4.32 mW cm^{-2}. All incident light intensities were measured using a UV meter with a calibrated UVA detector (UVP model MS-100 with MS125 UVA sensor).

The photocatalytic activities of the titania films were also assessed using a photocatalyst ink [28] comprising: 3 g of a 1.5 wt% aqueous solution of hydroxyethyl cellulose (HEC), 0.3 g of glycerol and 4 mg of the redox dye, resazurin, Rz. Typically, a 25 mm^2 section of the sample under test was coated with a few drops of this ink, spun at 500 rpm for 10 s, and dried in an oven at 70 °C for 10 min. Drying in air, rather than in an oven, did not alter the performance of the ink. A typical dried ink film was ca. 590 nm thick, as measured by weighing the film and using a weight-averaged density based on the relative amounts of HEC and glycerol present. In the ink tests, all UV irradiations were performed using a small UVA irradiation system (VWR), comprising two, 4 W black light blue lamps (typical output: 365 ± 20 nm); with an irradiance of 7.4 mW cm^{-2} when placed directly above the sample under test. All UV/Vis spectra were recorded using a Thermo Electron Helios Beta UV/Vis single beam spectrophotometer.

Contact angles were measured using an FTA200 contact angle instrument (Camtel). This instrument allows the deposition of a 10 μL water droplet onto the substrate under test via a 500 μL syringe coupled to a 27 gauge needle with a 90° bevel tip held above the test substrate. The shape of the droplet on the sample under test was stable for many minutes and so 30 s after its delivery its profile was recorded using a combination of a white light source, prism and CCTV, all in a horizontal plane, i.e., perpendicular, to that of its delivery. The resulting recorded profile image of the water droplet was then analysed and the contact angle determined using a computer and proprietary instrument software. In this part of the work, ultra-band gap irradiation of the films under test were carried out using two 8 W 254 nm germicidal lamps (BDH, UK) for 30 min.

3. Results and discussion

A popular method for assessing the activity of a self-cleaning titania photocatalyst film is the stearic acid (SA) test, in which a thin layer of SA is deposited onto the film and its photocatalytic destruction monitored as a function of time. This reaction has gained preference over the years [20–27] for a number of reasons, including (a) SA provides a reasonable model compound for the solid, wax-like, thin organic films that deposit on exterior and interior surfaces, (b) SA is very stable under UV illumination in the absence of a photocatalyst film, (c) SA films, typically >monolayer thick (i.e. >2.5 nm) [24], are very easily cast onto the photocatalytic film under test from a methanol or chloroform solution and (d) the kinetics of removal of >2.5 nm thick SA films are usually simple and zero-order, and the thickness of the deposited SA film on a titania film under test is not usually a critical factor when assessing the photocatalytic activity of the titania film, making the test much easier.

The overall photocatalytic mineralization of SA can be summarized as follows:

$$CH_3(CH_2)_{16}CO_2H + 26O_2 \xrightarrow[h\upsilon \geq E_{bg}]{TiO_2} 18CO_2 + 18H_2O \quad (2)$$

Although there are likely to be many intermediates involved in reaction (2), none of significance are detectable in the gas phase above the SA film [26]. The lack of volatile intermediates helps ensure that reaction (2) goes to completion and that all the SA present on the titania film is mineralized [27]. The most commonly employed method to monitor the kinetics of this reaction is via the disappearance of the SA film using infrared absorption spectroscopy, since SA absorbs strongly in the region 2800–3000 cm^{-1}, with peaks at 2958 cm^{-1}, 2923 cm^{-1}, and 2853 cm^{-1}, due to asymmetric in-plane C–H stretching in the CH_3 group and asymmetric and symmetric C–H stretching in the CH_2 groups, respectively.

A number of different photocatalytic films, including that produced by PAR-DC-MS, were tested using this technique. The variation in the FT-IR absorbance spectrum of a typical PAR-DC-MS film, with an initial coating of stearic acid, as a function of UV irradiation time is illustrated in Fig. 3(a). These results show that after 200 min exposure to UVA light the stearic acid film is completely removed, in contrast to a similar experiment, carried out under otherwise identical reaction conditions, but using plain glass, for which the SA film remained largely unchanged, as indicated by the results illustrated in Fig. 3(b). The amount of stearic acid present on any of the photocatalytic films tested is proportional to the integrated area, A_{int}, under the corresponding FT-IR absorbance spectrum [23]. Thus, data of the form illustrated in Fig. 3 can be converted into associated A_{int} versus UV irradiation time plots for the different photocatalytic films tested and the results of this work are illustrated in Fig. 4. From this plot it appears that the PAR-DC-MS titania film is markedly more active (ca. 6.9 times) as a photocatalyst for the removal of stearic acid than the commercial self-cleaning glass, Activ^{TM}. This marked difference is largely due to film thickness, since the PVD titania film is typically ca. 17 times thicker than the CVD titania film on Activ^{TM} glass. The most active of the films tested was a 90 nm film of P25, which was ca. 25 times more active than a film of Activ^{TM} glass and 3.8 times more active than the PVD titania film, as indicated by the initial rates for SA destruction given in Table 1.

One of the most active clear and robust photocatalyst titania films reported is produced using a sol–gel technique [20] and was used here to compare with the activity of the PAR-DC-MS film. Like the other two samples it utilizes an anatase film of titania, but is generated as a much thicker (ca. 4 μm) layer, so as to be able to absorb much more of the incident UVA light. As a consequence, in practice the best of the titania films tested in this work were the P25 and sol–gel films, as indicated by the results in Fig. 4 and summarized in Table 1, although the latter films are less robust physically than the PAR-DC-MS or CVD films. The initial rate of disappearance of stearic acid data in Table 1 can be recalculated in terms of activity per nanometer of titania and the results are also given in this table and show that the titania film on Activ^{TM} is the most active of the four titania coated samples

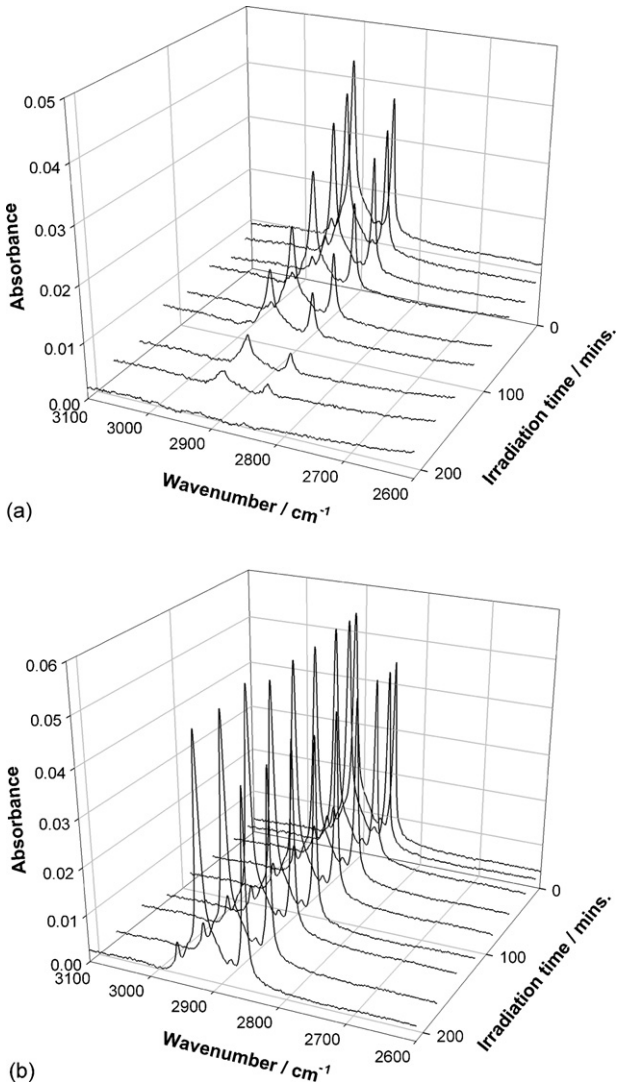

Fig. 3. Absorbance vs. wave number plot as a function of UV irradiation time of a stearic acid film on a sample of (a) PAR-DC-MS titania on glass and (b) plain glass.

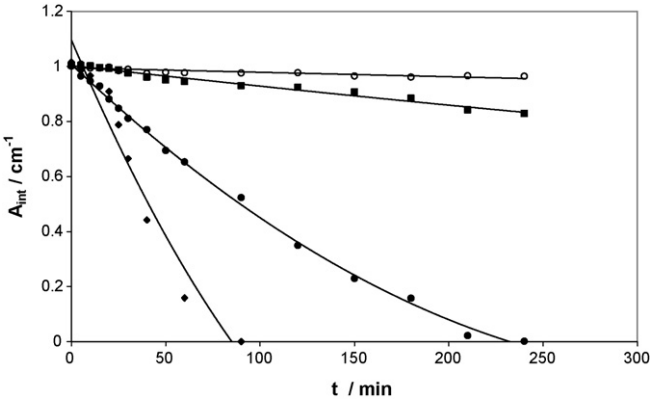

Fig. 4. Integrated IR absorbance (over the range 2800–3000 cm^{-1}) due to stearic acid, A_{int}, vs. UV irradiation time plots for the following underlying titania films on glass: (◯) plain glass, (■) Activ^{TM}, (●) PAR-DC-MS and (♦) sol–gel.

Table 1
Results of the stearic acid (SA) and resazurin (Rz) ink tests on the photocatalytic activities of various titania-on-glass films

Film	SA test		Rz ink test $R_{ink} = dAbs_{610}/dt$ (10^{-3} min^{-1})	Turnover number[a]
	$R_{SA} = dA_{int}/t$ (10^{-3} cm^{-1} min^{-1})	R_{SA}/thickness (10^{-6} cm^{-1} min^{-1} nm of titania^{-1})		
PAR-DC-MS	4.8	19	97.2	2.1[b]
Activ^{TM}	0.7	47	13.6	6.9
Sol–gel	12.8	3.2	[c]	0.03
P25[d]	17.8	20	[c]	12.6[e]

[a] Turnover number = No. of molecules of SA destroyed/No. of sites of TiO_2 present.
[b] Based on the data in Fig. 5.
[c] Too fast to measure accurately.
[d] Ninety nanometer film as prepared and used previously [19].
[e] Based on an initial SA absorbance of 11 data in Ref. [19].

tested for reasons which remain unclear, but could include differences in surface morphology, porosity, degree of crystallinity, to name but a few. The important difference between the PAR-DC-MS films and those produced by a sol–gel or CVD technique is that the latter two require a high temperature (≥450 °C) to create films with appreciable photocatalytic activity and a reasonable degree of mechanical stability, whereas the PAR-DC-MS titania films are prepared under ambient conditions, during which the substrate temperature does not exceed 100 °C.

An essential feature of any photocatalyst film is its ability to work many times without losing its activity. Titania is a very photoactive material that, upon UV activation, generates conductance band electrons and valence band holes that are extremely reactive, with the former able to reduce ambient oxygen present and the latter able to oxidise most organics and many inorganics either directly or, more usually, indirectly via the intermediate generation of adsorbed hydroxyl radicals [1–3]. The striking oxidizing power of photoactivated titania is one of its key features since it ensures that few materials adsorbed on its surface are able to resist complete oxidative mineralization. Titania is also a photocatalyst that is recognized as showing little evidence of photochemical wear with prolonged use. The photocatalytic durability of the PAR-DC-MS films was tested by studying the repeated photomineralization of a stearic acid film using the same sample and the results are illustrated in Fig. 5. These show that even after the destruction of five, relatively thick, films of stearic acid, each comprising ca. 9.7×10^{15} molecules of stearic acid cm^{-2}, the kinetics of reaction (2) remained largely unaltered. Since the density of anatase titania is 3.9 g cm^{-3}, the number of moles of sites per g of TiO_2 is 0.0004 [29] and the thickness of the film is ca. 250 nm, it follows that a typical PAR-DC-MS film has 2.35×10^{16} sites per cm^2, (assuming 0% porosity). Thus, the turnover number (TN) [30] for the PAR-DC-MS photocatalyst film is ≥($5 \times 9.7 \times 10^{15}/2.35 \times 10^{16}$), i.e., ≥2.06. On this basis, turnover numbers can also be calculated for the P25, sol–gel and Activ^{TM} films and the results are reported in Table 1. Turnover numbers for photocatalysts are rarely calculated, despite the fact that it has been argued that the epithet of 'photocatalyst' should be only applied when it has been established that the photocatalyst has a turnover number >1 [30]. From the results in Table 1, it appears that the PAR-DC-MS, P25 and CVD films of titania deserve to be called 'photocatalysts', whereas the thick, sol–gel film would need to destroy >ca. 38 consecutive layers of stearic acid to qualify.

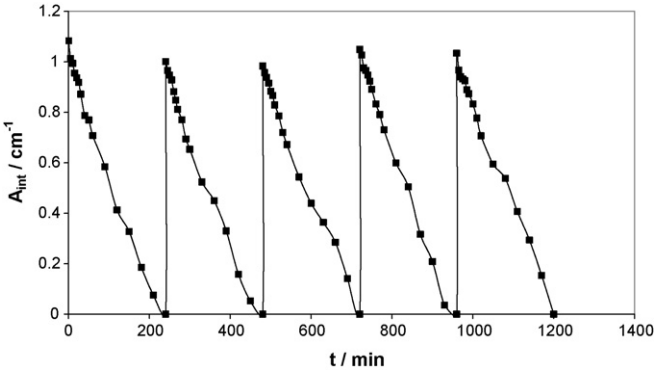

Fig. 5. A_{int} vs. UV irradiation time plot for a PAR-DC-MS sample of titania onto which a new layer of stearic acid is repeatedly deposited and then destroyed by photocatalysis.

A brief inspection of the results illustrated in Figs. 4 and 5 reveals the SA test is quite slow, even when a very active film, like that produced by PAR-DC-MS, is used. This is hardly surprising, given the film is thin (250 nm), only absorbing about 32% of the incident UVA light, and the photocatalytic reaction (2) is a 104 electron (each most probably generated by one photon) per SA molecule destroyed process, i.e. a process with a maximum possible quantum yield for reaction (2) of 0.96%.

In a recent paper [28], we reported on a much more photon efficient, rapid method for assessing photocatalytic activity, utilising a photocatalyst ink. This ink typically comprised a redox indicator dye, resazurin, Rz, a sacrificial electron donor, glycerol, a polymer binder, hydroxyl ethyl cellulose, and a solvent, water. Once deposited on a photocatalytic film for testing, upon its UV illumination, the Rz photocatalytic film interacts with different components of the ink, with the photogenerated electrons reducing the blue resazurin dye to its pink reduced form, resorufin (Rf), and the photogenerated holes oxidizing glycerol to glyceraldehye and/or glyceric acid (Gly_{ox}). These basic processes are illustrated in the schematic in Fig. 6. The main advantage of this ink over the SA test, is that it is very rapid, and easily observed and monitored. These features are well illustrated by the recorded changes in the absorbance spectrum of an Rz ink film on a typical sample of the PAR-DC-MS film as a function of UV irradiation time, as shown in Fig. 7. These

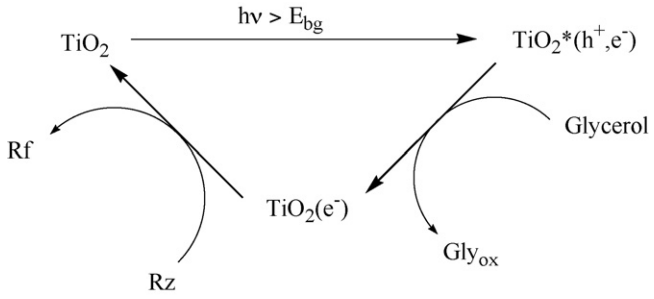

Fig. 6. Schematic highlighting the major photo-induced electron transfer processes associated with the Rz photocatalyst indicator ink.

results show that within 2 min irradiation, the initially blue films containing Rz (λ_{max} = 610 nm) turns pink as all the Rz is converted to Rf (λ_{max} = 580 nm). In contrast, the disappearance of a SA film takes hours and is not readily observed, with monitoring requiring FT-IR spectroscopy. Using the data illustrated in Fig. 7, the change in absorbance of the film at 610 nm, at any time, t, i.e. ΔAbs_{610}, can be calculated where

$$\Delta Abs_{610} = Abs_t - Abs_\infty \quad (3)$$

and Abs_t and Abs_∞ are the absorbances of the film at 610 nm at time, t, and when all the Rz has been converted to Rf, respectively. This approach was used to construct the plots of ΔAbs_{610} versus t for plain glass, Activ^{TM} and PVD films illustrated in Fig. 8 from the associated plots of absorption spectrum at different irradiation times, as illustrated in Fig. 7 for the PAR-DC-MS film. From the results in Fig. 8, it is clear that the PAR-DC-MS titania film is much more active than the CVD film (i.e. Activ), ca. 6.9 times, and that this assessment required only a few minutes UV irradiation to be made. In contrast, the SA test, which revealed a similar difference in activities between the PVD and CVD films (a factor ≅7.1, see Table 1), requires typically 60 min UV irradiation time in order to make this assessment. Thus, the Rz ink test is excellent for assessing thin, photocatalytic films, of limited activity, however, it is too sensitive (responds in <1 s),

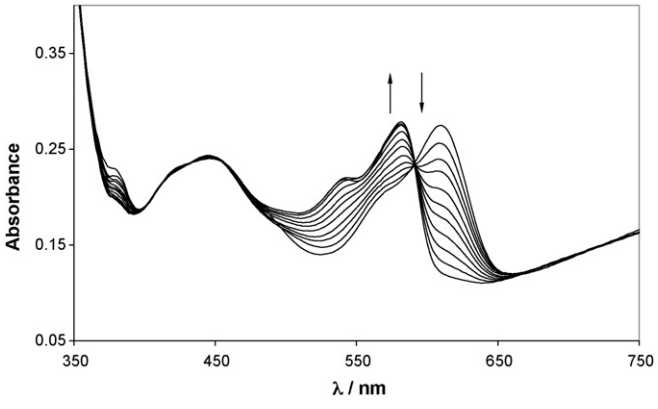

Fig. 7. UV/Vis absorption spectra of a PAR-DC-MS film with a coating of the Rz photocatalyst indicator ink recorded every 10 s upon exposure to UV light. With increasing irradiation time the absorbance of the peak due to Rz (610 nm) decreases and that due to the reduced form of the dye, Rf, at 580 nm, increases.

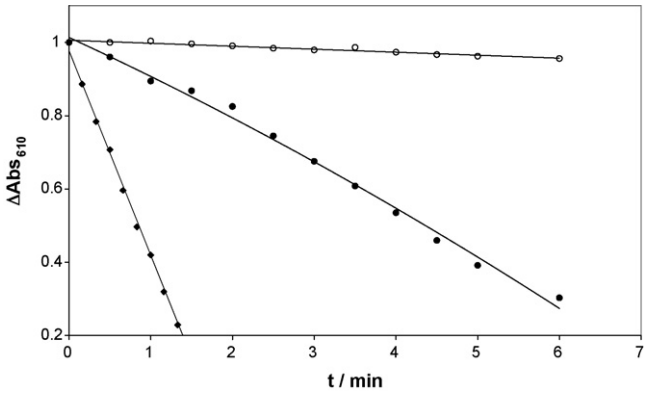

Fig. 8. Plots of the changes in absorbance at 610 nm of a Rz ink film, ΔAbs_{610}, as a function of UV irradiation time when the ink film was cast on: (◯) plain glass, (●) Activ^{TM} or (⧫) PAR-DC-MS glass.

at the UVA levels employed, to be used on thick, highly active, photocatalytic films, such as the sol–gel film samples also used in this work. Other work shows more appropriate, i.e. less sensitive, photocatalyst inks can be created by using less easy to reduce dyes in its formulation.

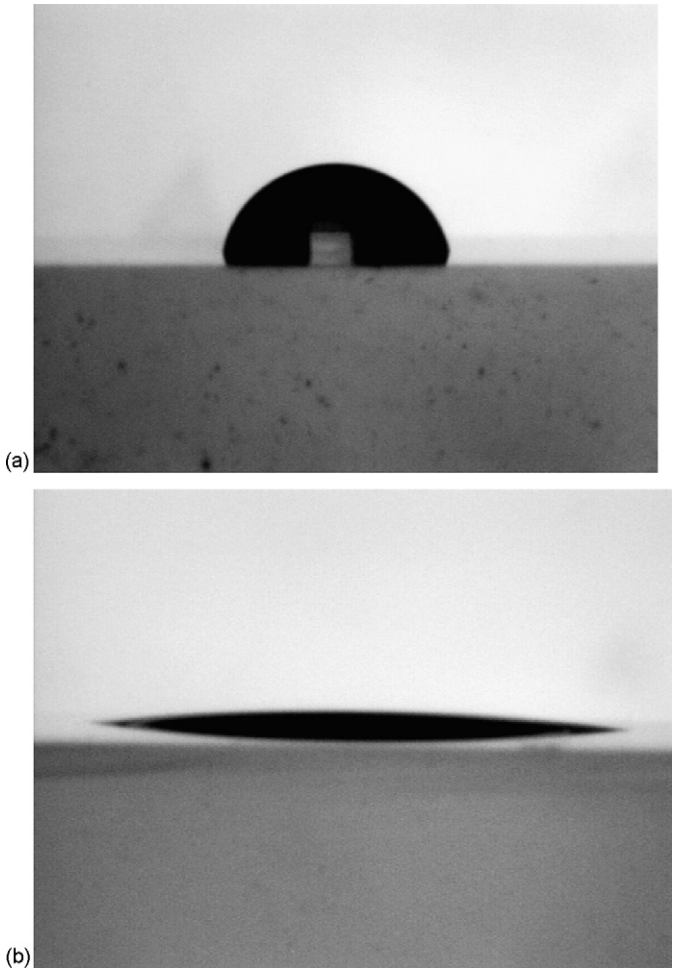

Fig. 9. CCTV profiles of a water droplet on the surface of PAR-DC-MS titania film (a) before and (b) after its illumination with UV light for 30 min. With a plain piece of glass the water droplet does not change shape with UV illumination.

Finally, all films were tested for photoinduced superhydrophilicity, i.e. PSH, which involves the conversion of the surface of the titania film from a hydrophobic to a hydrophilic nature, upon irradiation with UV light [31–33]. There is much debate as to the underlying cause of PSH, which may be simply due to the photocatalytic destruction of hydrophobic organics adsorbed on the surface of titania [32], i.e. reaction (1), or to a photo-induced hydration process [31,33], i.e.

$$\equiv \text{Ti–O–Ti} \equiv + \text{H}_2\text{O} \rightarrow \equiv \text{Ti–OHHO–Ti} \equiv \quad (4)$$

Included in the PSH process is the feature that, once rendered hydrophilic, the titania film slowly regains its initial hydrophilic character in the dark, e.g. via contamination by airborne organics or via the dehydration of the surface (i.e. the reverse of reaction (4)). It appears to be generally true that any titania photocatalytic film also exhibits the PSH effect. The change in shape of a water droplet on the surface of a PAR-DC-MS titania film before and after UV irradiation is illustrated in Fig. 9. These results were typical for all the titania films tested, i.e. P25, sol–gel, Activ™ and PAR-DC-MS, and are indicative of the PSH effect. This effect enhances the self-cleaning nature of the titania film, which is able to remove organics not only by a photocatalytic mineralization process, i.e. reaction (1), but also by PSH, since organics which would otherwise spoil the surface of the glass, adhere poorly to a hydrophilic surface and are readily washed away by (rain) water.

4. Conclusions

Robust, active, anatase titania films can be deposited onto glass at low temperatures, i.e. <100 °C, using a PVD technique: plasma-assisted, reactive dc magnetron sputtering. The films are transparent and colourless and truly photocatalytic, exhibiting turnover numbers >2.0 for the photocatalytic mineralization of stearic acid. These films are typically 6.9 times more active than a sample of commercial self-cleaning glass, mainly because they are much thicker and, therefore, absorb more of the incident UV light. All titania films tested, including those produced by magnetron sputtering exhibited photo-induced superhydrophilicity. The low temperatures used in the production of the PAR-DC-MS films makes this technique promising with respect to producing robust, very active photocatalyst titania films on low temperature substrates, such as plastics, metals and artificial fibres. Further work in this area is in progress.

References

[1] M.R. Hoffmann, S.T. Martin, W.Y. Choi, D.W. Bahnemann, Chem. Rev. 95 (1995) 69, and references therein.
[2] A.L. Linsebigler, G.Q. Lu, J.T. Yates, Chem. Rev. 95 (1995) 735, and references therein.
[3] A. Mills, S. LeHunte, J. Photochem. Photobiol. A: Chem. 108 (1997) 1, and references therein.
[4] M. Kaneko, I. Okura (Eds.), Photocatalysis, Springer, Berlin, 2002.
[5] A. Mills, S.K. Lee, J. Photochem. Photobiol. A: Chem. 152 (2002) 233.
[6] http://www.pilkington.com (accessed September 2006).
[7] http://www.toto.co.jp/products/hydro/genri_en.htm (accessed September 2006).
[8] J.T. Remillard, J.R. McBride, K.E. Nieteriing, A.R. Drews, X. Zhang, J. Phys. Chem. B. 104 (2000) 4440.
[9] L. Meng, M. Andritschky, M.P. dos Santos, Thin Solid Films 223 (1993) 242.
[10] P. Löbl, M. Huppertz, D. Mergel, Thin Solid Films 251 (1994) 72.
[11] D. Mardare, G.I. Rusu, Mater. Sci. Eng. B. 75 (2000) 68.
[12] S.K. Zheng, T.N. Wang, G. Xiang, C. Wang, Vacuum 62 (2001) 361.
[13] S. Takeda, S. Suzuki, H. Odaka, H. Hosono, Thin Solid Films 392 (2001) 338.
[14] Y.Q. Hou, D.M. Zhuang, G. Zhang, M. Zhao, M.S. Wu, Appl. Surf. Sci. 218 (2003) 97.
[15] W. Zhang, Y. Li, S. Zhu, F. Wang, Surf. Coat. Technol. 182 (2004) 192.
[16] M.C. Barnes, S. Kumar, L. Green, N.M. Hwang, A.R. Gerson, Surf. Coat. Technol. 190 (2005) 321.
[17] T. Frach, D. Glöss, C. Metzner, T. Modes, B. Scheffel, O. Zywitzki, Vacuum 80 (2006) 679.
[18] J. Huang, I. Ichinose, T. Kunitake, A. Nakao, Langmuir 23 (2002) 9048.
[19] A. Mills, A. Lepre, N. Elliott, S. Bhopal, I.P. Parkin, S.A. O'Neill, J. Photochem. Photobiol. A: Chem. 160 (2003) 213.
[20] A. Mills, N. Elliott, G. Hill, D. Fallis, J.R. Durrant, R.L. Willis, Photochem. Photobiol. Sci. 2 (2003) 591.
[21] Y. Paz, Z. Luo, L. Rabenberg, A. Heller, J. Mater. Res. 10 (1995) 2848.
[22] R. Fretwell, P. Douglas, J. Photochem. Photobiol. A: Chem. 143 (2001) 229.
[23] Y. Paz, A. Heller, J. Mater. Res. 12 (1997) 2759.
[24] T. Sawunyama, L. Jiang, A. Fujishima, K. Hashimoto, J. Phys. Chem. B. 101 (1997) 1100.
[25] T. Minabe, D.A. Tryk, P. Sawunyama, Y. Kikuchi, K. Hashimoto, A. Fujishima, J. Photochem. Photobiol. A: Chem. 137 (2000) 53.
[26] T.D. Manning, I.P. Parkin, R.J.H. Clark, D. Sheel, M.E. Pemble, D. Vernadou, J. Mater. Chem. 12 (2002) 2936.
[27] A. Mills, J. Wang, J. Photochem. Photobiol. A: Chem. 182 (2006) 181.
[28] A. Mills, J. Wang, S.-K. Lee, M. Simonsen, Chem. Commun. (2005) 2721.
[29] J. Cunningham, G.S. Al-Sayyed, in: G.R. Helz, R.G. Zepp, D.G. Crosby (Eds.), Srijaranai in Aquatic and Surface Chemistry, Lewis Publishers, Boca Raton, FL, 1994, Chapter 22.
[30] N. Serpone, A. Salinaro, A. Emerline, V. Ryabchuk, J. Photochem. Photobiol. A: Chem. 130 (2000) 83.
[31] A. Mills, G. Hill, S. Bhopal, I.P. Parkin, S.A. O'Neill, J. Photochem. Photobiol. A: Chem. 160 (2003) 185.
[32] J.M. White, J. Szanyi, M.A. Henderson, J. Phys. Chem. B. 107 (2003) 9029.
[33] K. Hashimoto, H. Irie, A. Fujishima, Jpn. J. Appl. Phys. 44 (2005) 8269.

ELSEVIER

Chemosphere 64 (2006) 1032–1035

CHEMOSPHERE

www.elsevier.com/locate/chemosphere

Technical Note

Photocatalytic oxidation of soot by P25 TiO_2 films

Andrew Mills *, Jishun Wang, Matthew Crow

Department of Pure and Applied Chemistry, University of Strathclyde, Thomas Graham Building, 295 Cathedral Street, Glasgow G1 1XL, UK

Received 18 December 2005; received in revised form 28 January 2006; accepted 30 January 2006
Available online 20 March 2006

Abstract

The photomineralisation of soot by P25 titania films is studied using FT-IR and the process shown to involve the oxidation of carbon to CO_2 exclusively. The efficiency of this process is low, however, with a formal quantum efficiency of 1.1×10^{-4} molecules of carbon oxidized per incident photon of UVA light. The cause of this low efficiency is attributed largely to the less than intimate contact between the fibrous soot layer and the surface of the photocatalyst.

Keywords: Soot; Photocatalysis; Titania; Carbon dioxide

1. Introduction

Soot, the product of the incomplete combustion of fossil and other fuels, is comprised of finely divided carbon particles, hydrocarbons and tar. Most soot is classified as ultra-fine (particle size <0.1 μm) particulate matter and as such can penetrate deep into the lungs and its cells, where it is able to cause serious health problems including chronic asthma and bronchitis (Barfknecht, 1983; Corporan et al., 2004). Soot particles can have an environmental lifetime of 1–3 weeks and travel long distances; for example, they have been found at the South Pole, where no major emission source exists for many thousands of miles (Barfknecht, 1983). In many industrial cities evidence of long-term past, if not present, high levels of airborne soot, is provided by the blackened state of the exteriors of its buildings. Any surface coating that is capable of completely mineralising soot is therefore of interest, not only with regard to health but also with respect to the maintenance of clean facades.

Self-cleaning materials, such as glass or tiles, have emerged recently as a tool to combat air-pollution and a route to provide buildings with longer-clean exteriors (Mills and Lee, 2002; Cassar, 2004; Scrivener and Van Danne, 2004). Such materials are usually based on a thin, photocatalytically active coating of titania that is able to mediate the oxidation of many airborne pollutants via the following solar-driven, general mineralisation reaction (Fujishima et al., 1999; Mills and Lee, 2002):

$$\text{organic} + O_2 \xrightarrow[TiO_2]{h\upsilon \geqslant 3\text{–}3.2\ \text{eV}} CO_2 + H_2O + \text{mineral acids} \qquad (1)$$

Since the bandgap of titania is large, i.e. 3–3.2 eV, only the UV component of sunlight is able to effect reaction (1). Recent work by others (Lee and Choi, 2002) and this group (Lee et al., 2004) has established that titania is also able to remove soot deposited on its surface, most likely via the following photocatalytic reaction:

$$C + O_2 \xrightarrow[TiO_2]{h\upsilon \geqslant 3\text{–}3.2\ \text{eV}} CO_2 \qquad (2)$$

However, the exact reaction stoichiometry associated with the photocatalytic removal of soot has not, as yet, been established. In mineralisation reactions, such as (1) or (2), it is important to establish that the products are just minerals and that there is no significant generation of any reactive intermediates that are environmentally less friendly than the reactants. Thus, in reaction (2) it is important to show that only CO_2 is produced and no other, possibly less 'green', forms of carbon, and carbon-containing

* Corresponding author. Tel.: +44 141 5482458; fax: +44 141 5484822.
E-mail address: a.mills@strath.ac.uk (A. Mills).

0045-6535/$ - see front matter © 2006 Elsevier Ltd. All rights reserved.
doi:10.1016/j.chemosphere.2006.01.077

compounds such as CO, are produced. If reaction (2) can be shown to be the correct reaction stoichiometry for soot removal by titania films this would be an encouraging result for the many commercial products, such as tiles and glass, that are currently being promoted for use as part of the exteriors of buildings. In this short paper, the results of a study of the stoichiometry and efficacy of reaction (2) are reported.

2. Experimental

Unless stated otherwise all chemicals were purchased from Aldrich Chemicals and used as received.

A typical Degussa P25 TiO_2-coated glass slide was prepared by dipping a cut-up, 1 mm thick microscope slide (final dimensions: 1 cm × 2.5 cm) in a 5 wt% P25 TiO_2 aqueous slurry, drying in an oven at 70 °C for 30 min, washing with water (to remove any loose material) and finally drying with compressed air, which provides a rapid and clean method of drying. The process was repeated three times to get a thick (ca. 0.9 μm) film on both sides of the slide; one of which was then wiped off to leave a final film that was white and semi-transparent as shown in Fig. 1a. A layer of soot (ca. 0.5 μm thick, as determined by SEM) was then deposited onto the TiO_2-coated glass slide using a burning 'T-lite'; a typical soot-coated film is illustrated in Fig. 1b. Scanning electron microscope, SEM, images of the soot layer revealed a layer of fibrous wisps, similar to those reported by others.

All UV/Vis absorption spectra were recorded using a Perkin Elmer Lambda 20 spectrophotometer and used to ensure that the TiO_2-film and TiO_2-plus-soot film preparation methods generated reproducible samples. All infra-red absorption spectra were recorded using a Perkin Elmer Spectrum One FT-IR spectrometer. In the latter work, a 10 cm quartz gas cell with demountable CaF_2 faces, thermostatted at 20 °C, and with purge gas inlet and taps and outlets, (Lidam Scientific, UK) was used to house a soot-covered Degussa P25 TiO_2-coated glass slide, as illustrated in Fig. 1c. This arrangement allowed any major carbon-containing volatiles, like CO_2, to be monitored as the film under test placed in the gas cell, usually in 101.3 kPa oxygen, was irradiated from above with UVA light.

All UV irradiations were carried out using six 8 W blacklight blue ($\lambda_{emission}(max) = 365$ nm; half-peak band width ca. 50 nm) fluorescent lamps set in a hemi-cylindrical arrangement with an aluminium back reflector. The irradiation source was placed about 10 cm above the samples under test and typically the incident UV light intensity was 4.28 mW cm^{-2}, measured using a UV meter with a calibrated UVA detector (UVP model MS-100 with MS125 UVA sensor).

Digital photography of the films was carried out using an Epson PhotoPC 3000Z digital camera.

3. Results and discussion

In a typical study of the photocatalytic decomposition of soot on a P25 TiO_2 film, the disappearance of the soot from the sample in the IR-gas cell was monitored via digital photography and the results are illustrated in Fig. 2. From these results it is clear that the overall process is very slow (ca. 45 d) and, as is apparent from Fig. 1b and was confirmed upon closer inspection of the film, that the deposited soot layer was patchy rather than of a uniform thickness. Not surprisingly, the thicker patches took longer to remove via reaction (2).

At the same time the destruction of a soot film was monitored photographically (see Fig. 2), it was also possible to monitor the evolution of any major, infrared-active volatile species, produced as part of this process, via FT-IR and the results of this work are illustrated in Fig. 3. Careful

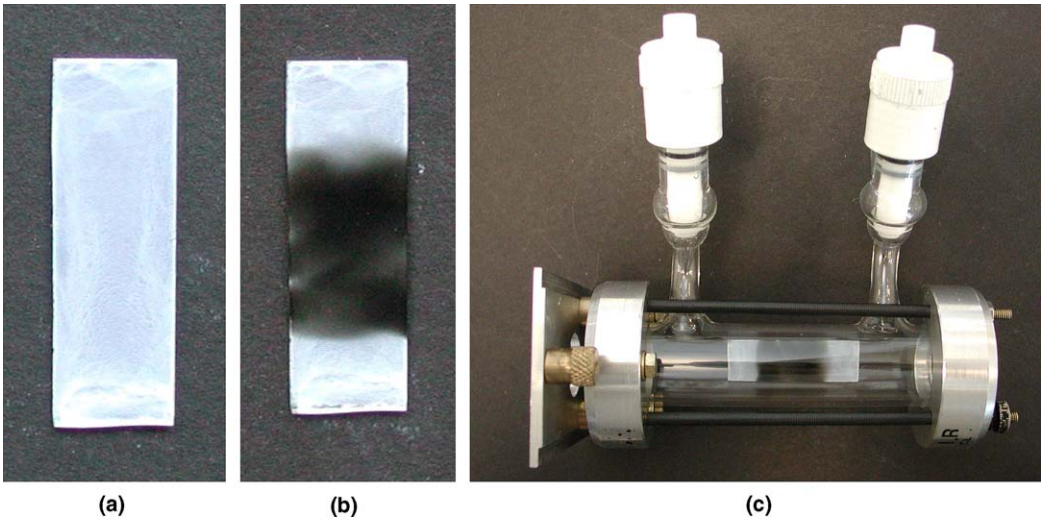

Fig. 1. Photographs of (a) a typical P25 TiO_2 film on glass, (b) a soot-covered P25 TiO_2 film and (c) the 10 cm FT-IR gas cell with soot-covered P25 TiO_2 film inside.

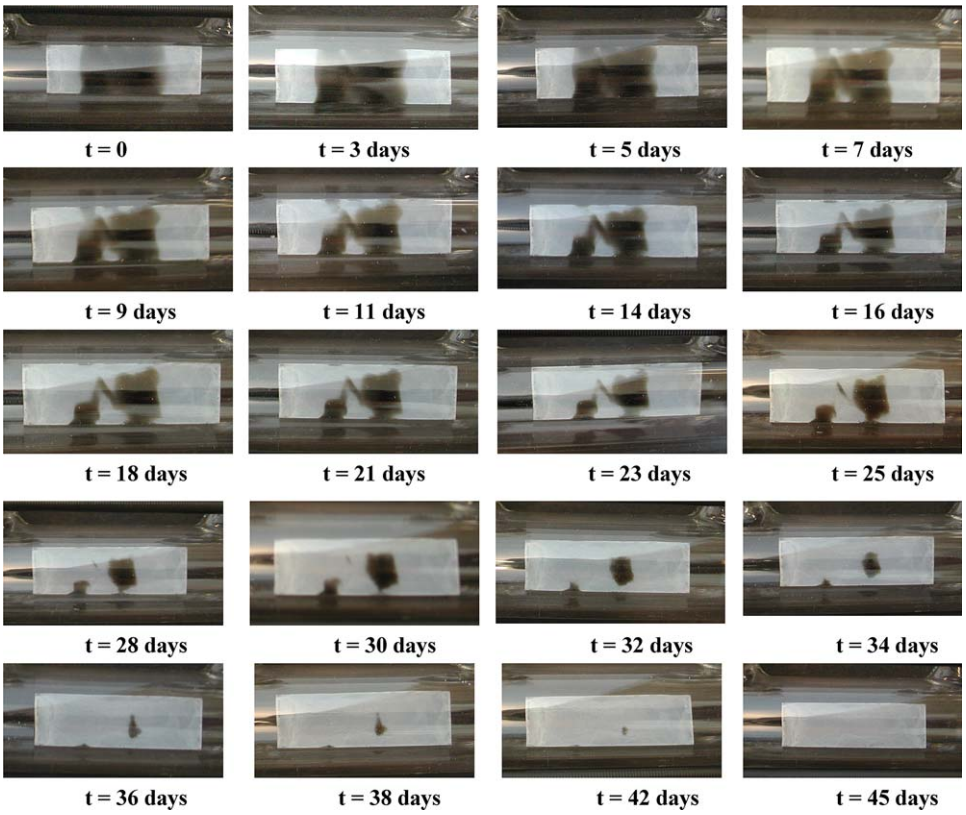

Fig. 2. Photographs of a typical P25 TiO_2 film on glass in a sealed FT-IR gas cell after various times of illumination with UVA light (4.28 mW cm^{-2}).

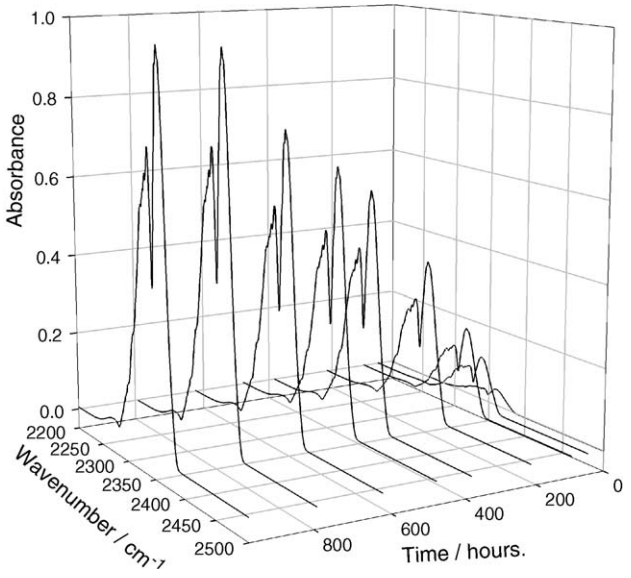

Fig. 3. Some of the infra-red absorption spectra recorded for the FT-IR gas cell in Fig. 1c, as a function of irradiation time. The observed spectra were all of the same shape and due to CO_2.

analysis of this latter data revealed that the shape of the infra-red spectrum of the observed volatiles did not change throughout the irradiation process and was identical to that of CO_2 alone. Thus, no evidence was found for any other volatile species, including CO, being produced during the photocatalytic oxidation of soot, sensitized by TiO_2. The FT-IR cell was calibrated with injections of known volumes of carbon dioxide and this allowed the data illustrated in Fig. 3 to be converted into a plot of the number of moles of CO_2 produced as a function of irradiation time, which is illustrated in Fig. 4. The final number of moles of CO_2 observed (22.5×10^{-6} mol) corresponded exceedingly well (i.e. 100% stoichiometry according to reaction (2)) to the measured mass loss observed for the TiO_2-soot film before and after irradiation (0.27 mg). The data in Fig. 4 give a reasonable fit to a first order process described by the following expression: $N_{CO_2} = 22.5(1 - \exp(-0.003\,t))$, where N_{CO_2} is the number of moles of CO_2 photogenerated after irradiation time, t.

From the data illustrated in Figs. 2 and 3, it is clear that the process is very slow and given an initial rate of CO_2 production of 1.91×10^{-11} mol s^{-1} (from the data in Fig. 4) and an incident light intensity of ca. 1.04×10^{17} photons s^{-1}, it is possible to estimate a formal quantum efficiency (FQE) for the process of 1.1×10^{-4} molecules $photon^{-1}$, implying an electron/photon formal quantum efficiency of 4.4×10^{-4}. This value is markedly (ca. 640 times) lower than that reported for the destruction of stearic acid (0.28 = electron/photon FQE) (Paz et al., 1995), presumably reflecting a more refractory nature for soot, possibly due to its less intimate contact with the surface. No attempt was made to optimise the latter, which might well have been improved by modifying the deposition procedure.

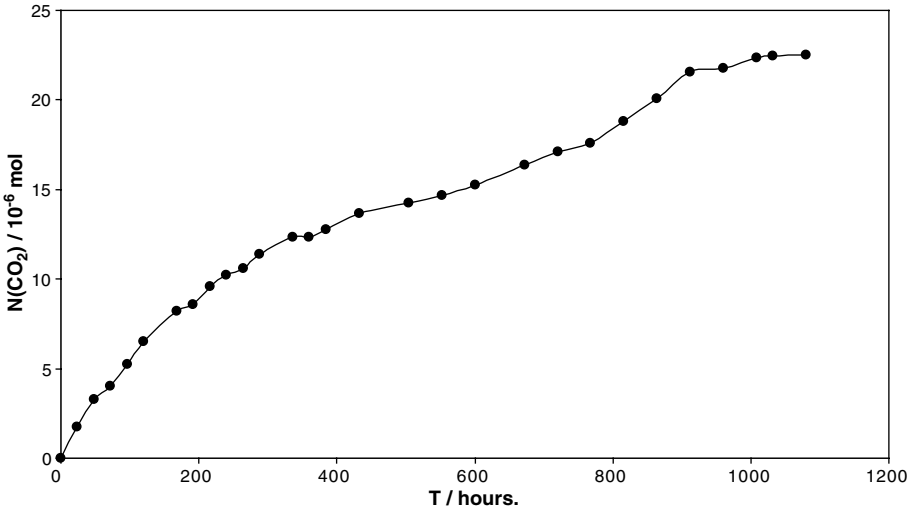

Fig. 4. Plot of the number of moles of CO_2 generated, calculated using the data in Fig. 3, as a function of irradiation time. Based on this data an initial rate for CO_2 generation of 1.91×10^{-11} mol s^{-1} was estimated. The line joining the points is not the result of a fit to the data.

From the results of this work it appears that self-cleaning titania films are able to remove soot particles from their surfaces via the semiconductor photomineralisation process summarized by reaction (2), in which CO_2 is the exclusive oxidation process. The fibrous, loosely-held nature of the soot layer is probably the main cause for the observed low formal quantum efficiency (1.1×10^{-4} molecules/photon) for the mineralisation process. These results offer encouragement to producers of titania-based self-cleaning materials for building exteriors, although the low FQE represents a concern. The titania used, P25, is an intimate mixture of anatase (70%) and rutile (30%). Further work is needed to establish if either of these two crystal phases are better or worse than P25 for the photocatalytic oxidation of soot.

References

Barfknecht, T.R., 1983. Toxicology of soot. Prog. Energy Combust. Sci. 9, 199–237.

Cassar, L., 2004. Photocatalysis of cementitious materials: clean buildings and clean air. MRS Bull. 29, 328–331.

Corporan, E., Dewitt, M., Wagner, M., 2004. Evaluation of soot particulate mitigation additives in a T63 engine. Fuel Process. Technol. 85, 727–742.

Fujishima, A., Hashimoto, K., Watanabe, T., 1999. TiO_2 Photocatalysis: Fundamentals and Applications. BCK Inc., Tokyo.

Lee, M.C., Choi, W., 2002. Solid phase photocatalytic reaction on the soot/TiO_2 interface: the role of migrating OH radicals. J. Phys. Chem. B 106, 11818–11822.

Lee, S.K., McIntyre, S., Mills, A., 2004. Light-driven oxygen scavenging by titania/polymer nanocomposite films. J. Photochem. Photobiol. A: Chem. 162, 203–206.

Mills, A., Lee, S.K., 2002. A web-based overview of semiconductor photochemistry-based commercial applications. J. Photochem. Photobiol. A: Chem. 152, 233–247.

Paz, Y., Luo, Z., Rabenberg, L., Heller, A., 1995. Photo-oxidative self-cleaning transparent titanium dioxide films on glass. J. Mater. Res. 10, 2842–2848.

Scrivener, K., Van Danne, H., 2004. Construction materials: from innovation to conservation. MRS Bull. 29, 308–310.

Photocatalytic Oxidation of Deposited Sulfur and Gaseous Sulfur Dioxide by TiO_2 Films

Andrew Mills,*,† Matthew Crow,† Jishun Wang,† Ivan P. Parkin,‡ and Nicolas Boscher‡

Department of Pure & Applied Chemistry, University of Strathclyde, Glasgow G1 1XL, UK, and Department of Chemistry, University College London, London, WC1H 0AJ, UK

Received: February 3, 2007

Thick (4 μm) films of anatase titania are used to photocatalyze the removal of deposited films of amorphous sulfur, ~2.8 μm, thick and under moderate illumination conditions ($I = 5.6$ mW cm^{-2}) on the open bench the process is complete within ~8 or 18 h using UVC or UVA light, respectively. Using UVA light, 96% of the product of the photocatalytic removal of the film of sulfur is sulfur dioxide, SO_2. The photonic efficiency of this process is ~0.16%, which is much higher (>15 times) than that of the removal of soot by the same films, under similar experimental conditions. In contrast to the open bench work, in a closed system the photocatalytic activity of a titania film toward the removal of sulfur decreased with repeated use, due to the accumulation of sulfuric acid on its surface generated by the subsequent photocatalytic oxidation of the initial product, SO_2. The H_2SO_4-inactivated films are regenerated by soaking in water. The problems of using titania films to remove SO_2 from a gaseous environment are discussed briefly.

Introduction

Titanium dioxide photocatalysis has emerged in recent years as a potentially useful tool for environmental remediation.[1−3] The usual role of such photocatalysis is to effect the mineralization of organic pollutants in air or water, i.e.

$$\text{organic} + O_2 \xrightarrow[h\nu \geq 3.2\ \text{eV}]{TiO_2} \text{minerals (such as } CO_2 \text{ and } H_2O) \quad (1)$$

In this work, titanium dioxide, TiO_2, is the preferred photocatalyst, because it is inexpensive, very active as a photocatalyst, easily cast as films which are mechanically robust (e.g., via CVD or sol−gel techniques), and biologically and chemically inert.[1−3] A number of building materials, such as glass, tiles, concrete blocks, and paving, are now being sold with TiO_2 photocatalyst coatings, and the market continues to grow.[4] Although most TiO_2 photocatalyst research has focused on the destruction of organics, there are a number of notable inorganic pollutants that also need to be addressed before this method can be considered as a general, effective tool for cleaning up the environment. One such pollutant is soot, i.e., ultrafine particles of carbon, which blackens most external building surfaces and can cause serious health problems including chronic asthma and bronchitis.[5,6] Another airborne, particulate, environmental pollutant is sulfur, generated as a byproduct in several industrial chemical processes, including sour natural gas processing.[7,8] Previous work by this group[9] and others[10] has shown that thick (>1 μm) anatase TiO_2 films, produced via a sol−gel technique, are very effective at photocatalyzing the oxidation of soot to carbon dioxide. Following on, this paper describes the results of a study of the photocatalytic oxidation of amorphous sulfur by these very active, thick, TiO_2 photocatalytic films. The initial product of the latter process is sulfur dioxide, SO_2, which represents a much bigger threat to the environment than particulate sulfur, due to its large-scale global production, and intimate involvement with acid rain production. Thus, this paper also investigates briefly the use of thick TiO_2 films as photocatalysts for the removal of SO_2 from the gas phase.

Experimental Section

Unless stated otherwise, all chemicals were purchased from Aldrich Chemicals and used as received.

All thick TiO_2 films were prepared using titanium (IV) isopropoxide as the precursor and a sol−gel technique, the details of which are given elsewhere.[11] The films were typically 4 μm thick, optically clear and colorless, and comprised ~13 nm particles of anatase titania in a porous network (~60% porosity). The films were laid down from a sol−gel, as 1 cm wide, 7.6 cm long strips on microscope glass slides and converted to robust, anatase crystalline films by annealing at 450 °C for 30 min.

Amorphous sulfur was deposited onto the surface of a photocatalyst film by dip-coating the slide into a 4.0 mol dm^{-3} solution of sulfur (100 mesh) dissolved in carbon disulfide and air-drying for 30 min. Using this technique, typically 4×10^{-5} g cm^2 of sulfur were deposited onto the titania films. Figure 1 illustrates a typical side-on scanning electron micrograph image of the sulfur-on-titania films, from which it is possible to estimate the thickness of the sulfur layer as ~2.8 μm, comprising particles, typically ~260 nm in diameter but with some ranging in size from 60−500 nm. This image also shows that both the darker, underlying titania layer and the lighter, top-coat of amorphous sulfur are very porous.

All UV/vis absorption spectra were recorded using a Perkin-Elmer Lambda 20 spectrophotometer. All infrared absorption spectra were recorded using a Perkin-Elmer Spectrum One FTIR spectrometer. In the latter work a 10 cm quartz cell with demountable CaF_2 faces, with purge gas inlet and outlet taps (Lidam Scientific, UK) were used to house any photocatalytic film under test. Typically, this arrangement allowed the major sulfur-containing volatiles, like SO_2, to be monitored as a sulfur-on-titania film was irradiated with UV light in a closed system.

* Author for correspondence. E-mail: a.mills@strath.ac.uk.
† University of Strathclyde.
‡ University College London.

10.1021/jp070947o CCC: $37.00
Published on Web 03/22/2007

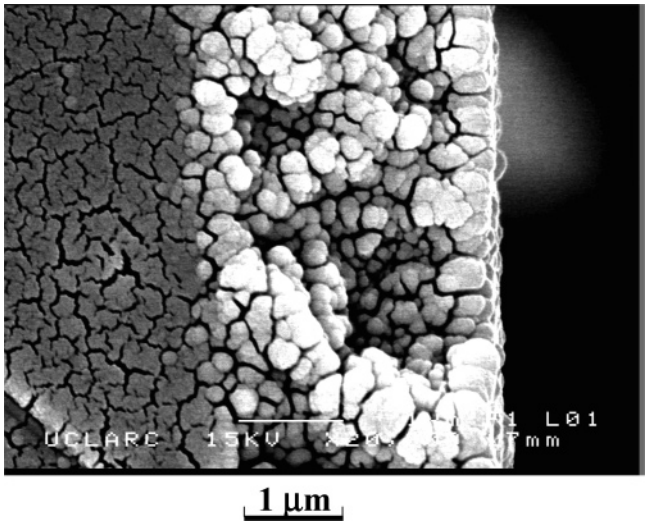

Figure 1. Electron micrograph of a typical amorphous sulfur layer (lighter-colored particles) deposited onto a thick sol−gel film of anatase titania (20,000× magnification).

The infrared spectrum of SO_2 has been reported elsewhere;[12] briefly, it comprises very strong bands at 1151 and 1362 cm^{-1} and a weaker one at 2499 cm^{-1}.

UV irradiations were carried out using six 8 W UV fluorescent tubes that were either UVC (i.e., λ_{max}(emission) = 254 nm), or UVA (λ_{max}(emission) = 365 ± 20 nm), set in a cylindrical hemisphere arrangement with an aluminum back reflector. Unless stated otherwise, all mentions of UVC or UVA light refer to these light sources. In both cases the incident light intensity was typically 5.6 mW cm^{-2}, as measured using a UV power meter (UVP model MS-100).

Digital photography of the films was carried out using an Epson PhotoPC 3000Z digital camera.

Results and Discussion

The disappearance of the sulfur layer on a typical thick titania film in air by semiconductor photocatalysis, achieved by irradiating the film on the open bench with the use of UVC light, was monitored initially by digital photography, and the results are illustrated in Figure 2. These results, and others obtained from the same experimental system but using UVA light, reveal that the sulfur film deposited on titania is removed within hours upon exposure to UV light, i.e., in ∼8 h (UVC) or 18 h (UVA), whereas, over the same time periods, sulfur deposited onto glass did not noticeably disappear upon irradiation with either UV light, under the same conditions (see Figure 2). The most likely initial process associated with the photocatalytic removal of sulfur is as follows:

$$S + O_2 \xrightarrow[h\nu \geq 3.2\ eV]{TiO_2} SO_2 \qquad (2)$$

It is probable that the photocatalytic oxidation of sulfur by oxygen proceeds via a mechanism similar to that which operates in the well-studied, photocatalytic oxidation of organics, i.e., reaction 1. Thus, the absorption of an *ultra*-band gap photon, i.e., $h\nu \geq 3.2$ eV, generates an electron−hole pair. Although many of the latter ultimately recombine, some photogenerated holes that reach the surface are able to either react directly with the sulfur or photo-oxidize adsorbed hydroxyl radicals which then react with the sulfur. The photogenerated electrons that reach the surface are able to react with oxygen to form superoxide, which can be further reduced, eventually forming water, or generating hydrogen peroxide, which can act as another source of hydroxyl radicals.

The removal of the amorphous sulfur film via the photocatalytic process (i.e., reaction 2), upon UV irradiation on the open bench, was also monitored via the change in the UV/visible absorption spectrum of the film and showed that the absorbance due to the sulfur on a sulfur-on-titania film, Abs(S), is proportional to the mass of sulfur remaining on the titania film at most wavelengths. For example, at 600 nm, Abs(S) is taken as the difference between the absorbance of the sulfur-on-titania film and that of a titania-only film at 600 nm, i.e., ΔAbs_{600}. The variation in the absorbance spectrum of a typical sulfur-on-titania film upon irradiation with UVC or UVA light on the open bench is illustrated in Figure 3a, and the data contained therein were used to create the plot of ΔAbs_{600} as a function of irradiation time, illustrated in Figure 3b. From these data it can be seen that the photocatalytic process, reaction 2, appears much slower (∼2.3 times) if UVA, rather than UVC, light is employed. Mass loss measurements made on these films reveal initial rates of sulfur removal of 90 or 41 $\mu g\ h^{-1}$ using a UVC or UVA light source, respectively.

A large part of the higher activity for reaction 2 using UVC light is due to the greater absorbance of the TiO_2 film of UVC light (i.e., 100% absorbed) compared to the UVA light (only ∼44% absorbed, a factor of 2.3). Another possible, but much smaller, contributor to the increased apparent photocatalytic activity when UVC light is used is the photoactivity of sulfur itself, since others have found that sulfur powder, when dispersed in an *aerated, aqueous solution*, is susceptible to photolytic oxidation, i.e.

$$2S + 3O_2 + 2H_2O \xrightarrow[UVC]{} 2H_2SO_4 \qquad (3)$$

when UVC (i.e., 254 nm) but not UVA (i.e., 365 nm) or visible light is used.[13,14] In our work, in order for reaction 3 to contribute to the loss of sulfur using UVC light, it must be assumed that the latter process occurs also in *ambient humid air*, using amorphous films of sulfur, as well as in *aerated aqueous solution*, using powder dispersions of crystalline sulfur, as reported by others.[13] In support of this, separate photolysis experiments carried out on an amorphous layer of sulfur deposited onto roughened glass, which was needed to make the sulfur layer stick well to the glass to form a layer, revealed that in ambient air (60% humidity, 20 °C), sulfur is, indeed, photo-oxidized in O_2 when exposed to UVC but not UVA light, albeit at a much slower rate (<5 times) compared to that observed using a TiO_2 photocatalytic film. In this work, FT-IR gas-phase measurements where the sulfur-on-titania film was in a closed FT-IR gas cell, reveal that the initial product of the photolysis of sulfur by UVC light is SO_2, and so the overall photoreaction can be described as follows:

$$S + O_2 \xrightarrow[UVC]{} SO_2 \qquad (4)$$

Since the above photolysis reaction is possible, it cannot be ruled out as making a small (<20%) contribution to the overall kinetics of sulfur removal on titania films when using UVC light. A brief inspection of the results illustrated in Figure 3b, coupled with the knowledge that the parameter, ΔAbs_{600}, is proportional to the mass of sulfur remaining on the photocatalyst film, reveals that the kinetics of sulfur removal are approximately zero-order with respect to the level of sulfur present. Such kinetics are not surprising, given that those for most photocatalytic processes are described by a Langmuir−Hinshelwood-type expression[1−3] and that the titania films used

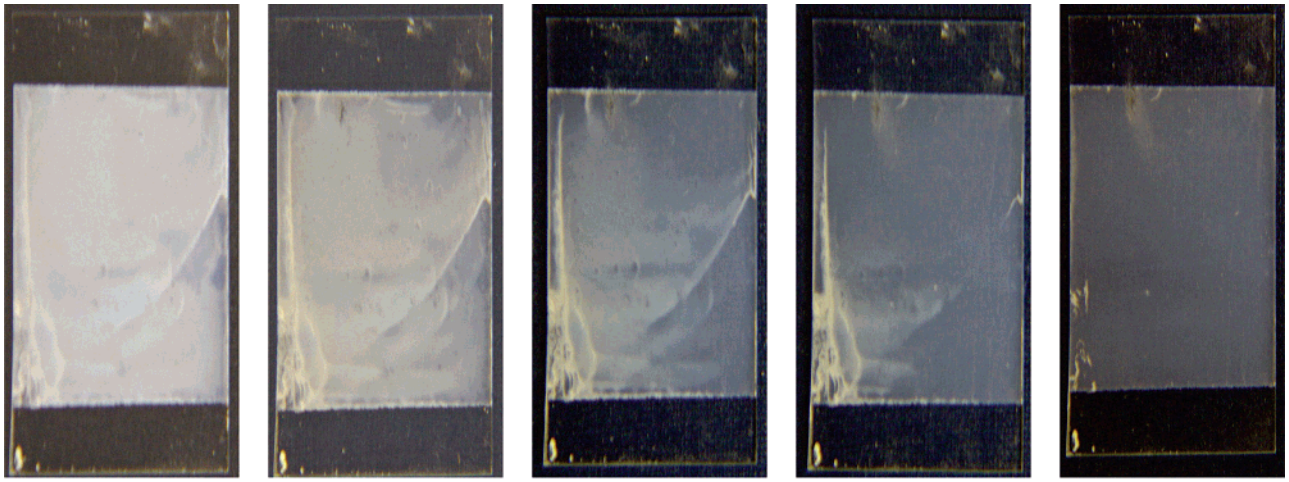

Figure 2. Time-sequence photographs of a typical sulfur-on-titania film as a function of UVC irradiation time. Note that the specks of sulfur *not* on the titania film, such as in the bottom left-hand corner of each photo, are not significantly changed during this irradiation process.

in this work were covered by a thick (~2.8 μm) layer of sulfur so that all the available photocatalytic sites would most likely be occupied and, as a consequence, only saturation, or zero-order, kinetics would be observed. The same argument is often used to explain the observed zero-order kinetics for the photocatalytic destruction of greater than monolayer deposits of stearic acid on titania films[15,16] and for soot removal by titania photocatalysis.[9,10] Although the titania films are covered by a relatively thick layer of sulfur, this layer does not appear to prevent either UVA or UVC light transmission through to the underlying titania layer, presumably via a scattering process.

In this study of the UVC- and UVA-driven photocatalytic oxidation of a sulfur-on-titania film, when monitored using FT-IR in a closed gas cell, SO_2 appears to be the initial product. However, when using UVC light, the kinetics of this process are complicated by the recognized UV sensitivity of the product, SO_2, since the latter has an absorbance maximum at ~285 nm[17] and in air is photo-oxidized by UVC light to form sulfur trioxide, SO_3, which, in turn, readily forms sulfuric acid, in the presence of water,[18] i.e.

$$2SO_2 + O_2 \xrightarrow[\text{UVC}]{} 2SO_3 \xrightarrow{2H_2O} 2H_2SO_4 \qquad (5)$$

As a consequence, when UVC is used as the illumination source, in a closed system the overall kinetics comprise a mixture of the photomineralization process, reaction 2, and the photolytic reactions 4 and, more notably, 5 of the reactant, sulfur, and the initial product, SO_2, respectively.

In order to avoid the above photolytic complications, in a subsequent study of the stoichiometry and quantum efficiency of the photocatalytic reaction 2, all illuminations were conducted using UVA light. Thus, a typical sulfur-on-glass film was irradiated with UVA in a gas stream (100 cm^3 min^{-1}) of oxygen, and the amount of SO_2 generated via the photocatalytic oxidation of the sulfur, i.e., reaction 2, was monitored by trapping the SO_2 from the gas stream by passing it through 100 mL of a 0.1 M sodium tetrachloromercurate (II) (TCM) scrubbing or trap solution. Such a TCM trap solution, upon contact with SO_2, is known to form rapidly a stable, nonvolatile, soluble disulfitomercury (II) salt (DSM) via the following reaction:[19]

$$\underset{\text{TCM}}{[HgCl_4]^{2-}} + 2SO_2 + 2H_2O \rightarrow \underset{\text{DSM}}{[Hg(SO_3)_2]^{2-}} + 4HCl \qquad (6)$$

During the course of the irradiation the TCM trap solution was sampled (1 mL samples) at regular time intervals, *t*, and each sample was reacted with a color-developing solution, comprising 1 mL of *p*-rosaniline hydrochloride (0.04 wt % dye in 6 wt % concentrated HCl acid), 1 mL of formaldehyde (0.2 wt %), and 4 mL 0.1 M TCM solutions. The colored product, *p*-rosaniline metasulfonic acid (*p*-RMSA) has an absorbance maximum at ~560 nm, and so the absorbance at this wavelength in the developed solution, i.e., Abs_{560}, is directly proportional to the level of DSM (and therefore the mass of SO_2 produced via reaction 2, i.e. $[SO_2]_t$) present in the scrubbing solution at the associated irradiation time,[19] *t*. Figure 4 illustrates the observed changes in the absorption spectrum of the developed *p*-RMSA solution, derived from the sampled TCM trap solution, as a function of irradiation time.

A calibration graph, relating $[SO_2]_t$ to Abs_{560}, was created by injecting in known amounts of sodium metabisulfite into the TCM scrubbing solution and measuring the absorbance at 560 nm in the subsequent developed solution, Abs_{560}. Thus, using the Abs_{560} data illustrated in Figure 4, the associated plot of $[SO_2]_t$ versus irradiation time, *t*, shown in Figure 5 was constructed. From this plot, and the overall loss of mass of the film, it appears that 903 μg of sulfur dioxide are generated via reaction 2 for a loss of 470 μg of sulfur from the film, indicating that the yield of SO_2 in photoreaction 2 is ~96%. This high efficiency is similar to that reported earlier (100% yield) by us for the photocatalytic oxidation of soot to carbon dioxide by the same thick, sol−gel based titania films.[9]

From the initial part of the plot of $[SO_2]_t$ vs *t* illustrated in Figure 5 it is possible to derive a value for the initial rate of generation of SO_2 of 58.9 μg h^{-1}, equivalent to 0.129 μg cm^{-2} min^{-1}, since the film had typically an area of 7.6 cm^2. The incident UVA light intensity was 7 mW cm^{-2}, equivalent to 7.7×10^{17} 365 nm photons/cm^2/min. Thus, the formal quantum efficiency for reaction 2 is ~0.16% which is much higher (~15 times) than that reported for the photocatalytic oxidation of soot,[9] 0.011%, probably partly due to the much more intimate contact of the dense sulfur particles with the titania film, when compared to the lighter, fibrous and more loosely attached films of soot used in the previous studies. The former are deposited by a precipitation method, as described earlier, whereas the latter are generated using a candle flame. It is also very likely that the

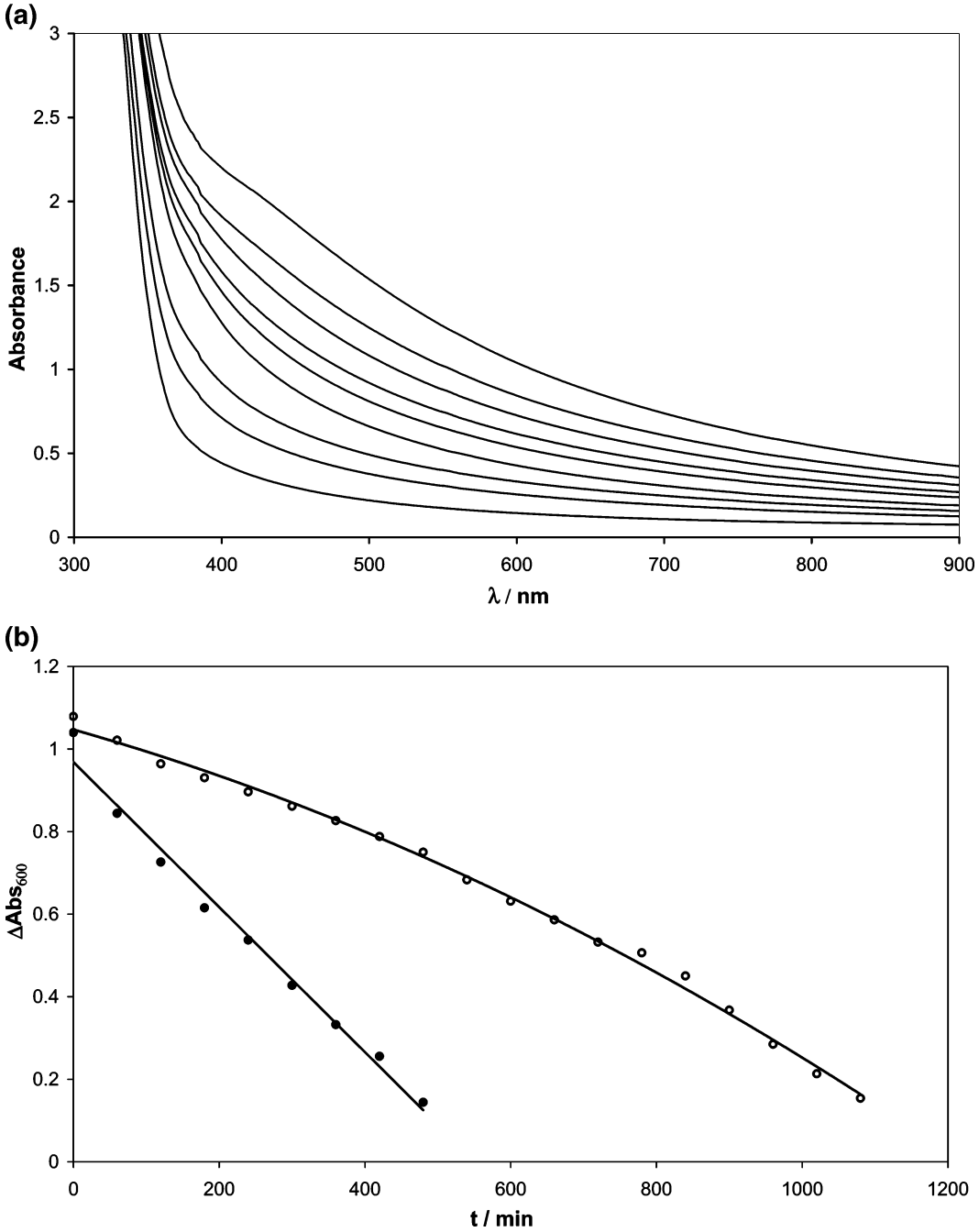

Figure 3. (a) Variation in the absorption spectra of a sulfur-on-titania film as a function of UVC irradiation time; spectra recorded every 60 min with top spectrum ($t = 0$). (b) Plot of the change in absorbance due to sulfur on a typical sulfur-on-titania film at 600 nm, ΔAbs_{600}, as a function of irradiation time, using either UVC (●) or UVA (○) light. The UVC data points were taken from the data in (a).

soot particles absorb more and scatter less UV light, and consequently, their transmission of the UV to the underlying titania film is significantly lower than that for a sulfur film of approximately the same thickness.

The generation of sulfur particles is an environmental problem associated with a number of industrial chemical processes but is confined largely to regions close to the factory, due to the dense nature of the sulfur particles. In contrast, and as noted earlier, SO_2 pollutant production is associated with many large industries and is a global environmental problem, due to its rapidly diffusing and toxic nature. Curiously, the use of photocatalysis for the removal of gaseous SO_2 has not been well studied. One possible reason for this emerges from the work of Shang et al. using titania nanoparticulate powder, prepared by a sol−gel process, to photo-oxidize SO_2 in the presence of oxygen:[18]

$$2SO_2 + O_2 \xrightarrow[\text{UV light}]{TiO_2} 2SO_3 \quad (7)$$

In the latter work the photo-oxidation of SO_2 was found to be ∼5.3 times faster in the presence of TiO_2, but the titania powder showed decreasing, and eventually no, activity after repeated use, although the deactivated titania could be regenerated by sonicating in water. Qualitative analysis by Shang et al. showed that the major product (i.e., >92%) was SO_3 or, in humid air, H_2SO_4 both of which accumulate on the surface of the titania and were responsible for the loss of photocatalytic activity by the titania observed by these workers with its repeated use.[18]

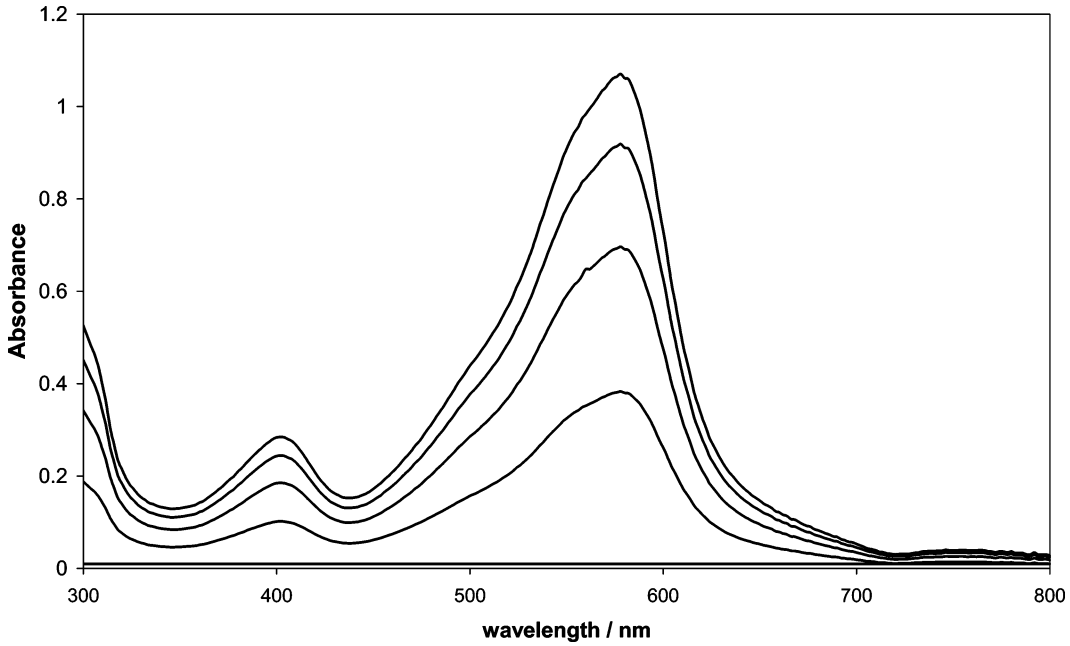

Figure 4. Absorption spectra of the *p*-RMSA-developed solution, derived from 1 mL samples of the DSM trap solution, for the following UVA irradiation times (from bottom to top): 0, 6, 24, 48, and 80 (and 96) h respectively, using a typical sulfur-on-titania film sample in a flowing stream of oxygen. Note: the 80 and 96 h spectra are identical.

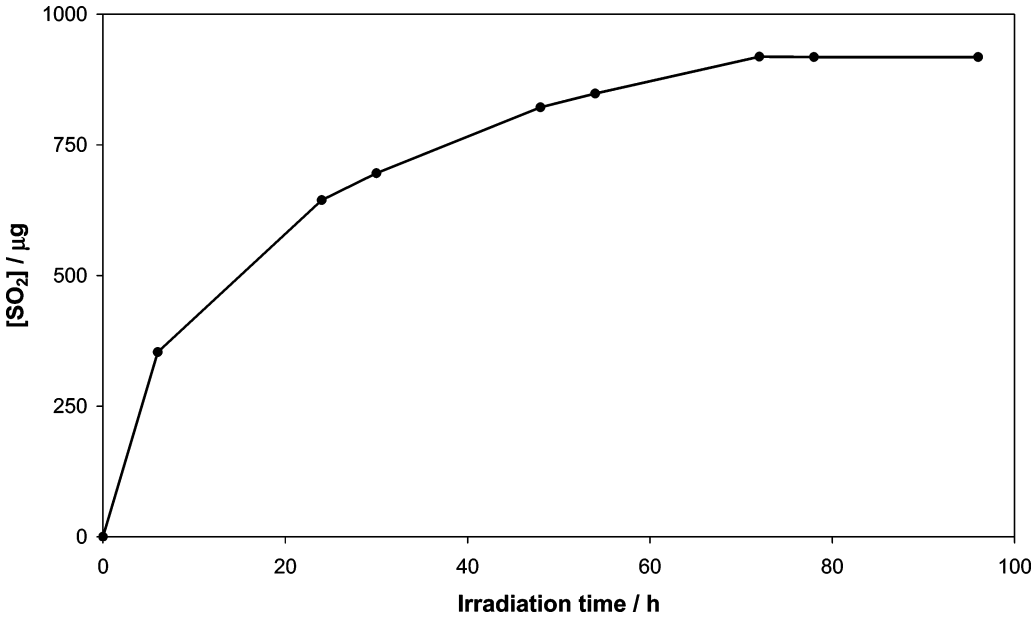

Figure 5. Plot of the mass of sulfur produced, [SO_2], from a typical sulfur-on-titania film sample, as a function of UVA irradiation time. Data are derived from the absorbances at 560 nm of the sampled DSM trap solution.

In our work on the photocatalytic oxidation of sulfur, i.e., reaction 2, the process went to completion within a few hours of UV irradiation under open bench conditions, i.e., in air with a typical relative humidity of 60%, as illustrated by the results in Figure 2 and noted earlier. Further work in the open air revealed that a titania film does not lose its photocatalytic activity for removing sulfur with repeated use, presumably because the oxidation product, SO_2, diffuses away from the titania film. In contrast, in a closed system, such as a sealed FT-IR gas cell, in which the SO_2 accumulates in the gas phase above the film, the kinetics of sulfur removal are much reduced ($<$4.6 times), and the titania film loses much of its initial photocatalytic activity with repeated use, presumably due to poisoning by the H_2SO_4 product generated via the photolytic or photocatalytic reactions 5 and 7, respectively. In support of this, and as indicated by Shang et al., soaking a repeatedly used, largely inactive titania film in water regenerates much of its initial photocatalytic activity.[18]

The above findings indicate that titania photocatalysis may not be appropriate for use in the removal of SO_2, since the likely product, SO_3, or more likely H_2SO_4 if any moisture is present, appears to poison the surface. However, since these poisons may be readily removed by water it might be possible to use titania photocatalysis to remove SO_2 from an ambient gaseous environment, if the photocatalyst was washed regularly with (rain) water. Although, even under these circumstances, the product, H_2SO_4, is a recognized environmental hazard in its own right and would require careful disposal. Alternatively, it could be collected as a possible commercial byproduct of photocatalysis-based, sulfur dioxide removal process.

Conclusion

Anatase titania films are able to photocatalyze the slow oxidation of amorphous sulfur to form SO_2. Using UVA light, the stoichiometry of this reaction is ~96%, with a photonic efficiency of ~0.16%. Using UVC light the photochemistry is complicated by the concomitant photolysis of sulfur to form SO_2 and of SO_2 to form SO_3 and/or H_2SO_4. In a closed environment, which allows the initial SO_2 product to accumulate, titania is able to photo-oxidize the SO_2, but the product, H_2SO_4, appears to poison the surface, and the photocatalytic activity of the film is only regenerated after soaking in water. This latter feature is a major problem in the use of titania photocatalyst films for air remediation, particularly in very dry environments where the possibility of photocatalyst film regeneration is much reduced. In addition, the photocatalytic removal of SO_2, and presumably NO_x, is not without its problems, as the product or products are also environmental hazards and can form acids which poison the titania photocatalyst.

References and Notes

(1) Hoffmann, M. R.; Martin, S. T.; Choi, W. Y.; Bahnemann, D. W. *Chem. Rev.* **1995**, *95*, 69.
(2) Mills, A.; LeHunte, S. *J. Photochem. Photobiol. A* **1997**, *108*, 1.
(3) Fujishima, A.; Hashimoto, K.; Watanabe, T. *TiO_2 Photocatalysis: Fundamentals and Applications*; BCK Inc: Tokyo, 1999.
(4) Mills, A.; Lee, S. K. *J. Photochem. Photobiol. A* **2002**, *152*, 233.
(5) Barfknecht, T. R. *Prog. Energy Combust. Sci.* **1983**, *9*, 199.
(6) Corporan, E.; Dewitt, M.; Wagner, M. *Fuel Process. Technol.* **2005**, *85*, 727.
(7) Kennedy, K. A.; Addison, P. A.; Maynard, D. G. *Environ. Pollut.* **1985**, *39*, 71.
(8) Kennedy, K. A.; Addison, P. A.; Maynard, D. G. *Environ. Pollut.* **1988**, *51*, 121.
(9) Mills, A.; Wang, J.; Crow, M. *Chemosphere* **2006**, *64*, 1032.
(10) Lee, M. C.; Choi, W. *J. Phys. Chem. B* **2002**, *106*, 11818.
(11) Mills, A.; Elliott, N.; Hill, G.; Fallis, D.; Durrant, J. R.; Willis, R. L. *Photochem. Photobiol. Sci.* **2003**, *2*, 591.
(12) Herzberg, G. *Molecular Spectra and Molecular Structure*, 2nd ed.; Krieger Publishing: London, 1991.
(13) Matsumoto, Y.; Nagal, H.; Sato, E. I. *J. Phys. Chem.* **1982**, *86*, 4664.
(14) Matsumoto, Y.; Yamaguchi, Y.; Sato, E. I. *Bull. Chem. Soc. Jpn.* **1985**, *58*, 1255.
(15) Paz, Y.; Luo, Z.; Rabenberg, L.; Heller, *J. Mater. Res.* **1995**, *10*, 2842.
(16) Minabe, T.; Tryk, D. A.; Sawunyama, P.; Kikuchi, Y.; Hashimoto, K.; Fujishima, A. *J. Photochem. Photobiol. A* **2000**, *137*, 53.
(17) Vattulainen, J.; Wallenius, L.; Stenberg, J.; Hernberg, R.; Linna, V. *Appl. Spectrosc.* **1997**, *51*, 1311.
(18) Shang, J.; Zhu, Y.; Du, Y.; Xu, Z. *J. Solid State Chem.* **2002**, *166*, 395.
(19) West, P. W.; Gaeke, G. C. *Anal. Chem.* **1956**, *28*, 1816.

In Situ, Continuous Monitoring of the Photoinduced Superhydrophilic Effect: Influence of UV-Type and Ambient Atmospheric and Droplet Composition

Andrew Mills* and Matthew Crow

Department of Pure & Applied Chemistry, University of Strathclyde, 295 Cathedral Street, Glasgow G1 1XL, United Kingdom

Received: December 4, 2006; In Final Form: February 1, 2007

A controlled-atmosphere chamber, combined with a CCTV system, is used to monitor continuously the change in shape of water droplets on the self-cleaning commercial glass, Activ, and a sol−gel TiO_2 substrate during their irradiation with either UVA or UVC light. This system allows the photoinduced superhydrophilic effect (PSH) exhibited by these materials to be studied in real time under a variety of different conditions. UVA was less effective than UVC in terms of PSH for both titania-coated glasses, and plain glass was unaffected by either form of UV irradiation and so showed no PSH activity. With UVA, ozone increased significantly the rate of PSH for both substrates, but had no effect on the wettability of plain glass. For both titania substrates and plain glass, no PSH activity was observed under an O_2-free atmosphere. A more detailed study of the PSH effect exhibited by Activ revealed that doping the water droplet with either an electron acceptor ($Na_2S_2O_8$), electron donor ($Na_2S_2O_4$), or simple electrolyte (KCl) in the absence of oxygen did not promote PSH. However, when Activ was UV irradiated, while immersed in a deoxygenated KCl solution, prior to testing for PSH activity, only a small change in contact angle was observed, whereas under the same conditions, but using a deoxygenated persulfate-containing immersion solution, it was rendered superhydrophilic. The correlation between organic contaminant removal and surface wetting was also investigated by using thick sol−gel films coated with stearic acid; the destruction of SA was monitored by FTIR and sudden wetting of the surface was seen to coincide with the substantial removal of the organic layer. The results of this work are discussed in the context of the current debate on the underlying cause of PSH.

Introduction

Semiconductor photocatalysis has, over the last 30 years, been shown to have wide-ranging technological and synthetic applications.[1−7] Its use in the field of environmental remediation—through the creation of photocatalytic water and air purification systems, and more recently self-cleaning surfaces—is an area where the transition from a promising technology to global market product ranges has occurred.[8,9] A key observation in the creation of titania-based, self-cleaning coatings is that of the photoinduced superhydrophilic effect (PSH), i.e. the greatly improved water wettability of titania films upon UV illumination. First noticed in 1988 by Kume and Nozu,[10] working for the Nippon Itagarasu company, it was ascribed initially to the simple photocatalytic destruction of adventitious hydrophobic organic material deposited on the titania coating on glass,[10] a photocatalytic model of PSH that has found increasing support in recent years. PSH in titania films was re-recognized in the mid-nineties by researchers at the TOTO Inc. laboratories, working with those at Tokyo University, who reported that TiO_2/SiO_2 films acquired superhydrophilic properties upon UV irradiation.[5,11] Thus, in this later work, preirradiation water droplets were formed on the TiO_2/SiO_2 film substrates, but postultraviolet irradiation, the water spread evenly across the surface, forming "sheets" instead.[11]

Over the past 10 years much research has been carried out to provide an appropriate mechanistic model for PSH. Not surprisingly, most models begin with the photogeneration of electron-holes pairs within the photocatalyst, which occurs when electromagnetic radiation of energy greater than the band gap—the energy difference between the valence band (VB) and the conductance band (CB)—is absorbed by the semiconductor and promotes an electron from the VB to the CB. These photogenerated electrons and holes are then able to migrate to the surface where, upon interaction with oxygen and adsorbed hydroxyl groups, respectively, they can take part in numerous reactions, including the photocatalytic mineralization of any organic material that may be present on the surface of the photocatalyst, i.e.

$$\text{organic} + O_2 \xrightarrow[h\nu \geq 3.2\ \text{eV}]{TiO_2} \text{minerals (such as } CO_2 \text{ and } H_2O) \quad (1)$$

The above process, the photocatalytic oxidation of organics, is a well-recognized and accepted feature of most forms of titania. However, when discussing the mechanism of PSH, it is the final fate of the photogenerated electrons and holes, when there is no apparent organic material on the surface of the photocatalyst, that is at the heart of the ongoing debate that is based largely on two very different models. The first assumes that the photogenerated electrons and holes responsible for PSH produce a restructuring of the surface of the titania, from one that is intrinsically hydrophobic to one that is hydrophilic and able to revert back to the former in the dark via a, usually slow (hours or days), dehydration process. A very simplified summary of this process is as follows:

* Address correspondence to this author. E-mail: a.mills@strath.ac.uk. Fax: +44-141-548-4822. Phone: +44-141-548-2458.

10.1021/jp068327v CCC: $37.00
Published on Web 03/31/2007

$$\equiv Ti-O-Ti\equiv + H_2O \underset{\text{dark}}{\overset{O_2,\ h\nu \geq E_{BG}}{\rightleftharpoons}} \equiv Ti-OH\ HO-Ti\equiv \quad (2)$$

The second model proposes that the photogenerated electrons and holes effect the photocatalytic destruction of very small amounts of adventitious, hydrophobic, and usually, almost undetectable (via FTIR for example), organic surface species, via reaction 1, to reveal the pristine, intrinsically hydrophilic surface of the titania photocatalyst underneath. In this case the slow return of the original hydrophobic nature of the titania in the dark is thought to be due to the re-contamination of the hydrophilic surface by air-borne hydrophobic organics.

Evidence supporting each mechanism has been reported. For example, in the case of the restructuring model, FTIR[5] and X-ray electron spectroscopy[12,13] (XPS) have been used to demonstrate the reversible adsorption of water on TiO_2 with UV illumination. The importance of bridging oxygen sites—also key to the restructuring model in PSH—was highlighted in this work by studying PSH using different crystal faces of rutile TiO_2, with the (001) face, which does not feature bridging oxygens, showing the least propensity for the PSH.[5,12] The UV-light-driven surface hydration/dark dehydration model was also supported by evidence that showed previously UV-irradiated samples recovered their hydrophobicity at increased rates in the dark when under vacuum.[14]

In contrast, other groups have reported strong evidence for the alternative "photocatalyst" model of PSH, summarized by reaction 1. For example, White[15] and Zubkov,[16] utilizing model organic layers of trimethyl acetate (TMA)[15] and hexane[16] to recreate the hydrophobic−hydrophilic change during UV irradiation of a titania surface, reported an induction period, presumably during which the hydrophobic organics are photooxidised, followed by rapid wetting of the surface. Another study, using sum frequency generation (SFG) analysis to successfully detect surface hydrocarbons at levels which FTIR would not normally have sufficient sensitivity,[17] showed that the intensity of the C−H stretches due to these hydrocarbons decreased upon UV irradiation of an apparently pristine but hydrophobic sample of titania on glass, and regenerated under ambient, dark conditions due to re-contamination of the surface by air-borne hydrocarbons.

Interestingly, work into PSH has been characterized by the observation of two very different types of kinetics associated with the change of water droplet contact angle, CA, with illumination time, namely: hyperbolic-shaped decay profiles—characterized by a linear plot of CA^{-1} versus UV irradiation time[5,18−22]—and those which are decidedly nonhyperbolic and better described by an initial slow decrease in CA for a period, followed by a rapid drop in CA;[13,19,23−25] examples of each can be seen in Figure 1. Interestingly, the examples illustrated in Figure 1 are from different reports by the same research group.[18,23] With respect to the above different shaped CA vs illumination time decay profiles illustrated in Figure 1, UV light intensity, and how well it is absorbed, is found to be significant, with low intensities and thin films appearing to give nonhyperbolic profiles,[19,25] and high intensities and thicker films displaying hyperbolic type profiles.[5,19,20,23] These differences, it has been suggested, could be due to a preliminary surface conditioning process, possibly the removal of low levels of organic impurities,[19,24] thus providing support for the organic impurity, i.e., reaction 1, model of PSH.

While the debate as to the mechanism of PSH continues there is still a great deal of fundamental work that can be carried out and which should lead to an improved understanding of PSH and its mechanism. To date the majority of PSH research has been carried out either on single crystals or on substrates derived by a variety of different sol−gel procedures. While the latter are nearer to the CVD-coated, poly-nanocrystalline titania films used in most examples of self-cleaning glass, the variety of the different sol−gel formulations and fabrication conditions employed by the different research groups has not been conducive to comparing and contrasting the PSH results. To help avoid this problem, in this work the self-cleaning photocatalytic glass, Activ (Pilkington), which has already been suggested as a possible reference photocatalyst,[19] is used. In addition, some work is also carried out with a much more active, photocatalyst film, prepared by a sol−gel procedure, to aid comparison with PSH work carried out by others[5,18,24] using similar, highly active films.

In the study of PSH, most evaluations are invariably made by measuring the contact angle exhibited by a water droplet on the substrate under test, i.e., CA, usually before and after a period of UV irradiation. Until now, to generate a CA vs UV irradiation time profile, such as illustrated in Figure 1, a number of identical samples of the titania film under test needed to be prepared, irradiated for different times, and have their CAs measured. This is very time-consuming work and the generation of identical titania film samples is not usually achieved. As a result the CA vs time profile that results from such work provides only an average picture of the kinetics of PSH and any subtleties in the decay profile and kinetics are likely to be lost. In contrast, the PSH features of any titania film type would be assessed much more easily, quickly, and accurately by monitoring the actual CA vs UV irradiation real time profile for a single sample. In this paper a controlled-atmosphere chamber, combined with a CCTV system, is used to monitor *continuously* the change in shape of water droplets on the self-cleaning commercial glass, Activ, and a sol−gel TiO_2 substrate during their irradiation with either UVA or UVC light. This system allows the PSH activities of these samples to be studied quickly and easily under a wide range of different conditions, generating results which help provide a better understanding of the mechanism behind the PSH effect.

Experimental Section

Unless stated otherwise all chemicals were purchased from Aldrich Chemicals and used as received. The two types of titania-coated substrates used in this work were 2 square cm Activ samples, supplied by Pilkington Glass, and 1 cm × 2 cm sized, ∼4 μm thick, doctor-blade-cast paste films, made by a sol−gel method, using titanium isopropoxide as a precursor, as described elsewhere.[26] The Activ glass samples were comprised of a 4 mm thick float glass coated with an approximately 15 nm layer of TiO_2, deposited by an in-line CVD process.[19] Films of both types were left in a sealed box in the dark for in excess of 1 month before use. In work in which an additional layer of stearic acid (SA) was coated onto a sol−gel film, this was achieved by spin coating 3 droplets of a 2 g of SA L^{-1} of chloroform solution at 135 rpm for 10 s and gave very thin layers of SA—typically comprising 1.2×10^{16} molecules cm^{-2}.[27] Monitoring of the SA destruction was achieved by using a Perkin-Elmer Spectrum One FTIR spectrometer to measure the peak absorbance area in the region 2700−3000 cm^{-1} as a function of irradiation time, which provided a measure of the amount of SA remaining on the substrate under test.

Contact angles were measured with an FTA100 system, comprising a CCTV camera interfaced with a computer, which

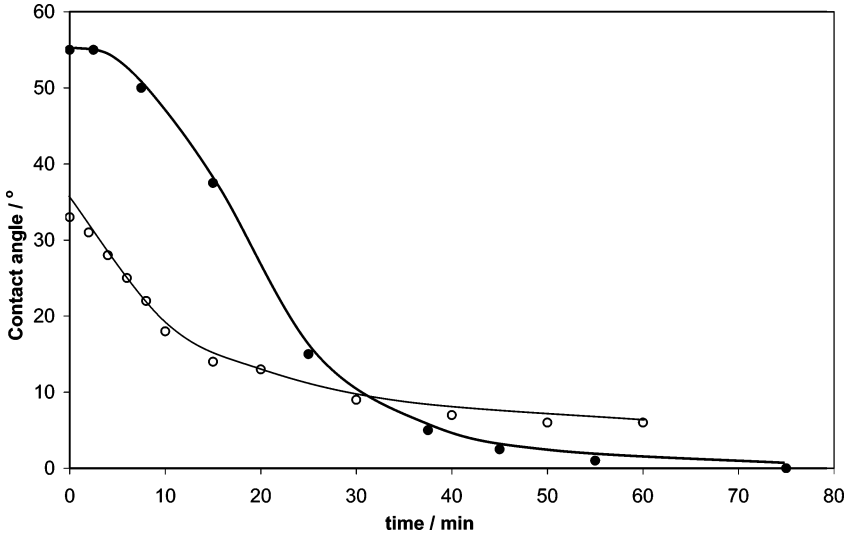

Figure 1. Time dependence of the contact angle (CA) made by a water droplet on two different TiO_2 films under UV illumination with different light intensities, showing nonhyperbolic (●, 0.1 mW cm^{-2})[23] and hyperbolic CA vs irradiation time profiles (○, 0.2 mW cm^{-2}).[18]

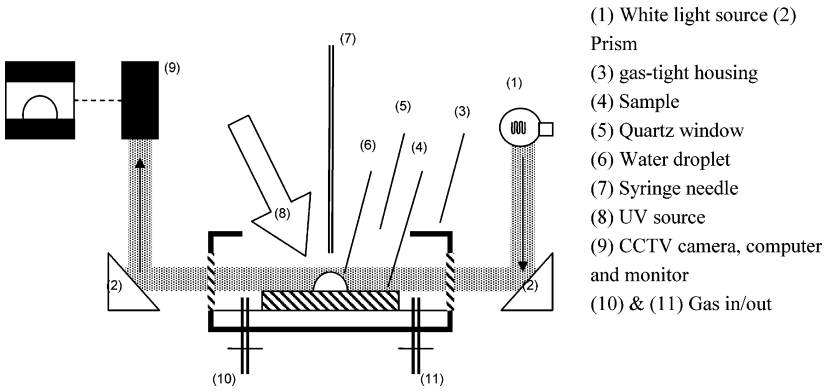

Figure 2. Schematic of the environmental chamber system used for in situ CA measurements on TiO_2 photocatalyst and blank substrates.

provided a continuous stream of images of any water droplet after its initial deposition onto the photocatalyst substrate under test. Droplets were deposited using a 500 μL Gastight (Hamilton) syringe, via a 30-gauge stainless steel needle with 0° bevel (Kahnetics), which deposited reproducible 5 μL water droplets. The software package associated with the instrument allowed calculation of the contact angle made by the water droplet deposited on the substrate by curve-fitting the droplet image outline. This system allowed the contact angle of a water droplet on a substrate under test to be monitored continuously in situ as a function of UV irradiation time. At all times unless stated otherwise, when contact angle changes were measured in situ, an environmental chamber was used to keep the ambient atmosphere at 100% relative humidity (RH), with $T = 22$ °C, to limit evaporation of the water droplet.

The environmental chamber noted above had a brass body, fitted with two glass windows to allow CCTV observation in the plane of the droplet for contact angle analysis. A circular quartz window on top permitted both UVA and UVC irradiation of the underlying TiO_2 films; this window also featured a rubber septum through which the syringe needle was passed for the initial water droplet deposition. A schematic illustration of this system is given in Figure 2. Irradiation of the substrates for PSH studies was carried out by using either UVC or UVA light. In either case, two 8-W bulbs were used and gave a typical intensity of ~0.5 mW cm^{-2} of UV light inside the experimental chamber. A small desk fan was used to cool the system continuously and minimize any local heating effects due to the low-energy UV lamps. The environmental chamber allowed flushing by water-saturated (i.e., 100% RH) oxygen, nitrogen, or air gas stream and was typically run at 100 mL min^{-1} during the recording of the variation of CA vs illumination time for any sample. In some experiments an ozone generator (OZ500, Dryden Aqua) was also connected into the gas system to purge the chamber with an atmosphere containing approximately 1700 ppm ozone in an otherwise 100% RH, oxygen atmosphere.

Results and Discussion

In Situ, Continuous Observation of PSH. In a typical experiment, a sample of Activ glass was placed in the environmental chamber, in a 100% RH O_2 atmosphere, and a water droplet then deposited onto its surface. Figure 3a shows a set of images of the water droplet on the Activ glass, taken at different times during the UV irradiation process. Initial work on Activ and paste films showed that the water droplet contact angles decreased with increasing UV irradiation time, indicative of the PSH effect. The blank experiment, using water droplets on plain glass, showed that upon their irradiation with UV the CA did not decrease rapidly but, instead, decreased gradually due to evaporation with a typical initial rate ($-r_i$) of 0.17 deg min^{-1}, which did not change over many hours of irradiation. Figure 3b shows the measured variations in CA on Activ under UVC and UVA irradiation, from which $-r_i$ values of 1.38 and 0.27 deg min^{-1}, respectively, were calculated. With UVC light, the surface of Activ is rendered superhydrophilic, i.e., CA ≤

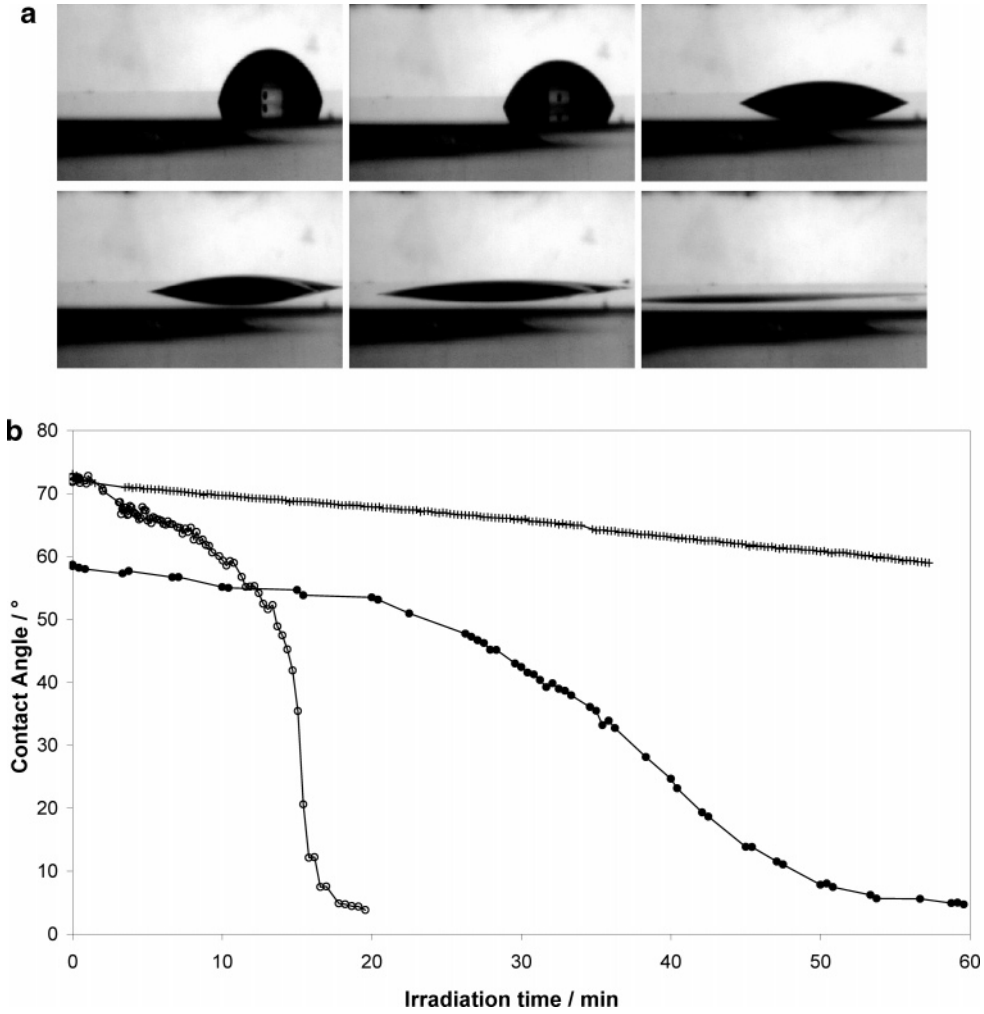

Figure 3. (a) CCTV images of water droplet on Activ taken in situ during UV irradiation. $CA_i = 69°$, final CA = ~0° (b) CA versus irradiation time profiles recorded using Activ sample irradiated from above in water-saturated oxygen atmosphere and either UVC (○) or UVA (●) light, or in a water-saturated N_2-only atmosphere with UVC light (+). Note that although the CAs were monitored continuously, the values of sampled contact angles are depicted here, and in other figures, using different symbols, to aid differentiation between the different CA vs time profiles. [In O_2: UVA, $-r_i = 0.27$ deg min^{-1}, $-r_{max} = 2.0$ deg min^{-1}; UVC, $-r_i = 1.38$ deg min^{-1}, $-r_{max} = 22.4$ deg min^{-1}.]

5°, after ~20 min, while with UVA this process takes ~55 min; the difference is probably due to the higher fraction of light absorbed, *f*, by the 15 nm layer of TiO_2 in the UVC region—i.e., ca. $f = 0.53$ for 254 nm, compared to 0.07 for 365 nm light.[19,26]

Both CA vs time profiles illustrated in Figure 3b are decidedly nonhyperbolic in shape, which is typical of a low-activity, titania photocatalyst film, such as Activ. Such nonhyperbolic shapes can be loosely characterized by two parameters, namely, the maximum rate of wetting, $-r_{max}$, and the time taken for the latter to occur, δ. From the data in Figure 3b, for UVA, $-r_{max}$ is 2.0 deg min^{-1} and δ is ~38 min, whereas with UVC irradiation, $-r_{max}$ is 22.4 deg min^{-1} and δ is ca. 16 min. It appears likely that $-r_{max}$ and the delay time (δ) are negatively correlated to some extent and related closely to the photocatalytic activity of a sample, i.e., the greater the photocatalytic activity of the sample, the larger its r_{max} value and the lower the value of δ exhibited.

The simplest explanation for such a relationship is the existence of a layer of hydrophobic surface organic contaminants on low-activity samples such as Activ, which are removed faster (resulting in a low value of δ and high value of $-r_{max}$) the greater the photocatalytic activity exhibited by the sample. The photocatalytic activity of such low-activity photocatalyst films can be increased a number of ways, including by, as in Figure 3b, using light, such as UVC, which is absorbed much more strongly than UVA or by using a greater intensity of the same wavelength of light. These results, and the photocatalytic model of PSH, suggest that any titania-based photocatalytic film is PSH active and can be made to exhibit a hyperbolic CA vs time decay profile, for which δ is zero and $-r_{max}$ is very high, if its activity can be increased sufficiently. In this context, the high UVA absorbances of thick, sol−gel films of titania help explain why these films are often reported to exhibit hyperbolic-type CA vs time decay profiles with use of UVA light sources, in contrast to thin titania films, such as Activ. Not surprisingly, initial work shows that δ for Activ decreases with increasing UV irradiance.

In the presence of a water-saturated, nitrogen-only atmosphere, rather than oxygen, no PSH effect was observed for both Activ (see Figure 3b) and thick paste titania films, in agreement with the recent results of others.[16] This observation highlights the need for oxygen—or some other sacrificial electron acceptor, SEA, for PSH to operate, a feature that is common to both PSH mechanisms.

Effect of an Ozone-Containing Atmosphere. In another set of experiments the chamber was flushed with a water-saturated, oxygen gas stream containing ozone (1700 ppm) and irradiated with UVA; the latter UV light was used so as not to electronically excite the ozone. The resulting CA vs time profiles for a

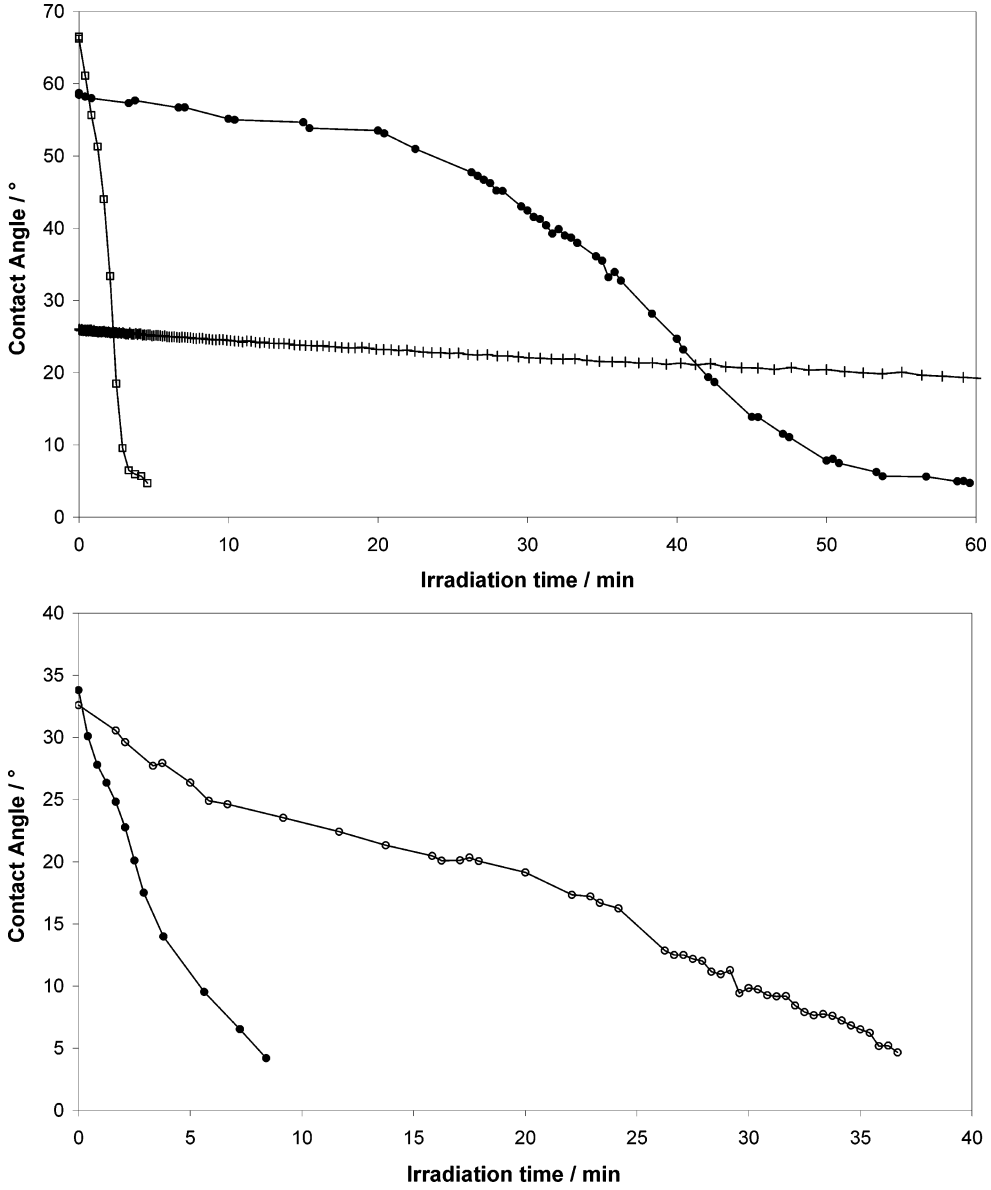

Figure 4. (a) CA vs UVA irradiation time for hydrated oxygen (●) and ozone (□) atmospheres with Activ samples, and UVA/ozone for plain glass (+) [Activ: UVA/O_2, $-r_i = 0.27$ deg min^{-1}; UVA/ozone, $-r_i = -r_{max} = 14.8$ deg min^{-1}] [plain glass: UVA/ozone, $-r_i = 0.10$ deg min^{-1}]. (b) CA vs UVA irradiation time for pure oxygen (○) and ozone (●) atmospheres for sol−gel paste films [UVA/O_2, $-r_i = -r_{max} = 1.3$ deg min^{-1}; UVA/ozone, $-r_i = -r_{max} = 5.1$ deg min^{-1}].

typical water droplet on Activ and paste films are shown in Figure 4, parts a and b, respectively. With both substrates the presence of ozone was found to increase markedly the rate of the photoinduced hydrophilic conversion process, and decrease the time taken for the superhydrophilic state to be reached, i.e., from ∼55 to <5 min for Activ and from ∼38 to ∼8 min for the paste film. In contrast, the CA for a droplet on plain glass, subjected to the same UVA/ozone process, remained largely unchanged, showing that the very rapid PSH effect exhibited by Activ and sol−gel titania films under similar conditions is not due to ground state, or UV excited, ozone reacting with the surface of the substrate supporting the water droplet. Instead, in the latter systems, ozone appears to be acting as a super sacrificial electron acceptor. Note that the combination of UVC and ozone renders all three substrates superhydrophilic with a few minutes of irradiation due, most probably, to the highly effective oxidizing action of electronically excited ozone. The suggestion that ozone is a more effective SEA than oxygen in semiconductor photocatalysis is not without precedent, as ozone in combination with UVA light has been shown to increase the rate of photocatalytic decomposition of toluene.[28]

Also notable from the data illustrated in Figure 4a is that the considerable (ca. 38 min) delay time observed in the CA vs time profile for an Activ film irradiated in O_2 with UVA is eliminated, and the maximum rate of PSH is increased when ozone is present, i.e., $-r_{max}$[UVA/ozone] (=14.8 deg min^{-1}) ≫ $-r_{max}$[UVA/O_2] (=2.0 deg min^{-1})), presumably reflecting the marked increase in the rate of the photocatalytic mineralization of the surface organic species brought about by the presence of the super-electron acceptor, ozone, and the negative correlation between r_{max} and δ, noted earlier. Note also in Figure 4b that the CA vs t profile for the much thicker, and so more UVA absorbing, paste titania film exhibits no real delay time in the absence or presence of ozone, i.e., $\delta \approx 0$ min, although the rate of PSH is much faster (compare $-r_{max}$[UVA/O_2] (=1.3 deg min^{-1}) to $-r_{max}$[UVA/ozone] (=5.1 deg min^{-1})) in the latter case. Presumably, this lack of a delay, and consequent generation of a hyperbolic decay in CA, is due to the titania paste film's

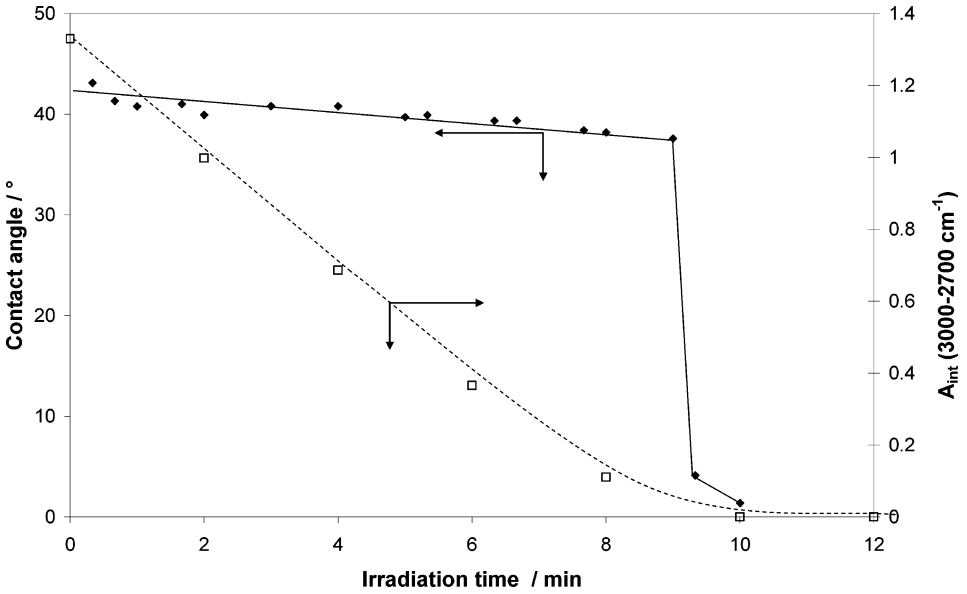

Figure 5. CA (♦) and FTIR (□) integrated area, A_{int}, measured from 2700 to 3000 cm^{-1}, versus UVA irradiation time for stearic acid coated paste film in an ozone-containing (1700 ppm) oxygen, water-saturated atmosphere. A blank of a stearic acid-coated paste film treated with only ozone produced no change in integrated area over 30 min.

much greater photocatalytic activity compared to Activ, due to its greater absorbance of UVA light ($f = 0.83$, cf. 0.07 for Activ). It also shows that above a certain PSH activity, as measured by $-r_{max}$, the delay time is zero and so is no longer correlated with $-r_{max}$, for films not deliberately contaminated with hydrophobic organics.

PSH on Deliberately Contaminated Titania Films. As noted above the thick titania sol−gel films do not exhibit any delay in their CA vs *t* plots, even in the absence of ozone, see Figure 4b, and follow a more conventional hyperbolic profile, as would be expected for films of high activity, which absorb strongly any incident UV light, based on the photocatalyst model of PSH. In contrast, and as indicated earlier, thin titania films and/or low incident UV light intensities have been shown to give rise to such nonhyperbolic CA vs irradiation time profiles and appear associated with low rates of PSH.[19,23] Interestingly and not surprisingly, such nonhyperbolic CA vs *t* profiles can be effected by using very active, thick, sol−gel films, even in an ozone-containing environment, through the application of a stearic acid (SA) film onto the substrate's surface before water droplet deposition, as shown by the CA vs UVA irradiation time profile in Figure 5. Figure 5 also illustrates the variation of the integrated area under the FTIR peaks due to the SA layer on the same thick paste titania film, i.e., A_{int} vs UV irradiation time. This concomitant monitoring of the SA layer by FTIR on an identical film shows that there is a strong correlation between the end of the induction period − characterized by a sudden wetting process − and the removal of the final, FTIR-detectable, traces of the stearic acid layer. These results appear to lend support to the elegant work of Yates et al.[16] and their proposal that such delay periods are due to organic film contaminant removal by photocatalysis.

PSH and Salt Doping of Water Droplets. In the previous section ozone was seen to increase the rate of PSH by acting as a super, i.e., much more effective than O_2, sacrificial electron acceptor, and no PSH effect was observed on Activ and sol−gel samples in the absence of an electron acceptor such as ozone, or atmospheric oxygen. These results raise the following question: Does the electron acceptor have to be oxygen or oxygen-containing, or can it be another SEA? Certainly in some examples of semiconductor photocatalysis, i.e., reaction 1, other SEAs have been used with great effect.[29] Thus, in this work the role of electron-acceptor in PSH was investigated further by dissolving various salts in the water used to generate the deposited water droplets. Thus, water droplets containing 0.1 M sodium persulfate (an SEA), potassium chloride, and sodium dithionite (an oxygen scavenger) were each, in turn, deposited onto an Activ titania film. As shown in Figure 6a all three salt-containing drops made the PSH process faster, i.e., typically reaching a CA < 5° in <10 min rather than the usual ∼18 min, in 100% RH oxygen. The CA vs *t* profiles generated by this work suggest that having an electrolyte in the water droplet accelerates the photocatalytic process and thus the rate of PSH. The fact that the electrolyte may also act as either an SEA (as in the case of persulfate) or a scavenger of O_2 (as in the case of dithionite) in the water droplet appears to make no difference to the kinetics of PSH. These results imply that PSH depends more on what happens to the surface surrounding the water droplet rather than underneath the droplet itself.

Possibly of greater initial surprise is the observation that PSH is not exhibited by Activ with use of any of the different salt-containing droplets under an anaerobic, rather than oxygen, atmosphere. This is surprising because sodium persulfate is a proven effective SEA for the TiO_2-sensitized photooxidation of organics in water,[29] so if the photocatalytic model of PSH is correct, persulfate's presence in a water droplet, in an otherwise anaerobic atmosphere, should allow any organic material directly beneath the water droplet to be destroyed, effectively burning a hole into any underlying organic film. Given this, initially it seems odd that the water droplet does not spread, i.e., no PSH activity is exhibited, when a persulfate droplet is UV irradiated under anaerobic conditions. However, a possible reason for the persulfate-containing water droplet not spreading would be that, apart from underneath the water droplet, the surrounding titania film would, presumably, remain covered with a thin, albeit undetectable (by FTIR at least), layer of organic material that renders it hydrophobic, as indicated by the schematic illustration in Figure 6b. Support for the above "hole-burning" model, as illustrated in Figure 6b, was provided by a demonstration that persulfate is able to effect readily the complete cleaning of the surface of an Activ sample of the hydrophobic organics by semiconductor photocatalysis under anaerobic conditions, thereby

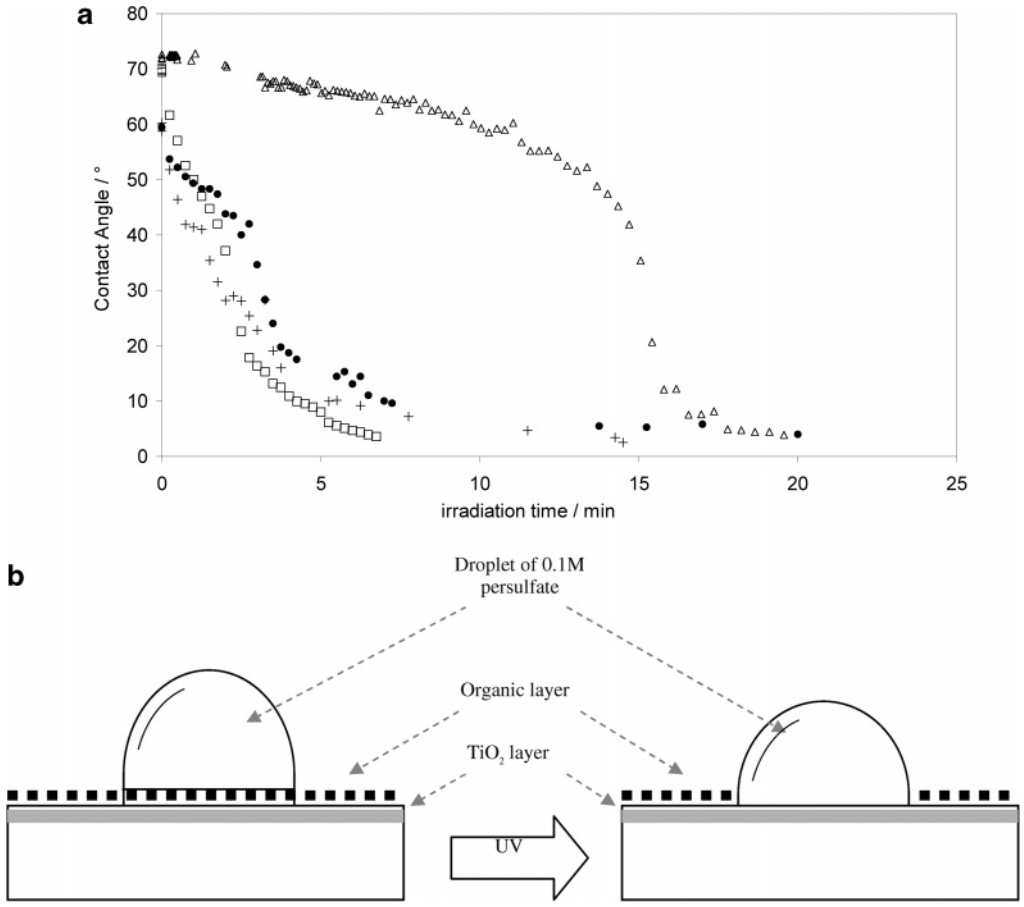

Figure 6. (a) CA versus UVC irradiation time for pure water (△), sodium persulfate (□), potassium chloride (●), and sodium dithionite (+) on Activ in hydrated oxygen atmosphere. (b) Schematic of the suggested hole-burning effect of irradiation on 0.1 M persulfate solution droplet on Activ in deoxygenated atmosphere.

rendering it superhydrophilic. This was achieved by preirradiating an Activ film, submerged in an anaerobic, 0.1 M persulfate solution, with UVA light. The results of this work showed that the titania film was rendered superhydrophilic by this process whereas, in contrast, films which had been treated similarly, but with 0.1 M KCl or sodium dithionite as the immersion solution, retained their initial hydrophobic character.

Conclusions

Contact angles were measured in situ during irradiation with UVC and UVA to generate both hyperbolic (on thick paste films) and nonhyperbolic (on Activ) profiles. Ozone, or the presence of an electrolyte in the deposited droplet, increases the rate of PSH on Activ TiO_2 substrates significantly. In contrast, the combination of UVA and ozone revealed plain glass to have no PSH activity, indicating that ozone acts as a superelectron acceptor that is able to enhance significantly the PSH activities of titania-based films. The deposition of a thin film of stearic acid causes a delay in the onset of the usual rapid drop in CA as a function of UV irradiation time. Concomitant monitoring, by FTIR, of the stearic acid layer revealed a strong correlation between its final removal and the sudden wetting on a TiO_2 film, i.e., the onset of PSH. PSH was not observed for samples of Activ using sodium persulfate-doped droplets in a deoxygenated atmosphere, but when such samples were preirradiated in a deoxygenated solution of persulfate, they were rendered superhydrophilic; showing that persulfate can be used as a replacement for oxygen as an electron acceptor in PSH. The combination of all these results appears to provide strong support for the Yates et al.[16] model of PSH, namely that it is simply a manifestation of the well-established photocatalytic mineralization of hydrophobic organic material and that most pristine, polycrystalline titania films, such as those found in commercial, self-cleaning glass, are intrinsically superhydrophilic, due to the van der Waals−London forces, hydrogen bonding, and electrostatic interactions.[30]

It can be argued that, as all the experiments reported above were carried out at a 100% RH, a photocatalytic water chemisorption mechanism for PSH cannot be ruled out. However, work carried out with the high boiling point, not easily oxidized, polar liquid, DMSO, as the droplet medium, in the absence of water vapor, showed that the titania films continued to exhibit a clear PSH effect. This observation, and the observation of PSH with use of water droplets in an ambient oxygen atmosphere of 0% RH, appears at odds with a photocatalytic water chemisorption mechanism.

References and Notes

(1) Chen, D.; Ray, A. K. *Chem. Eng. Sci.* **2001**, *56*, 1561.
(2) Fox, M. A. *Acc Chem. Res.* **1983**, *16*, 314.
(3) Fox, M. A.; Dulay, M. T. *Chem. Rev.* **1993**, *93*, 342.
(4) Fujishima, A.; Honda, K. *Nature* **1972**, *238*, 37.
(5) Fujishima, A.; Rao, T. N.; Tryk, D. A. *J. Photochem. Photobiol., C* **2000**, *1*, 1.
(6) Kamat, P. *Chem. Rev.* **1993**, *93*, 267.
(7) Hoffman, M. R.; Martin, S. T.; Choi, W.; Bahnemann, D. *Chem. Rev.* **1995**, *95*, 69.
(8) Mills, A.; Lee, S.-K. *J. Photochem. Photobiol., A* **2002**, *152*, 233.
(9) http://www.selfcleaningglass.com (accessed February 2007).
(10) Kume, S.; Nozu, T. Difficulty stainable glass product. JP Patent Office Application. No. Sho 63-100042, 1988.
(11) Wang, R.; Hashimoto, K.; Fujishima, A.; Chikuni, M.; Kojima, E.; Kitamura, A.; Shimohigoshi, M.; Watanabe, T. *Nature* **1997**, *388*, 431.

(12) Wang, R.; Sakai, N.; Fujishima, A.; Watanabe, T.; Hashimoto, K. *J. Phys. Chem. B* **1999**, *103*, 2188.
(13) Watanabe, T.; Nakajima, A.; Wang, R.; Minabe, M.; Koizumi, S. *Thin Solid Films* **1999**, *351*, 260.
(14) Irie, H.; Hashimoto, K. In *Environmental Photochemistry Part II*: *Photocatalytic Active Surfaces and Photo-Induced High Hydrophilicity*/*High Hydrophobicity*; Boule, P., Robertson, P. K. J., Bahnemann, D. W., Eds.; Springer-Verlag: Duesseldorf, Germany, 2005; Vol. 2, p 425.
(15) White, J. M.; Szanyi, J.; Henderson, M. *J. Phys. Chem. B* **2003**, *107*, 9029.
(16) Zubkov, T.; Stahl, D.; Thompson, T. L.; Panayatov, D.; Diwald, O.; Yates, J. T. *J. Phys. Chem. B* **2005**, *109*, 15454.
(17) Wang, C.-Y.; Groenzin, H.; Shultz, M. J. *Langmuir* **2003**, *19*, 7330.
(18) Sakai, N.; Fujishima, A.; Watanabe, T.; Hashimoto, K. *J. Phys. Chem. B* **2003**, *107*, 1028.
(19) Mills, A.; Lepre, A.; Elliott, N.; Bhopal, S.; Parkin, I. P.; O'Neill, S. A. *J. Photochem. Photobiol., A* **2003**, *160*, 213.
(20) Sakai, N.; Fujishima, A.; Watanabe, T.; Hashimoto, K. *J. Phys. Chem. B* **2001**, *105*, 3023.
(21) Sakai, N.; Fukuda, K.; Shibata, T.; Ebina, Y.; Takada, K.; Sasaki, T. *J. Phys. Chem. B* **2006**, *110*, 6198.
(22) Sakai, N.; Wang, R.; Fujishima, A.; Watanabe, T.; Hashimoto, K. *Langmuir* **1998**, *14*, 5918.
(23) Sun, R.; Fujishima, A.; Watanabe, T.; Hashimoto, K. *J. Phys. Chem. B* **2001**, *105*, 1984.
(24) Langlet, M.; Permpoon, S.; Riassetto, D.; Berthome, G.; Pernot, E.; Joud, J. C. *J. Photochem. Photobiol., A* **2006**, *181*, 203.
(25) Zhang, X.-T.; Sato, O.; Taguchi, M.; Einaga, Y.; Murakami, T.; Fujishima, A. *Chem. Mater.* **2005**, *17*, 696.
(26) Mills, A.; Hill, G.; Bhopal, S.; Parkin, I. P.; O'Neill, S. A. *J. Photochem. Photobiol., A* **2003**, *160*, 185.
(27) Mills, A.; Wang, J. *J. Photochem. Photobiol., A* **2006**, *182*, 181.
(28) Pengyi, Z.; Fuyan, L.; Gang, Y.; Qing, C.; Wanpeng, Z. *J. Photochem. Photobiol., A* **2003**, *156*, 189.
(29) Mills, A.; Valenzuela, M. A. *J. Photochem. Photobiol., A* **2004**, *165*, 25.
(30) Kanta, A.; Sedev, R.; Ralston, J. *Langmuir* **2005**, *21*, 2400.

Hindawi Publishing Corporation
International Journal of Photoenergy
Volume 2008, Article ID 470670, 6 pages
doi:10.1155/2008/470670

Research Article

A Study of Factors that Change the Wettability of Titania Films

Andrew Mills and Matthew Crow

Department of Pure and Applied Chemistry, University of Strathclyde, 295 Cathedral Street, Glasgow, G1 1XL, UK

Correspondence should be addressed to Andrew Mills, a.mills@strath.ac.uk

Received 25 July 2007; Accepted 3 January 2008

Recommended by Russell Howe

The effect of several pretreatment methods on the wettability of polycrystalline titania-coated glass (Pilkington Activ) and plain glass are investigated. UV/ozone, immersion in aqua regia, and heating ($T > 500^\circ C$) render both substrates superhydrophilic (i.e., water contact angle (CA) $< 5^\circ$). The dark recovery of the contact angles of these superhydrophilic substrates, monitored after treatment in either an evacuated or an ambient atmosphere, led to marked increases in CA. Ultrasound treatment of superhydrophilic Activ and glass samples produced only small increases in CA for both substrates, but rubbing the samples with a cloth produced much larger increases. The results of this study are discussed in the context of the current debate over the mechanism of the photo-induced superhydrophilic effect.

1. INTRODUCTION

Titanium dioxide films have been widely observed to become superhydrophilic, that is, water droplet contact angle $< 5^\circ$, when exposed to ultraviolet (UV) light, a phenomenon termed photoinduced superhydrophilicity (PSH) [1–7]. Its effects have been pivotal in the development of self-cleaning surfaces for glazing and other applications, but the precise mechanism by which this change is effected remains the subject of some debate, although it is clear that PSH is initiated by the photogeneration of electron/hole pairs and their migration to the surface. An essential feature of the overall PSH phenomenon is not only the initial, photo-induced hydrophobic to hydrophilic change, but also the reverse, dark process, whereby a superhydrophilic titania film recovers its original hydrophobic form. Any mechanism of PSH must embrace both the light-induced superhydrophilic process and the dark hydrophobic recovery step.

In 1985 Kume and Nozu of Nihon Itagarasu, Japan reported that sheet glass coated with TiO_2 had the ability to stay clean by "…rapidly and automatically decomposing and removing organic stains adhered to the glass surface…" [8]. Most importantly, part of their patent application involved the observation that the contact angle made by a water droplet on the glass, that is, CA, was reduced as a function of UV irradiation time. This appears to be the first clear claim of a PSH effect relating to titania films on glass and explanation for the effect, namely, it is due to the removal of hydrophobic organic stains on the surface, via the following, well-established, photocatalytic oxidative (PCO) process:

$$\text{organic} + O_2 \xrightarrow[h\nu \geq 3.2\,\text{eV}]{TiO_2} \text{minerals} \quad (\text{e.g., } CO_2 \text{ and } H_2O). \quad (1)$$

In contrast, in 1997, Wang et al. [6], reporting on the UV-induced PSH of TiO_2/SiO_2 films, proposed that the effect was not due to PCO but rather the dissociative adsorption of water at surface defects created by UV light [9]. The defects, it was suggested, were formed by the trapping of holes at bridging oxygen lattice points close to the surface, the Ti^{4+} sites being reduced to Ti^{3+} by the electrons and oxygen atoms being ejected to form vacancies [10]. The oxygen vacancies were thought to cause an increase in the adsorbed hydroxyl group density and lead to the formation of hydrophilic regions. It was proposed that storage in the dark, in the presence of oxygen, removed the defects replacing the chemisorbed hydroxyl groups with oxygen and so returning the surface to its original hydrophobic state. A very simple summary of this surface reorganisation

mechanism for PSH is as follows:

$$\equiv \mathrm{Ti} - \mathrm{O} - \mathrm{Ti} \equiv + \mathrm{H_2O} \underset{\text{dark}}{\overset{\mathrm{O_2}, h\nu \geq E_{BG}}{\longleftrightarrow}} \equiv \mathrm{Ti} - \mathrm{OH}\ \ \mathrm{HO} - \mathrm{Ti} \equiv . \quad (2)$$

It has been suggested that the above mechanism is specific to only a few materials of which titania is most notable, for example, it is not exhibited by silica substrates, that is, glass. This photo-induced surface reorganisation (PISR) model of PSH has received support from a number of different studies including examination of the creation of Ti^{3+} defects on single-crystal rutile TiO_2 using XPS [11]; FTIR measurements that reveal anatase TiO_2 is able to adsorb water reversibly upon UV irradiation [10]; and AFM studies which show apparent "roughening" of the surface as a result of UV exposure (attributed to defect formation) [12]. The importance of bridging oxygen, an integral part of the PISR model, has also been illustrated using rutile single crystals, with the (001) face—which does not feature bridging oxygens—showing the least propensity to photo-induced hydrophilic change [10, 13].

Recently, support for the more simplistic PCO model of PSH, based on reaction (1), namely, the photocatalytic removal of hydrophobic organic surface contaminants, has increased with a number of different groups reporting evidence for this model using test hydrophobic surface contaminants such as trimethyl acetate [14] and hexane [15], and the detection of previously unobserved layers of hydrocarbons on titania surfaces [16]. These results have presented a significant challenge to the PISR model of PSH.

Key to any model of PSH is an explanation of the dark recovery step, and significant support for this aspect of the PISR model of PSH effectively a dark, dehydration step (see reaction (2)) has been provided by studies [10, 17, 18] which show that titania films regain their original hydrophobicity at an increased rate when stored at increased temperatures [18, 19] or under an evacuated (H_2O free) atmosphere [17]. The PISR model rationale behind this is that heat and vacuum cause the metastable water/hydroxyl groups, responsible for the superhydrophilic surface of titania, to dissociate more quickly. It has also been demonstrated that hydrophilic TiO_2-glass films exhibit a measurable increase in contact angle when subjected to ultrasound [20]. The use of ultrasound to render a superhydrophilic film slightly more hydrophobic was interpreted initially by advocates of the PISR model as being due to the reoxidation of the surface by sonically produced OH radicals [20], but more recently as simply the breaking down of the photo-induced hydrophilic metastable state by an external stimulus [18]. A similar interpretation has been used to explain the effect of wet rubbing [21], which reconverts superhydrophilic titania to its original hydrophobic state via a mechanochemical effect.

In this paper, the effects of UV/O_3, heating, and strong acid pretreatment on initially hydrophobic samples of Activ and plain glass were studied. In addition, the effects of vacuum, ultrasound, and rubbing on the wettability of clean, superhydrophilic samples of titania-coated, self-cleaning glass (Activ), and plain glass were examined and the results discussed in terms of the two different mechanisms of the PSH effect.

2. EXPERIMENTAL

All reagents, unless otherwise stated, were supplied by Aldrich and used as received. The titania-coated substrates used in this work were 2 cm × 2 cm Activ samples, supplied by Pilkington Glass, comprising 4 mm thick float glass coated with an approximately 15 nm layer of TiO_2, deposited by an inline CVD process [22]. The reverse side of Activ provided the samples of uncoated float-glass used in all "plain glass" blank experiments. Additional experiments revealed no difference in behaviour between that of the reverse side of Activ and uncoated float glass samples. Typically, all glass samples, that is, Activ or plain, were cleaned with chloroform and left in a sealed box in the dark for in excess of one month before use. Unless otherwise stated, both types of glass were rendered superhydrophilic by pretreating with UVC/ozone, effected by irradiation with 2 × 6 W UVC (254 nm) bulbs (Vilber-Lourmat, Torcy, France), irradiance ~1 mW cm^{-2}, in a water saturated, that is, 100% relative humidity (RH), oxygen atmosphere containing ~1700 ppm ozone, produced by a corona-discharge ozone generator (OZ500, Dryden Aqua, Edinburgh, UK).

Other pretreatment methods used included a heat-treatment process, using a muffle furnace, in which the samples were kept at the desired temperature for 1 hour before removing to cool to room temperature in a covered Petri dish. Aqua regia was also used as a pretreatment method and involved immersing the samples for 1 hour in the aqua regia before being removed, rinsed with doubly-distilled, deionised water and dried in a stream of cylinder air.

Water droplet contact angles, CAs, were measured using an FTA100 system comprising a CCTV camera interfaced with a computer, which provided a continuous stream of images of any water droplet after its initial deposition onto the surface of the substrate under test. Droplets were deposited using a 500 μL Gastight (Hamilton) syringe, via a 30-gauge stainless steel needle with 0° bevel (Kahnetics), which deposited reproducible 5 μL water droplets. The software package associated with the instrument allowed calculation of the contact angle made by the water droplet deposited on the substrate by curve fitting the droplet image outline. Three droplets were deposited per sample and the average of the contact angles determined with a typical variance of <5%.

The study of the kinetics of contact angle recovery of samples held under vacuum was carried out using a vacuum desiccator connected to a vacuum line. Noncovered samples were simply left on the benchtop in a light-free laboratory. For the investigation of ultrasonic (US) recovery, samples of superhydrophilic Activ or glass were immersed in doubly-distilled, deionised water and placed in a US bath (VWR model: USC100T). All glassware for this section was thoroughly cleaned with chloroform and rinsed with water before use. Sample handling was carried out using plastic

Table 1: Table of water contact angles for Activ and glass samples before and after pretreatment.

Pretreatment method	Activ		Glass	
	initial CA/°	final CA/°	initial CA/°	final CA/°
UVC/O_3[(a)]	71	<5	35	<5
Δ 500°C[(b)]	70	<5	37	<5
Aqua regia[(c)]	70	<5	38	<5

[(a)] Samples irradiated by 2 × 6 W UVC bulbs in ~1700 ppm O_3 for 1 hour.
[(b)] Samples heated to 500°C and held at temp for 1 hour before cooling under Petri dish.
[(c)] Immersion in 25 mL aqua regia for 1 hour before rinsing and drying.

forceps and the samples were dried with compressed air from a cylinder.

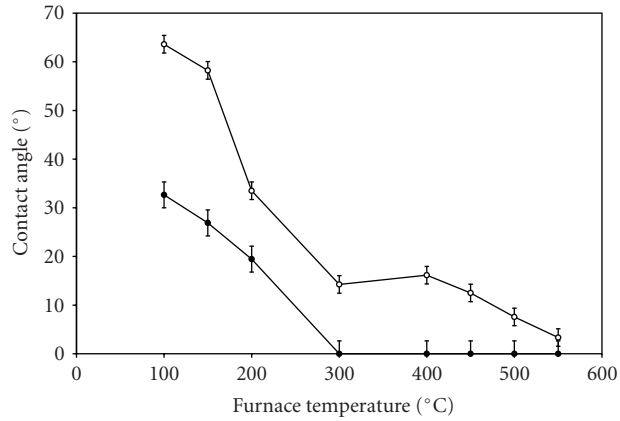

Figure 1: Plot of contact angle versus pretreatment temperature for Activ (∘) and for glass (•).

3. RESULTS AND DISCUSSION

3.1. Pretreatment cleaning methods

The combination of short wavelength ultraviolet light and ozone to create electronically excited ozone, O_3^*, a very effective oxidising agent, is well documented in its use for destroying organic materials and scouring the latter from surfaces such as semiconductor wafers [23, 24]. Recent work by this group has found that the combination of UVC and ozone as a pretreatment produces a superhydrophilic surface on Activand plain glass. These findings imply that the intrinsic state of a titania film or pristine glass is superhydrophilic, as indicated by other work on both plain glass [25] and titania [26]—such as found on Activ—and that this state requires simply the removal of all surface contaminants, particularly hydrophobic organics for its production.

The finding that UV/O_3 pretreatment renders Activ superhydrophilic fits in with both the PSIR and PCO models of PSH. However, the observation that plain glass is also rendered superhydrophilic indicates that the initial hydrophobic nature of the plain glass, and most probably Activ, is due to contamination of the surface by hydrophobic organics, at a level too low to be detected by simple FTIR. Thus, there appears no need to invoke a surface reorganisation mechanism, that is, PISR to explain PSH in titania, since the above results imply any oxidative process that removes hydrophobic surface organics, such as UVC/O_3, will render the surface of titania and glass superhydrophilic. The typical water droplet contact angles of plain and Activ glass samples before and after UV/O_3 treatment are given in Table 1.

A series of experiments were carried out to investigate a variety of other oxidising pretreatment methods, including heating and strong acid immersion, to ascertain if all were able to render Activ and plain glass superhydrophilic (i.e., CA < 5°). Thus, heating Activ and plain glass at different temperatures and testing their hydrophilic natures, via CA measurements, produced the results illustrated in Figure 1. These results show that for both substrates, the CA decreases with increasing temperature, with glass falling from an initial contact angle, CA_i, ~35° to <5° by 300°, and Activ from CA_i~70° to <5° by 550°.

That the titania substrates become hydrophilic with heat treatment appears at odds with the PSIR model of PSH, that is, reaction (2), which suggests that the dark dehydration process should be promoted by high temperatures [27], leading to either no change, or an increase in its hydrophobic nature and *not*, as observed in Figure 1, a decrease. Instead, the results in Figure 1 indicate that the initial hydrophobic character of Activ and plain glass is due to organic surface contaminants that are readily oxidised by high-heat treatment to reveal the intrinsic superhydrophilic nature of glass and titania films. From the data in Figure 1, it appears that the plain glass samples become hydrophilic at lower temperatures than Activ, probably due to a lower level of contamination on glass, which is much smoother than the titania films, rendering the latter more susceptible to organic adsorption.

In a final set of experiments, Activ and plain glass samples that were initially hydrophobic were pretreated with the very oxidising reagent, aqua regia, and all found to be rendered superhydrophilic (see Table 1).

From the above results, it appears that all three methods of pretreatment, that is, UVC/O_3, heat (>550°C), and aqua regia are able to effect the conversion of both Activ and plain glass samples from an initial hydrophobic state to a superhydrophilic state. All three methods use very strong oxidising agents/conditions to render plain and Activ glass samples superhydrophilic, most probably due to the oxidation of any surface hydrophobic organic species. These results provide significant support for the PCO model of PSH and reveal that the pristine, that is, organic-free, surfaces of these materials are superhydrophilic.

3.2. Studies of the "dark" hydrophilic to hydrophobic process

The "dark" recovery of contact angle, that is, the regeneration of hydrophobicity, exhibited by superhydrophilic titania films has been widely reported [10, 17, 22, 28], and opinion

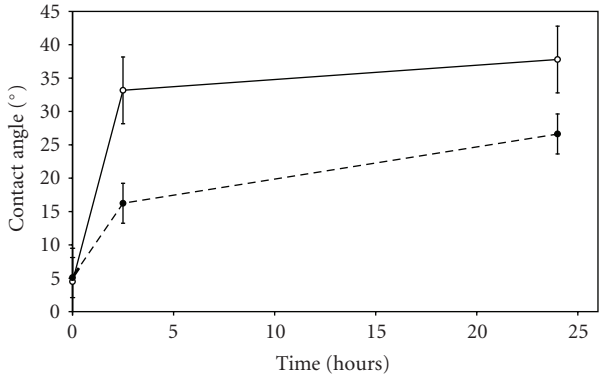

Figure 2: Water droplet contact (CA) angle versus exposure time in an evacuated atmosphere for Activ (∘) and glass (•); CA measurements recorded under ambient conditions.

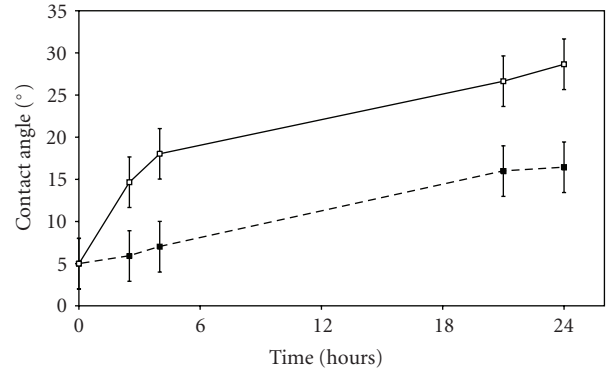

Figure 3: Variation in CA versus time for initially pristine superhydrophilic sample of Activ (□) and glass (■) under ambient laboratory conditions.

over its cause is polarised between a recontamination of the surface by airborne organics (the PCO model of PSH) and the reverse of reaction (2), that is, a dehydroxylation/dehydration process on the surface of the titania (the PISR model of PSH). Work carried out by others [17] shows that superhydrophilic samples of titania become more hydrophobic when stored in an evacuated atmosphere. These results are interpreted as providing strong evidence of the PISR model, in which vacuum storage accelerates water desorption and therefore CA recovery in superhydrophilic samples of titania. In replicating this work, we also found that the CA of Activ increases markedly when the samples are stored under vacuum, but also, and more revealing, that plain glass exhibits the same feature, although to a lesser extent. These results, illustrated in Figure 2, indicate that the phenomenon of the CA increasing for superhydrophilic titania films held under vacuum—used to support the "surface reorganisation" model, that is, reaction (2)—is not specific to titania films but is also exhibited by plain glass and so not likely to be associated with a PISR mechanism, which is attributed to titania but not to glass. Instead, the more likely explanation is that it is due to organic contamination of a clean surface, that is, glass or titania in this work, produced by exposing the sample to air when making the CA measurement after storage in a vacuum.

The effect of airborne contamination of a pristine, superhydrophilic glass, and Activ surface was demonstrated by leaving two freshly prepared samples out on the bench and monitoring the change in CA as a function of time. The results of this work are illustrated in Figure 3, from which it is clear that, on the open bench, a pristine, superhydrophilic sample of glass, or Activ can be rendered noticeably hydrophobic within few hours of exposure. Note that, as expected from its lower surface roughness, over the same time plain glass is rendered less hydrophobic than Activ due to this surface contamination. Simple IR analysis of these glass samples revealed no indication of contamination of their surfaces by hydrophobic organics, implying that the level is very low and below that detectable by conventional FTIR spectroscopy.

Table 2: Table of water contact angle for Activ and glass samples before and after either sonication or immersion for 10 minutes in deionised (DI) water.

Treatment	Activ		Glass	
	initial CA/°	final CA/°	initial CA/°	final CA/°
Sonication for 10 minutes in DI water	<5	8.9	3.8	8.2
DI water immersion for 10 minutes	<5	6.4	4.3	5.3

Previous work carried out by others [20] has shown that a superhydrophilic titania film is rendered more hydrophobic upon exposure to ultrasound (10 minutes). In another set of experiments, both glass and titania films, rendered superhydrophilic by treatment with UVC/O_3, were placed in high-purity water in clean beakers and treated with ultrasound. The measured CAs of these samples before and after exposure to ultrasound are given in Table 2 and show that for both samples upon sonication the CA rises slightly, by 3–5°, whereas without sonication the CA remains largely unchanged. These results imply that the effect of ultrasound on superhydrophilic films, be they glass or titania, is very small and most probably due to a roughening of the substrate, and/or some organic contamination. This effect is, once again, not specific to titania and would have been expected if the PISR model was appropriate.

Other work shows that any wiping or rubbing of a pristine superhydrophilic glass or titania film using a tissue or cloth renders the film hydrophobic, and this is attributed, once again, to organic contamination of the surfaces of these substrates. It appears unlikely that rubbing is able to effect the reverse of reaction (2) via a mechanochemical effect as claimed by others [21] since plain glass is affected in the same way as titania.

4. CONCLUSIONS

UV light is well known to render titania samples superhydrophilic, but this can also be effected for glass and titania

films by the combination of UVC and ozone or pretreatment with a highly oxidising solution (e.g., aqua regia) or by heating at $T > 500^{\circ}$C, suggesting that a common process is responsible for the cleaning of both substrates, namely, the removal of adventitious hydrophobic organic surface species via oxidation. These findings indicate that the pristine surfaces of plain glass and titania are intrinsically superhydrophilic and imply that the photocatalytic oxidation of organics on titania (PCO) is the most likely cause of the PSH effect.

Investigations of the recovery of the initial hydrophobicity exhibited by untreated titania or plain glass showed that, once rendered superhydrophilic, the dark hydrophilic to hydrophobic process is exhibited by both titania and plain glass films and is most likely due to contamination by airborne, hydrophobic organics. Thus, storage of titania or plain glass under vacuum, or on the open bench, leads to a noticeable increase in CA. The effect of ultrasonic treatment on contact angle recovery is very small for both plain and titania-coated glass, and probably due to surface roughening. Rubbing or wiping the hydrophilic plain glass or titania films produces a marked rise in hydrophobicity and is attributed to contamination of the surfaces by hydrophobic organics.

The work presented here provides further support for the proposal that the PSH effect is due to the UV-driven removal of hydrophobic surface organics by PCO, and the dark, slow readsorption of airborne organics.

REFERENCES

[1] M. Langlet, S. Permpoon, D. Riassetto, G. Berthomé, E. Pernot, and J. C. Joud, "Photocatalytic activity and photo-induced superhydrophilicity of sol-gel derived TiO_2 films," *Journal of Photochemistry and Photobiology A*, vol. 181, no. 2-3, pp. 203–214, 2006.

[2] A. Mills, G. Hill, S. Bhopal, I. P. Parkin, and S. A. O'Neill, "Thick titanium dioxide films for semiconductor photocatalysis," *Journal of Photochemistry and Photobiology A*, vol. 160, no. 3, pp. 185–194, 2003.

[3] M. Miyauchi, A. Nakajima, T. Watanabe, and K. Hashimoto, "Photocatalysis and photoinduced hydrophilicity of various metal oxide thin films," *Chemistry of Materials*, vol. 14, no. 6, pp. 2812–2816, 2002.

[4] I. P. Parkin and R. G. Palgrave, "Self-cleaning coatings," *Journal of Materials Chemistry*, vol. 15, no. 17, pp. 1689–1695, 2005.

[5] R.-D. Sun, A. Nakajima, A. Fujishima, T. Watanabe, and K. Hashimoto, "Photoinduced surface wettability conversion of ZnO and TiO_2 thin films," *Journal of Physical Chemistry B*, vol. 105, no. 10, pp. 1984–1990, 2001.

[6] R. Wang, K. Hashimoto, A. Fujishima, et al., "Light-induced amphiphilic surfaces," *Nature*, vol. 388, no. 6641, pp. 431–432, 1997.

[7] N. Stevens, C. I. Priest, R. Sedev, and J. Ralston, "Wettability of photoresponsive titanium dioxide surfaces," *Langmuir*, vol. 19, no. 8, pp. 3272–3275, 2003.

[8] S. Kume and T. Nozu, J. P. Patent Office, "Difficult stainable glass product," application no.: Sho 63-100042, 1988.

[9] A. Fujishima, K. Hashimoto, and T. Watanabe, *TiO_2 Photocatalysis: Fundamentals and Applications*, BKC, Tokyo, Japan, 1999.

[10] A. Fujishima, T. N. Rao, and D. A. Tryk, "Titanium dioxide photocatalysis," *Journal of Photochemistry and Photobiology C*, vol. 1, no. 1, pp. 1–21, 2000.

[11] A. N. Shultz, W. Jang, W. M. Hetherington III, D. R. Baer, L.-Q. Wang, and M. H. Engelhard, "Comparative second harmonic generation and X-ray photoelectron spectroscopy studies of the UV creation and O_2 healing of Ti^{3+} defects on (110) rutile TiO_2 surfaces," *Surface Science*, vol. 339, no. 1-2, pp. 114–124, 1995.

[12] K.-I. Katsumata, A. Nakajima, T. Shiota, et al., "Photoinduced surface roughness variation in polycrystalline TiO_2 thin films," *Journal of Photochemistry and Photobiology A*, vol. 180, no. 1-2, pp. 75–79, 2006.

[13] R. Wang, N. Sakai, A. Fujishima, T. Watanabe, and K. Hashimoto, "Studies of surface wettability conversion on TiO_2 single-crystal surfaces," *Journal of Physical Chemistry B*, vol. 103, no. 12, pp. 2188–2194, 1999.

[14] J. M. White, J. Szanyi, and M. A. Henderson, "The photon-driven hydrophilicity of titania: a model study using $TiO_2(110)$ and adsorbed trimethyl acetate," *Journal of Physical Chemistry B*, vol. 107, no. 34, pp. 9029–9033, 2003.

[15] T. Zubkoy, D. Stahl, T. L. Thompson, D. Panayotov, O. Diwald, and J. T. Yates Jr., "Ultraviolet light-induced hydrophilicity effect on $TiO_2(110)$ (1×1). Dominant role of the photooxidation of adsorbed hydrocarbons causing wetting by water droplets," *Journal of Physical Chemistry B*, vol. 109, no. 32, pp. 15454–15462, 2005.

[16] C.-Y. Wang, H. Groenzin, and M. J. Shultz, "Molecular species on nanoparticulate anatase TiO_2 film detected by sum frequency generation: trace hydrocarbons and hydroxyl groups," *Langmuir*, vol. 19, no. 18, pp. 7330–7334, 2003.

[17] H. Irie and K. Hashimoto, "Photocatalytic active surfaces and photo-induced high hydrophilicity/high hydrophobicity," in *Environmental Photochemistry Part II*, P. Boule, P. K. J. Robertson, and D. W. Bahnemann, Eds., Springer, Berlin, Germany, 2005.

[18] K. Hashimoto, H. Irie, and A. Fujishima, "TiO_2 photocatalysis: a historical overview and future prospects," *Japanese Journal of Applied Physics*, vol. 44, no. 12, pp. 8269–8285, 2005.

[19] M. Miyauchi, N. Kieda, S. Hishita, et al., "Reversible wettability control of TiO_2 surface by light irradiation," *Surface Science*, vol. 511, no. 1–3, pp. 401–407, 2002.

[20] N. Sakai, R. Wang, A. Fujishima, T. Watanabe, and K. Hashimoto, "Effect of ultrasonic treatment on highly hydrophilic TiO_2 surfaces," *Langmuir*, vol. 14, no. 20, pp. 5918–5920, 1998.

[21] M. Kamei and T. Mitsuhashi, "Hydrophobic drawings on hydrophilic surfaces of single crystalline titanium dioxide: surface wettability control by mechanochemical treatment," *Surface Science*, vol. 463, no. 1, pp. L609–L612, 2000.

[22] A. Mills, A. Lepre, N. Elliott, S. Bhopal, I. P. Parkin, and S. A. O'Neill, "Characterisation of the photocatalyst Pilkington Activ™: a reference film photocatalyst?" *Journal of Photochemistry and Photobiology A*, vol. 160, no. 3, pp. 213–224, 2003.

[23] J. R. Vig, "UV/ozone cleaning of surfaces," *Journal of Vacuum Science and Technology A*, vol. 3, no. 3, pp. 1027–1034, 1985.

[24] R. R. Sowell, R. E. Cuthrell, D. M. Mattox, and R. D. Bland, "Surface cleaning by ultraviolet radiation," *Journal of Vacuum Science and Technology*, vol. 11, no. 1, pp. 474–475, 1974.

[25] S. Takeda, M. Fukawa, Y. Hayashi, and K. Matsumoto, "Surface OH group governing adsorption properties of metal oxide films," *Thin Solid Films*, vol. 339, no. 1-2, pp. 220–224, 1999.

[26] M. Takeuchi, K. Sakamoto, G. Martra, S. Coluccia, and M. Anpo, "Mechanism of photoinduced superhydrophilicity on the TiO_2 photocatalyst surface," *Journal of Physical Chemistry B*, vol. 109, no. 32, pp. 15422–15428, 2005.

[27] A. Kanta, R. Sedev, and J. Ralston, "Thermally- and photoinduced changes in the water wettability of low-surface-area silica and titania," *Langmuir*, vol. 21, no. 6, pp. 2400–2407, 2005.

[28] N. Sakai, A. Fujishima, T. Watanabe, and K. Hashimoto, "Quantitative evaluation of the photoinduced hydrophilic conversion properties of TiO_2 thin film surfaces by the reciprocal of contact angle," *Journal of Physical Chemistry B*, vol. 107, no. 4, pp. 1028–1035, 2003.